

METABOLIC FATE OF JASMONATES

Dissertation

for the award of the degree

“*Doctor rerum naturalium*”

of the University of Goettingen

within the doctoral program

“Plant Responses To Eliminate Critical Threats”

of the Georg-August University School of Science (GAUSS)

submitted by

Sven Haroth

from Alfeld (Leine), Germany

September 2018

Department of Plant Biochemistry

Albrecht-von-Haller-Institute for Plant Sciences

Georg-August University Goettingen

Thesis committee

Prof. Dr. Ivo Feussner, Department of Plant Biochemistry, Albrecht-von-Haller-Institute for Plant Science, University of Goettingen

Prof. Dr. Christiane Gatz, Department of Plant Molecular Biology and Physiology, Albrecht-von-Haller-Institute for Plant Science, University of Goettingen

Prof. Dr. Ralf Ficner, Department of Structural Biology, Institute for Microbiology and Genetics, University of Goettingen

Members of the Examination Board

Referee: Prof. Dr. Ivo Feussner, Department of Plant Biochemistry, Albrecht-von-Haller-Institute for Plant Science, University of Goettingen

2nd Referee: Prof. Dr. Christiane Gatz, Department of Plant Molecular Biology and Physiology, Albrecht-von-Haller-Institute for Plant Science, University of Goettingen

Further members of the Examination Board

Prof. Dr. Ralf Ficner, Department of Structural Biology, Institute for Microbiology and Genetics, University of Goettingen

Prof. Dr. Andrea Polle, Department for Forest Botany and Tree Physiology, Buesgen-Institute, University of Goettingen

Prof. Dr. Volker Lipka, Department of Plant Cell Biology, Albrecht-von-Haller Institute for Plant Sciences, University of Goettingen

Prof. Dr. Petr Karlovsky, Molecular Phytopathology and Mycotoxin Research, University of Goettingen

Date of oral examination: 16th October 2018

TABLE OF CONTENTS

Affidavit	IV
Acknowledgements	V
Abstract	VI
Abbreviations	VII
List of figures	IX
List of tables	XI
1. Introduction	1
1.1. Jasmonates as plant hormones	1
1.1.1. JA-biosynthesis	2
1.1.2. JA-Ile signaling	4
1.1.3. JA-Ile inactivation.....	6
1.1.4. Jasmonate crosstalk.....	9
1.2. Glycosyltransferases in phytohormone homeostasis.....	10
1.2.1.1. Glycosylation of Jasmonates	15
2. Aims of the study	17
3. Material and Methods	18
3.1. Material	18
3.1.1. Equipment.....	18
3.1.2. Software.....	19
3.1.3. Consumables.....	19
3.1.4. Chemicals	20
3.1.5. Enzymes, size markers, antibodies, and molecular biological kits	21
3.1.6. Media.....	21
3.1.7. Plasmids.....	22
3.1.8. Bacteria strains	23
3.1.9. Plant lines	23
3.1.10. Oligonucleotides	23
3.2. Methods.....	25
3.2.1. Plant growth and treatment	25
3.2.1.1. Plant growth and cultivation	25
3.2.1.2. Seed propagation from JA-deficient plants by JA methyl ester treatment	26
3.2.1.3. Wounding of Arabidopsis	26
3.2.2. Molecular biological methods	26
3.2.2.1. Extraction of genomic plant DNA	26
3.2.2.2. Extraction of total plant RNA	27
3.2.2.3. Synthesis of complementary DNA	28
3.2.2.4. Cultivation of <i>E. coli</i> bacteria	28
3.2.3. Cloning of coding sequences from <i>A. thaliana</i> into recombinant plasmids.....	29
3.2.3.1. Amplification of DNA fragments using PCR	29
3.2.3.2. Separation of nucleotides by electrophoresis	29
3.2.3.3. Purification of Plasmids and DNA fragments.....	30
3.2.3.4. Restriction and ligation of DNA	30
3.2.3.5. Transformation of competent <i>E. coli</i> cells	31

3.2.3.6.	Colony PCR	32
3.2.4.	Generation of plant mutants.....	32
3.2.4.1.	Gene editing by clustered regularly interspaced short palindromic repeats / CRISPR associated protein 9.....	32
3.2.4.2.	Transformation of <i>Agrobacterium tumefaciens</i>	33
3.2.4.3.	<i>Agrobacterium</i> -mediated transformation of <i>A. thaliana</i>	33
3.2.4.4.	Quantitative real-time PCR expression analysis	34
3.2.5.	Purification of heterologous expressed proteins	35
3.2.5.1.	Cell disruption of <i>E. coli</i> cells.....	35
3.2.5.2.	Recombinant protein purification	35
3.2.5.3.	Protein separation by SDS-PAGE.....	39
3.2.5.4.	Protein detection by western blot.....	40
3.2.6.	Enzyme characterization.....	41
3.2.6.1.	Protein activity assay	41
3.2.6.2.	Determination of optimal temperature and pH values	41
3.2.6.3.	Analysis of the Substrate specificity of UGTs by using UDP- ¹⁴ C(U)-Glc	42
3.2.6.4.	Determination of the kinetic parameters	43
3.2.7.	Substrate synthesis.....	45
3.2.7.1.	Enzymatic syntheses of 9- and 13-hydroxy-octadecatrienoic acids.....	45
3.2.7.2.	Purification of 9- and 13-HOT.....	45
3.2.8.	Metabolite analyses	46
3.2.8.1.	Homogenizing plant material.....	46
3.2.8.2.	Extraction of plant material	46
3.2.8.3.	Targeted LC-MS/MS analysis of phytohormones	47
3.2.8.4.	Metabolite analysis by LC-high resolution-MS	48
3.2.8.5.	Non-targeted <i>ex vivo</i> metabolite fingerprinting	49
3.2.8.6.	Structure determination by fragmentation	50
4.	Results	51
4.1.	Identification of four UGTs as candidates for 12-OH-JA glycosylation	51
4.1.1.	<i>UGT76E1</i> and <i>UGT76E2</i> may be related to 12-OH-JA metabolism.....	51
4.1.2.	Transcriptome analysis of wounded <i>A. thaliana</i> leaves confirmed <i>UGT76E1</i> , <i>UGT76E2</i> and identified <i>UGT76E11</i> and <i>UGT76E12</i> as wound induced transcripts	53
4.1.3.	Real time PCR analyses confirm, that <i>UGT76E1</i> , <i>UGT76E11</i> , and <i>UGT76E12</i> are induced after wounding	54
4.1.4.	<i>UGT76E1</i> and <i>UGT76E2</i> are assigned to JA metabolism by co-expression analyses.....	55
4.2.	Sequence analyses of the candidates.....	57
4.2.1.	<i>UGT76E1</i> , <i>UGT76E2</i> , <i>UGT76E11</i> , and <i>UGT76E12</i> have similar gene structures.....	57
4.2.2.	<i>UGT76E1</i> and <i>UGT76E2</i> as well as <i>UGT76E11</i> and <i>UGT76E12</i> cluster as homologues	57
4.2.3.	Protein parameters of <i>UGT76E1</i> , <i>UGT76E2</i> , <i>UGT76E11</i> , and <i>UGT76E12</i> are similar ..	59
4.3.	Biochemical characterization of <i>UGT76E1</i> , <i>UGT76E2</i> , <i>UGT76E11</i> , and <i>UGT76E12</i> ..	60
4.3.1.	<i>UGT76E1</i> , <i>UGT76E2</i> , <i>UGT76E11</i> , <i>UGT76E12</i> , and <i>UGT74F1</i> were heterologously expressed in <i>E. coli</i>	60
4.3.2.	<i>UGT76E1</i> , <i>UGT76E2</i> , <i>UGT76E11</i> , <i>UGT76E12</i> , and <i>UGT74F1</i> were purified to homogeneity.....	61
4.3.3.	<i>UGT76E1</i> , <i>UGT76E2</i> , <i>UGT76E11</i> , <i>UGT76E12</i> , and <i>UGT74F1</i> show activity towards ω-OH-hexadecanoic acid and some towards 12-OH-JA	65
4.3.4.	The UGT enzymes prefer mild alkaline pH.....	68
4.3.5.	<i>UGT76E1</i> and <i>UGT76E2</i> show substrate preference for 12-OH-JA.....	69

4.3.6.	Homogenous enzymes can be brought back to their native substrates	72
4.3.7.	UGT76E1, UGT76E2, UGT76E12, and UGT74F1 show activity towards their known substrates	74
4.3.8.	UGT76E1, UGT76E2, UGT76E11, UGT76E12, and UGT74F1 show activity towards native substrates	76
4.3.8.1.	12-OH-JA-Ile is no substrate for the analyzed UGTs	78
4.3.9.	Substrate preferences of UGT76E1, UGT76E2, UGT76E11, UGT76E12, and UGT74F1	79
4.3.10.	The kinetic Parameters of UGT76E1, UGT76E2, UGT76E11, and UGT76E12 were estimated by A coupled photometric	80
4.4.	Jasmonates accumulate after wounding	85
4.5.	Gene editing enables investigating <i>UGT76E1</i> , <i>UGT76E2</i> , <i>UGT76E11</i> , and <i>UGT76E12</i> in <i>A. thaliana</i>	86
4.5.1.	The optimized vector system targets four candidates to Cas9	87
4.5.2.	CRISPR/Cas9 initiates a loss-of-function mutation in <i>UGT76E1</i>	88
5.	Discussion	90
5.1.	Comprehensive characterization of the JA-related UGTs revealed their catalytic preferences	91
5.2.	UGT76E1, UGT76E11, and UGT76E12 are slow catalysts	93
5.3.	UGT76E1 glycosylates 12-OH-JA with high specificity	96
5.4.	UGT76E2 forms 12- <i>O</i> -Glc-JA with high specificity and turnover numbers	98
5.5.	UGT76E11 shows activities towards oxylipins and a so far unknown metabolite	99
5.6.	UGT76E12 prefers other oxylipins over 12-OH-JA	100
5.7.	Evidence for physiological relevance of 12- <i>O</i> -Glc-JA	102
5.7.1.	12- <i>O</i> -Glc-JA-Ile cannot be identified in <i>A. thaliana</i>	104
5.7.2.	12-COOH-JA was identified in wounded leaves of <i>A. thaliana</i>	104
6.	Outlook	106
7.	References	108
8.	Supplemental data	117
	<i>Curriculum vitae</i>	135

AFFIDAVIT

Hereby, I confirm that this dissertation entitled “Metabolic fate of jasmonates” has been written independently and no other sources and aids were used than quoted.

Sven Haroth

Goettingen September 3rd, 2018

ACKNOWLEDGEMENTS

The space here is far too little to thank everybody as I should but I will give it a try:

First of all, I thank Prof. Dr. Ivo Feussner for supervising me for a long time. He took care of my scientific education from *Bachelors*, over *Masters*, to this dissertation in his department of Plant Biochemistry. Thank you a lot for all your support and trust through many years! I am also indebted to Prof. Dr. Chrsitiane Gatz and Prof. Dr. Ralf Ficner as members of the thesis committee and for helpful and interesting discussions.

In addition, I am deeply grateful for the support of Dr. Kirstin Feussner. She answered many everyday questions, helped me with metabolite measurements, fragmentations, with her MarVis-experience, as well as with uncountable discussions, and not to forget for critical reading of this thesis. Kirstin, thank you so much for all your support and patience with me. Furthermore, I thank Dr. Ellen Hornung, she helped and supported me over a long time of my study. I cannot tell how much helpful advice and motivating words she had for me, thank you Ellen – also for many delicious lunch meals. Dr. Amélie Kelly was a great support with the gene editing method, and by critical reading parts of this thesis. Dr. Cornelia Herrfurth and Dr. Krzysztof Zienkiewicz supported me a lot with phytohormone measurements. I thank Dr. Stefanie König for initiating the work. Sabine Freitag not only produced and purified oxylipins for my work and helped me with liquid chromatography, but also supported me as a good friend over years. You cheered me up every day, thank you. Furthermore, I want to thank Susanne Mester for taking care of my plants. I thank Dr. Alexander Kaefer and Manuel Landesfeind for providing the MarVis software as well as Prof. Dr. Sabine Rosahl (University of Halle/Wittenberg, Germany) for providing the pET3B vector with the potato lipoxygenase. This thesis was performed within the International Research Training Group 2172 “PRoTECT: Plant Responses To Eliminate Critical Threats”, which gave me great scientific opportunities and many new friends.

I thank all members of the department of Plant Biochemistry, especially all PhD students, Dmitrij, Milena, Yi-Tse, Hanno, Katharina, Jasmin, Elisa, Athanas, and Franziska as well as former doctoral students Dr. Viktoria Bruckhoff, Dr. Daniel Bruckhoff, and Dr. Heike Siegler for the wonderful atmosphere, great barbeques and evenings – I enjoyed working here every day. My fellow students and friends, Sven Johansson, Sören Rindfleisch, and Florian Harmann, made studying a great time of my life, thank you so much! Next, I want to thank my mother Ute Haroth and my grandmother Inge Bensch for endless understanding and support during the last years and forever. Nothing would have been possible without you. Last but not least, I want to thank my girlfriend Marlene Jost! Especially, the last weeks were hard for both of us, thank you for all your love. On to the next adventure...

ABSTRACT

Jasmonoyl-isoleucine (JA-Ile) is a phytohormone that orchestrates responses to wounding, feeding insects or necrotrophic pathogens in plants. JA-Ile-metabolism has been studied intensively (Wasternack, 2015) and most of the enzymes of the JA-Ile-synthesis as well as of its catabolism have been described (Koo, 2018; Wasternack, 2015). However, the enzyme(s) responsible to specifically glycosylate 12-hydroxy-JA (12-OH-JA) are still elusive although the metabolite 12-*O*-glucosyl-JA (12-*O*-Glc-JA) has been described in plants (Koo, 2018; Miersch *et alia* (*et al.*), 2008; Seto *et al.*, 2009). 12-*O*-Glc-JA triggers tuber formation in potato (Yoshihara *et al.*, 2014) and induces leaf-closing in Mimosa (Nakamura *et al.*, 2011). Furthermore, the glycoside might have individual functions as storage- or transport-compound (Miersch *et al.*, 2008).

Therefore, this work investigated the glycosylation of 12-OH-JA. Four *UDP-dependent glycosyltransferases* (UGTs) (*UGT76E1*, *UGT76E2*, *UGT76E11*, and *UGT76E12*) were identified as wound-induced and JA-related and sequence-analyses identified the catalytic motifs in all of them. *UGT76E1*, *UGT76E2*, *UGT76E11*, and *UGT76E12* were heterologously expressed and purified from bacterial cultures. The UGT enzymes were characterized biochemically by different activity assays in conditions as equal as possible to determine their individual substrate tolerances and specificities. In addition, a new approach was established which exposes the enzymes to their native substrate to challenge their selectivity. Through this approach, it was possible to investigate purified proteins as close as possible to their natural environment. Finally, the kinetic parameters of the UGTs were recorded with their preferred substrates in a continuous assay. Altogether, *UGT76E1* and *UGT76E2* were characterized as 12-OH-JA-UGTs. *UGT76E11* showed activity towards oxylipins and an unknown compound with the calculated sum formula C₁₁H₁₈O₃. *UGT76E12* showed high activity towards an artificial hydroxy-FA, and three oxylipins as well as to 12-OH-JA with minor extent.

This is the first report of UGTs that specifically glycosylate oxylipins. So far, glycosylated oxylipins have been found in *L. paucicostata* (Kai *et al.*, 2010) but not in *A. thaliana*. However, glycosylation may increase the solubility of the FA-derived compounds in the plant cell and may be involved in oxylipin regulation or even signaling (*confer* Wasternack & Feussner, 2018).

To investigate the physiological role of the candidate UGTs, a CRISPR/Cas9 approach was designed. A *ugt765e1* mutant plant line was originally identified by screening for an altered metabolite profile of 12-OH-JA, 12-OH-JA sulfate, and 12-*O*-Glc-JA. Due to potential redundancy of the candidates forming 12-*O*-Glc-JA, higher order mutants will be necessary to investigate the consequences of a 12-*O*-Glc-JA-depletion *in vivo*.

ABBREVIATIONS

[E]	Concentration of enzyme	cps	Counts per second
[S]	Concentration of substrate	CRISPR	Clustered regularly interspaced short palindromic repeats
11-HHT	(7Z,9E,13Z)-11-Hydroxy-7,9,13-hexadecatrienoic acid	CTAB	Cetyltrimethylammonium
11- <i>O</i> -Glc-HHT	11- <i>O</i> -Glycosyl-hydroxy-hexadecatrienoic acid	d	Days
12,13-EOT	12,13-Epoxy-octadecatrienoic acid	<i>dde2-2</i>	<i>Delayed dehiscence 2-2</i>
12-COOH-JA	12-Carboxy-jasmonic acid	ddh-JA	Didehydro-jasmonic acid
12-COOH-JA-Ile	12-Carboxy-jasmonoyl-isoleucine	DEPC	Diethyl pyrocabonate
12-HSO ₄ -JA	12-Hydroxy-jasmonic acid sulfate	DES	Divinyl ether synthase
12- <i>O</i> -Glc-JA	12- <i>O</i> -Glucosyl-jasmonic acid	dh-Kaempferol	Dihydro-kaempferol
12- <i>O</i> -Glc-JA-Ile	12- <i>O</i> -Glucosyl-jasmonoyl-isoleucine	dh-Myricetin	Dihydro-myricetin
12-OH-JA	12-Hydroxy-jasmonic acid	dnOPDA	Dinor-12-oxo-phytodienoic acid
12-OH-JA-Ile	12-Hydroxy-jasmonoyl-isoleucine	dNTP	Deoxyribonucleoside triphosphates
12-OPDA	<i>cis</i> -(+)-12-Oxo-phytodienoic acid	DP	Declustering potential
13-HOT	(9Z,11E,15Z)-13-Hydroxy-9,11,15-octadecatrienoic acid	DTT	Dithiothreitol
13-HPOT	(9Z,11E,15Z)-13-Hydroperoxy-9,11,15-octadecatrienoic acid	<i>e. g.</i>	<i>Exempli gratia</i>
13-LOX	13-Linoleate lipoxygenase	EAS	Epoxy alcohol synthase
¹⁴ C(U)-Glc	Uniformly ¹⁴ C labelled glucose	EDTA	Ethylenediaminetetraacetic acid
16:0	Hecadecanoic acid	EIC	Extracted ion chromatogram
1D-SOM	One-dimensional self-organizing map	EP	Entrance potential
2- <i>O</i> -Glc-SA	2- <i>O</i> -Glucosyl-salicylic acid	ESI	Electrospray ionization
2-OH-16:0	2-Hydroxy-hexadecanoic acid	<i>et al.</i>	<i>Et alia</i>
3-OH-16:0	3-Hydroxy-hexadecanoic acid	EVC	Empty vector control
9-HOT	(10E,12Z,15Z)-9-Hydroxy-10,12,15-octadecatrienoic acid	f. w.	Fresh weight
9-HPOT	(10E,12Z,15Z)-9-hydroxy-10,12,15-octadecatrienoic acid	FA	Fatty acid
9-LOX	9-Linoleate lipoxygenase	GA	Gibberellic acid
ABA	Abscisic acid	GE	Glycosyl ester
ACN	Acetonitrile	GH3	Gretchen Hagen 3
AOC	Allene oxide cyclase	Glc	Glucose
AOS	Allene oxide synthase	GmLOX	Lipoxygenase from <i>Glycine max</i>
AP	Alkaline phosphatase	gRNA	GuideRNA
appr.	approximately	GTR1	Glucosinolate transporter 1
AU	Absorption unit	h	Hours
BA	Benzoic acid	HisTag	Hexa-histidine tag
bp	Base pairs	HMPA-Glc	(2R,3R)-2-Hydroxy-3-methylpentanoic acid glycoside
BRB	Britton-Robinson buffer	HPL	Hydroperoxide lyase
BSA	Bovine serum albumin	HPLC	High performance liquid chromatography
c	Concentration	hpw	Hours post wounding
Cas9	Clustered regularly interspaced short palindromic repeats associated protein 9	IAA	Indole-3-acetic acid
CAZy	Carbohydrate-active enzyme	IAR3	Indole-3-acetic acid-alanine resistant 3
cDNA	Complementary DNA	IBA	Indole-3-butyric acid
CE	Collision energy	ICA	Indole-3-carboxylic acid
<i>cf.</i>	<i>Confer</i>	ILL6	Indole-3-acetic acid-leucine-like 6
COI1	Coronatine insensitive 1	IMAC	Immobilized metal affinity chromatography
Col-0	Columbia 0	JA	Jasmonic acid
		JA-GE	Jasmonic acid-glucosyl ester
		JA-Ile	Jasmonoyl-isoleucine
		JA-Ile/Leu	Jasmonoyl-isoleucine/leucine
		JA-Leu	Jasmonoyl-leucine
		JA-ME	Jasmonic acid-methyl ester
		JAR1	Jasmonic acid resistance 1

JAT1	Jasmonic acid transporter 1	Q-TOF	
JAZ	Jasmonate inflorescence meristem domain protein	Red	Reductase
JGT1	UDP-glucose:jasmonic acid glucosyltransferase 1	R-O-Glc	O-Glucosyl-substrate
JOX	Jasmonate-induced oxygenase	R-OH	Hydroxy-substrate
k _{cat}	Maximal turnover number	rpm	Rotations per minute
K _M	Michaelis-Menten constant	RT	Retention time
LB	Luria-Bertani	SA	Salicylic acid
LC	Liquid chromatography	SA-GE	Salicylic acid-glucosyl ester
LC-HR-MS	liquid chromatography coupled to high resolution mass spectrometry	SCF	Skp1/Cullin/F-box
LC-MS	Liquid chromatography coupled to mass spectrometry	SDS	Sodium dodecyl sulfate
LDH	Lactate dehydrogenase	SEC	Size exclusion chromatography
LOX	Lipoxygenase	SP	Straight phase
M	Mol per liter	SRM	Single reaction monitoring
m/z	Mass-to-charge ratio	ST2a	Sulfotransferase 2a
mAU	Milli Absorption units	St-RA	2-Oxothiazolidine-4-carboxylic acid
MeOH	Methanol of liquid chromatography coupled to mass spectrometry grade	t	Reaction time
min	Minutes	T1	Transformants of the generation 1
MR	Mutual rank	T2	Transformants of the generation 2
MRM	Multiple reaction monitoring	TAE	Tris/acetic acid/ethylenediaminetetraacetic acid
MS	Mass spectrometry	TBS	Tris buffered saline
MS/MS	Mass spectrometry fragmentation	T-DNA	Transfer DNA
MTBE	Methyl <i>tert</i> -butylether	TEMED	Tetramethylethylenediamine
MW	Molecular weight	TIC	Total ion chromatogram
NADH/NAD ⁺	Nicotinamide adenine dinucleotide	TLC	Thin-layer chromatography
NtSA-UGT	Salicylic acid Uridine diphosphate -dependent glycosyltransferase from <i>Nicotina tabacum</i>	tracrRNA	Trans-activating crRNA
OD ₆₀₀	Optical density at 600 nm	tri-OH-18:1	(10 <i>E</i>)-9,12,13-Trihydroxy-10-octadecadienoic acid
OH-16:0	Hexadecanol	tri-OH-18:2	(10 <i>E</i> ,15 <i>Z</i>)-9,12,13-Trihydroxy-10,15-octadecadienoic acid
OPC-6	3-Oxo-2-pentenylcyclopentane-1-hexanoic acid	T-TBS	Tween-Tris buffered saline
OPC-8	3-Oxo-2-pentenylcyclopentane-1-octanoic acid	UDP	Uridine diphosphate
OPR2	12-Oxo-phytodienoate reductase 2	UDP-Glc	Uridine diphosphate glucose
OPR3	12-Oxo-phytodienoate reductase 3	UGT	Uridine diphosphate -dependent glycosyltransferase
OsSA-UGT	Salicylic acid Uridine diphosphate -dependent glycosyltransferase from <i>Oryza sativa</i>	UPLC	Ultra performance liquid chromatography
p.d.u.	Procedure defined unit	UTP	Uridine triphosphate
P450	Cytochrome P450	V	Reaction rate
PAGE	Polyacrylamide gel electrophoresis	v/v	Volume per volume
PAM	Protospacer adjacent motif	VvGT1	Glycosyltransferase UGT78A5 from <i>Vitis vinifera</i>
PAX1	Peroxisomal ATP-binding cassette transporter 1	w/v	Weight per volume
PCR	Polymerase chain reaction	ZYP-5052	Auto-induction medium for protein expression
PDA	Photo diode array detector	ε	Extinction coefficient
PEP	Phosphoenolpyruvate	ω-O-Glc-16:0	ω-Glucosyl-hexadecanoic acid
pI	Isoelectrical point	ω-OH-16:0	ω-Hydroxy-hexadecanoic acid
Pip	Pipecolic acid		
PK	Pyruvate kinase		
POX	Peroxygenase		
PUFA	Polyunsaturated fatty acid		
qPCR	Quantitative real-time polymerase chain reaction		

LIST OF FIGURES

Figure 1-1: Biosynthesis of jasmonic acid and jasmonoyl-isoleucine in plants.....	3
Figure 1-2: The LOX pathway is the major pathway of oxylipin formation	4
Figure 1-3: Metabolic fate of jasmonates in plants	7
Figure 1-4: Nomenclature of UDP-dependent glycosyltransferases of family 1	11
Figure 1-5: Catalytic motifs of UDP-dependent glycosyltransferases	13
Figure 1-6: Phylogenetic tree of <i>UGTs</i> of <i>A. thaliana</i> related in hormone homeostasis.....	14
Figure 4-1: Expression of UGT76E1, UGT76E2, UGT76E11, UGT76E12, and UGT74F1 in <i>A. thaliana</i> leaves after wounding	55
Figure 4-2: Phylogenetic tree of group H UGTs in <i>A. thaliana</i>	58
Figure 4-3: UGT76E1, UGT76E2, UGT76E11, and UGT76E12 show the catalytic motifs.....	58
Figure 4-4: UGT76E1, UGT76E2, UGT76E11, UGT7 E12, and UGT74F1 were expressed in <i>E. coli</i>	61
Figure 4-5: Optimization of the protein purification of UGT76E1 by affinity chromatography	63
Figure 4-6: Protein purification for UGT76E1, UGT76E2, UGT7E11, UGT76E12, and UGT74F1	64
Figure 4-7: LC-MS based activity assays of UGT76E1, UGT76E2, UGT7E11, UGT76E12, and UGT74F1 with ω -OH-hexadecanoic acid and 12-hydroxy-JA as substrates.....	66
Figure 4-8: Structure confirmation of 12- <i>O</i> -glucosyl-JA	67
Figure 4-9: Optimum pH of UGT7E1, UGT76E2, UGT76E11, and UGT7E12	68
Figure 4-10: Substrate specificity of UGT7E1, UGT7E2, UGT76E11, UGT76E12, and UGT74F1	71
Figure 4-11: Search for native substrates of UGT76E1, UGT7E2, UGT76E11, UGT76E12, UGT74F1 by non-targeted <i>ex vivo</i> analysis	73
Figure 4-12: Activity of UGT76E1, UGT7E2, UGT76E11, UGT76E12, and UGT74F1 for 12-hydroxy-JA, salicylic acid, and ω -hydroxy-hexadecanoic acid in total metabolite extracts	75
Figure 4-13: Native substrates of UGT76E1, UGT7E2, UGT76E11, UGT76E12, UGT74F1 identified by a non-targeted <i>ex vivo</i> analysis	77
Figure 4-14: MS/MS analysis of the unknown substrate C11H18O3.....	78
Figure 4-15: Scheme of a coupled spectrophotometric assay to record reactions of uridine diphosphate-dependent glycosyltransferases.....	81
Figure 4-16: Enzyme kinetics of UGT76E1 with 12-hydroxy-JA.....	82
Figure 4-17: Enzyme kinetics of UGT76E2 with 12-hydroxy-JA.....	83
Figure 4-18: Jasmonate profiles of <i>A. thaliana</i> after wounding.....	86
Figure 4-19: Vector maps of the CRISPR-Cas9 constructs for four UGT-target genes	87
Figure 4-20: Identification of a mutation in the ORF of <i>UGT76E1</i> by CRISPR-Cas9 activity.....	89
Figure 5-1: UGT76E1, UGT76E2 complete the set of jasmonate-enzymes after wounding.....	99
Figure 5-2: The candidate UGTs glycosylate oxylipins.....	102
Supplemental figure 1: Phylogenetic tree of glycosyltransferases of <i>A. thaliana</i>	117
Supplemental figure 2: Search for glycosyltransferase genes products by co-expression analysis	118

Supplemental figure 3: Expression of <i>UGT76E1</i> , <i>UGT76E2</i> , <i>UGT76E11</i> , and <i>UGT76E12</i> in <i>A. thaliana</i> leaves after wounding	119
Supplemental figure 4: Expression of <i>UGT76E1</i> and <i>UGT7E2</i> after abiotic stresses	120
Supplemental figure 5: Expression of <i>UGT76E11</i> and <i>UGT7E12</i> after abiotic stresses	121
Supplemental figure 6: Expression of <i>UGT76E1</i> , <i>UGT76E2</i> , <i>UGT76E11</i> , <i>UGT76E12</i> , and <i>UGT74F1</i> in Col-0 and JA-deficient mutant after wounding.....	122
Supplemental figure 7: Co-expression analysis of <i>UGT76E1</i> and <i>UGT76E2</i>	123
Supplemental figure 8: Co-expression analysis of <i>UGT76E11</i> and <i>UGT76E12</i>	124
Supplemental figure 9: Gene structures of <i>UGT76E1</i> , <i>UGT76E2</i> , <i>UGT76E11</i> , and <i>UGT76E12</i> in <i>A. thaliana</i> genome	125
Supplemental figure 10: Sequencing results of <i>UGT76E1</i> , <i>UGT76E2</i> , <i>UGT76E11</i> , <i>UGT76E12</i> , and <i>UGT74F1</i> integrated into the expression vector	126
Supplemental figure 11: Optimum temperature of <i>UGT7E1</i> , <i>UGT76E2</i> , <i>UGT76E11</i> , and <i>UGT7E12</i>	127
Supplemental figure 12: <i>UGT76E12</i> shows side activity towards ethanol.....	128
Supplemental figure 13: 12-carboxy-JA was identified in leaves after wounding.....	130
Supplemental figure 14: 12- <i>O</i> -glucosyl-jasmonoyl-isooleucine is not detected in plants	131
Supplemental figure 15: Enzyme kinetics with 9- and 13-hydroxy-octadecatrienoic acid	133
Supplemental figure 16: Phytohormone profiles of <i>A. thaliana</i> after wounding	134

LIST OF TABLES

Table 3-1: Equipment	18
Table 3-2: Software	19
Table 3-3: Consumables	19
Table 3-4: Chemicals	20
Table 3-5: Enzymes, size markers, antibodies, and molecular biological kits.....	21
Table 3-6: Antibiotics	21
Table 3-7: Media for plant cultivation	21
Table 3-8: Media for <i>E. coli</i> cultivation.....	22
Table 3-9: Plasmids	22
Table 3-10: Bacterial strains	23
Table 3-11: Plant lines	23
Table 3-12: Oligonucleotides.....	23
Table 3-13: Cetyltrimethylammonium bromide solution.....	27
Table 3-14: Solutions for RNA extraction	27
Table 3-15: Buffer system for agarose gel electrophoresis	30
Table 3-16: Buffer systems for protein purification of UGT76E1	37
Table 3-17: Buffer systems for protein purification of UGT76E2.....	37
Table 3-18: Buffer systems for protein purification of UGT76E11	38
Table 3-19: Buffer systems for protein purification of UGT76E12.....	38
Table 3-20: Buffer systems for protein purification of UGT74F1	38
Table 3-21: Wash buffer for protein purification.....	39
Table 3-22: Composition of 2x Laemmli sample buffer.....	40
Table 3-23: Composition of 10 % SDS-PAGE gel.....	40
Table 3-24: Composition of stock buffers for SDS-PAGE.....	40
Table 3-25: Coomassie staining solution	40
Table 3-26: Substances, which were tested as substrates for the UGTs.	43
Table 3-27: Reaction mixture of the coupled spectrophotometric assay.	44
Table 3-28: Internal standards for quantitative LC-MS/MS analysis	46
Table 3-29: Transitions of the multiple reaction monitoring mode of the LC-MS/MS analysis	48
Table 4-1: Search for glycosyltransferase genes as candidates for JA-glycosylation.....	52
Table 4-2: Co-expression analysis of <i>UGT76E1</i> , <i>UGT76E2</i> , <i>UGT76E11</i> , and <i>UGT76E12</i>	56
Table 4-3: Amino acid sequence comparison for UGT76E1, UGT76E2, UGT76E11, and UGT76E12.....	59
Table 4-4: Relative substrate preference of UGT76E1, UGT76E2, UGT76E11, UGT76E12, and UGT74F1.....	80
Table 4-5: Kinetic parameters of the UGT76E1, UGT76E2, UGT76E11, UGT76E12, and UGT74F1 towards their best substrates	84
Table 4-6: CRISPR target sequences for UGT76E1, UGT76E2, UGT76E11, and UGT76E12.....	88

Table 5-1: Comparison of kinetic parameters of UDP-dependent glycosyltransferases.....	95
Supplemental table 1: Calculated protein parameters and predicted localizations for UGT76E1, UGT76E2, UGT76E11, UGT76E12 and UGT74F1.....	125
Supplemental table 2: Chemical structures of the UGT-substances	128
Supplemental table 3: Identification of specific metabolite markers by fragmentation.....	132

1. INTRODUCTION

Providing food for the increasing human population is a critical issue nowadays. Increasing the yield is thus a common way to optimize the existing agricultural resources. However, humans have to share their revenues. Especially, feeding insects and pathogen infections cause losses in agriculture. Within optimizing agricultural processes, genetic and biochemical approaches help to understand plant defense as well as pathogen invasion and have already pushed the limits (Guo *et alia* (*et al.*), 2018). “A detailed understanding of plant immunity to arthropod herbivores will provide new insights into basic mechanisms of chemical communication and plant-animal coevolution and may also facilitate new approaches to crop protection and improvement” (Howe & Jander, 2008). Thereby, plants actively respond to threats by producing toxins, defensive proteins and emitting volatiles that recruit insect predators. Interestingly, insects and injured plant cells initiate the defense responses themselves. These initial stimuli are processed by conserved pathways of plant hormones and the group of jasmonates promote many defense responses to a broad spectrum of insects and pathogens (Koo, 2018).

1.1. JASMONATES AS PLANT HORMONES

In addition to defense against biotic attackers, jasmonates are involved in abiotic stress responses (Farmer, 2007; Wasternack *et al.*, 1998) and influence developmental processes like flower development and root growth (Ueda & Kato, 1980; Yoshihara *et al.*, 2014). Jasmonates are molecules that derive from the core molecule jasmonic acid (JA) (Wasternack *et al.*, 1998). They may have similar evolutionary origin and biosynthetic similarities to eicosanoids, which act in mammalian wound and inflammatory responses (Koo, 2018). Eicosanoids like leukotrienes and prostaglandins have been studied extensively due to their clinical importance (Bensinger & Tontonoz, 2008).

To study the formation of jasmonates and processes regulated by them in plants, mechanical tissue damage is often used to elicit the core of inducible defense responses (Koo & Howe, 2009). Thereby, the jasmonate pathway can be stimulated in a controlled and reproducible way. On top of this, jasmonates induce systemic responses by either acting as a mobile signal or being synthesized *de novo* at the distal site (Gasperini *et al.*, 2015; Glauser *et al.*, 2009; Koo & Howe, 2009).

Initially, the odorant molecule JA-methyl ester (JA-ME) was isolated from *Jasminium grandiflorum* flowers (Demole *et al.*, 1962), which gave the name to the whole class of jasmonates. Since then, many aspects of the biosynthesis, signal perception, hormonal activity and different physiological effects have been elucidated (Wasternack, 2015).

1.1.1. JA-BIOSYNTHESIS

A variety of oxidized fatty acids (FAs) – so-called oxylipins – have functions in intra- and intermolecular signaling in animals, plants and fungi (Andreou *et al.*, 2009; Wasternack & Feussner, 2018). In plants, jasmonoyl-isoleucine (JA-Ile) – the active form of JA – is the major oxylipin acting as phytohormone.

The synthesis of oxylipins may start with the peroxidation of polyunsaturated fatty acids (PUFAs). In case of JA, an unspecific glycerolipase may release α -linolenic acid ((9Z,12Z,15Z)-9,12,15-octadecatrienoic acid) from one of the two positions of a galactolipid of the plastidial membrane (Figure 1-1) (Koo, 2018). This molecule is oxygenated at the C13 to 13-hydroperoxy-octadecatrienoic acid (13-HPOT) by specific 13-linoleate lipoxygenase (LOX) enzymes (13-LOX). In *A. thaliana* leaves, LOX2 is responsible for the bulk of JA synthesis in the first hour post wounding (hpw) (Glaser *et al.*, 2009). However, in this plant up to four isoenzymes can contribute to JA formation (Caldelari *et al.*, 2011; Chauvin *et al.*, 2012). In addition, two other LOXs (9-LOX) specifically catalyze 9-hydroperoxy-octadecatrienoic acid (9-HPOT) from α -linolenic acid. Altogether, this LOX-pathway feeds the substrate pool of this branch with 9- and 13-HPOT (Blée, 2002). Several enzymes may compete for this substrate pool (Figure 1-2) (Feussner & Wasternack, 2002). In plants, a specific group of cytochrome P450 (P450) enzymes of the CYP74 family primarily metabolizes the LOX-products. As a member of this family, a hydroperoxide lyase (HPL) cleaves the hydroperoxides and produces green-leaf volatiles, which may attract beneficial predators to fight against herbivores (Chehab *et al.*, 2008). Noticeable, the *A. thaliana* accession Columbia 0 (Col-0) is natural *HPL*-mutant (Duan *et al.*, 2005), which promotes JA-production by elevated substrate availability (Chehab *et al.*, 2008). Furthermore, glycosylated oxylipins were identified (Kai *et al.*, 2010). Such molecules may be formed from hydroxy or carboxy derivatives such as (10E,12Z,15Z)-9-hydroxy-10,12,15-octadecatrienoic acid (9-HOT) and (9Z,11E,15Z)-13-hydroxy-9,11,15-octadecatrienoic acid (13-HOT), which are synthesized from α -linolenic acid by LOX and reductase activity (Figure 1-2).

The second member of the CYP74 family is allene oxide synthase (AOS). In *A. thaliana*, a single copy gene is detectable in its genome. This enzyme reaction may be the first step with 13-HPOT as substrate of JA-biosynthesis (Figure 1-2) by producing an unstable allene oxide 12,13-epoxy-octadecatrienoic acid (12,13-EOT, Figure 1-1). The allene oxide cyclase (AOC) subsequently converts 12,13-EOT to the stable *cis*-(+)-12-oxo-phytodienoic acid (12-OPDA). Those three reactions take place in the plastid, from where 12-OPDA gets exported by a yet unknown protein and imported into the peroxisome by the peroxisomal ATP-binding cassette transporter 1 (PAX1) (Theodoulou *et al.*, 2005). There, the double bond of 12-OPDA within the cyclopentene ring is reduced to yield 3-oxo-2-pentenylcyclopentane-1-octanoic acid (OPC-8) by the

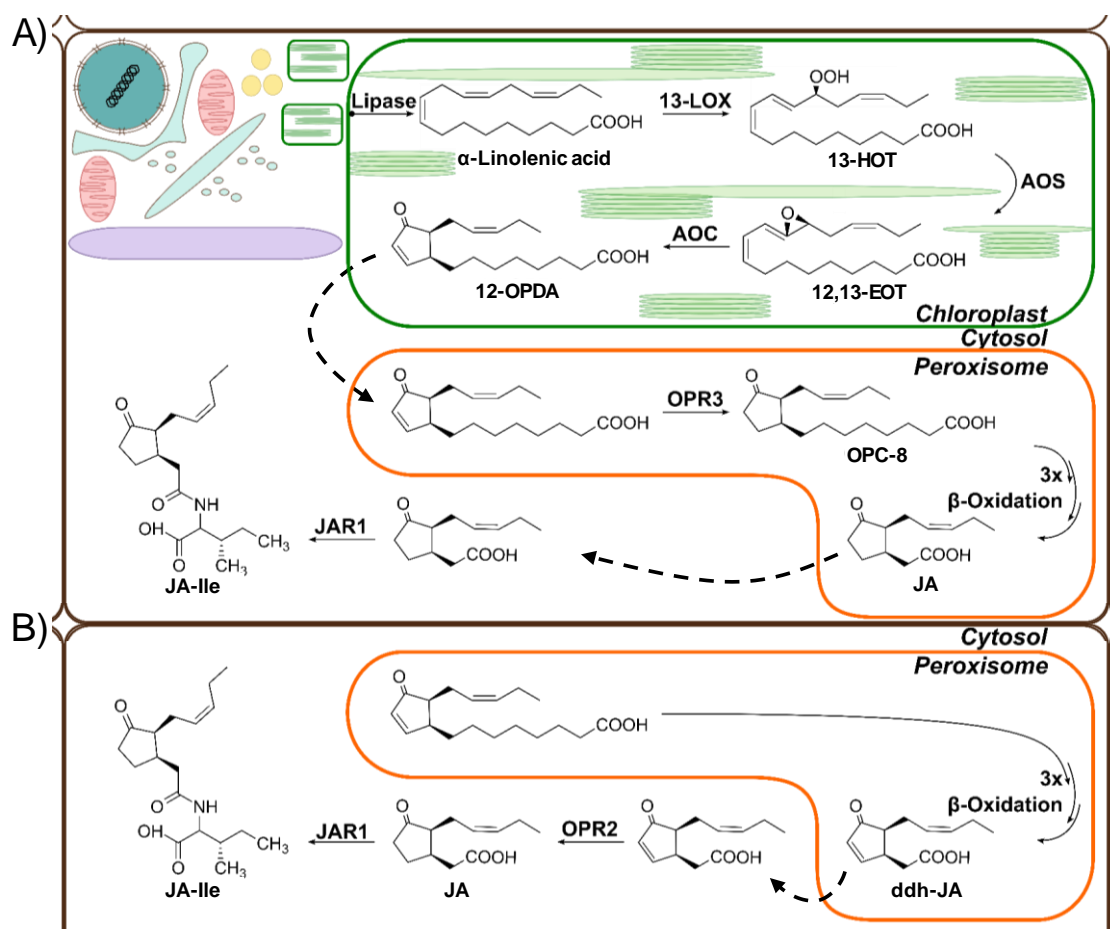


Figure 1-1: Biosynthesis of jasmonic acid and jasmonoyl-isoleucine in plants

The biosynthesis of jasmonic acid (JA) is spread over three cell compartments. **A)** Linolenic acid, released from the inner plastidial membrane by a lipase, is oxidized to 13-hydroperoxy-octadecatrienoic acid (13-HPOT) by a 13-lipoxygenase (13-LOX). 13-HPOT is dehydrated to 12,13-epoxy-octadecatrienoic acid (12,13-EOT) by the allene-oxide synthase (AOS) and cyclized to the 12-oxo-phytyldienoic acid (12-OPDA) by the allene-oxide cyclase (AOC). 12-OPDA is transported from the chloroplast into the peroxisome where it is reduced to 3-oxo-2-pentenyl-cyclopentane-1-octanoic acid (OPC-8) by the oxo-phytyldienoate reductase isoform 3 (OPR3). Shorted in three rounds of β -oxidation, JA is formed and exported into the cytoplasm. There, it gets hormonal activity by the conjugation to isoleucine by jasmonic acid resistant 1 (JAR1) forming jasmonoyl-isoleucine (JA-Ile). **B)** An alternative JA pathway lacks the reduction in the peroxisome yielding didehydro-JA (ddh-JA) after the β -oxidations. Final reduction of cytosolic ddh-JA to JA is performed by OPR isoform 2 (OPR2). Transports over biological membranes are indicated by dashed arrows. Figures modified from Wasternack & Hause, 2013 and Chini *et al.*, 2018.

12-oxo-phytyldienoate reductase isoform 3 (OPR3). Finally, three rounds of β -oxidation shorten OPC-8 to yield JA. Each β -oxidation cycle includes activation by the OPC-8 Coenzyme A ligase 1 (Koo *et al.*, 2006), dehydrogenation, hydration, and oxidation by the three enzymes of the FA- β -oxidation (Figure 1-1A).

Another route in JA synthesis is the initial release and peroxidation of roughanic acid (16:3 [n-3]) leading to dinor-12-OPDA (dnOPDA) (Weber *et al.*, 1997). Parallel to 12-OPDA, this molecule is thought to be translocated and reduced by OPR3 (Chini *et al.*, 2018) yielding JA *via* 3-oxo-2-pentenylcyclopentane-1-hexanoic acid (OPC-6). Recently, another alternative path was

identified, which lacks the initial reduction of 12-OPDA to OPC-8 in the peroxisome. Here, the 12-OPDA undergoes the three cycles of β -oxidation yielding didehydro-JA (ddh-JA), which, in turn, gets exported to the cytoplasm and is reduced to JA by OPR isoform 2 (OPR2, Figure 1-1B) (Chini *et al.*, 2018).

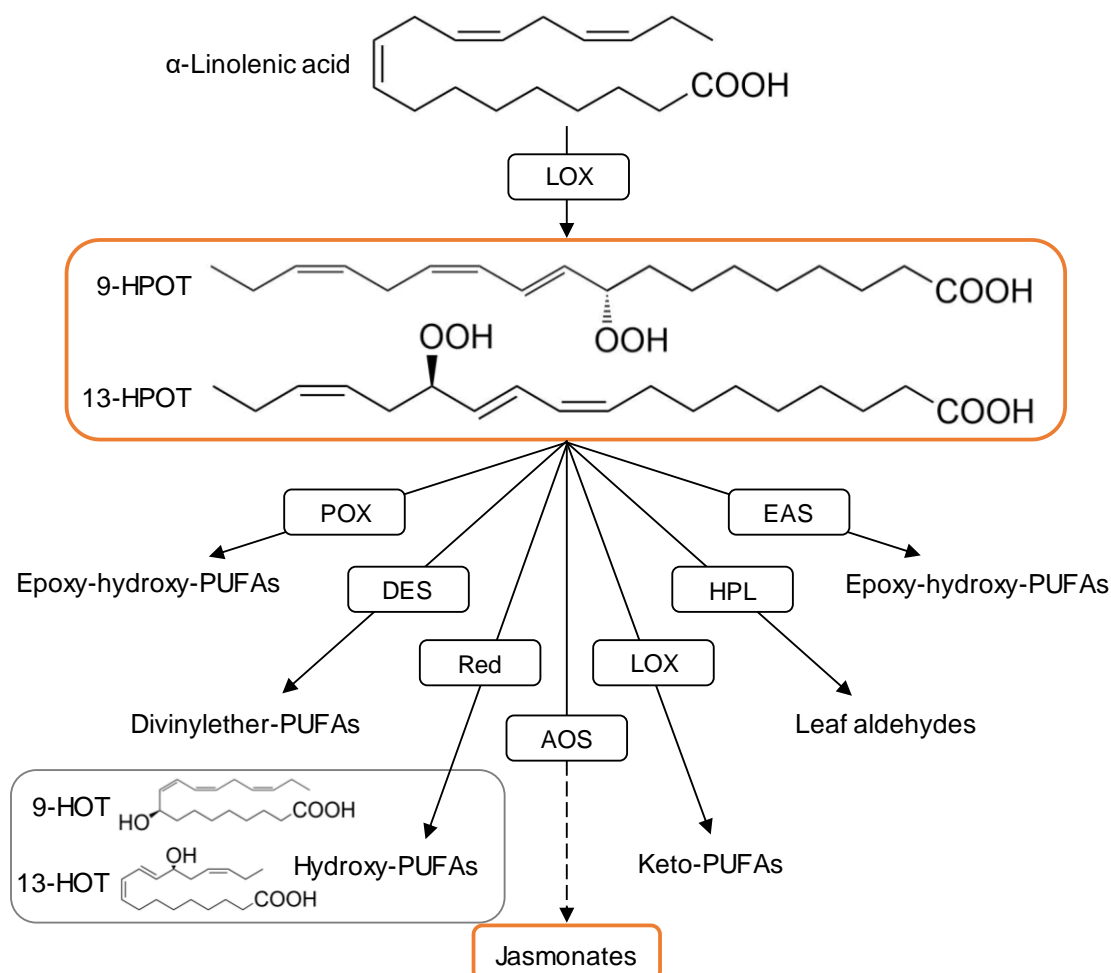


Figure 1-2: The LOX pathway is the major pathway of oxylipin formation

Lipoxygenases (LOX) oxygenate polyunsaturated fatty acids (PUFAs) such as α -linolenic acid to the 9-LOX- and 13-LOX-derived hydroperoxides, 9-hydroperoxy-octadecatrienoic acid (9-HPOT) or 13-hydroperoxy-octadecatrienoic acid, (13-HPOT). Those molecules can be metabolized to diverse oxylipins: epoxy-hydroxy PUFA by a peroxygenase (POX), divinyl ether PUFAs by a divinyl ether synthase (DES), hydroxy PUFAs by a reductase (Red), jasmonates by an allene oxide synthase (AOS), keto PUFAs by a LOX, leaf aldehydes by a hydroperoxide lyase (HPL), and to epoxy-hydroxy PUFAs formed by an epoxy alcohol synthase (EAS). Figure is modified from Feussner & Wasternack, 2002.

1.1.2. JA-ILE SIGNALING

In plant defense, JA-Ile orchestrates a rapid defense towards herbivores, wounding or necrotrophic pathogen attacks. Signal transduction pathways like calcium ion fluxes and phosphorylation cascades assist jasmonate signaling (Howe & Jander, 2008). In *A. thaliana*, JA

levels rise within 30 s in the local leaf and in 120 s in the systemic leaves (Glauser *et al.*, 2009). For its activation, JA is conjugated with the amino acid isoleucine to form JA-Ile by the jasmonic acid-amido synthetase, named JA resistance 1 (JAR1), a member of the acyl acid-amido synthetase family Gretchen Hagen 3 (GH3, GH3.11, Figure 1-3) (Westfall *et al.*, 2012). It de-represses transcription of the JA-responsive genes (Wasternack & Hause, 2013). Transcription activators, *exempli gratia* (*e. g.*) the leucine-zipper MYC2, are constitutively bound to promoter regions of these genes which are in turn repressed by jasmonate zinc-finger inflorescence meristem domain (JAZ) proteins. Additionally, the gene transcription is successfully down regulated by the interaction of the co-repressors novel interactor of JAZ in complex with topless (Pauwels *et al.*, 2010). Upon de-repression of JA-responsive genes, JA-Ile enables molecular binding of coronatine insensitive 1 (COI1) – as F-box ligase of the Skp1/Cullin/F-box(COI1) (SCF^{COI1}) complex – to JAZ. Likewise, the JA-repressors are targeted for poly ubiquitination and protein degradation by the proteasome (Wasternack & Hause, 2013). Subsequently, MYC2 and its bound co-activator mediator 25 can activate JA-responsive gene expression. Such genes include new JAZ and MYC2, which suppress further transcription in the absence of an additional JA-Ile signal as negative feedback regulation (Koo *et al.*, 2014). The real situation in the nucleus involves more regulative proteins like histone acetyltransferases or additional repressors competitive for MYC2-binding called jasmonate associated MYC2-like proteins (Wasternack & Song, 2017). This complex regulation directs the interaction with other phytohormones and balances growth and defense related pathways (see 1.1.4) (*confer* (*cf.*) Guo *et al.*, 2018; Wasternack & Song, 2017),

So far, two transporters have been described that are involved in this pathway: PXA1 and the jasmonic acid transporter 1 (JAT1). JAT1 has dual function. It imports JA-Ile into the nucleus and transports JA or JA-Ile through the plasma membrane (Li *et al.*, 2017; Nguyen *et al.*, 2017). Further, intercellular transport of both maybe mediated by the multifunctional glucosinolate transporter 1 (GTR1) transporting gibberellins and jasmonates (Ishimaru *et al.*, 2018; Saito *et al.*, 2015).

Concerning the JA-precursor 12-OPDA and its amino acid conjugate 12-OPDA-Ile, it has been discussed that they may have their individual set of responsive genes (Arnold *et al.*, 2016). The structural and metabolic relation of 12-OPDA-Ile to JA-Ile suggests similar behavior but, for 12-OPDA-Ile, neither the enzymatic conjugation, the transport mechanism, nor the perception have been studied in *A. thaliana* yet. However, in early land plants like bryophytes, the active compound JA-Ile is not present. In liverworts for example, the alternative precursor dnOPDA stimulates COI1-JAZ interaction within the molecular machinery (Monte *et al.*, 2018). Furthermore, several jasmonate derivatives were tested to have activating or inactivating functions (see Figure 1-3) (Miersch *et al.*, 2008; Wasternack & Feussner, 2018).

As a result, JA-Ile signaling may stimulate the synthesis of chemicals that act as insect deterrents, toxins, or anti-nutritive substances (Wu & Baldwin, 2010). Such compounds are often stored in specialized defensive organs like trichomes (Yoshida *et al.*, 2009). It also promotes defense by deposition of callose, surface lipids, and phenolics (Koo, 2018). In addition, jasmonates promote the emission of volatiles that may alert neighboring plants or attract insect predators (Kessler & Baldwin, 2001). Physiologically, the JA-Ile pathway readjusts growth and development for defense (Guo *et al.*, 2018).

1.1.3. JA-Ile INACTIVATION

As a phytohormone, JA-Ile reprograms plants to defense meaning signal-termination is important to restore growing conditions (Guo *et al.*, 2018; Koo, 2018). Other phytohormones are also conjugated to amino acids. In contrast to JA-Ile, auxin is inactivated by conjugation whereas the free molecule is active. However, GH3 enzymes catalyze the reaction in analogy to JAR1 (Staswick & Tiriyaki, 2004). For JA-Ile, there are at least two ways to terminate the signal: de-conjugation of the active conjugate and oxidation of the molecule at the ω -terminus of the pentenyl side chain. However, both pathways may overlap and co-operate in inactivating the JA-Ile signal (Figure 1-3).

So far, the oxidation of the active JA-Ile to the 12-hydroxy-JA-Ile (12-OH-JA-Ile) may be the initial and direct modification for the inactivation. Further oxidation yields 12-carboxy-JA-Ile (12-COOH-JA-Ile) (Heitz *et al.*, 2012). All three oxidation states – JA-Ile, 12-OH-JA-Ile, and 12-COOH-JA-Ile – can be de-conjugated by the amidohydrolase indole-3-acetic acid (IAA)-alanine resistant 3 (IAR3, Figure 1-3) (Zhang *et al.*, 2016). In addition, IAA-leucine resistant-like 6 (ILL6) is capable to cleave off the amino acid from JA-Ile and 12-OH-JA-Ile (Figure 1-3) (Widemann *et al.*, 2013; Zhang *et al.*, 2016). An *ill6iar3* double mutant with increased JA-Ile/12-OH-JA-Ile levels and overexpressing lines with reduced levels confirm the redundant action of ILL6 or IAR3 *in planta* (Zhang *et al.*, 2016).

However, cleavage of JA-Ile to JA alone retains the potential of a re-activation whereas oxidation to 12-OH-JA-Ile indeed reduces activity towards transcriptional activation (Koo *et al.*, 2014; Koo *et al.*, 2011). Generally, oxidation is a common step of inactivating phytohormones and is often catalyzed by P450 enzymes. For instance, hydroxylation of abscisic acid (ABA), gibberellic acid (GA) and brassinosteroids are essential steps in signal termination (Mizutani & Sato, 2010). Metabolomic data have shown that oxidized jasmonates like 12-OH-JA-Ile and 12-COOH-JA-Ile accumulate when JA-Ile levels decrease (Bruckhoff *et al.*, 2016). Three P450s – CYP94B1, CYP94B3, and CYP94C1 – have been identified to oxidize JA-Ile with different specificities (Heitz *et al.*, 2012; Kitaoka *et al.*, 2011; Koo *et al.*, 2014; Koo *et al.*, 2011; Widemann *et al.*, 2016). CYP94B1 and CYP94B3 preferentially form 12-OH-JA-Ile during plant defense and

CYP94C1 catalyzes the reaction in flower maturation (Widemann *et al.*, 2016). Here again, the three P450s act redundantly (Bruckhoff *et al.*, 2016; Koo *et al.*, 2014). However, CYP94C1 exclusively forms 12-COOH-JA-Ile (Figure 1-3) (Bruckhoff *et al.*, 2016; Widemann *et al.*, 2016). Besides its accumulation after wounding, 12-COOH-JA-Ile is formed during flower opening (Widemann *et al.*, 2016). However, possible functions of the different oxidized JA-Ile derivatives have to be investigated.

Subsequent de-conjugation of 12-OH-JA-Ile may yield 12-hydroxy-JA (12-OH-JA), which did not exhibit JA-typical responses like inhibition of root growth, germination or expression of JA responsive genes (Gidda *et al.*, 2003; Miersch *et al.*, 2008). Although residual amounts of 12-OH-JA were present in different mutant lines theoretically impaired in 12-OH-JA formation by

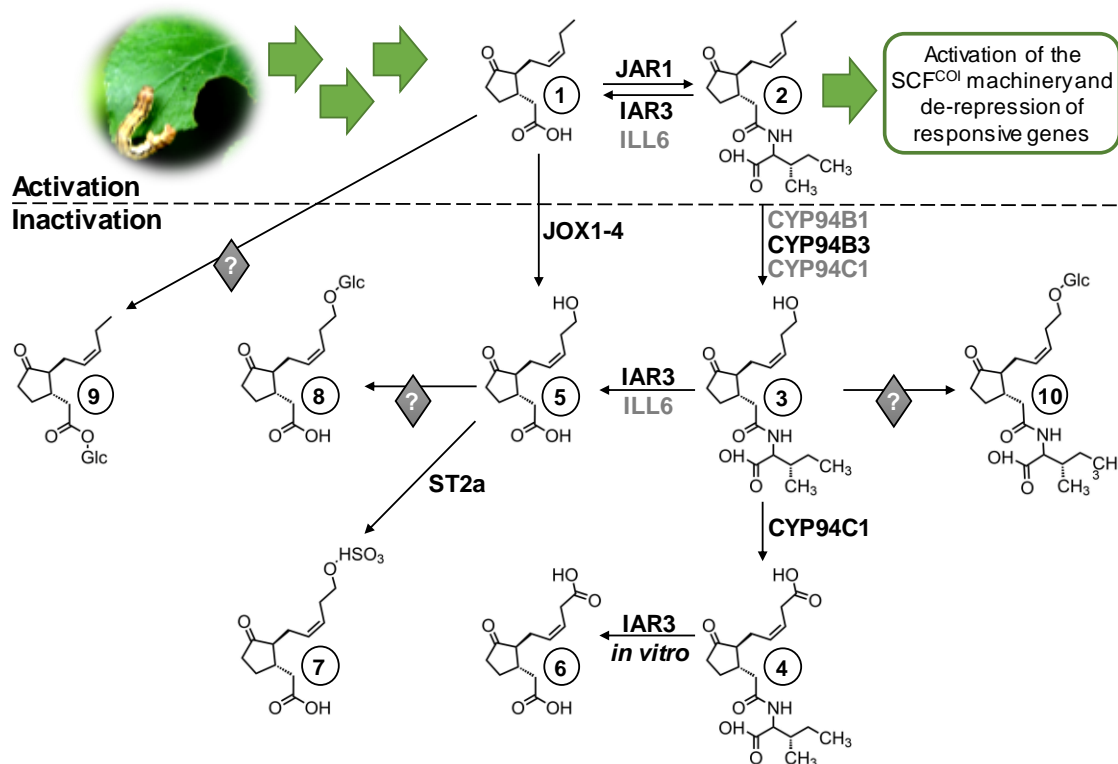


Figure 1-3: Metabolic fate of jasmonates in plants

Wound stimuli like feeding insects lead to the activation of jasmonic acid (JA, 1) biosynthesis. JA gets active as hormone by the conjugation to isoleucine. Jasmonoyl-isoleucine (JA-Ile, 2) stimulates de-repression of JA-responsive genes *via* proteasomal degradation. The amounts of JA and JA-Ile in the cell are controlled by ω -oxidations and/or de-conjugation of the isoleucine-moiety. CYP94B1, CYP94B3, and CYP94C1 oxidize JA-Ile to 12-hydroxy-JA-Ile (12-OH-JA-Ile, 3) and CYP94C1 to 12-carboxy-JA-Ile (12-COOH-JA-Ile, 4). JA-Ile, 12-OH-JA-Ile, and 12-COOH-JA-Ile get de-conjugated by IAA-alanine-resistant 3 (IAR3) and IAA-leucine-resistant-like 6 (ILL6) forming JA, 12-hydroxy-JA (12-OH-JA, 5) and 12-carboxy-JA (12-COOH-JA, 6), respectively. JA is oxidized to 12-OH-JA by jasmonate-induced oxidases 1 to 4 (JOX1-4). 12-OH-JA gets modified to 12-OH-JA sulfate (12-HSO₄-JA, 7) by sulfotransferase 2a (ST2a) or glycosylated to 12-O-glucosyl-JA (12-O-Glc-JA, 8). Question marks indicate so far unknown enzymes for the reactions to 12-O-Glc-JA, jasmonic acid-glucosyl ester (JA-GE, 9), and 12-O-glucosyl-JA-Ile (10). Scheme modified from Wasternack & Hause, 2013, additions from Carls *et al.*, 2017; Kitaoka *et al.*, 2014; Widemann *et al.*, 2016; Zhang *et al.*, 2016. Photo was taken from Iven *et al.*, 2014.

serial hydroxylation and de-conjugation of JA-Ile (cf. Bruckhoff *et al.*, 2016; Widemann *et al.*, 2013; Zhang *et al.*, 2016), this path was the only route to form 12-OH-JA known until recently. After the direct oxidation of JA had been suggested (Bruckhoff *et al.*, 2016), the responsible enzymes were independently identified twice (Caarls *et al.*, 2017; Smirnova *et al.*, 2017). These jasmonate-induced oxygenase 1 to 4 (JOX1-4) belong to the family of 2-oxoglutarate Fe(II)-dependent oxygenases (Figure 1-3) (Caarls *et al.*, 2017). The respective quadruple mutant showed elevated JA-levels and reduced levels of 12-OH-JA resulting in higher resistance to a necrotrophic fungus and feeding insects. Although induced by JA, JOX1-4 down-regulate the JA-Ile-dependent responses (Caarls *et al.*, 2017) like it has been observed for their metabolic product 12-OH-JA before (Miersch *et al.*, 2008). Trying to explain this dual synthesis routes of 12-OH-JA, Smirnova and co-workers suggested specificity of the de-conjugation path in response to wounding and the oxidative path for necrotrophic pathogen attack. Besides its dual synthesis paths, 12-OH-JA can be modified by two different ways (Figure 1-3). On the one side, the specific sulfotransferase 2a (ST2a) is known to form 12-hydroxy-JA sulfate (12-HSO₄-JA) (Gidda *et al.*, 2003). On the other side, the 12-hydroxy group can be glycosylated to form 12-*O*-glucosyl-JA (12-*O*-Glc-JA) (Wasternack & Feussner, 2018). Here, the responsible enzymes are still elusive (Koo, 2018; Wasternack & Feussner, 2018). Similar to 12-OH-JA, 12-HSO₄-JA and 12-*O*-Glc-JA may be part of the inactivation process of the JA-Ile defense (Gidda *et al.*, 2003; Miersch *et al.*, 2008). All three metabolites (12-OH-JA, 12-HSO₄-JA, and 12-*O*-Glc-JA) have been identified in many plant species in an organ-specific manner (Miersch *et al.*, 2008; Seto *et al.*, 2009). In addition, 12-OH-JA has been identified as tuber-inducing compound in *Solanum tuberosum*, which is reflected in its trivial name tuberonic acid (Yoshihara *et al.*, 2014).

In analogy to the oxidation products of conjugated jasmonates, also JA, 12-OH-JA, and 12-COOH-JA are present in *A. thaliana*. The metabolite 12-COOH-JA has been found in open flowers of *A. thaliana* (Bruckhoff *et al.*, 2016). Although, the biosynthesis is unknown the abundance of 12-COOH-JA is connected to CYP94C1-activity (Bruckhoff *et al.*, 2016). Furthermore, IAR3 is capable to de-conjugate 12-COOH-JA-Ile to 12-COOH-JA *in vitro* (Figure 1-3) (Zhang *et al.*, 2016). On top of this, the abundance of 12-COOH-JA in open flowers might be connected to the accumulation of 12-COOH-JA-Ile upon flower opening (Widemann *et al.*, 2016). Hence, 12-COOH-JA is likely to be another catabolic derivative by serial oxidation and de-conjugation of jasmonates.

In summary, six different inactivating metabolites are found around the two active molecule JA-Ile. Mainly, two catabolic routes terminate the defense signal by terminal oxidation and de-conjugation. Three different oxidation states have been identified for the core molecule JA and the active form JA-Ile. Within the catabolic fate, 12-OH-JA has an emphasized position, since it is produced in two ways (oxidation of JA and de-conjugation of 12-OH-JA-Ile) and metabolized

in two ways to 12-HSO₄-JA and 12-O-Glc-JA. Surprisingly, no individual metabolic functions of any of the catabolic derivatives has been identified yet.

1.1.4. JASMONATE CROSSTALK

Major plant processes like growth, development, and defense are orchestrated by different phytohormones. Therefore, a precise balance of these general processes and the actually needed pathways is essential for an effective plant growth and metabolism. A complex network of signal transduction pathways regulated by the different phytohormones regulates and balances the interaction of plants with their environment (Guo *et al.*, 2018). In this respect, the enzymes of the different pathway are good examples how this crosstalk is achieved. As mentioned above, the amidohydrolases IAR3 and ILL6 were initially identified and named as auxin hydrolases (Zhang *et al.*, 2016) however they use JA-Ile as substrate as well. Besides JAR1, another member of the GH3 family (AtGH3.5) conjugates auxin, benzoic acid (BA), and salicylic acid (SA) (Westfall *et al.*, 2016). Such broad substrate tolerances for different plant hormones allow common modification patterns of different phytohormones leading to a complex and fine-tuned crosstalk between the different phytohormones that can influence each other. In the case of jasmonates, the crosstalk with other phytohormones or day and night signaling pathways regulates the balance between growth and defense (Guo *et al.*, 2018; Pieterse *et al.*, 2009).

JA-Ile inhibits root growth by crosstalk with auxin (Yoshihara *et al.*, 2014) but also promotes the activation of auxin biosynthesis and *vice versa* (Koo, 2018). On top of this, both pathways share a similar genetic regulation *via* a SCF complex-mediated degradation of repressors (Koo, 2018). This might explain the overlapping activities of JA- or auxin-related enzymes. A crosstalk between JA-Ile and GA may be synergistic in stamen development but also antagonistic during plant growth and defense (Wasternack & Hause, 2013). Here, the main regulators JAZ and DELLA repress each other (Koo, 2018). Next, the interaction of JA-Ile and ABA is mostly antagonistic due to their roles in different stress responses – water control after drought or heat is regulated by ABA, while the wound response is controlled by JA-Ile. However, the crosstalk of JA-Ile and ABA can also have a synergistic character since wounding may cause water loss and ABA receptors are expressed *via* JA-Ile in *Nicotina tabacum* (*N. tabacum*) and *A. thaliana* (Lackman *et al.*, 2011). In defense, JA-Ile and ethylene generally act synergistically in response to necrotrophic pathogens (Pieterse *et al.*, 2013; Xu *et al.*, 1994). Here, JAZ-degradation activates both, JA-Ile and ethylene controlled responses (Zhu *et al.*, 2011). Anyhow, the best studied phytohormone crosstalk is between JA-Ile and SA. Both hormones act in plant defense but SA is involved in the response towards biotrophic pathogens, while JA-Ile reacts towards necrotrophic pathogens and tissue damage. In nature, plants often have to face both infections simultaneously

and JA-Ile and SA levels are well balanced until one particular stimulus pushes the response towards one defense pathway (Wasternack & Hause, 2013).

A complex network of interaction between JA-Ile and different other phytohormones may be assisted by chemical modifications, which potentially change the signaling character of JA-Ile. In case of jasmonates, different modifications are known to take place in plants, like conjugation, oxidation, de-conjugation, methylation, sulfation, and glycosylation (see Figure 1-3) (Iven *et al.*, 2014) but most of the physiological roles of such modifications are elusive (Koo, 2018). In contrast to this, many specific enzymes catalyzing the different modifications of jasmonates are well studied. The only modification where the enzymes enzymatic are not known yet is the glycosylation of different jasmonates (JA, 12-OH-JA, 12-OH-JA-Ile, Figure 1-3).

1.2. GLYCOSYLTRANSFERASES IN PHYTOHORMONE HOMEOSTASIS

Glycosylated forms of all phytohormones except ethylene are well known in *A. thaliana* (Bowles *et al.*, 2006). All individual steps in phytohormone-metabolism are regulated and balanced by specific modifications whereby glycosylation is often the final step (Vogt & Jones, 2000). Glycosylation increases the solubility of lipophilic compounds like anthocyanin pigments (Vogt & Jones, 2000). Furthermore, it promotes metabolic transport and likewise changes the inter- or intracellular localization of the metabolites, *e. g.* the glycosylated anthocyanin pigments are stored in the vacuole. In combination with a specific hydrolase enzyme, glycosylated molecules can serve as reversible storage forms. Whereas, without a hydrolase the molecule can be trapped in the organelle to regulate the cellular pool of bioactive compounds. In both cases, the activity of glycosyltransferases regulate the bioactivity and the homeostasis of specialized metabolites and phytohormones. Hereby, the responsible UGT is often controlled on the transcriptional level to regulate its mode and time of action (Bowles *et al.*, 2006; Ross *et al.*, 2001; Vogt & Jones, 2000). In analogy, glycosylation of specialized molecules is part of a three-step detoxification-strategy: Phase I is an activation of the molecule by oxidation or hydrolytic cleavage. Phase II is the glycosylation itself. It is a second layer of chemical modification, which prepares the compound for elimination from the cytosol. Phase III is the transport of the modified molecule into the vacuole or the apoplast (Coleman *et al.*, 1997). Besides the plants vacuole, the apoplast is another storage site, which accumulates inert derivatives for further storage or degradation (Dietz *et al.*, 2000).

Glycosyltransferase enzymes catalyze the transfer of a hexose-moiety to a chemical. There are different classifications of glycosyltransferases known. The database of carbohydrate-active enzyme (CAZy) ranks all glycosyltransferases known into 106 sequence-based families by their co-substrate usage *e. g.* nucleotide diphosphate-sugars, nucleotide monophosphate-sugars or

sugar phosphates (<http://www.cazy.org/>, access 20.08.2018) (Campbell *et al.*, 1997). Glycosylation of natural products and small lipophilic compounds is catalyzed by glycosyltransferases of the family 1. This is the biggest family of all glycosyltransferases known and uses uridine diphosphate (UDP)-activated sugars for catalysis (Bowles *et al.*, 2006). This subgroup was then used as basis for more detailed groupings (Campbell *et al.*, 1997): All glycosyltransferases using UDP-activated sugars are called UDP-dependent-glycosyltransferases (UGTs) and are grouped into one superfamily. The UGT-superfamily is divided into families by at least 40 % amino acid sequence homology. Here, the families 71 to 100 are specific for plants. These 30 UGT families are further separated into subfamilies by at least 60 % homology and are classified by individual numbers (Figure 1-4) (Mackenzie *et al.*, 1997). This nomenclature will be used throughout this work to describe the analyzed glycosyltransferases.

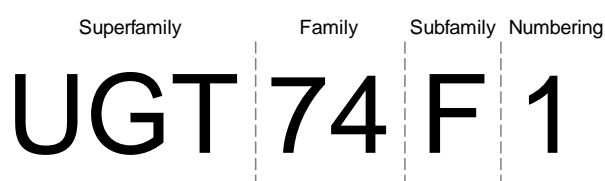
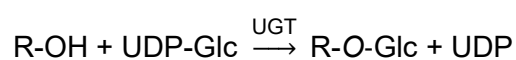


Figure 1-4: Nomenclature of UDP-dependent glycosyltransferases of family 1

The scheme illustrates the systematic nomenclature of the superfamily of UDP-dependent glycosyltransferases of the family 1 (UGTs). Further grouping is achieved in families with $\geq 40\%$ and in subfamilies with $\geq 60\%$ amino acid sequence homology. Lastly, all members of one subfamily are individually numbered (Mackenzie *et al.*, 1997).

All UGTs transfer the activated sugar moiety from a donor onto the acceptor molecule. In plants, the donor is mostly UDP-glucose (UDP-Glc) but can also be UDP-galactose, UDP-xylose, UDP-glucuronic acid or UDP-rhamnose (Vogt & Jones, 2000). The glucose (Glc) moiety of UDP-Glc derives from Glc-1-phosphate reacts with UTP-nucleotide releasing pyrophosphate. For this reaction two UTP-Glc-1-phosphate uridylyltransferases are known in *A. thaliana* (Meng *et al.*, 2009). Then, the actual UGT-reactions can take place: The UGT individual binds the co-substrate and transfers the Glc moiety from the donor onto the deprotonated group of a substrate-acceptor (Reaction 1). Usually, hydroxy groups (OH-), thioles (SH-), secondary amines (NH-), and rarely methines (CH-) can be used for glycosylation by UGTs (Bowles *et al.*, 2006).

Reaction 1



R-OH: Hydroxy-substrate, sugar acceptor
 UDP-Glc: Uridine diphosphate glucose, sugar-donor
 UGT: Uridine diphosphate-dependent glycosyltransferase
 R-O-Glc: Product, *O*-glucosyl-substrate
 UDP: Uridine diphosphate

All plant UGTs that could be analyzed by x-ray crystallography so far share a common protein structure (fold-B). This structure features two domains split by a cleft. The UDP-Glc-binding motif is located at the C-terminal domain and harbors a general Rossmann-fold motif to coordinate the sugar-nucleotide (Albesa-Jové & Guerin, 2016; Bowles *et al.*, 2006). This Rossmann-fold motif is a general structural feature of proteins to coordinate nucleotides by an alternating order of β -sheets and α -helices (Lesk, 1995). This C-terminal motif is highly conserved and characteristic for all UGT enzymes. In this 40-44 amino acid-long region, six characteristic amino acids achieve the direct UDP-Glc binding (Figure 1-5A) (Albesa-Jové & Guerin, 2016; Bowles *et al.*, 2006). This motif was identified by x-ray crystallography of the glycosyltransferase UGT78A5 from *Vitis vinifera* (*V. vinifera*, VvGT1), with the bound cofactor in the crystal structure (Figure 1-5A) (Offen *et al.*, 2006). On the other side of the cleft, the N-terminal domain is specific for substrate binding. Thus, the general sequence homology is much lower but the motif of a catalytic histidine and an assisting aspartate is well conserved (Figure 1-5B). This motif was proposed by the x-ray crystal structure of VvGT1 and the glucosyltransferase UGT74F2 from *A. thaliana* (George Thompson *et al.*, 2017; Offen *et al.*, 2006). UGT74F2 uses SA as substrate to form specifically the SA-glucosyl ester (SA-GE), (George Thompson *et al.*, 2017; Lim *et al.*, 2002). Here, a tyrosine, an aspartate and the catalytic histidine coordinate SA as substrate in a way that the hydroxy group of the acid can attack the anomeric carbon of UDP-Glc by a S_N2 -reaction mechanism (see Figure 1-5B) (Albesa-Jové & Guerin, 2016; Bowles *et al.*, 2006). In the case of a glycosidic product formed, the assisting aspartate deprotonates the secondary amine in the imidazole ring of the catalytic histidine. Consequently, the second nitrogen of the imidazole ring, which is a tertiary amine, compensates for that by deprotonating the hydroxy group of the substrate (Albesa-Jové & Guerin, 2016; George Thompson *et al.*, 2017). Subsequently, the substrate anion targets the C1 of the sugar-donor by a nucleophilic attack. These reaction mechanisms explain the so-called inverting reaction of this class of UGTs (Lairson *et al.*, 2008): The activated sugar donor is in the α -configuration and nucleophilic attack of the substrate-anion from behind leads to a flip into the β -conformation of the sugar in a S_N2 -reaction mechanism. Hence, the orientation of the substrate to the catalytic histidine is crucial for catalysis. In the case of a hydroxy group, the anionic oxygen atom forms a glycosidic product with the sugar. In the case of a carboxy group, the carbanion forms a glycosyl ester (GE) as product (see Figure 1-5B). For example, the two homologue proteins UGT74F1 and UGT74F2 are characterized as SA-UGTs in *A. thaliana*. Thereby, UGT74F1 coordinates the SA-substrates *via* the carboxy group of the benzoate and the 2-hydroxy group gets deprotonated to form a glycoside. UGT74F2, on the other side, coordinates the SA-molecule *via* the hydroxy group and the carboxy group gets deprotonated to form a GE (George Thompson *et al.*, 2017). However, UGT74F1 and UGT74F2 have overlapping activates towards the respective other

reaction (George Thompson *et al.*, 2017; Lim *et al.*, 2002). Generally, the catalytic sites of the UGT enzymes show high regio-selectivity and -specificity for the reactive groups, whereas, the substrate specificity tends to be broad (Vogt & Jones, 2000).

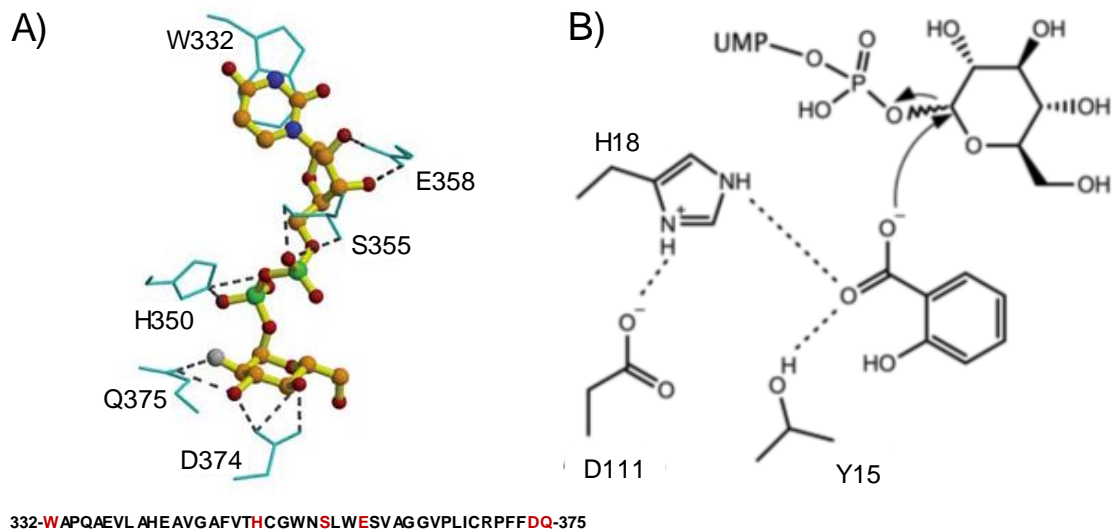


Figure 1-5: Catalytic motifs of UDP-dependent glycosyltransferases

UDP-dependent glycosyltransferases (UGTs) use an activated sugar donor, e.g. UDP-Glc, to transfer the sugar moiety onto the substrate. Hence, all UGTs share a conserved motif for the binding of the sugar donor and the catalytic site. **A)** Conserved binding motif of UDP-Glc in the active site of VvGT1. The UDP-Glc orientation is achieved by six conserved amino acids (marked in the amino acid sequence by red letters) (taken from Bowles *et al.*, 2006; Offen *et al.*, 2006). **B)** The catalytic site of UGT74F2 with the coordinated substrates salicylic acid (SA) and UDP-Glc. Hydrogen bonds are given as dashed lines. The reaction mechanism is indicated with arrows: Y15, H18, and D111 coordinate SA; S_N2 attack by the hydroxy group of the acid to the anomeric carbon of UDP-Glc results in the formation of SA-glucosyl ester (taken from George Thompson *et al.*, 2017).

There are 120 genes encoding *UGTs* predicted in the *A. thaliana* genome. Thereof, 109 carry the specific UDP-Glc-binding motif and 107 out of these 109 share nine conserved sequence-regions (Ross *et al.*, 2001). These UGTs were arranged in a phylogenetic tree into 14 groups depending on the amino acid similarity of the nine characteristic motifs (named A-N, Supplemental figure 1, membership > 60 % similarity) (Ross *et al.*, 2001). Although general catalytic preferences cannot be predicted, the group L (consisting of members of the UGT-subfamilies UGT74, UGT75 and UGT 84) contains UGTs, which form mainly GE-products with IAA and SA. UGT84B1, UGT74E2, and UGT74D1 are described to glycosylate auxins like indole-3-carboxylic (ICA) acid and indole-3-butyric acid (IBA) (Jackson *et al.*, 2001; Jin *et al.*, 2013; Tanaka *et al.*, 2014). For IAA the glycosylation has major influence on the hormone homeostasis. In this case, 90 % of all IAA is conjugated *via* an amide bond, 10 % are linked as GE for inactivation and storage and only 1 % is free IAA (Woodward & Bartel, 2005). UGT84A1 and UGT84A3 are described to produce phenylpropanoid-GE as precursors of lignin synthesis. Here, the glycosylation is thought to promote export of the monomers for extracellular polymerization (Lim *et al.*, 2001). In this L

group, also UGT74F1 and UGT74F2, which glycosylate SA, are clustered (see above, (George Thompson *et al.*, 2017; Lim *et al.*, 2002)). For 2-*O*-glucosyl-SA (2-*O*-Glc-SA), it has been reported to be localized in the vacuole (in soybean (Dean *et al.*, 2003) and in tobacco (Dean *et al.*, 2005)). The group H of UGTs harbors all UGT76 enzymes. This subfamily is not yet well characterized. Here, UGT76B1 is published to form a (2*R*,3*R*)-2-hydroxy-3-methylpentanoic acid glycoside (HMPA-Glc). The activity was found after *UGT76B1* was identified as the top induced UGT-gene after various biotic and abiotic stresses. UGT76B1 might regulate SA and JA-Ile crosstalk in plant stress response by producing HMPA-Glc

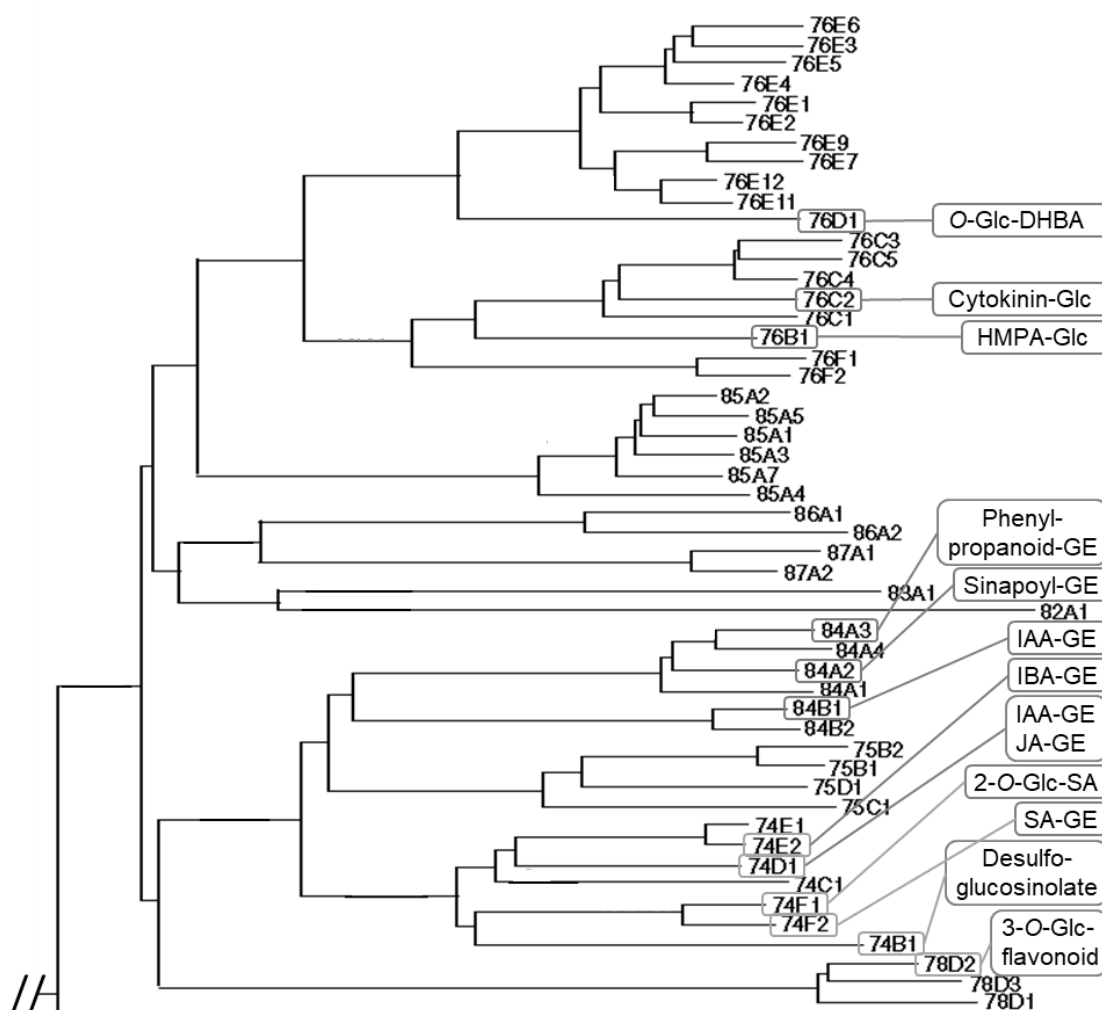


Figure 1-6: Phylogenetic tree of UGTs of *A. thaliana* related in hormone homeostasis

Phylogenetic tree of 51 out of 107 UGT genes of *A. thaliana*. The selected branch includes several genes (indicated by grey ellipses), whose gene products are involved in hormone homeostasis or stress response. Enzymatic products of selected UGTs are given in black boxes. The complete phylogenetic tree is shown in Supplemental figure 1. GE, glycosyl ester; HMPA-Glc, (2*R*,3*R*)-2-hydroxy-3-methylpentanoic acid glycoside; DHBA, dihydroxy-benzoic acid; IAA, indole-3-acetic acid; IBA, indole-3-butylic acid; JA, jasmonic acid; 3-*O*-Glc-flavonoid, 3-*O*-glycosyl-flavonoid. Indicated activities are taken from Bowles *et al.*, 2006; George Thompson *et al.*, 2017; Hou *et al.*, 2004; Huang *et al.*, 2018; Jackson *et al.*, 2001; Lim *et al.*, 2002; Ross *et al.*, 2001; Song, 2005; Tanaka *et al.*, 2014; von Saint Paul *et al.*, 2011.

(von Saint Paul *et al.*, 2011). In addition to that, UGT76C2 was characterized as being specific for the amine-glycosylation of cytokinins after drought stress (Hou *et al.*, 2004). Although not much is known about the group H, the activities that are known could point towards diverse glycosylation activities within the plant's defense response and phytohormone homeostasis.

1.2.1.1. GLYCOSYLATION OF JASMONATES

Glucose derivatives of jasmonates, like JA-glucosyl ester (JA-GE) (Miersch *et al.*, 1987; Swiatek *et al.*, 2004), the 12-*O*-Glc-JA (Miersch *et al.*, 2008), and the 12-*O*-glucosyl-JA-Ile (12-*O*-Glc-JA-Ile) (Kitaoka *et al.*, 2014) have been identified in many plant species (Figure 1-3) (Wasternack & Feussner, 2018). Furthermore, a JA-Ile glucosyl ester has been postulated as putative natural compound (Wasternack & Hause, 2013). Although, there is a set of glycosylated jasmonate, no intra- and intercellular functions are known for any of them (Koo, 2018). In *N. tabacum* cell cultures (Bright Yellow-2-cells), JA-application promotes the formation of JA-GE but also the export of 12-OH-JA (Swiatek *et al.*, 2004). In *A. thaliana*, UGT74D1, named UDP-glucose:JA glucosyltransferase 1 (JGT1), was published to produce JA-GE but already that study showed higher affinities towards auxins and even dihydro-JA (Song, 2005). Anyhow, the same enzyme was found to be specific for IAA and 2-oxindole-3-acetic acid but without JA being tested as mentioned above (Jin *et al.*, 2013; Tanaka *et al.*, 2014). In summary, UGT74D1 seems to be rather unspecific and forms GEs of different phytohormones. This might point towards a putative function in homeostasis by balancing levels of several phytohormones.

In the case of the ω -glycosylation of 12-OH-JA and 12-OH-JA-Ile, the addition of the Glc requires hydroxylation beforehand. Likewise, it follows the detoxification phases I and II (see above). Possibly, a similar inactivation mechanism could exist as described for SA in the vacuole (Dean *et al.*, 2005; Dean *et al.*, 2003) or possibly in the apoplast (Dietz *et al.*, 2000).

So far, one study has detected 12-*O*-Glc-JA-Ile after wounding in *A. thaliana*, *N. tabacum*, and *Glycine max* (Kitaoka *et al.*, 2014). However, the levels were much lower than for 12-OH-JA. Nevertheless, the same group found 12-*O*-Glc-JA-Ile to be de-conjugated to 12-*O*-Glc-JA by IAR3 *in vitro* (Zhang *et al.*, 2016). Together, there might be a physiological activity of 12-*O*-Glc-JA-Ile.

12-OH-JA and 12-*O*-Glc-JA may induce tuber formation in *S. tuberosum* (Yoshihara *et al.*, 2014). Despite, 12-OH-JA and 12-HSO₄-JA do not induce typical JA-responses like inhibiting root growth and germination rates in *Solanum lycopersicum* (*S. lycopersicum*) (Gidda *et al.*, 2003; Miersch *et al.*, 2008). All three JA-derivatives are induced by JA-Ile/COI but do not stimulate the defense-signaling themselves. Thus, it is highly unlikely that those derivatives can be metabolized back to JA (Gidda *et al.*, 2003; Miersch *et al.*, 2008). Nevertheless, the balance of 12-HSO₄-JA and 12-*O*-Glc-JA seems to be tightly regulated. On the one hand, a ST2a over-expressing line

shows enhanced levels of 12-HSO₄-JA over 12-*O*-Glc-JA in *S. lycopersicum* (Wasternack & Hause, 2013). On the other hand, a mutant with disrupted 12-HSO₄-JA-levels shows elevated 12-*O*-Glc-JA-abundance (Mugford *et al.*, 2009). Both reactions seem to compete for the joint substrate 12-OH-JA. In addition to this, 12-OH-JA and/or 12-*O*-Glc-JA are mobile compounds in *S. tuberosum* and *N. tabacum*. After application of radiolabeled 12-OH-JA, both radiolabel metabolites (12-OH-JA and 12-*O*-Glc-JA) could be detected in distal leaves (Seto *et al.*, 2009). Hence, glycosylation might change or retain the localization of 12-OH-JA. On top of this, there is a β -glucosidase specifically hydrolyzing 12-*O*-Glc-JA to 12-OH-JA in *Oryza sativa* (*O. sativa*) (Wakuta *et al.*, 2010). In *O. sativa* and *N. tabacum*, there are UGTs specific for SA-glycosylation (UGT74H3 and UGT74G1-like respectively), which also tolerate 12-OH-JA (Seto *et al.*, 2011; Seto *et al.*, 2009). Nevertheless, no specific UGTs have been found for any of those glycosylation reactions of jasmonates yet (Koo, 2018; Wasternack & Feussner, 2018).

Up to now, there is just one physiological effect of 12-*O*-Glc-JA known, which acts as a COI1-JAZ independent leaf-closing factor in *Samanea saman* (*S. saman*). Noticeable, this effect is induced to a lesser extent by 12-OH-JA application, too (Nakamura *et al.*, 2011). Therefore, specific and individual functions of 12-OH-JA and its glycoside cannot be addressed without knowing the catalytic enzymes and using the respective plant mutants.

2. AIMS OF THE STUDY

The overall topic concerns the metabolic fate of jasmonates in plant defense of wounded *A. thaliana*. Especially the catabolic fate may be highly diverse including signal termination, degradation, storage as well as regulation and balance with other phytohormones. The initial hydroxylation of the active JA-Ile leads to inactivation (Heitz *et al.*, 2012). On top of this, there are three different glycosylated jasmonates in *A. thaliana*, which change the properties of the free compounds. In such cases, a glycosylation reaction increases the solubility of jasmonates and might tag the molecules for an altered localization *e. g.* for deposition in the vacuole or the apoplast (Dean *et al.*, 2005; Dean *et al.*, 2003; Dietz *et al.*, 2000). All these derivatives are yet without a function. Consequently, it is important to identify the specific UGTs first. Hereby, it is crucial to characterize them enzymatically in respect to their substrate specificity and selectivity. In addition, kinetic parameters will give detailed information about the UGT's preference and activity. Vogt and Jones, 2000, stress the importance of detailed enzymatic data to conclude real activities. Such findings will complete the set of catalytic enzymes acting on jasmonates (see Figure 1-3). Generally, the responsible UGT(s) will dramatically increase the understanding on the whole pathway in response to wounding, feeding insects or necrotrophic pathogens and phytohormone signal termination. Then, investigations of all reactions, their crosstalk, and regulation might address different roles of the glycosylated jasmonates.

This work follows the approach to mimic defense by mechanical wounding in the model plant *A. thaliana* (Koo & Howe, 2009). After wounding, jasmonates follow a chronological sequence of metabolic modifications (Bruckhoff *et al.*, 2016; Iven *et al.*, 2014). This work wants to use this knowledge and postulates that also the gene expression of the responsible UGT-candidates might follow such temporal order since UGTs are usually regulated on this level (Vogt & Jones, 2000). In this way, the stringent series of metabolic modifications of jasmonates can be achieved by exact and controlled gene activations. Once putative candidates have been identified, the UGTs will be tested with multiple experimental layers to characterize them enzymatically. On top of this, the UGT candidates will be investigated *in vivo* using gene editing to generate plant mutants. Likewise, it may be possible to separate the physiological functions of 12-OH-JA and 12-O-Glc-JA.

3. MATERIAL AND METHODS

3.1. MATERIAL

3.1.1. EQUIPMENT

Table 3-1: Equipment

Equipment	Supplier
Acquity UPLC BEH RP 18 column (1x100 mm, 1.7 µm particle size)	Waters Corporation (Milford, USA)
Acquity UPLC HSS T3 column (1x100 mm, 1.8 µm particle size)	Waters Corporation (Milford, USA)
Acquity UPLC system with (or without) UPLC eLambda 800 nm PDA detector	Waters Corporation (Milford, USA)
Agilent 1100 HPLC system	Agilent Technologies (Waldbronn, Germany)
Agilent 1200 UHPLC system	Agilent Technologies (Waldbronn, Germany)
ÄKTA prime plus	GE Healthcare (Little Chalfont, UK)
ÄKTA prime system	GE Healthcare (Little Chalfont, UK)
Applied Biosystems 4000 quadrupole/linear ion trap mass spectrometer	MDS Sciex (Framingham, USA)
Agilent 6540 Accurate-Mass Quadrupole-Time Of Flight (Q-TOF) mass spectrometer	Agilent Technologies (Waldbronn, Germany)
Arium pro Ultrapure Water System	Sartorius AG (Goettingen, Germany)
Avanti J-25 centrifuge	Beckmann Coulter GmbH (Krefeld, Germany)
Biometra BioDocAnalyzer	Analytik Jena AG (Jena, Germany)
CanonScan 8000F scanner	Canon Incorporated (Tokyo, Japan)
Centrifuge 5415 D	Eppendorf AG (Hamburg, Germany)
Centrifuge 5417 R	Eppendorf AG (Hamburg, Germany)
Centrifuge 5810 R	Eppendorf AG (Hamburg, Germany)
Climate chambers	YORK Refrigeration, YORK Industriekaelte GmbH & Co. KG (Mannheim, Germany)
Fluorescent image analyzer FLA-3000	Fujifilm Corporation (Tokyo, Japan)
HiLoad 16/600 Superdex 75 prep grade	GE Healthcare (Little Chalfont, UK)
HiLoad 26/600 Superdex 200 prep grade	GE Healthcare (Little Chalfont, UK)
HisTALON Superflow Cartridge, 1 mL, 5 mL	Takara Bio Europe (Saint-Germain-en-Laye, France)
HisTrap HP, 1 mL, 5 mL	GE Healthcare (Little Chalfont, UK)
HiTrap Desalting 5 mL	GE Healthcare (Little Chalfont, UK)
ZORBAX RX-SIL (4.6 x 50 mm, 1.8 µm particle size)	Agilent (Waldbronn, Germany)
PCR detection systems iQ5 real-time	Bio-Rad Laboratories GmbH (Muenich, Germany)
JA10 rotor	Beckman Coulter GmbH (Krefeld, Germany)
JA25.50 rotor	Beckman Coulter GmbH (Krefeld, Germany)
LCT Premier TOF-MS	Waters Corporation (Milford, USA)
Mastercycler gradient	Eppendorf AG (Hamburg, Germany)
Mastercycler personal	Eppendorf AG (Hamburg, Germany)
Microfluidizer M-110L	Microfluidic (Westwood, USA)
Mini-PROTEAN 3 electrophoresis system	Bio-Rad Laboratories GmbH (Munich, Germany)
Mixer Ball Mill MM200 with stainless steel grinding jars or PTEE-jars	Retsch GmbH (Haan, Germany)
NanoDrop 2000 spectrophotometer	Thermo Fisher Scientific (Waltham, USA)
NGM 68 Nitrogen-Membrane-Generator	cmc Instruments (Eschborn, Germany)
Percival CU-36L/D	Percival Scientific Inc. (Perry, USA)
Premium Freezer	Liebherr (Bulle, Switzerland)
Quartz SUPERSIL cuvettes	Hellma Analytics, Muellheim, Germany

RK 51005 Ultrasonic cleaner	Sonorex (Moerfelden-Walldorf, Germany)
Sterile bench Prettl-Telstar BioII-A	Telstar (Terrassa, Spain)
TriVersa NanoMate	Advion (Ithaca, USA)
Ultraflow Freezer	Nuaire (Plymouth, USA)
Ultrasonic unit Branson Sonifier Cell disruptor B15	Branson Ultrasonics Corporation (Danbury, USA)
V-630 UV/Vis Spectrophotometer	JASCO Corporation (Hachioji, Japan)

3.1.2. SOFTWARE

Table 3-2: Software

Software	Supplier
Analyst software 1.6.2	Applied Biosystems (Darmstadt, Germany)
Bildanalyseprogramm 1.0.4.6	Datinf GmbH (Tuebingen, Germany)
Biometra BioDocAnalyzer 2.2	Analytik Jena AB (Jena, Germany)
ChemBioDraw 14.0.0.117	PerkinElmer (Waltham, USA)
Geneious 8.1	Biomatter Ltd. (Auckland, New Zealand)
Inkscape Vector Graphics Editor 0.92.1.1	Inkscape Project
MarkerLynx for MassLynx software	Waters Corporation (Milford, USA)
Marvis Suite 2.6	Kaever <i>et al.</i> , 2014
MassHunter Quantitative Analysis B.05.00	Agilent Technologies (Santa-Clara, USA)
MassHunter Workstation Acquisition software B.04.00	Agilent Technologies (Santa-Clara, USA)
MassLynx software 4.1	Waters Corporation (Milford, USA)
Microsoft Office 2016	Microsoft Corporation (Redmond, USA)
NanoDrop	Thermo Fisher Scientific (Waltham, USA)
Origin 8.5	Origin Lab (Northampton, Massachusetts, USA)
Photoshop CS6	Adobe Systems Incorporated (San Jose, California, USA)
Pymol v0.99	DeLano Scientific LLC (San Francisco, USA)
iQ5 Optical System Software	Bio-Rad Laboratories GmbH (Muenich, Germany)
SigmaPlot	Systat Software GmbH (Erkrath, Germany)
Spectra Manager II Software	JASCO Corporation (Hachioji, Japan)

3.1.3. CONSUMABLES

All general consumables were purchased from Sarstedt AG & Co. KG (Nuembrecht, Germany), if not stated otherwise.

Table 3-3: Consumables

Product	Supplier
Glass vials for HPLC	Macherey-Nagel (Dueren, Germany)
Glass vials for UPLC	Macherey-Nagel (Dueren, Germany)
Micropore tape	3M Science. Applied to Life (St Paul, USA)
Roti-NC, pore size 2 µm	Carl Roth & Co. (Karlsruhe, Germany)
Silica gel 60 plate	Merck KGaA, Darmstadt, Germany
Spin-X UF 6, 30 kDa cut-off	Corning B.V. Life Science (Amsterdam, Netherlands)
Soil: Fruehstofer Erde	Industrie Erdwerk Archut (Lauterbach-Wallenrod, Germany)
Soil: Fruehstofer Erde, T25 fein	Industrie Erdwerk Archut (Lauterbach-Wallenrod, Germany)

3.1.4. CHEMICALS

All chemicals were purchased from Carl Roth & Co. (Karlsruhe, Germany) and Merck KGaA (Darmstadt, Germany) if not stated otherwise. Solvents like methanol, ethanol, dichlormethane, and acetonitrile (ACN) were supplied by Thermo Fisher Scientific (Waltham, USA) in high performance liquid chromatography (HPLC)- or liquid chromatography (LC) coupled to mass spectrometry (MS) (LC-MS)-grade. Ultra-pure water was taken from an Arium pro Ultrapure Water System (Sartorius, Goettingen, Germany).

Table 3-4: Chemicals

Chemical	Manufacturer
11-Hydroxy-JA	Kindly provided by Dr. Otto Miersch (University of Halle/Wittenberg, Germany)
12-Hydroxy-JA methyl ester	Kindly provided by Dr. Otto Miersch (University of Halle/Wittenberg, Germany)
12-Hydroxy-JA	Kindly provided by Dr. Otto Miersch (University of Halle/Wittenberg, Germany)
12- <i>O</i> -Glycosyl-hydroxy-JA	Kindly provided by Dr. Otto Miersch (University of Halle/Wittenberg, Germany)
3-Hydroxy-hexadecanoic acid	Larodan (Solna, Sweden)
Dihydro-kaempferol	PhytoLab GmbH & C. KG (Vestengergsgreuth, Germany)
Dihydro-myricetin	PhytoLab GmbH & C. KG (Vestengergsgreuth, Germany)
9,12,13-Trihydroxy-octadecadienoic acid	Larodan (Solna, Sweden)
Gibberellic acid 3	Duchefa Biochemie B.V (Haarlem, Netherlands)
Microagar	Duchefa Biochemie B.V (Haarlem, Netherlands)
Silwet L-77 silicone surfactant	Momentive Performance Materials Inc., Waterford, USA
9,12,13-Trihydroxy-octadecaenoic acid	Larodan (Solna, Sweden)
D ₅ 12-oxophytodienoic acid	Kindly provided by Dr. Otto Miersch (University of Halle/Wittenberg, Germany)
D ₅ jasmonic acid	Kindly provided by Dr. Otto Miersch (University of Halle/Wittenberg, Germany)
D ₄ jasmonoyl-leucine	Kindly provided by Dr. Otto Miersch (University of Halle/Wittenberg, Germany)
D ₄ salicylic acid	Isotopes (Quebec, Canada)
D ₅ indole-3-acetic acid	Eurisotop (Freising, Germany)
D ₆ abscisic acid	Isotopes (Quebec, Canada)
2-oxothiazolidine-4-carboxylic acid	Merck KGaA (Darmstadt, Germany)
Uridine diphosphate glucose [glucose ¹⁴ C(U)]	PerkinElmer Inc. (Waltham, USA)

3.1.5. ENZYMES, SIZE MARKERS, ANTIBODIES, AND MOLECULAR BIOLOGICAL KITS

Table 3-5: Enzymes, size markers, antibodies, and molecular biological kits

Enzymes	Supplier
DNase I from bovine pancreas	Merck KGaA (Darmstadt, Germany)
Jump-start RedTaq ready mix	Merck KGaA (Darmstadt, Germany)
Lactatdehydrogenase	Boehringer Mannheim GmbH (Mannheim, Germany)
Lysozyme from chicken egg white, ~ 70 000 U/mL	Merck KGaA (Darmstadt, Germany)
Phusion High-Fidelity Polymerase	Thermo Fisher Scientific (Waltham, USA)
Pyruvatkinase	Boehringer Mannheim GmbH (Mannheim, Germany)
Restriction endonuclease enzymes	Thermo Fisher Scientific (Waltham, USA)
T4-DNA-Ligase	Thermo Fisher Scientific (Waltham, USA)
Takyon No ROX SYBR Mastermix blue dTTP	Kaneka Eurogentec S.A. (Seraing, Belgium)
Size marker	
Gel Filtration Standard	Bio-Rad Laboratories GmbH (Muenich, Germany)
Gene-Ruler 1kb DNA Ladder	Thermo Fisher Scientific (Waltham, USA)
Roti-Mark standard	Carl Roth GmbH & Co. KG (Karlsruhe, Germany)
Unstained Protein Molecular Weight Marker	Thermo Fisher Scientific (Waltham, USA)
Molecular biological kits	
GenElute Plasmid Miniprep Kit	Merck KGaA (Darmstadt, Germany)
Nucleospin Gel and PCR Clean-up	Macherey-Nagel (Dueren, Germany)
Antibodies	
Tetra-His Antibody	Quiagen (Hilden, Germany)
Goat anti mouse IgG	Merck KGaA (Darmstadt, Germany)

3.1.6. MEDIA

Table 3-6: Antibiotics

Given are the final concentrations of the antibiotics.

Antibiotics	Concentration [$\mu\text{g/mL}$]
Kanamycin	25
Carbenicillin	100
Rifampicin	50
Chloramphenicol	35
Hygromycin	50

Table 3-7: Media for plant cultivation

In sterile conditions, plants were cultivated on plates with 1/2 Murashige Skoog medium. The ingredients were dissolved in water. Weight per volume, w/v.

Murashige Skoog powder	0.22 % [w/v]
sucrose	0.05 % [w/v]
Microagar	0.2 % [w/v]

Table 3-8: Media for *E. coli* cultivation

The cultures were used for DNA-amplification and cloning as well as pre-cultures and main-cultures for protein expression. *E. coli* were transformed with different plasmids and cultivation was always connected to antibiotic selection (Table 3-6). The standard medium for bacteria cultivation was Luria-Bertani (LB) medium. Protein expression was done in special auto-induction medium (ZYP-5052) like in Studier, 2002. During preparation, ammonium and phosphate salts were added last to avoid precipitation. Volume per volume, v/v; weight per volume, w/v.

LB medium	
NaCl	5 g/L
Peptone	10 g/L
Yeast extract	10 g/L
ZY medium	
Peptone	10 g/L
Yeast extract	5 g/L
ZYP-5052 expression medium	
MgSO ₄	1 mM
FeCl ₃	10 μM
CaCl ₂	4 μM
MnCl ₂	2 μM
ZnSO ₄	2 μM
CoCl ₂	0.4 μM
CuCl ₂	0.4 μM
NiCl ₂	0.4 μM
NaMoO ₄	0.4 μM
Na ₂ SeO ₃	0.4 μM
H ₃ BO ₃	0.4 μM
(NH ₄) ₂ SO ₄	25 mM
KH ₂ PO ₄	50 mM
Na ₂ HPO ₄	50 mM
Glycerol	0.5 % [v/v]
Glucose	0.05 % [w/v]
α-lactose	0.2 % [w/v]
ZY medium	93 % [v/v]

3.1.7. PLASMIDS

Table 3-9: Plasmids

Plasmid	Selection marker	Reference
pCambia	Kanamycin resistance BASTA resistance	Dr. Ellen Hornung, (University of Goettingen, Germany, (Hornung <i>et al.</i> , 2005)
pET24a	Kanamycin resistance	Novagen (Schwalbach, Germany)
pET28a	Kanamycin resistance	Novagen (Schwalbach, Germany)
pJET1.2/blunt	Ampicillin resistance	Thermo Fisher Scientific (Waltham, USA)
pUC18-Entry	Carbenicillin resistance	Dr. Ellen Hronung, University of Goettingen, Germany (Hornung <i>et al.</i> , 2005)
pHEE401E	Kanamycin resistance / Streptomycin resistance	Addgene (Cambridge, USA, Wang <i>et al.</i> , 2014)

3.1.8. BACTERIA STRAINS

Table 3-10: Bacterial strains

Strain	Genotype	Reference
<i>Agrobacterium tumefaciens</i> EHA 105		Dr. Ellen Hornung (University of Goettingen, Germany)
<i>Escherichia coli</i> Rosetta II (DE3)	$\Delta(ara-leu)7697\Delta lacX74 \Delta phoA$ <i>PvuII phoR araD139 ahpC galE galK rpsL F'[lac+ lacIq pro] gor522::Tn10 trxB pRARE2 (CamR, StrR, TetR)</i>	Novagen (Schwalbach/Ts., Germany)
<i>Escherichia coli</i> BL21 Star (DE3)	<i>F- ompT hsdSB (rB-mB-) gal dcm rne131 (DE3)</i>	Thermo Fisher Scientific (Waltham, USA)
<i>Escherichia coli</i> DH5 α	<i>fhuA2 lac(del)U169 phoA glnV44 Φ80' lacZ(del)M15 gyrA96 recA1 relA1 endA1 thi-1 hsdR17</i>	New England Biolabs Ltb (Ontario, Canada)
<i>Escherichia coli</i> XL-1-blue	<i>recA1 endA1 gyrA96 thi-1 hsdR17 supE44 relA1 lac[F' proAB lac9z M15 Tn19(Tetr)]</i>	Agilent Technologies (Santa-Clara, USA)

3.1.9. PLANT LINES

All plant lines used in this work are *A. thaliana* plants of the accession Col-0.

Table 3-11: Plant lines

Locus of mutation	Plant	Plant line	Reference
At5g42650	Col-0 <i>delayed-dehiscence 2-2 (dde2-2)</i>	N65993	Nottingham Arabidopsis Stock Centre Dr. Michael Stumpe (University of Goettingen, Germany, von Malek <i>et al.</i> , 2002)

3.1.10. OLIGONUCLEOTIDES

Table 3-12: Oligonucleotides

No.	Name	Sequence	Item	rest. site
P005	UGTE12-fwd-pET28	ACGCATATGATGCAGGTTTTGGGAATGGAGG	Cloning	NdeI
P006	UGTE12-rev-pET28	ACGCTCGAGTCATAGAGTCCCTTATGAAGTGAC	Cloning	XhoI
P007	UGTE1-fwd-pET28	ACGCATATGATGGAAGAAGTACAGGAGTGAAGAGAAG	Cloning	NdeI
P008	UGTE1-rev-pET28	ACGCTCGAGGTGAACAATGATTTTTGTCTATAAATGC	Cloning	XhoI
P026	pJET fwd	CGACTCACTATAGGGAGAGCGGC	Sequencing	
P027	pJET rev	AAGAACATCGATTTTCCATGGCAG	Sequencing	
P028	T7-for	TAATACGACTCACTATAGGG	Sequencing	
P029	T7-rev	GCTAGTTATTGCTCAGCGG	Sequencing	
P044	pJet for outer	ACCATATCCATCCGGCGTAA	Sequencing	
P045	pJet rev outer	AAGAAAACCCACGCCACCTA	Sequencing	
P129	E1-q-left	TGCCAACTTCAGCATTTGGG	qPCR	
P130	E1-q-right	ACCATGCCAAAGATGAGCTC	qPCR	
P131	E12-q-left	TCGTCACCATTCCAGAAAGC	qPCR	

P132	E12-q-right	TTGTTGCAGCACCAACTGAC	qPCR	
P133	Actin8-RT_for	GGTTTTCCCCAGTGTGTTG	qPCR	
P134	Actin8-RT_rev	CTCCATGTCATCCCAGTTGC	qPCR	
P135	UBQ5-RT_fwd	GACGCTTCATCTCGTCC	qPCR	
P136	UBQ5-RT_rev	GTAAACGTAGGTGAGTCCA	qPCR	
P137	E2-fwd	ACGCATATGGAGGAAAAGCAAG	Cloning	NdeI
P138	E2-rev	ACGCTCGAGCATGGAATTAAC	Cloning	XhoI
P139	E11-fwd	ACGCATATGGAGGAAAAGCC	Cloning	NdeI
P140	E11-rev	ACGCTCGAGTAGAGTCCCTCATG	Cloning	XhoI
P157	U6-29p-F	TTAATCCAAACTACTGCAGCCTGAC	CRISPR- Sequencing	
P158	U6-29-p-R	AGCCCTCTTCTTTTCGATCCATCAAC	CRISPR- Sequencing	
P159	U6-1t-F	GCTAAGACAAAGTGATTGGTCCGTT	CRISPR- Sequencing	
P160	U6-1t-R	AACGGACCAATCACTTTGTCTTAGC	CRISPR- Sequencing	
P161	A-DT1-BsF	ATATATGGTCTCGATTGCGGGAAGGCTCTTTACTCCAGTT	CRISPR/Cas9	
P162	A-DT1-F0	TGCGGGAAGGCTCTTTACTCCAGTTTTAGAGCTAGAAATAGC	CRISPR/Cas9	
P163	A-DT0-BsR2	ATATTATTGGTCTCAATCTCTTAGTCGACTCTACCAAT	CRISPR/Cas9	
P164	A-DT2-BsF2	ATATTATTGGTCTCAAGATTGCAGACTCAGTTAAGCTGCCTG TT	CRISPR/Cas9	
P165	A-DT2-F0	TGCAGACTCAGTTAAGCTGCCTGTTTTAGAGCTAGAAATAGC	CRISPR/Cas9	
P166	A-DT0-BsR3	ATATTATTGGTCTCATCACTACTTCGTCTCTAACCAT	CRISPR/Cas9	
P167	A-DT3-BsF3	ATATTATTGGTCTCAGTGATTGCTCTGGTAAGCTTTCTGGAA GTT	CRISPR/Cas9	
P168	A-DT3-F0	TGCTCTGGTAAGCTTTCTGGAAGTTTTAGAGCTAGAAATAGC	CRISPR/Cas9	
P169	A-DT4-R0	AACAACAGTCCTTGAAGCTCACCAATCACTACTTCGACTCTA GCTGTAT	CRISPR/Cas9	
P170	A-DT4-BsR	ATTATTGGTCTCTAAACAACAGTCCTTGAAGCTCAC	CRISPR/Cas9	
P171	B-DT1-BsF	ATATATGGTCTCGATTGAACAGTGATGGAGAAGCCCTGTT	CRISPR/Cas9	
P172	B-DT1-F0	TGAACAGTGATGGAGAAGCCCTGTTTTAGAGCTAGAAATAGC	CRISPR/Cas9	
P173	B-DT0-BsR2	ATATTATTGGTCTCAATCTCTTAGTCGACTCTACCAAT	CRISPR/Cas9	
P174	B-DT2-BsF2	ATATTATTGGTCTCAAGATTGTCGTGCTAAAGACGACACTGT T	CRISPR/Cas9	
P175	B-DT2-F0	TGTCGTGCTAAAGACGACACTGTTTTAGAGCTAGAAATAGC	CRISPR/Cas9	
P176	B-DT0-BsR3	ATATTATTGGTCTCATCACTACTTCGTCTCTAACCAT	CRISPR/Cas9	
P177	B-DT3-BsF3	ATATTATTGGTCTCAGTGATTGTTTCAGCACCACAAGTGCCA GTT	CRISPR/Cas9	
P178	B-DT3-F0	TGTTTCAGCACCACAAGTGCCAGTTTTAGAGCTAGAAATAGC	CRISPR/Cas9	
P179	B-DT4-R0	AACTTCCAGAAAGCTTACCAGAGCAATCACTACTTCGACTCT AGCTGTAT	CRISPR/Cas9	
P180	B-DT4-BsR	ATTATTGGTCTCTAAACTTCCAGAAAGCTTACCAGAG	CRISPR/Cas9	
P183	SGT-fwd	ACGGAATTCGAGAAGATGAGAGG	Cloning	EcoRI
P184	SGT_rev	ACGGGATCCTTTGATTTGAATTTTTG	Cloning	BamHI
P187	SGT_rev_new	ACGCTCGAGTCATTTGATTTGAATTT	Cloning	XhoI
P188	2A-DT1-BsF	ATATATGGTCTCGATTGCGGGAAGGCTCTTTACTCCAGTT	CRISPR/Cas9	
P189	2A-DT1-F0	TGCGGGAAGGCTCTTTACTCCAGTTTTAGAGCTAGAAATAGC	CRISPR/Cas9	
P190	2A-DT2-R0	AACAGGCAGCTTAACTGAGTCTGCAATCTCTTAGTCGACTCT AC	CRISPR/Cas9	
P191	2A-DT2-BsR	ATTATTGGTCTCGAAACAGGCAGCTTAACTGAGTCTGCAA	CRISPR/Cas9	
P192	2B-DT1-BsF	ATATATGGTCTCGATTGAGGGCTTCTCCATCACTGTTGTT	CRISPR/Cas9	
P193	2B-DT1-F0	TGAGGGCTTCTCCATCACTGTTGTTTTAGAGCTAGAAATAGC	CRISPR/Cas9	
P194	2B-DT2-R0	AACAGTGTGCTCTTAGCAGACCAATCTCTTAGTCGACTCT AC	CRISPR/Cas9	
P195	2B-DT2-BsR	ATTATTGGTCTCGAAACAGTGTCGTCTTTAGCAGACCAA	CRISPR/Cas9	
P237	E1-detect (rev)	CGGTCAAGCTGCCTGGG	Seq-CRISPR	
P238	E2-detect (rev)	CAGGATCTTTCATGTCTG	Seq-CRISPR	

P239	E11-detect (rev)	CGTTTTGTTGTCCTTTGGG	Seq-CRISPR
P240	E12-detect (rev)	CTTTGGCTGCAGCTTCAGC	Seq-CRISPR
P241	E2-q-left	TTGGGCCAATAGAGAGTACGC	qPCR
P242	E2-q-right	ACCGGAACCTGCAGTTGTTG	qPCR
P243	E11-q-left	TTTTGGAGCCATTGCGGATG	qPCR
P244	E11-q-right	ATCACTGGAAAACGGCTTGC	qPCR
P245	SGT-q-left	AAACCTTCGGCTCCAAAACC	qPCR
P246	SGT-q-right	ATCCATTGCAAGGTCAAGCG	qPCR
P247	E2-q-left_new	GAGCTCATCTTTGGCAAGGTTG	qPCR
P248	E2-q-right_new	TTCAACCACTCAACGCAACTC	qPCR

3.2. METHODS

The plant work dealing with *A. thaliana* was generally performed according to Weigel & Glazebrook, 2002.

3.2.1. PLANT GROWTH AND TREATMENT

3.2.1.1. PLANT GROWTH AND CULTIVATION

Plants were grown either on soil or on plates in sterile conditions.

For standard growth conditions, plants were grown on soil (Fruehstofer Erde, Industrie Erdwerk Archut, Lauterbach-Wallenrod, Germany). Therefore, the seeds were sowed on steamed soil (80 °C, 8 hours (h)) and stored at 4 °C in the dark for 2 days (d) to guarantee a synchronized germination. Then, the plants were transferred either into climate chambers with long day conditions (16 h light / 8 h dark, 22 °C, 60 % humidity, and light intensity of 100 $\mu\text{mol m}^{-2}\text{s}^{-1}$) for seed propagation and homozygosity tests or into Percival CU-36L/D (Percival Scientific Inc., Perry, USA) with short day conditions (8 h light / 16 h dark, 22 °C, 60 % humidity, and light intensity of 100 $\mu\text{mol m}^{-2}\text{s}^{-1}$) for wounding experiments (see 3.2.1.3).

For sterile growth conditions, the seeds were sterilized with bleach first. Approximately (appr.) 200 seeds were treated with 1 mL sterilization solution (66 % Na-hypochlorite [12 %], 0.1 % Tween 20 in water) and incubated for 10 min. Following, the solution was discarded and the seeds were washed with 0.5 mL pure ethanol five times and air dried. These seeds were brought onto 1/2 Murashige Skoog plates (Table 3-7). Therefore, the seeds were given in sterile 0.1 % Agarose in water [weight per volume (w/v)] and applied onto the plates. The suspension was allowed to dry for appr. 1 h under the sterile bench. Then, the covered plate was sealed with Micropore-tape (3M Science, St Paul, USA). The plates were transferred to long day conditions (16 h light / 8 h dark, 22 °C).

3.2.1.2. SEED PROPAGATION FROM JA-DEFICIENT PLANTS BY JA METHYL ESTER TREATMENT

JA-deficient plants tend to be male sterile (Caldelari *et al.*, 2011; Stintzi & Browse, 2000; von Malek *et al.*, 2002). This causes problems in propagating seeds because such mutants are impaired in elongating the anthers in the flowers and, hence, not able to self-fertilize. To propagate the JA-deficient mutant *dde2-2* (Table 3-11) (von Malek *et al.*, 2002), plants were grown under long-day conditions and the flowers were sprayed every day with a solution of 0.01 % JA-ME, 95 %, Merck KGaA, Darmstadt, Germany) in 0.1 % Tween 20.

3.2.1.3. WOUNDING OF ARABIDOPSIS

Plant were wounded like described in (Mosblech, 2010). For the wounding experiment, five plants per pot (9 x 9 x 8 cm) were grown under short day conditions (8 h light /16 h dark, 22 °C) for six weeks. Leaves were wounded three times across the mid vein by squeezing with forceps. In this work, non-arresting Kocher's forceps were used controlled wounding of the leaves. Damaged rosette leaves were harvested by cutting the aboveground part of the plants. Usual harvesting time points were 1, 2, and 5 hpw. Control plants were harvested without of wounding. All harvested rosettes were immediately flash-frozen in liquid N₂. 10 plants per time point were pooled as one replicate. The plant material was stored at -80 °C for further analyses.

3.2.2. MOLECULAR BIOLOGICAL METHODS

If not mentioned otherwise, all molecular biological methods were performed according to Ausubel *et al.*, 1993, or Sambrook *et al.*, 1989.

3.2.2.1. EXTRACTION OF GENOMIC PLANT DNA

Genomic DNA was extracted from homogenized plant material following the method of Doyle & Doyle, 1987. It was used to amplify specific gene fragments for genotyping of plants and to detect single nucleotide polymorphisms. Therefore, appr. 100 mg of the sample were homogenized in 250 µL cetyltrimethylammonium bromide (CTAB) solution (Table 3-13) and incubated at 65 °C for 15 minutes (min). Then, 250 µL of chloroform : isoamyl alcohol [24:1, volume per volume (v/v)] were added and mixed. After centrifugation at 7 500 xg at room temperature for 4 min, 180 µL of the aqueous phase were taken and mixed with the same volume of isopropanol. After 2 min of incubation, the sample was centrifuged at 20 000 xg at room temperature for 10 min. The supernatant was carefully removed and the pellet was washed with 75 % ethanol and dried at 65 °C. Finally, the dry pellet was dissolved in 70 µL H₂O.

Table 3-13: Cetyltrimethylammonium bromide solution

Cetyltrimethylammonium bromide (CTAB) extraction solution was used for extracting genomic DNA from plant tissue. Ethylenediaminetetraacetic acid (EDTA). Weight per volume, w/v.

2 % [w/v]	CTAB
100 mM	Tris/HCl pH 8.0
20 mM	EDTA
1.4 M	NaCl

3.2.2.2. EXTRACTION OF TOTAL PLANT RNA

RNA from *A. thaliana* was isolated to amplify coding sequences of processed gene products and to monitor the expression of Arabidopsis genes quantitatively. To isolate total RNA from vegetative tissue, a modified protocol from (Onate-Sanchez & Vicente-Carbajosa, 2008) was used. 300 µL of extraction buffer (Table 3-14) were pipetted in a 1.5 mL reaction tube and 100 mg frozen tissue-powder were weighted into the tube. The suspension was mixed roughly and incubated for 5 min at room temperature. Then, 100 µL of protein precipitation solution (Table 3-14) were added and the suspension was incubated at 4 °C for at least 10 min. Following, the suspensions was centrifuged at 20 000 xg and 4 °C for 10 min. The supernatant was transferred to a fresh tube and mixed with 300 µL isopropanol. This volume was centrifuged at 20 000 xg and 4 °C for 4 min to precipitate poly-nucleotides. Then, the supernatant was carefully removed and the pellet was washed with 500 µL 70 % ethanol and centrifuged as before. The supernatant was taken again and the pellet was dried at 50 °C. The dry residue was resuspended in 20 µL diethyl pyrocarbonate DEPC-water (Table 3-14). The entire volume was used for DNase I treatment. Therefore, 3 µL of 10x DNase buffer were mixed with the RNA and 2 µL (2 units) of DNase I (Thermo Fisher Scientific, Waltham, USA) were added and incubated at 37 °C for 30 min. The reaction was stopped by adding 2 µL 50 mM ethylenediaminetetraacetic acid (EDTA) and incubating at 65 °C for 10 min. 70 µL of DEPC-water were added to the 30 µL of DNase-treated RNA and this was mixed with 50 µL 7.5 M NH₄Ac and 400 µL 100 % ethanol. This solution was centrifuged at

Table 3-14: Solutions for RNA extraction

Diethyl pyrocarbonate (DEPC), ethylenediaminetetraacetic acid (EDTA), sodium dodecyl sulfate (SDS).

Cell lysis solution	
2 %	SDS
68 mM	Sodium citrate
138 mM	Citric acid
1 mM	EDTA
Protein-DNA precipitation solution	
4 M	NaCl
16 mM	Sodium citrate
32 mM	Citric acid
DEPC-water	
0.1 %	DEPC in water dissolved 2 h at 37 °C and autoclaved

20 000x g and 4 °C for 20 min to separate RNA from degraded DNA. Afterwards, the pellet was washed with 200 µL ethanol at 20 000x g and 4 °C. The supernatant was removed and the pellet was dried at 50 °C. Finally, the residue was resuspended in 20 µL water. The extracted RNA was stored at -80 °C.

3.2.2.3. SYNTHESIS OF COMPLEMENTARY DNA

To check the expression of genes or to clone correctly processed gene products for protein expression, RNA has to be used as template. While, especially for polymerase chain reaction (PCR), it is necessary to use DNA. Therefore, complementary DNA (cDNA) has to be synthesized from the RNA.

1 µg RNA was reversely transcribed into cDNA. Initially, the RNA was incubated with 1 µL 0.5 µg/µL olido dT₁₈-primer at 65 °C for 10 min. Then, 2 µL 5x buffer for the reverse transcriptase, 2 µL 10 mM deoxyribonucleoside triphosphates (dNTP) mix, and 1 µL (200 units) reverse transcriptase (RevertAid, Thermo Fisher Scientific, Waltham, USA) were added to a final volume of 10 µL. The transcription reaction was carried out in a thermo cycler (Eppendorf cycler, Hamburg, Germany) at 37 °C for 1 h and at 70 °C for 10 min. For further use, 90 µL water were added to obtain cDNA-concentrations of 300 – 500 ng/µL.

3.2.2.4. CULTIVATION OF *E. COLI* BACTERIA

Bacteria were cultivated either in liquid culture or on solid medium. A cultivation was always connected with a selection against specific antibiotics (Table 3-9). The first selection after ligation usually was performed on plates (LB-medium (Table 3-8) with 1.5 % [w/v] agar, (Duchefa Biochemie B.V, Haarlem, Netherlands)). Incubation at 37 °C overnight allowed positively transformed cells to form single colonies, which were investigated further.

For plasmid amplification, 5 mL liquid LB medium containing the respective antibiotic (Table 3-9) were inoculated with one single colony of a plate-culture and incubated at 37 °C and 200 rotations per minute (rpm) overnight.

In preparation of protein expression, the expression cells, the vector, and the expression medium were optimized. Best yields were obtained from heterologous protein expression with the pET28a vector in BL21 Star (DE3) cells in ZYP-5052 by using auto-induction medium (Table 3-8) (Studier, 2005). This kind of medium automatically induced protein expression at low glucose and high lactose conditions without further stimulation. Firstly, 50 mL pre-culture were inoculated with several colonies from a cultivation plate or with the 0.5 mL of a glycerol stock (an aliquot of an earlier pre-culture with 30 % glycerol [v/v], stored at -80 °C) and cultivated in LB medium at 37 °C overnight. Thereof, a main expression culture was prepared. Therefore,

250 mL liquid expression medium (Table 3-8) in a 1 L flask were inoculated with pre-culture to an optical density at 600 nm (OD_{600}) of 0.1 and the cultures were incubated at 16 °C for 3 d. After protein expression, the cells were harvested by centrifugation at 4 000 xg and 4 °C for 20 min. The pellets were transferred into 50 mL tubes and flash-frozen in liquid N₂ for storage at -80 °C.

3.2.3. CLONING OF CODING SEQUENCES FROM *A. THALIANA* INTO RECOMBINANT PLASMIDS

3.2.3.1. AMPLIFICATION OF DNA FRAGMENTS USING PCR

PCR is the standard method to amplify DNA fragments from a template sequence. The general method consists of three steps: (i) a DNA double strand is melted into single strands at a temperature of 94 – 98 °C. (ii) Specific primers bind to the complement sequence of the single stranded template DNA. This works best at a temperature appr. 3 °C under the specific melting temperature of the primers. (iii) The primer sequences are elongated by the DNA-polymerase at its optimal temperature. These three steps are repeated for 20 - 40 circles. Thereby, the sequence of interest flanked by the two primers is multiplied exponentially. Here, two polymerase enzymes were used: Jump-start RedTaq (Merck KGaA, Darmstadt, Germany) and Phusion High-fidelity polymerase (Thermo Fisher Scientific, Waltham, USA). Both enzymes were used following the manufacturers protocol for reactions mixtures and PCR settings. All PCRs were carried out in thermo cyclers (Eppendorf cyclers, Hamburg, Germany).

Noticeably, the coding sequence of *UGT74F1* was amplified from root-RNA to express the protein heterologously in bacteria (see 3.2.2.4). Interestingly, the obtained PCR product corresponds to gene product *At2g43840.1* on The Arabidopsis Information Research. This differs in three base pairs (bp) from the variant *At2g43840.2*: at position 625 bp from the start, the amplified sequence is adenine-adenine-guanine in variant 1 compared to tyrosine-tyrosine-adenine in variant 2. This position corresponds to exon-intron border of exon 1 and intron 1. This differences change the amino acid sequence of variant 1 to 2 as following: valine₂₀₉ to glutamic acid and lysine₂₁₀ to glutamic acid.

3.2.3.2. SEPARATION OF NUCLEOTIDES BY ELECTROPHORESIS

Polynucleotides carry negative charges on their sugar-phosphate backbones, which are proportional to the length of the nucleotide sequence. Thus the molecules can be separated according to their size along an electrical field in a gel matrix retarding DNA movement. Here, electrophoretic separation of nucleotides was performed in horizontal 1 % agarose gels in Tris/acetic acid/EDTA (TAE) buffer (Table 3-15). In case of separating RedTaq-PCR products, no additional dye was added since the RedTaq buffer already includes a dye. Other DNA samples were mixed with 1/6 volume loading dye (Table 3-15). For size calibration of the nucleotide

fragments, 5 μ L of the Gene-Ruler 1 kb DNA Ladder (Thermo Fisher Scientific, Waltham, USA) were added to the gel. After running the electrophoresis, the DNA was stained in 2 μ g/mL ethidium bromide in TAE buffer (Table 3-15) for appr. 10 min. DNA signals were visualized by exiting with UV light in a Biometra BioDocAnalyzer (Analytik Jena AG, Jena, Germany).

Table 3-15: Buffer system for agarose gel electrophoresis

Agarose gel electrophoresis was used to separate DNA- or RNA-fragments by size. DNA was separated in 1 % agarose gels in Tris/acetic acid/ethylenediaminetetraacetic acid (EDTA) (TAE) buffer. If necessary, the DNA samples were prepared with 6x loading dye. Volume per volume, v/v; weight per volume, w/v.

TAE buffer	
40 mM	Tris
20 mM	Acetic acid
2 mM	EDTA
6x loading dye	
40 mM	Tris
2 mM	EDTA
50 % [v/v]	Glycerol
0.4 % [w/v]	Bromphenole blue

3.2.3.3. PURIFICATION OF PLASMIDS AND DNA FRAGMENTS

Isolation of pure plasmids was performed using the GenElute Plasmid Miniprep Kit (Merck KGaA, Darmstadt, Germany) according to the protocol provided by the manufacturer. For purification of DNA fragments, the DNA solutions were separated by agarose electrophoresis (3.2.3.2) first. These separated DNA fragments were cut from the gel and purified using the NucleoSpinExtract II Kit (Macherey-Nagel, Dueren, Germany) according to the protocols provided by the manufacturer.

3.2.3.4. RESTRICTION AND LIGATION OF DNA

Specific restriction of double-stranded DNA enables site-directed cloning. The restriction sites are normally added during PCR from the primers sequences. These specific sites are cut by endonuclease restriction enzymes (Thermo Fisher Scientific, Waltham, USA) leaving complementary overhangs which can be ligated again. Originally, these enzymes defend bacteria against attacking phages by cutting foreign DNA. Commercially used endonucleases type II recognize specific palindromic DNA sequences and cut them. Type I enzymes cut next to the recognition site. In this work, digestion reactions of double stranded DNA were performed in reaction volumes of 20-50 μ L at 37 °C for 1 h up to overnight. Reaction solutions were prepared as recommended by the manufacturer. Digested fragments were separated by agarose gel electrophoresis (3.2.3.2) and analyzed by UV light.

DNA ligation was performed with at least two double stranded DNA fragments with complementary overhanging sequences to gain one functional DNA plasmid. The ligation reaction was performed in 10 μ L volume following the manufacturers concentrations for T4-Ligase and buffers (Thermo Fisher Scientific, Waltham, USA) and incubated for 30 min at room temperature. Concerning DNA concentrations, it is important to mix the fragments in optimal amounts. The concentration of open ends of the smaller insert is best five times higher than that of the bigger fragment, the vector (Equation 1). Nucleotide concentrations were determined in a NanoDrop spectrophotometer (Thermo Fischer Scientific, Waltham, USA) at 260 nm. Following ligation, the reaction solutions were subsequently transformed into competent cells optimized for plasmid-amplification (Table 3-10).

Equation 1

$$\text{Volume}(\text{insert}) = \frac{5 \cdot \text{size}(\text{insert}) \cdot c(\text{vector}) \cdot \text{Volume}(\text{vector})}{\text{size}(\text{vector}) \cdot c(\text{insert})}$$

Volume (insert): Volume of the insert fragment for an effective ligation

Size (insert): Size of the insert in base pairs

c (insert): Concentration of the insert

Volume (vector): Volume of the vector fragment

Size (vector): Size of the vector in base pairs

c (vector): Concentration of the vector

3.2.3.5. TRANSFORMATION OF COMPETENT *E. COLI* CELLS

Transformation of bacteria was used for different purposes: amplification of DNA and plasmids, propagation of correctly ligated DNA fragments, heterologous expression of proteins for purification, and *Agrobacteria*-mediated plant transformation. Therefore, 1 μ L (appr. 200 ng) of plasmid was mixed with 100 μ L of chemical competent cells ($> 10^7$ colony forming units, Table 3-10, provided by Dr. Ellen Hornung, University of Goettingen, Germany) or, in case of transformation after ligation, the whole ligation volume was mixed with the competent cells. All transformations were incubated on ice for 20 min. Subsequently, the transformation of the cells was stimulated by a heat shock at 42 $^{\circ}$ C for 45 s. This treatment loosens the cell wall of the bacteria and enables assimilation of the plasmid of interest. The suspension was chilled on ice for 5 min before 900 μ L Luria-Bertani (LB) medium (Table 3-8) were added. The cultures were incubated at 37 $^{\circ}$ C and 200 rpm for appr. 90 min to recover and express the antibiotic resistance proteins. In case of ligation, all cells or, in case of plasmid transformation, just a part of the cultures were plated on a LB-agar plate (LB-medium (Table 3-8) with 1.5 % [w/v] microagar (Duchefa Biochemie B.V, Haarlem, Netherlands)) containing the appropriate antibiotics. The plates were incubated overnight at 37 $^{\circ}$ C. In case of transformation into *Agrobacterium tumefaciens* (*A. tumefaciens*), plates and cultures were incubated for 2 d at 28 $^{\circ}$ C.

3.2.3.6. COLONY PCR

Colony PCR was used to identify those cells of a transformation reaction (3.2.3.5) that contain the correct plasmid. Therefore, positively selected colonies were analyzed for the insert of interest on the respective plasmid. A single colony was picked and first streaked on a fresh LB-agar plate (1.5 % [w/v] agarose, (Duchefa Biochemie B.V, Haarlem, Netherlands) in LB-medium (Table 3-8)) with the respective antibiotics and then dissolved in 20 μ L PCR reaction solution: 10 μ L Jump-start Red Taq master mix (Thermo Fisher, Waltham, USA), 1.25 mM primer forward, and 1.25 mM primer reverse in water. The PCR program was set as recommended by the manufacturer. Primers were specific for the insert or specific for the vector backbone flanking the insert. PCR products were analyzed by agarose gel electrophoresis (3.2.3.2) and visualized by UV-light.

3.2.4. GENERATION OF PLANT MUTANTS

3.2.4.1. GENE EDITING BY CLUSTERED REGULARLY INTERSPACED SHORT PALINDROMIC REPEATS / CRISPR ASSOCIATED PROTEIN 9

The method of clustered regularly interspaced short palindromic repeats (CRISPR) / CRISPR associated protein 9 (Cas9) is based on a bacterial defense system against viruses. Viral sequence information from a previous attack are stored in the bacterial genome as so-called CRISPR. The molecular tool CRISPR/Cas9 was optimized for scientific usage: the guide RNAs (gRNAs) is designed to contain all information to direct Cas9 to its target sequence for cutting the double stranded protospacer adjacent motif (PAM).

The targets for *UGT76E1*, *UGT76E2*, *UGT76E11*, and *UGT76E12* were identified with three different online tools: (i) CRISPRdirect (<https://crispr.dbcls.jp/>) gives target candidates by comparing the given gene sequence to the selected genome (*A. thaliana*). The guanine/cytosine-content of the gRNA should be higher than 40 % and stop-sites for the RNA-Pol III should be avoided. Further, the tool gives the number of off-targets in the genome scored by the position of a mismatch to the PAM. (ii) CRISPR-P (<http://crispr.hzau.edu.cn/CRISPR2/>) scored candidate targets by the number of off-target sites in the genome (*A. thaliana*) without judging the position of the mismatch. (iii) The Genetic Perturbation Platform for designing sgRNAs for CRISPRko (<http://portals.broadinstitute.org/gpp/public/analysis-tools/sgrna-design>) tested the on-target efficiency of candidate targets. Besides misleading results for the human genome (default taxon = human), the “On-Target Efficacy Score” (which is independent of the taxon) gives the power of target sequence for the gene of interest. Values above 0.5 were treated as good candidates, values above 0.7 were judged as very good candidates (oral communication Dr. C. Thurow, Georg-August-University, Goettingen, Germany).

The best candidates from above (see Table 4-6) were used to design a constructs with four targets and replaced the dummy nucleotides in CRISPR/Cas9 construct according to the protocol from (Xing *et al.*, 2014) (supplemental material S2 and S3). Differing from the protocol, the gRNAs were first ligated into the pJET vector for DNA-amplification and sequencing. The pJET-constructs and the donor vector, pHEE401E (Addgene, Cambridge, USA) were subsequently cut with the endonuclease enzyme BsaI (Thermo Fisher Scientific, Waltham, USA) overnight at 37 °C. The fragments were purified by agarose electrophoresis (3.2.3.2) and extracted from the gel (Nucleospin Gel and PCR Clean-up, Macherey-Nagel, Dueren, Germany). The four fragments were ligated into the acceptor vector corresponding to (Equation 1). The ligations were incubated at room temperature overnight, transformed into ultra-high-competent DH5 α cells (Table 3-10), and selected on kanamycin plates. Positive colonies were re-streaked on both kanamycin and streptomycin (separately), to select for the loss of the streptomycin-resistance gene originally present in the cloning site of pHEE401E. Positive colonies were screened for the presence of a newly introduced HindIII (Target UGT76E11) restriction site, resulting in a fragment of 1580 bp. Candidates were confirmed through sequencing with vector-specific sequencing primers (Table 3-12) (Xing *et al.*, 2014) (supplemental material S2 and S3). Correct plasmids were transformed into *A. tumefaciens* for plant transformation by floral dip (Table 3-10, 3.2.4.3).

3.2.4.2. TRANSFORMATION OF AGROBACTERIUM TUMEFACIENS

Chemically competent *A. tumefaciens* were provided by Dr. Ellen Hornung (Georg-August-University, Goettingen, Germany). Competent cells were thawed, mixed with 3 μ g plasmid DNA, and incubated on ice for 30 min. The transformation of the cells was stimulated by shock freeze at -80 °C for 2 min. After the suspension has been thawed again, 900 μ l LB medium were added and the culture was incubated for 3-4 h at 28 °C for recovery. Following, all the cells were plated on LB-plates (1.5 % [w/v] agar, (Duchefa Biochemie B.V, Haarlem, Netherlands) in LB-medium (Table 3-8)) supplemented with kanamycin and rifampicin (Table 3-6). The plates were incubated at 28 °C for 2 d. Resulting clones were used for plant transformation.

3.2.4.3. AGROBACTERIUM-MEDIATED TRANSFORMATION OF A. THALIANA

An important part of the CRISPR/Cas9 gene editing in *A. thaliana* is the presence of the CRISPR/Cas9-plasmid in the plant. Therefore, *A. tumefaciens* was used to mediate the gene transfer into the plant embryo by floral dip (Clough & Bent, 1998). After transformation of the agrobacteria with the plasmid of interest (Table 3-9), several colonies were used to inoculate a pre-culture. 20 ml culture (LB medium (Table 3-8), kanamycin and rifampicin (Table 3-6)) were incubated at 28 °C and 200 rpm overnight. This pre-culture was used to inoculate 400 ml LB medium as main-culture. After growing overnight at 28 °C and 200 rpm the cells were harvested by centrifugation at 8000x g for 20 min and the resulting pellet was resolved in 300 ml 5 % [w/v]

sucrose solution. Then, 70 μ l Silwet L-77 (Momentive Performance Materials Inc., Waterford, USA) were added. Subsequently, the flowering inflorescences of *Arabidopsis* (grown for appr. 4 – 5 weeks in long-day conditions, 16 h light / 8 h dark, 22 °C) were dipped into this bacteria suspension. The plants were covered overnight. The flower dipping transformation was repeated one week later. Positive T1 transformed lines were selected by hygromycin (Table 3-6).

3.2.4.4. QUANTITATIVE REAL-TIME PCR EXPRESSION ANALYSIS

To analyze the expression status of selected genes quantitative real-time PCR (qPCR) was used. It determines the amount of gene product in a biological sample. The amounts were determined in a cDNA pool, which has been synthesized from total RNA of *A. thaliana* (3.2.2.2). The analysis monitors the amount of DNA synthesized in a PCR reaction in real-time. Here, the reactions were carried out in an iQ5 real-time PCR detection systems (Bio-Rad Laboratories GmbH, Muenich, Germany) with the appropriate filter for the emitting wavelength of the fluorescent chromophore SYBR-green (Thermo Fisher Scientific, Waltham, USA). The molecule intercalates into the DNA formed during the reaction and gives fluorescent signals, which are detected during the PCR run at the end of every cycles. The amount of template in the cDNA pool defines how many cycles will be needed for that particular PCR-product to reach the exponential phase. Likewise, higher and earlier fluorescent signals are detected in the PCR when the gene had been expressed with higher rates. The amount of transcript of different genes under certain conditions can be quantified and compared by the number of cycles which it took to synthesis a certain amount of DNA in the qPCR. The obtained qPCR data of genes of interest were compared to the expression of the reference gene actin 8 (*At1g49240*). This gene has been chosen because its expression is not altered in the response to wounding and not directly involved in genetic JA-response.

Here, the Takyon No ROX SYBR Mastermix (Kaneka Eurogentec S.A., Seraing, Belgium) was used as a 2x ready to use mix. For a reaction 10 μ L Takyon No ROX SYBR Mastermix, 2 μ L primer mix (25 mM), 5.5 mL water, and 2.5 μ L cDNA (300-500 ng/ μ L) were mixed in PCR stripes with flat caps. The reaction was performed with 40 cycles. Special qPCR-primers were designed with the online tool primer3plus (<https://primer3plus.com/cgi-bin/dev/primer3plus.cgi>). The DNA sequences of *UGT76E1*, *UGT76E2*, *UGT76E11*, *UGT76E12*, and *UGT74F1* were submitted to primer3prefold (<https://primer3plus.com/cgi-bin/dev/primer3prefold.cgi>) and regions tending to form secondary structure were identified and neglected for primer design. These results were send to primer3plus to score candidate primer pairs (server setting qPCR). The best primer pairs for every gene were tested by PCR. Positive testing means that one specific DNA product is formed exclusively and no unspecific DNA fragments are co-amplified. Positive and specific primers (Table 3-12) were used for qPCR.

3.2.5. PURIFICATION OF HETEROLOGOUS EXPRESSED PROTEINS

3.2.5.1. CELL DISRUPTION OF *E. COLI* CELLS

After heterologous protein expression (see 3.2.2.4), the bacterial cells were harvested and disrupted for the following protein purification. Therefore, a cell pellet was resuspended in the His A buffer (Table 3-16 – Table 3-20). Appr. 3 mL buffer per 1 g cells were used to get a dense suspension for effective disruption. This suspension was treated with 1 mg/mL lysozyme from chicken egg white (Merck KGaA, Darmstadt, Germany) and 0.01 mg/mL DNase I from bovine pancreas (Merck KGaA, Darmstadt, Germany) and stirred for 20 min. Following that pretreatment, small volumes (< 30 mL) were disrupted by pulsed ultrasonic treatment (Branson Sonifier Cell Disruptor B15, Branson Ultrasonics Corporation, Danbury, USA) at 40 % power and 50 % impulse level for 5 x 1 min and cooled down in between for 1 min. Larger volumes of around 120 mL were disrupted by high pressure in a Microfluidizer device (Fluidizer 110L, Microfluidic, Westwood, USA). The crude lysate was centrifuged at 50 000 xg for at least 30 min to pellet the cell debris. The resulting cleared lysate was introduced to protein purification.

3.2.5.2. RECOMBINANT PROTEIN PURIFICATION

For preparing protein purification, the protein parameters were calculated with the ProtParam online tool (<https://web.expasy.org/protparam/>). Calculated properties were: the molecular weights (MWs), the isoelectric points (pIs), and the specific extinction coefficients at 280 nm. Here, the calculations take into account the numbers of the aromatic amino acids tryptophan, tyrosine and cysteine and the MW. Furthermore, the amino acid sequences were analyzed for signal peptides by SignalP (<http://www.cbs.dtu.dk/services/SignalP/>), for target peptides by TargetP (<http://www.cbs.dtu.dk/services/TargetP/>), and for transmembrane domains with the TMHMM tool (<http://www.cbs.dtu.dk/services/TMHMM/>).

Protein purification was applied for proteins tagged with an N-terminal hexa-histidine tag (HisTag), which were heterologously expressed in *E. coli*. A two-step purification strategy of immobilized metal affinity chromatography (IMAC) and size exclusion chromatography (SEC) was used. The ÄKTAprime plus systems (GE Healthcare (Little Chalfont, UK) was used for protein purification at 4 °C. The IMAC was done with 5 mL HisTrap columns (GE Healthcare (Little Chalfont, UK) or 5 mL HisTALON columns (Takara Bio Europe, Saint-Germain-en-Laye, France). The SEC was performed with a S75 Sepharose gel filtration column (GE Healthcare, Little Chalfont, UK).

The first purification step was an IMAC. Here, the purification bases on the affinity of the imidazole groups of the histidine amino acids of the HisTag of the protein to form octahedral complexes with incomplete-chelated bivalent cations (Ni^{2+} or Co^{2+}) on the resin. Meaning that

the tagged proteins were bound to the equilibrated column while all the other proteins of the cleared lysate flowed through the column. This protein loading was done with a flowrate of 1.5 mL/min. Loading conditions were also used to wash all unspecific proteins from the matrix. In some cases, this washing was not sufficient to remove unspecific bound proteins. Especially, bacterial chaperons are often bound to the proteins of interests directly and rigidly. Those chaperones are native bacterial proteins assisting in correct protein folding during protein biosynthesis and require metabolic energy to be released again. In that cases, a second washing step was applied: a wash buffer (50 mM Tris pH 7.5, 100 mM NaCl, 2 mM dithiothreitol (DTT), 5 mM ATP, 5 mM MgCl₂, 20 mM Imidazole, Table 3-21) was used to elute strongly interacting proteins from the matrix or the tagged protein. For protein elution, the His-tagged proteins was displaced from the complex by imidazole (150 mM for HisTrap and 40 mM for HisTALON). At the end of every purification run, a washing with imidazole was performed (500 mM for HisTrap and 200 mM for HisTALON) to elute every protein from the column and to start recovery of the column. The entire purification process was recorded by UV-Vis spectroscopy at 280 nm. Samples of all purification steps were analyzed by denaturing sodium dodecyl sulfate (SDS)-polyacrylamide gel electrophoresis (PAGE).

For a second purification step a SEC was used. SEC separates proteins by their specific radius of gyration, which is the mean of all the distances from the surface of the protein to the center of gravity. Generally, radius of gyration corresponds to the size of the protein. It ensure that co-purified proteins from the IMAC purification are separated in a second purification step by a different chromatographic principle (SEC). Technically, the sepharose matrix of the gel filtration has a defined pore size in which molecules might or might not diffuse corresponding to their radius of gyration - their size. Consequently, smaller molecules diffuse in pores and have more interaction. Physically, longer distance at a constant speed equals more time. Hence, bulky molecules elute earlier from the gel filtration than smaller ones. Like this, the elution volume of a specific protein from the gel filtration column can be calculated by calibrating the column (Equation 2). Here, the real protein sizes of the expressed amino-acid chain with HisTag were used for calculations. The HiLoad 16/600 Superdex 75 prep grade (GE Healthcare, Little Chalfont, UK) is capable to separate proteins up to 70 kDa. Again, protein elution was monitored

Equation 2

$$\text{Volume}_{S75}(\text{protein}) = \frac{\log_{10}(\text{MW}(\text{protein})) - 6.9219}{(-0.0352)}$$

Volume_{S75}(protein): Elution volume of the protein of interest on the HiLoad 16/600 Superdex 75 prep grade (GE Healthcare, Little Chalfont, UK)

MW(protein): Molecular weight of the protein of interest

by UV-Vis spectroscopy at 280 nm and SDS-PAGE. For further use and tests, the homogeneous proteins were concentrated to > 1 mg/mL with concentrators (Spin-X UF6, 30 kDa cut-off, Corning B.V. Life Science, Amsterdam, Netherlands), flash-frozen in liquid N₂ and stored at -80 °C.

Table 3-16: Buffer systems for protein purification of UGT76E1

Specific buffer systems were used to purify heterologous expressed proteins. His A buffer was used for equilibrating the HisTALON Superflow Cartridge (Takara Bio Europe, Saint-Germain-en-Laye, France), loading the cleared lysate, and washing. His B was the elution buffer to displace proteins from the affinity columns. Following, proteins were purified with size exclusion chromatography. The gel filtration buffer was a low-salt buffer without special additives.

His A		
50	mM	Tris/HCl pH 9.0
100	mM	NaCl
0.1	%	Tween 20
His B		
50	mM	Tris/HCl pH 9.0
100	mM	NaCl
0.1	%	Tween 20
200	mM	Imidazole
Gel filtration		
50	mM	Tris/HCl pH 9.0
100	mM	NaCl

Table 3-17: Buffer systems for protein purification of UGT76E2

Specific buffer systems were used to purify heterologous expressed proteins. His A was used for equilibrating the HisTrap HP (GE Healthcare, Little Chalfont, UK), loading the cleared lysate, and washing. His B was the elution buffer to displace proteins from the affinity columns. Following, proteins were purified with size exclusion chromatography. The gel filtration buffer was a low-salt buffer without special additives.

UGT76E2		His A
50	mM	Tris/HCl pH 8.0
100	mM	NaCl
0.1	%	Tween 20
UGT76E2		His B
50	mM	Tris/HCl pH 8.0
100	mM	NaCl
0.1	%	Tween 20
500	mM	Imidazole
UGT76E2		Gel filtration
50	mM	Tris/HCl pH 8.0
100	mM	NaCl

Table 3-18: Buffer systems for protein purification of UGT76E11

Specific buffer systems were used to purify heterologous expressed proteins. His A was used for equilibrating the affinity columns, loading the cleared lysate, and washing. His B was the elution buffer to displace proteins from the affinity columns. Following, proteins were purified with size exclusion chromatography. The gel filtration buffer was a low-salt buffer without special additives.

His A		
20	mM	Tris/HCl pH 7.5
50	mM	NaCl
10	%	Glycerol
0.1	%	Tween 20
His B		
20	mM	Tris/HCl pH 7.5
50	mM	NaCl
10	%	Glycerol
0.1	%	Tween 20
500	mM	Imidazole
Gel filtration		
20	mM	Tris/HCl pH 7.5
50	mM	NaCl

Table 3-19: Buffer systems for protein purification of UGT76E12

Specific buffer systems were used to purify heterologous expressed proteins. His A was used for equilibrating the affinity columns, loading the cleared lysate, and washing. His B was the elution buffer to displace proteins from the affinity columns. Following, proteins were purified with size exclusion chromatography. The gel filtration buffer was a low-salt buffer without special additives.

His A		
50	mM	Tris/HCl pH 8.0
100	mM	NaCl
10	%	Glycerol
His B		
50	mM	Tris/HCl pH 8.0
100	mM	NaCl
10	%	Glycerol
500	mM	Imidazole
Gel filtration		
50	mM	Tris/HCl pH 8.0
100	mM	NaCl

Table 3-20: Buffer systems for protein purification of UGT74F1

Specific buffer systems were used to purify heterologous expressed proteins. His A was used for equilibrating the affinity columns, loading the cleared lysate, and washing. His B was the elution buffer to displace proteins from the affinity columns. Following, proteins were purified with size exclusion chromatography. The gel filtration buffer was a low-salt buffer without special additives.

His A		
50	mM	Tris/HCl pH 8.0
100	mM	NaCl
0.1	%	Tween 20
His B		
50	mM	Tris/HCl pH 8.0
100	mM	NaCl
0.1	%	Tween 20
500	mM	Imidazole
Gel filtration		
50	mM	Tris/HCl pH 8.0
100	mM	NaCl

Table 3-21: Wash buffer for protein purification

To remove unspecific proteins from the affinity purification column, a special wash buffer was used. It was applied between loading of proteins and specific elution of the proteins of interests. Dithiothreitol, DTT; adenine triphosphate, ATP.

His wash buffer		
50	mM	Tris/HCl pH 7.5
100	mM	NaCl
2	mM	DTT
5	mM	ATP
5	mM	MgCl ₂
20	mM	Imidazole

3.2.5.3. PROTEIN SEPARATION BY SDS-PAGE

SDS-PAGE (Davis, 1964; Kellenberger, 1968; Laemmli, 1970; Ornstein, 1964) was used to record the protein purification process. The samples were sonified and boiled before the proteins were separated by SDS-PAGE. For SDS-PAGE, samples of 20 µL were mixed with 20 µL of 2x Laemmli sample buffer (Table 3-22). Thereof, 5-10 µL were loaded on a 10 % acryl amide gel (Table 3-23). For molecular weight determination 5 µL Unstained Molecular Weight Marker (MBI Fermentas, St. Leon Roth, Germany) were loaded on a separate lane of the gel. The separation itself was performed in a Mini-Protean3 electrophoresis system (Bio-Rad Laboratories GmbH, Munich, Germany) at 30 mA per gel until the running front was just run out of the gel. The proteins in the gel were visualized with Coomassie Brilliant Blue staining solution, which is prepared of 1 mL of Coomassie staining stock solution in appr. 50 mL of fixation solution (Table 3-25). The gel was boiled in the staining solution and incubating for 10 min for protein staining. For de-staining the gel was several times boiled in water and incubated with a dye-absorbing tissue for 10 min.

For SDS-PAGE of whole bacterial cells, aliquots of the expression culture (Equation 3) were centrifuged at 10 000x g for 4 min. The pellet was dissolved in 50 µL water and 50 µL 2x Laemmli sample buffer. The samples were sonified and boiled before the proteins were separated by SDS-PAGE as before.

Equation 3

$$\frac{0.5 \text{ mL}}{\text{OD}_{600}} = \text{Volume (aliquot)}$$

OD₆₀₀: Optical density of the bacterial culture at 600 nm

Volume (aliquot): Volume of the aliquot in mL

Table 3-22: Composition of 2x Laemmli sample buffer

Dithiothreitol (DTT), sodium dodecyl sulfate (SDS). Volume per volume, v/v; weight per volume, w/v.

100 mM	Tris/HCl pH 6.8
200 mM	DTT
4 % [w/v]	SDS
0.002 % [w/v]	Bromphenole blue
40 % [v/v]	Glycerol

Table 3-23: Composition of 10 % SDS-PAGE gel

Tetramethylethylenediamine (TEMED). The volume of the recipe is sufficient for 4x 0.75 mm gels (Bio-Rad Laboratories GmbH, Munich, Germany).

	4 % Stacking gel (mL)	10 % Separation gel (mL)
Separation gel buffer	-	4.25
Stacking gel buffer	1.90	-
Water	4.50	6.92
(Bis) acrylamide (30 % [w/v])	1.00	5.67
Ammonium persulfate	$70 \cdot 10^{-3}$	$153 \cdot 10^{-3}$
TEMED	$7.5 \cdot 10^{-3}$	$17 \cdot 10^{-3}$

Table 3-24: Composition of stock buffers for SDS-PAGE

Stacking gel buffer	
0.5 M	Tris/HCl pH 6.8
0.1 % [w/v]	SDS
Separation gel buffer	
1.5 M	Tris/HCl pH 8.8
0.1 % [w/v]	SDS

Table 3-25: Coomassie staining solution

Volume per volume, v/v; weight per volume, w/v.

Coomassie staining stock solution	
0.25 % [w/v]	Brilliant blue G-250
0.25 % [w/v]	Brilliant blue R-250
In 100 % [v/v]	Ethanol
Fixation solution	
5 % [v/v]	Acetic acid
10 % [v/v]	Ethanol
85 % [v/v]	H ₂ O

3.2.5.4. PROTEIN DETECTION BY WESTERN BLOT

His-tagged proteins were detected in whole bacterial cell after protein expression. After SDS-PAGE of the samples, the stacking gel was removed and the proteins in separation gel were transferred onto a nitrocellulose membrane (Roti-NC, pore size 2 μ m, Carl Roth & Co., Karlsruhe, Germany). Therefore, a Mini-Protean3 electrophoresis system was used with a Mini Trans-Blot Cell (both Bio-Rad Laboratories GmbH, Munich, Germany). The transfer was carried out in wet conditions in transfer buffer (25 mM Tris, 192 mM glycine, 20 % methanol [v/v]) at 240 mA and 80 V for 2 h. The transfer cassette was dismantled and membrane was checked for successful

protein blotting by staining with Ponceau S (0.1 % [w/v] in water : acetic acid, [99 : 1, v/v] for 5 min. The staining was removed with water before the membrane was incubated in 0.05 % [v/v] Tween 20, 10 mM Tris/HCl, pH 7.9, 150 mM NaCl (Tween-Tris buffered saline, T-TBS) containing 3 % milk powder (blotting grade, Carl Roth & Co., Karlsruhe, Germany). The blocking was performed at room temperature for 1 h. Following, the membrane was incubated within a solution of the primary antibody (0.1 µg/mL in T-TBS, 3 % milk powder, Tetra-His Antibody, Quiagen, Hilden, Germany) at 10 rpm and 4 °C overnight. Next, the primary antibody solution was removed and membrane was washed four times with T-TBS, 3 % milk powder at room temperature on a rotary shaker for 10 min. Primary antibody-antigen conjugates were detected using an alkaline phosphatase-conjugated secondary antibody (goat anti mouse IgG, Merck KGaA, Darmstadt, Germany) diluted 1 : 30 000 in T-TBS, 3 % milk powder. The membrane was incubated with this secondary antibody solution at room temperature on a rotary shaker for 1 h. The antibody solution was removed and membrane were washed with T-TBS for 10 min (two times) and for 5 min (two times) with Tris buffered saline (TBS). For activity staining mediated by the alkaline phosphatase (AP), the membrane was equilibrated in AP buffer (100 mM Tris/HCl pH 9.5, 100 mM NaCl, 5 mM MgCl₂) and incubated with staining solution (15 mL AP buffer, 49.5 µL Nitro-blue-tetrazolium-chloride (50 mg/mL in 70 % dimethylformamide), 99 µL 5-bromo-4-chloro-3'-indolylphosphate p-toluidine salt (50 mg/mL in dimethylformamide) in the dark for 30-300 min. The staining reaction was stopped by transferring into water.

3.2.6. ENZYME CHARACTERIZATION

3.2.6.1. PROTEIN ACTIVITY ASSAY

A fast and simple protein activity assay was performed to monitor the activity of an enzyme during protein purification, to check enzymatic activity towards new potential substrates, and to test the activity of so far not characterized UGT-enzymes. Therefore, reactions were set up in 100 µL assay volume containing 10 µg enzyme, 0.1 mM substrate and 0.5 mM UDP-Glc. The assay were incubated at room temperature for 1 h and stopped by adding 100 µL ACN. The solvent precipitates. The samples were centrifuged at 20 000x g at room temperature for 5 min and 50 µL of the supernatant were transferred into glass vials. The substrates and products of the reaction were analyzed by LC coupled to mass spectrometer (LC-MS), 3.2.8.4).

3.2.6.2. DETERMINATION OF OPTIMAL TEMPERATURE AND pH VALUES

The enzymatic characterization of UGT76E1, UGT76E2, UGT76E11, and UGT76E12 required the determination of optimal parameters for the reaction, like pH and temperature optima.

The enzymatic product formation was evaluated at different pH conditions. The reactions were performed in 200 µL solutions containing 0.1 mM ω-hydroxy-hexadecanoic acid (ω-OH-16:0,

dissolved in ACN), 0.5 mM UDP-Glc, and 30 µg pure enzyme. To test a broad pH range from 2 to 12 with the high buffering capacity, the Britton-Robinson buffer (BRB) system (Britton & Robinson, 1931) was used. Tested were 13 pH conditions: pH 3.0, 4.0, 5.0, 6.0, 7.0, 7.5, 8.0, 8.5, 9.0, 9.5, 10.0, 11.0. All reactions were started by adding the enzyme and incubated at 25 °C for 1 h. The reactions were stopped by adding 50 µL ACN. After centrifugation at 20 000x g at room temperature for 5 min, 50 µL of the supernatant were used for detecting relative amounts of ω-*O*-glucosyl-hexadecanoic acid (ω-*O*-Glc-16:0) by LC-MS.

The optimal reaction temperature of the UGTs was investigated similarly just at fixed pH and different temperatures: 4 °C, 10 °C, 15 °C, 20 °C, 25 °C, 30 °C, 35 °C, 42 °C, 50 °C. 0.1 mM ω-OH-16:0, 5 mM UDP-Glc were mixed in 50 mM Tris-HCl, 100 mM NaCl buffer at pH 8.5 in a volume of 200 µL. These reactions were pre-incubated at the indicated reactions temperature for 10 min. Reactions at temperature lower than room temperature were incubated in water baths and reactions at temperatures above room temperature were incubated in heating blocks. 30 µg enzyme was added and the reactions were carried out for 1 h before the reactions were terminated by the addition of 50 µL ACN. The reaction products were analyzed as before.

3.2.6.3. ANALYSIS OF THE SUBSTRATE SPECIFICITY OF UGTs BY USING UDP-¹⁴C(U)-GLC

The substrate specificity of the UGTs was tested against different substrates with free hydroxy and/or carboxy groups. To describe the product formation in a half quantitative way radioactive product determination was used to contrast a set of different aglycones for their performance as substrate of one enzyme. Hereby, the Glc moiety is uniformly ¹⁴C labelled (¹⁴C(U)-Glc) one, which is transferred onto the aglycone upon catalysis. Like this, every turnover produces the same signal intensity and the signal intensities of all products can be compared.

Different aglycones (Table 3-26) were tested as substrates for UGT76E1, UGT76E2, UGT76E11, UGT76E12, and UGT74F1. The enzymatic reactions were carried out in a total volume of 20 µL with 60 µM substrate, 3.3 µM labeled UDP-¹⁴C(U)-Glc (0.02 µCi), 28 µM UDP-Glc, and 5 µg enzyme. The reaction assays and one negative control with inactivated enzyme were started by adding the enzyme and incubating at 25 °C for 1 h. 30 µL of n-butanol were added to stop the reactions and to extract the metabolites (modified from Huang *et al.*, 2015; Suzuki *et al.*, 2007). This solution was mixed thoroughly and centrifuged at 13 200x g for 5 min. The organic phase was taken and transferred into a new reaction tube. The residue was extracted again, mixed, and centrifuged as before. Both extractions were pooled and evaporated under stream of nitrogen. The residue was resolved in 20 µL 70 % [v/v] ethanol and spotted on thin-layer chromatography (TLC) plates (Silica gel 60 plate, Merck KGaA, Darmstadt, Germany). The TLC-plates were placed in an equilibrated TLC-chamber and run in dichlormethane : methanol : water [80 : 20 : 2,

v/v/v] (modified from Augustin *et al.*, 2012). Then, the plates were air-dried and covered with cling film and placed on phosphor screens in storage cassettes (Fujifilm Corporation Tokyo, Japan). After 3 d of incubation, the screens were scanned with a FLA-3000 fluorescent image analyzer (Fujifilm Corporation Tokyo, Japan). Data analysis was done with the “Bildanalyseprogramm1.0.4.6” (Datinf GmbH, Tuebingen, Germany) at a picture contrast of 4 220 – 41 200 pixel. Signal intensities were determined as within a signal detection boxes. Background signals were subtracted by a neighboring box. Product signals were calculated as product signal minus background over area.

Table 3-26: Substances, which were tested as substrates for the UGTs.

Substrates	
1	Hexadecanoic acid (16:0)
2	ω -Hydroxy-hexadecanoic acid (ω -OH-16:0)
3	2-Hydroxy-hexadecanoic acid (2-OH-16:0)
4	3-Hydroxy-hexadecanoic acid (3-OH-16:0)
5	Hexadecanol (OH-C16)
6	Benzoic acid (BA)
7	Salicylic acid (SA)
8	Pipelic acid (Pip)
9	Indole-carboxylic acid (ICA)
10	Abscisic acid (ABA)
11	Zeatin
12	Gibberellic acid (GA)
13	<i>cis</i> -(+)-12-Oxo-phytodienoic acid (12-OPDA)
14	Jasmonic acid (JA)
15	12-Hydroxy-JA (12-OH-JA)
16	11-Hydroxy-JA (11-OH-JA)
17	12-Hydroxy-JA-methyl ester (12-OH-JA-ME)
18	Quercetin
19	Dihydro-myricetin(dh-myricetin)
20	Dihydro-kaempferol(dh-kaempferol)
21	Control with inactivated enzyme

3.2.6.4. DETERMINATION OF THE KINETIC PARAMETERS

To record steady-state kinetics, a coupled spectrophotometric assay has been modified from (Brown *et al.*, 2012). UGTs catalyze the transfer of a Glc-moiety from the donor UDP-Glc to the hydroxyl-aglycone releasing the respective glycone and UDP. Via the co-product UDP, the UGT-reaction is coupled to the pyruvate kinase (PK) and lactate dehydrogenase (LDH) to record the UGT reaction kinetics in 1 : 1 : 1 stoichiometry: The PK phosphorylates UDP to UTP while metabolizing phosphoenolpyruvate (PEP) to pyruvate. LDH catalyzes the reduction of pyruvate to lactate by oxidizing nicotinamide adenine dinucleotide (NADH) to NAD⁺, which shows in contrast to NADH no absorption maximum at 340 nm. All measurements were performed in biological triplicates in Quartz SUPERSIL cuvettes (Hellma Analytics, Muellheim, Germany) in a V-630 UV/Vis Spectrophotometer (JASCO Corporation, Hachioji, Japan). The detailed reaction mixture is given in Table 3-27. UGT76E1 had be stabilized with bovine serum albumin (BSA, 0.13 % [w/v]). For the assay, the NADH stock-solution was prepared freshly in the gel filtration buffer of the respective enzyme (Table 3-16 – Table 3-20). The exact concentration of NADH was determined in 1/100 dilutions in the photometer with the Lambert Beer law (Equation 4). Therewith, a 2x master mix was prepared to reduce pipetting errors between the different measurements. The setup was blanked with an empty cuvette. The master mix was added to the

substrate and the buffer in the cuvette. This solution was checked to have an absorption at 340 nm of appr. 0.9 - the calculated value for the working concentration of 0.15 mM NADH in the cuvette is 0.96 (Equation 4). To start the reactions, the enzyme was added and mixed carefully by pipetting. The reaction was recorded at 340 nm for 300 - 600 s depending on the velocity of the reaction. The linear slope of the reaction was determined with the Spectra Manager II Software (JASCO Corporation, Hachioji, Japan). A high concentration of UDP was used to ensure that the rate limiting reaction is the UGT reaction. For evaluation, the reaction velocities were plotted against the given substrate concentration by the SIMGA-Plot software. Finally, the velocities were calculated to k_{cat} values by a modified Lambert-Beer equation (Equation 5)

Equation 4

$$c(\text{analyte}) = \frac{\text{Absorption}}{\varepsilon(\text{analyte}) \cdot l}$$

$c(\text{analyte})$: Concentration of the analyte of interest

$\varepsilon(\text{analyte})$: Specific extinction coefficient of the analyte

l : Path length, for cuvettes normally = 1 cm

Equation 5

$$k_{cat} = \frac{V_{max}}{[E]} = \frac{\Delta \text{Absorption}}{\varepsilon(\text{NADH}) \cdot l \cdot [E] \cdot t} = [s^{-1}]$$

k_{cat} : Maximal turnover number

V_{max} : Maximal reaction velocity; change of absorption per min

$[E]$: Concentration of enzyme

$\varepsilon(\text{NADH})$: Specific extinction coefficient of NADH, 6 220 M⁻¹cm⁻¹

l : Path length (for the used cuvettes) = 1 cm

t : Reaction time

Table 3-27: Reaction mixture of the coupled spectrophotometric assay.

Phosphoenolpyruvate, PEP; pyruvate kinase, PK; lactate dehydrogenase, LDH; uridine diphosphate glucose, UDP-Glc; nicotinamide adenine dinucleotide, NADH; UDP-dependent glycosyltransferase, UGT. Bovine serum albumin, BSA. Components marked with asterisks were mixed in a 2x master mix.

Volume	Component		Final concentration
1 μL	KCl (1 M in water)	*	5 mM
15 μL	MgCl ₂ (1 M in water)	*	75 mM
1 μL	PEP (100 mM in water)	*	0.8 mM
4 μL	PK (2.5 mg/mL in buffer)	*	50 μg/mL
4 μL	LDH (2.5 mg/mL in buffer)	*	50 μg/mL
1 μL	UDP-Glc (1 M in buffer)	*	5 mM
1.2 μL	NADH (25 mM in buffer)	*	150 μM
5 - 30 μg	UGT		50 - 150 μg/mL
2 - 90 μL	Substrate (1 mM in buffer)		10-450 μM
0.26 mg	BSA (only for UGT76E1)	*	0.13 % [w/v]
X μL	Gel filtration buffer		
200 μL	Final volume		

3.2.7. SUBSTRATE SYNTHESIS

3.2.7.1. ENZYMATIC SYNTHESSES OF 9- AND 13-HYDROXY-OCTADECATRIENOIC ACIDS

(10E,12Z,15Z)-9-Hydroxy-10,12,15-octadecatrienoic acid (9-HOT) and (9Z,11E,15Z)-13-hydroxy-9,11,15-octadecatrienoic acid (13-HOT) were used as substrates for the UGT reactions. Both compounds were synthesized enzymatically and purified to homogeneity afterwards by Sabine Freitag (University of Goettingen, Germany).

In case of 9-HOT, the LOX from *Solanum tuberosum* was expressed from pET3b in BL21 Star (DE3) like described in Andreou *et al.*, 2009. The bacterial cell pellet of 10 mL culture was used for the synthesis of 9-HOT. The pellet was resuspended in 1 mL lysis buffer (50 mM Tris/HCl pH 7.5, 300 mM NaCl, 10 % glycerol) supplemented with 1 μ L Tween 20. The suspension was lysed by sonication as described above (see 3.2.5.1). The cell debris was sedimented by centrifugation at 3 220x g and 4 °C for 4 min. 4 mL of the crude lysate were mixed with 6 mL reaction buffer (100 mM Tris/HCl, pH 7.5) and 60 μ L linolenic acid (250 mg/mL). The reaction was incubated stirring on ice for 30 min. Noticeable, every 5 min, fresh air was bubbled into the solution with a Pasteur pipette. The reaction was determined by adding 10 mL SnCl₂ solution (0.375 % [w/v] in methanol) and incubating at room temperature for 10 min. Likewise, the hydroperoxide products were reduced to the respective hydroxides. 9-HOT was extracted similar to Bligh & Dyer, 1959: 100 μ L concentrated acetic acid and 10 mL chloroform were added to the reduced reaction solution of the LOX from *Solanum tuberosum*. The solution was vigorously mixed and centrifuged at 3 220x g for 10 min. The lower phase was transferred to a new reaction tube and the remaining solution was extracted with chloroform again. The second lower phase was combined with the first phase and the whole volume was evaporated under a stream of nitrogen. The residue was dissolved in 500 μ L ethanol.

In case of 13-HOT, the LOX from *G. max* (GmLOX, Merck KGaA, Darmstadt, Germany) was used to produce the compound. 100 μ L of GmLOX (0.250 mg/mL) were mixed with 2 mL borate buffer (200 mM borate, pH 9) and 60 μ L linolenic acid (250 mg/mL) and incubated in an open vessel at room temperature for 30 min. Here, the reaction is stopped by adding appr. 0.1 g sodiumborohydride for reduction and proteins were precipitated by adding 100 μ L concentrated acetic acid.

3.2.7.2. PURIFICATION OF 9- AND 13-HOT

After synthesis and extraction, the compounds 9- and 13-HOT were purified by HPLC by S. Freitag (University of Goettingen, Germany). Both were purified by straight-phase HPLC SP HPLC: isocratic conditions with 0.8 mL/min in hexane : isopropanole : trifluoroacetic acid

[100 : 1 : 0.02, v/v/v] on a ZORBAX RX-SIL (4.6 x 50 mm, 1.8 μm particle size, Agilent, Waldbronn, Germany). The elution of 9-HOT and 13-HOT was monitored by 234 nm and their identity confirmed by coelution with the authentic standards. The concentration of 9-HOT and 13-HOT were determined with the NanoDrop 2000 spectrophotometer (Thermo Fisher Scientific, Waltham, USA) at 234 nm. The shared molar extinction coefficient of 23 000 $\text{M}^{-1}\text{cm}^{-1}$ was used to calculate the concentration of 9-HOT and 13-HOT by the Lambert-Beer law (Equation 4).

3.2.8. METABOLITE ANALYSES

3.2.8.1. HOMOGENIZING PLANT MATERIAL

Plant material was homogenized before analyses. Therefore, two techniques were used: (i) for extracting DNA or RNA, one leaf was collected in a reaction tube and flash-frozen in liquid N_2 . The frozen tissue was grinded with a small pistil in the tube. (ii) Samples from a wounding experiment were homogenized using a Mixer Ball Mill MM200 (Retsch GmbH, Haan, Germany) at 30 s^{-1} for 120 s. The device and the samples were constantly cooled with liquid N_2 .

3.2.8.2. EXTRACTION OF PLANT MATERIAL

The quantification of the plant hormones and, in particular jasmonates was essential to investigate their function *in vivo*. Here, a two phased methyl *tert*-butyl ether (MTBE) extraction was modified from Matyash *et al.*, 2008. Briefly, appr. 100 mg of the frozen tissue powder were weighted into 750 μL methanol (LC-MS grade, MeOH). 2.5 mL MTBE and 80 μL of an internal standard mixture (Table 3-28) were added and the solution was shaken in the dark at 4°C and 200 rpm for 1 h. 600 μL water were added for phase separation and mixed roughly before centrifugation at 450x g for 10 min at 22°C. Then, the upper phase was taken and transferred to another glass tube.

Table 3-28: Internal standards for quantitative LC-MS/MS analysis

For quantification, internal standards were added to the extraction solutions. Five-fold deuterated 12-oxophytodienoic acid, D₅-12-OPDA; five-fold deuterated jasmonic acid; D₅-JA; four-fold deuterated jasmonoyl-leucine, D₄-JA-Leu; four-fold deuterated salicylic acid, D₄-SA; five-fold deuterated indole-3-acetic acid, D₅-IAA; six-fold deuterated abscisic acid, D₆-ABA; 2-oxothiazolidine-4-carboxylic acid (St-RA).

Substance	(concentration)	Volume
D ₅ -12-OPDA	(3 ng/ μL)	10 μL
D ₅ -JA	(1 ng/ μL)	10 μL
D ₃ -JA-Leu	(1 ng/ μL)	20 μL
D ₆ -SA	(1 ng/ μL)	10 μL
D ₅ -IAA	(1 ng/ μL)	10 μL
D ₆ -ABA	(1 ng/ μL)	10 μL
St-RA	(5 ng/ μL)	10 μL

700 μL MeOH: water [3 : 2.5, v/v] and 1.3 mL MTBE were mixed to the remaining phase for re-extraction. After centrifugation as before, the upper and the lower phase were taken and pooled with the first upper phase. This solution was evaporated under a stream of nitrogen. The residue was dissolved in 100 μL MeOH twice and transferred to a reaction tube. For LC-MS measurements, the extracts were evaporated again and resolved in 20 μL solvent B (ACN : water, [90 : 10, v/v], 0.3 mM NH_4COOH , pH 3.5) first. Then, 80 μL solvent A (0.3 mM NH_4COOH in water, pH 3.5) were added to fit to the starting conditions of the chromatographic separation by LC.

3.2.8.3. TARGETED LC-MS/MS ANALYSIS OF PHYTOHORMONES

The LC-MS/MS measurement of the phytohormones were performed by Dr. Cornelia Herrfurth and Dr. Krzysztof Zienkiewicz (both University of Goettingen, Germany). The extracts were analyzed by ultra-performance-LC (UPLC) nano-electrospray ionization (ESI) MS-fragmentation (MS/MS) method according to Ghareeb *et al.*, 2011. An Acquity UPLC system equipped with ACQUITY UPLC HSS T3 column (100 mm x 1 mm, 1.8 μm particle size; both from Waters Corp., Milford, MA, USA) was coupled to a nanoESI chip ion source (TriVersa NanoMate; Advion BioSciences, Ithaca, USA). The MS analysis was performed with an Applied Biosystems 4000 quadrupole/linear ion trap mass spectrometer (MDS Sciex, Ontario, Canada). For analysis, 10 μL of the extract were injected (see 3.2.8.2). The binary gradient system consisted of solvent A, water and solvent B, ACN : water, 90 : 10 [v/v], both containing 0.3 mM NH_4COOH (adjusted to pH 3.5 with formic acid) was used. Elution was performed with the following gradient program: 10 % solvent B for 0.5 min, followed by a linear increase of solvent B up to 40 % within 1.5 min held for 2 min and followed by increase of solvent B up to 95 % solvent B in 1 min. An isocratic run at 95 % solvent B was then held for 2.5 min. To recover starting conditions a linear decrease to 10 % B within 3 min was performed. The flow rate was 0.16 mL/min. For stable nanoESI conditions, 70 $\mu\text{L}/\text{min}$ of 2-propanol/ACN/water [70 : 20 : 10, v/v/v] containing 0.3 mM NH_4HCOO (adjusted to pH 3.5 with formic acid) delivered by a Pharmacia 2248 HPLC pump (GE Healthcare, Munich, Germany) were added just after the column via a mixing tee valve. By using a second post column splitter 502 nl/min of the eluent were directed to the nanoESI chip with 5 μm internal diameter nozzles. Ionization voltage was set to -1.7 kV, phytohormones were negatively ionized and detected in a scheduled multiple reaction monitoring (MRM) mode with AB Sciex 4000 QTRAP tandem mass spectrometer (AB Sciex, Framingham, MA, USA). For the scheduled mode, the MRM detection window was 72 s and a target scan time of 1.2 s was set. Mass transitions were optimized for every compound individually (Table 3-29). The mass analyzers were adjusted to a resolution of 0.7 amu full width at half height. The ion source temperature was 40 $^\circ\text{C}$ and the curtain gas was set at 10 – given in arbitrary units. Quantification was carried out using a calibration curve of intensity relations of the mass-to-

charge ratio (m/z) of standard substances vs. molar amounts of unlabeled metabolites (0.3 – 1 000 pmol, [unlabeled]/[deuterium-labeled]).

Table 3-29: Transitions of the multiple reaction monitoring mode of the LC-MS/MS analysis

Metabolite in the LC-MS/MS analysis were identified in the multiple reaction monitoring mode by selecting their mother ion and an fragment for quantification. Every fragmentation scan has its individual clustering potential (DP), entrance potential (EP), and collision energy (CE). 12-Oxophytodienoic acid, 12-OPDA; jasmonic acid, JA; 11/12-hydroxy-JA, 11/12-OH-JA; 12-hydroxy-jasmonoyl sulfate, 12-HSO₄-JA; 12-glycosyl-*O*-JA, 12-*O*-Glc-JA; jasmonoyl-isoleucine/leucine, JA-Ile/Leu; 12-hydroxy-JA-Ile, 12-OH-JA-Ile; 12-carboxy-JA-Ile, 12-COOH-JA-Ile, abscisic acid, ABA; ABA-glycosyl ester, ABA-GE; salicylic acid, SA; 2-*O*-glycosyl-SA, 2-*O*-Glc-SA; indole-3-carboxylic acid, ICA; indole-3-acetic acid, IAA; five-fold deuterated 12-oxophytodienoic acid, D₅-12-OPDA; five-fold deuterated jasmonic acid; D₅-JA; four-fold deuterated jasmonoyl-leucine, D₄-JA-Leu; four-fold deuterated salicylic acid, D₄-SA; five-fold deuterated indole-3-acetic acid, D₅-IAA; six-fold deuterated abscisic acid, D₆-ABA.

Q1	Q3	Analyte	DP (V)	EP (V)	CE (eV)
291	165	12-OPDA	-70	-8.5	-28
209	59	JA	-30	-4.5	-24
225	59	11/12-OH-JA	-35	-9.0	-28
305	97	12-HSO ₄ -JA	-30	-4.0	-32
387	59	Glc- <i>O</i> -JA	-85	-9.0	-52
322	130	JA-Ile/Leu	-45	-5.0	-28
352	130	12-COOH-JA-Ile	-45	-10.0	-30
338	130	12-OH-JA-Ile	-45	-10.0	-30
263	153	ABA	-35	-4.0	-14
425	263	ABA-GE	-30	-10.0	-16
137	93	SA	-25	-6.0	-20
299	137	2- <i>O</i> -Glc-SA	-30	-4.0	-18
160	113	ICA	-40	-6.5	-22
174	130	IAA	-35	-9.0	-14
396	107	D ₅ -12-OPDA	-65	-4.0	-28
214	62	D ₆ -JA	-35	-8.5	-24
325	133	D ₄ -JA-Leu	-80	-4.0	-30
141	97	D ₄ -SA	-25	-6.0	-22
153	109	D ₅ -IAA	-50	-4.0	-22
293	179	D ₆ -ABA	-80	-10.0	-42

3.2.8.4. METABOLITE ANALYSIS BY LC-HIGH RESOLUTION-MS

The metabolite fingerprinting experiments were performed by LC-high resolution-MS (LC-HR-MS) together with Dr. Kirstin Feussner (University of Goettingen, Germany) according to Nahlik *et al.*, 2010. The samples were separated by an Acquity UPLC system with UPLC eLambda 800 nm PDA detector and equipped with an Acquity UPLC BEH SHIELD RP18 column (1x100 mM, 1.7 μ m particle size, Waters Corporation, Milford, USA). A flow rate of 0.2 ml min⁻¹ at 40 °C was applied. Separation was gained with a binary gradient of solvent A (water : formic acid [100 : 0.1, v/v]) and solvent B (ACN : formic acid [100 : 0.1, v/v]). The run was set with 0 – 0.5 min at 10 % solvent B, 0.5 – 3 min gradual to 28 % solvent B, 3 – 8 min gradual to 95 % solvent B, 8 – 10 min at 95 % solvent B, and 10 – 14 min 10 % solvent. The LC-HR-MS was operated in negative ESI mode with W optics to ensure a mass resolution larger than 10 000. Data were acquired by MassLynx 4.1 software in centroid format over a mass range of m/z 85 – 1 200

with a scan duration of 0.5 s and an interscan delay of 0.1 s. The capillary and the cone voltage were maintained at 2 600 V and 30 V and the desolvation and source temperature at 350 °C and 80 °C respectively. Nitrogen was used as cone (30 L h⁻¹) and desolvation gas (800 L h⁻¹). The Dynamic Range Enhancement mode was used for data recording. All analyses were monitored by using Leucine-enkephaline ([M-H]⁻ 554.2615 or [M+H]⁺ 556.2771 as well as its ¹³C isotopomer [M-H]⁻ 555.2615 or its double ¹³C isotopomer [M+H]⁺ 558.2836 as lock spray reference compound at a concentration of 0.5 µg mL⁻¹ in ACN : water [50 : 50, v/v] and a flow rate of 30 µL min⁻¹. For targeted data analysis, the MassLynx 4.1 software was used to investigate metabolites.

3.2.8.5. NON-TARGETED *EX VIVO* METABOLITE FINGERPRINTING

The non-targeted *ex vivo* experiments were performed together with Dr. Kirstin Feussner (Georg-August-University, Goettingen, Germany). It uses the metabolite fingerprinting platform (Kaefer *et al.*, 2014) and connects it to activity assays with purified enzymes. The purified enzyme were incubated with an enriched metabolite extracts from both phases of the MTBE-extraction (see 3.2.8.2). Here, the plant material of a wounding experiment (see 3.2.1.3) was used to provide the enzyme with the enriched metabolite extract including wound-accumulated metabolites like 12-OH-JA. The reactions were measured by the non-targeted fingerprinting pipeline (Kaefer *et al.*, 2014). The activity assays were performed as following: 100 µg homogeneous protein were incubated with 83 µL enriched plant extract (of 100 µL from 120 mg plant material), and 10 µM UDP-Glc. As positive control, known substrates were spiked into a selected number of reactions: 10 µM 12-OH-JA, 10 µM SA, and 10 µM ω-OH-16:0. The reactions were incubated at 25 °C for 1 h and terminated by adding 20 µL ACN. For measurement, the solutions were centrifuged at 20 000x g at 4 °C for 10 min and 70 µL were transferred into UPLC-vials. The non-targeted *ex vivo* activity assay was performed as three independent experiments which were performed at the same time, treated equally and measured together.

The technical parameters of the LC-HR-MS were set as described in 3.2.8.4. Samples were measured in positive and negative ionization mode. For data processing, the raw data of all samples of one experiment were taken and processed with MarkerLynx Application Manager for MassLynx 4.1 software resulting in two data matrices – from the two ionization modes. The toolbox MarVis (MarkerVisualization, <http://marvis.gobics.de>) was used for further data processing including ranking by ANOVA combined with the multiple testing by Benjamini-Hochberg, filtering the data, adduct and isotope correction as well as combining of the selected data of the two data matrixes (MarVis Filter) for clustering and visualization (MarVis Cluster). For database search, metabolite set enrichment analyses (MarVis Pathway) were used. Here, also internal databases optimized for *e. g.* jasmonates and their glucosides were integrated. Selected high quality features (false discovery rate < 10⁻⁶) were chosen for clustering and data base search.

The identity of selected features was confirmed by coelution with authentic standards and/or by fragmentation analysis.

3.2.8.6. STRUCTURE DETERMINATION BY FRAGMENTATION

Detailed structural information of different markers identified by metabolite fingerprinting were confirmed by fragmentation (MS/MS) using a LC 1290 Infinity (Agilent Technologies, Santa Clara, USA) coupled with an Applied Biosystems 6540 UHD Accurate-Mass triple quadrupole time of flight mass spectrometer (Agilent Technologies, Santa Clara, USA). The MS/MS analyses were done by Dr. Kirstin Feussner (Georg-August-University, Goettingen, Germany).

For LC an Acquity UPLC HSS T3 column (1 x 100 mm, 1.8 μm particle size, Waters Corporation, Milford, USA) was used at a flow rate of 0.5 ml min^{-1} and a temperature of 40 $^{\circ}\text{C}$. The binary solvent system consists of A (water : formic acid [100 : 0.1, v/v]) and B (ACN : formic acid [100 : 0.1, v/v]). The gradient was set as for LC-HR-MS analysis (3.2.8.4). The MS-instrument was operated with a detection frequency of 2 GHz in the Extended Dynamic Range and the targeted MS/MS mode. The source conditions were set with gas temperature: 250 $^{\circ}\text{C}$, drying gas flow: 8 L min^{-1} , nebulizer pressure: 35 psi, sheath gas temperature: 300 $^{\circ}\text{C}$, sheath gas flow: 8 L min^{-1} , VCap voltage: 3 kV, nozzle voltage: 200 V, and fragmentor voltage: 100 V. Samples were ionized in negative and/or positive ESI mode with collision energy 12-32 eV. Isolation of precursor ions occurred within the narrow isolation width of 1.3 m/z . Data were acquired by Mass Hunter Workstation Acquisition software B.05.01 (Agilent Technologies, Santa Clara, USA). Mass Hunter Qualitative Analysis B.06.01 (Agilent Technologies, Santa Clara, USA) was used for data analysis.

4. RESULTS

The JA-pathway has been studied intensively (Koo, 2018; Wasternack, 2015) and many of the enzymes of the JA-Ile-synthesis as well as for its catabolism have been described (see Figure 1-3). Up to now, the enzyme(s) responsible for the glycosylation of the 12-hydroxy group of 12-OH-JA are still elusive although the metabolite 12-*O*-Glc-JA is known in *A. thaliana* (Koo, 2018; Miersch *et al.*, 2008).

Here, four uncharacterized UGTs are investigated towards their activity on jasmonates – in particular towards 12-OH-JA. The work was divided into several subtopics: (i) the identification of potential candidate *UGTs* and (ii) their expression analysis in wounded *A. thaliana*. Then, (iii) the candidate enzymes were characterized biochemically in respect to their preferred substrate and their kinetic parameters. On top of this, (iv) the *in vivo* analysis of the candidates was started. Therefore, the CRISPR/Cas9 approach was used to knock out the candidate genes specifically.

4.1. IDENTIFICATION OF FOUR UGTs AS CANDIDATES FOR 12-OH-JA GLYCOSYLATION

After wounding, the modifications within the JA metabolic fate follow a time-course (see 4.4). This temporal distribution is reflected in the expression of such genes, too. Likewise, it may be possible to identify genes involved in the glycosylation of 12-OH-JA by co-expression analysis of gene products, which are known to synthesize and metabolize 12-OH-JA. The UGT family of *A. thaliana* has been studied phylogenetically before (Lim *et al.*, 2002; Ross *et al.*, 2001) and, hence, the putative genes connected to jasmonates are annotated and can be identified by online searches.

4.1.1. *UGT76E1* AND *UGT76E2* MAY BE RELATED TO 12-OH-JA METABOLISM

12-OH-JA is directly oxidized from JA by *JOX 1* to *JOX 4* (Caarls *et al.*, 2017). Therefore, the gene products of *JOX1* to *JOX4* were used as bait genes for RNA-seq co-expression analyses. For *JOX1*, *JOX2*, and *JOX4*, no co-regulations with predicted *UGTs* were found (data not shown). Whereas, *JOX3* shows co-expression with its homologue *JOX4*, *At2g39030*, *At4g37990*, *At1g52890*, *At2g36080*, and, interestingly, with *At5g59580* encoding for *UGT76E1* (Table 4-1). *UGT76E1* is a so far uncharacterized *UGT*. Searching against expression data from micro-array analysis, *JOX3* is co-regulated with other members in the JA-metabolism *CYP94B3*, *ILL6*, *TIFY7*, *TIFY 9*, and *TIFY 10* (Supplemental figure 2A) but not with *UGT76E1* here. Next, *ST2a*, which's

gene product forms 12-HSO₄-JA from 12-OH-JA, was used as a bait gene for the RNA-seq data. No co-expression is shown for known players around jasmonates. Anyhow, *ST2a* is co-expressed with *At5g59590* encoding for *UGT76E2* (Table 4-1) – a second uncharacterized *UGT*. Further, the available micro-array data of *ST2a* were evaluated but no co-regulations with *UGT76E2* or other putative *UGTs* were given (Supplemental figure 2B).

Furthermore, gene products, which are known to be involved in the jasmonate inactivation were investigated. *ILL6* and *IAR3*, whose gene products produce 12-OH-JA by de-conjugating 12-OH-JA-Ile, did not show co-regulation with putative *UGTs* (data not shown). Additionally, *CYP94B1*, *CYP94B3*, and *CYP94C1* oxidizing JA-Ile to 12-OH-JA-Ile were used as baits for co-expression searches. The 12-hydroxy group could be a target for further glycosylation to potentially form 12-Glc-O-JA-Ile. However, no co-expressions of putative *UGTs* were found with the JA-Ile oxidizing P450s as baits (data not shown).

Taken together, the search for gene products involved in the jasmonate catabolism identified two uncharacterized *UGTs* as candidates for the glycosylation of 12-OH-JA: *UGT76E1* and *UGT76E2*.

Table 4-1: Search for glycosyltransferase genes as candidates for JA-glycosylation

RNA-seq co-expression analysis of gene products involved in 12-hydroxy-JA metabolism. Jasmonic acid oxidase 3 (*JOX3*, *At3g55970*) and sulfotransferase 2a (*ST2a*, *At5g07010*) were used as bait genes to search for candidates for JA-glycosylation. Two uncharacterized glycosyltransferases, *UGT76E1* and *UGT76E2*, were identified (red frame). Given are the complete outputs of the data base search for every bait. The gene products are ranked by Mutual Rank (MR) giving an average correlation of two genes. Smaller MR-values indicate stronger correlation. Access 02.05.2018; the page was prepared on Dec. 14. 2017 for ATTED-II version 9.1

MR	Locus	Function
Bait gene: <i>JOX3</i> (<i>At3g55970</i>)		
1.6	<i>At2g38240</i>	2-Oxoglutarate and Fe(II)-dependent oxygenase Superfamily protein, JOX 4
1.8	<i>At2g39030</i>	Acyl-CoA N-acyltransferases superfamily protein
3.2	<i>At4g37990</i>	Elicitor-activated gene 3-2
3.4	<i>At1g52890</i>	NAC domain containing protein 19
18.9	<i>At5g59580</i>	<i>UGT76E1</i>
33.4	<i>At2g36080</i>	AP2/B3-like transcriptional factor family protein
Bait gene: <i>ST2a</i> (<i>At5g07010</i>)		
7.7	<i>At1g54100</i>	Aldehyde dehydrogenase 7B4
19.3	<i>At2g38240</i>	2-Oxoglutarate and Fe(II)-dependent oxygenase Superfamily protein, JOX 4
20.9	<i>At1g64660</i>	Methionine gamma-lyase
37.1	<i>At4g31380</i>	FPF1-like protein 1
44.1	<i>At5g59590</i>	<i>UGT76E2</i>
50.9	<i>At1g75450</i>	Cytokinin oxidase 5

4.1.2. TRANSCRIPTOME ANALYSIS OF WOUNDED *A. THALIANA* LEAVES CONFIRMED *UGT76E1*, *UGT76E2* AND IDENTIFIED *UGT76E11* AND *UGT76E12* AS WOUND INDUCED TRANSCRIPTS

A second source was used to support the candidates *UGT76E1* and *UGT76E2* and to search for additional *UGTs*, which could be involved in the catabolism of 12-OH-JA. Therefore, a combined transcriptome and metabolome study of a wounding time course for *A. thaliana* leaves was used (Kaefer, 2014). The data were recorded 0, 0.5 and 2 hpw in leaves of wild type Col-0 and the JA-deficient mutant *delayed dehiscence 2-2* (*dde2-2*) (Park *et al.*, 2002). This mutant is a loss-of-function point mutation in the *AOS*, which results in JA-deficient plants. The transcriptome data were recorded by a 44 k Affimetrix micro-array analysis.

There, the candidates *UGT76E1* and *UGT76E2* showed detectable signals at 2 hpw exclusively; all other time points and the *dde2-2* show just trace signals. Yet, the intensity of *UGT76E2* is below the signal threshold (> 500 procedure defined units (p.d.u.), oral communication Milena Lewandowska, University of Goettingen, Germany). In addition, a *UGT* related screening (*cf.* Figure 4-2) identified *UGT76E11* (*At3g46670*) and *UGT76E12* (*At3g46660*). *UGT76E11* shows constitutive expression with additional induction at 2 hpw in Col-0 (5-fold) and *dde2-2* (2-fold). Similar to *UGT76E1* and *UGT76E2*, *UGT76E12* displays wound induction in Col-0 at 2 hpw exclusively but with 5-fold higher intensities (Supplemental figure 3). Altogether, *UGT76E1* and *UGT76E2* show low signal intensities around the signal threshold whereas *UGT76E12* depicts robust induction. The accumulations of *UGT76E1*, *UGT76E2*, and *UGT76E12* at 2 hpw are strongly JA-dependent and the reduced expression of *UGT76E11* in *dde2-2* at 2 hpw suggest a JA-influence.

The Arabidopsis Information Resource provides another source of expression data. There, the online tool Arabidopsis eFP Browser offers transcriptome data for various stimuli, tissues, or developmental stages (Winter *et al.*, 2007). In this context, focus was given to the expression of the candidate *UGTs* after abiotic stress like wounding (Kilian *et al.*, 2007), cold, osmotic, salt, drought, UV-B, and heat stress.

UGT76E1 is exclusively expressed in *A. thaliana* shoots in response to wounding (1 hpw, Supplemental figure 4A). *UGT76E2* displays also a specific expression 1 hpw in shoots and, in addition, a constitutive expression in roots (Supplemental figure 4B). The expression of *UGT76E1* and *UGT76E2* is not induced by other kinds of abiotic stress like cold, osmotic, salt, drought, UV-B, and heat stress. In contrast to that, *UGT76E11* shows constitutive expression in shoots, which could be enhanced mainly by cold (3 hours after all stimulus) and salt stress (12 hours after all stimuli) but no expression in roots. Interestingly, in response to wounding, the expression of *UGT76E11* is reduced at 0.5 hpw similar to the results of the in-house transcriptome analysis shown above (Supplemental figure 5A, see Supplemental figure 3C) and started to

increase 1 hpw. *UGT76E12* illustrated specific expressions at 1 hpw, 24 h after oxidative stress, and highest inductions at 24h after osmotic stress in shoots. No expression of *UGT76E12* is depicted in roots (Supplemental figure 5B). The expression data of the Arabidopsis eFP Browser highlighted differential expression of *UGT76E1* and *UGT76E2* in roots and confirmed the findings in respect to the wound induction of the four candidate genes.

4.1.3. REAL TIME PCR ANALYSES CONFIRM, THAT UGT76E1, UGT7E11, AND UGT76E12 ARE INDUCED AFTER WOUNDING

To support the data of the co-expression analyses and transcriptome array, *UGT76E1*, *UGT76E2*, *UGT76E11*, and *UGT76E12* were analyzed by a quantitative expression analysis performed by qPCR. The expression analysis was performed with cDNA, which had been synthesized from RNA of wounded leaves (0, 1, 2, and 5 hpw, see 4.4). Here, *UGT74F1* (*At2g43840*) was added as control gene to the set of candidate genes: *UGT74F1* encodes a glycosyltransferase, that specifically glycosylates SA (George Thompson *et al.*, 2017; Lim *et al.*, 2004) and acts as wound-unrelated control here.

The obtained raw data were normalized to the basal expression of the respective genes at 0 hpw. At 1 hpw, *UGT76E1* and *UGT76E2* show slight elevation with 2-fold higher expression. While, *UGT76E11* and *UGT76E12* already show significant accumulation with 4-fold and 3.5-fold enrichment, respectively. At 2 hpw, the expression rates of *UGT76E1*, *UGT76E11*, and *UGT76E12* accumulated significantly with about 6- to 8-fold higher expressions. Whereas, *UGT76E2* shows no further accumulation. At 5 hpw, the expressions of *UGT76E1* and *UGT76E12* decreases to levels of *UGT76E2* (2-fold higher expression), while *UGT76E11* still displays 5.5-fold higher expression in comparison to the unwounded plants. The control, *UGT74F1* shows no induction after wounding at any of the time points (Figure 4-1A). Without normalization, *UGT76E1*, *UGT76E2*, *UGT76E11*, and *UGT74F1* display similar low constitutive expression levels. Only *UGT76E12* shows 2-fold elevated levels without wounding stimulus (Supplemental figure 6A). Furthermore, the expressions were compared between Col-0 and *dde2-2* at 0 and 2 hpw. The relative expression values of *UGT76E1*, *UGT76E2*, and *UGT76E12* show control-like levels in *dde2-2* at 2 hpw whereas *UGT76E11* shows 3-fold elevated levels (Supplemental figure 6B).

In summary, the quantitative expression analysis of the four candidate *UGTs* illustrates that *UGT76E1*, *UGT76E11*, and *UGT76E12* are significantly upregulated in Col-0 after wounding. In contrast to that, *UGT76E2* accumulates slightly but not significantly after wounding. The results of the quantitative expression analysis confirm the expression pattern of the transcriptome analysis for *UGT76E1*, *UGT76E11*, and *UGT76E12*, even though the relative expression rates

and fold changes are different (see 4.1.2). Contradictory to the transcriptome data, *UGT76E12* did not show significant accumulation after wounding.

So far, three different approaches – the co-expression analysis, the 44 k Affimetrix transcriptome analysis of wounded *A. thaliana* leaves, and the quantitative expression analysis by qPCR – identified *UGT76E1*, *UGT76E2*, *UGT76E11*, and *UGT76E12* as related to the JA-mediated wound-response in *A. thaliana*, even if the results for the three data sources are not completely consistent.

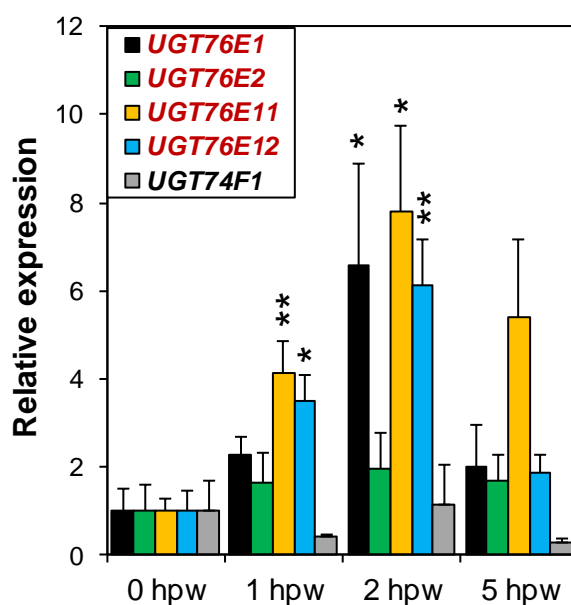


Figure 4-1: Expression of *UGT76E1*, *UGT76E2*, *UGT76E11*, *UGT76E12*, and *UGT74F1* in *A. thaliana* leaves after wounding

Quantitative real-time PCR of *UGT76E1* (red), *UGT76E2* (green), *UGT76E11* (orange), *UGT76E12* (blue), and *UGT74F1* (grey). Plants were grown for six weeks at 22 °C under short day conditions (8 h light/16 h dark). Leaves were wounded three times across the mid vein by squeezing with forceps. Damaged rosette leaves were harvested at indicated time points (hours post wounding (hpw)), RNA was isolated, and appr. 1 µg transcribed complementary DNA were used for PCR. All expression values are normalized to *actin 8* as reference. Relative expression of the transcripts normalized to their respective expression levels at 0 hpw. Each data point represents the mean value + SD of three biological replicates. 10 plants per time point were pooled for one replicate. Asterisks indicate significance by one-sided T-Test with * $p < 0.05$, ** $p < 0.01$

4.1.4. *UGT76E1* AND *UGT76E2* ARE ASSIGNED TO JA METABOLISM BY CO-EXPRESSION ANALYSES

UGT76E1, *UGT76E2*, *UGT76E11*, and *UGT76E12* have been identified as candidates for the glycosylation of jasmonates by co-expression with known players in jasmonate metabolism. Now, the candidates were used as baits for co-expression analysis to support the connection to jasmonates from the other side.

UGT76E1 displays connections to *JAZ2*, *ILL6*, and *JOX3*, which are members of the JA-mediated wound-response in *A. thaliana* (Table 4-2). *UGT76E2* shows co-regulation with genes induced by osmotic stress (data not shown, eFP-Browser, access 02.05.2018) like *cinnamyl alcohol dehydrogenase 5* (cf. Lee *et al.*, 2013), *Myzus persicae-induced lipase 1* (cf. Louis *et al.*, 2010) and *UGT71B8*, which glycosylates ABA (Dong *et al.*, 2014). Furthermore, *UGT76E2* is co-regulated with *ST2a*, by which it also was identified before (Table 4-2). Next, *UGT76E11* shows co-regulation with genes connected to drought response but not wounding. Like for *UGT76E11* itself, the co-regulated genes are induced by different abiotic stimuli with generally high expressions (data not shown, eFP-Browser, access 02.05.2018). *UGT76E12* is co-regulated with genes induced by osmotic stress (data not shown, eFP-Browser, access 02.05.2018) like *elicitor-activated gene 3-2* (cf. Somssich *et al.*, 1996), *CYP76C2* (cf. Hofer *et al.*, 2014), and *phenolic lucoside malonyltransferase 1* (cf. Khan *et al.*, 2016). None of them is known to have functions in wounding.

Table 4-2: Co-expression analysis of *UGT76E1*, *UGT76E2*, *UGT76E11*, and *UGT76E12*

RNA-seq co-expression analysis of gene products correlated with *UGT76E1* (At5g59580), *UGT76E2* (At5g59590), *UGT76E11* (At3g46670), and *UGT76E12* (At3g46660). Identified gene products related to JA metabolism are given in bold. *JAZ2*, *jasmonate-ZIM-domain protein 2*; *JOX3*, *jasmonic acid oxidase 3*. Given are the complete outputs of the database for every bait. Gene products are ranked by Mutual Rank (MR) giving an average correlation of two genes indicating stronger correlation by smaller values. Access 02.05.2018; the page was prepared on Dec. 14. 2017 for ATTED-II version 9.1

MR	Locus	Function
Bait gene: UGT76E1 (At5g59580)		
8.5	<i>At1g74950</i>	TIFY domain/Divergent CCT motif family protein, JAZ2
14.4	<i>At1g44350</i>	IAA-leucine resistant (ILR)-like gene 6, ILL6
18.9	<i>At3g55970</i>	Jasmonate-regulated gene 21, JOX3
Bait gene: UGT76E2 (At5g59590)		
42.2	<i>At4g34230</i>	<i>Cinnamyl alcohol dehydrogenase 5</i>
44.1	<i>At5g07010</i>	Sulfotransferase 2A, ST2a
45.7	<i>At5g14180</i>	<i>Myzus persicae-induced lipase 1</i>
102.6	<i>At3g21800</i>	<i>UDP-glucosyl transferase 71B8</i>
Bait gene: UGT76E11 (At3g46670)		
6.1	<i>At5g65890</i>	<i>ACT domain repeat 1</i>
8.0	<i>At2g40435</i>	<i>Transcription factor SCREAM-like protein</i>
8.2	<i>At5g24150</i>	<i>FAD/NAD(P)-binding oxidoreductase family protein</i>
16.3	<i>At2g36590</i>	<i>Proline transporter 3</i>
29.0	<i>At5g43745</i>	<i>Protein of unknown function (DUF1012)</i>
45.5	<i>At5g15240</i>	<i>Transmembrane amino acid transporter family protein</i>
Bait gene: UGT76E12 (At3g46660)		
5.8	<i>At4g37990</i>	<i>Elicitor-activated gene 3-2</i>
6.3	<i>At5g45570</i>	<i>Cytochrome P450, family 76, subfamily C, polypeptide 2</i>
12.4	<i>At5g39050</i>	<i>Phenolic lucoside malonyltransferase 1, PMAT1</i>

In addition to that, the available micro-array data of *UGT76E1*, *UGT76E2*, *UGT76E11*, and *UGT76E12* were checked. Here, the data did not show direct evidence for a potential role of any candidate in the glycosylation of jasmonates (Supplemental figure 7, Supplemental figure 8). Interestingly, *UGT76E12* is co-regulated with a gene encoding for β -glucosidase 11 (*At1g02850*)

(Supplemental figure 8B). This gene is expressed late after wounding – 12 hpw – but also after other abiotic stresses (data not shown, eFP-Browser, access 02.05.2018). Since β -glucosidases cleave glycosidic bonds, it might be connected to *UGT76E12*.

4.2. SEQUENCE ANALYSES OF THE CANDIDATES

4.2.1. *UGT76E1*, *UGT76E2*, *UGT76E11*, AND *UGT76E12* HAVE SIMILAR GENE STRUCTURES

In the *A. thaliana* genome, the four candidate genes are found in two loci. *UGT76E1* (*AT5g59580*) and *UGT76E2* (*At5g59590*) are located right next to each other on the chromosome five. Similarly, *UGT76E11* (*At3g46670*) and *UGT76E12* (*At3g46660*) are also located side by side on the chromosome three. Altogether, the gene structures of all four genes are similar: they have two exons split by one intron located at the first third of the genes (Supplemental figure 9). No splice-variants are known for the candidates. This is supported by findings that *UGTs* are clustered in groups of two to seven genes and harbor none to two introns (Ross *et al.*, 2001).

4.2.2. *UGT76E1* AND *UGT76E2* AS WELL AS *UGT76E11* AND *UGT76E12* CLUSTER AS HOMOLOGUES

As members of the UGT subfamily E, *UGT76E1*, *UGT76E2*, *UGT76E11*, and *UGT76E12* are related with ≥ 60 % amino acid sequence homology (Mackenzie *et al.*, 1997). In the phylogenetic tree of all UGTs of *A. thaliana*, the four candidates for 12-OH-JA glycosylation cluster in the group H, which contains all members of the *UGT76* family. The tree was generated by comparing ten conserved motifs of all UGTs in *A. thaliana* (Figure 4-2, see Supplemental figure 1). Therefore, the candidates share > 60 % motif-similarity as members of the same group (Ross *et al.*, 2001). In detail, *UGT76E1* and *UGT76E2* as well as *UGT76E11* and *UGT76E12* respectively cluster as homologs (Figure 4-2). The group H of the glycosyltransferase family has not been investigated in detail yet. No studies have been done on *UGT76E1*, *UGT76E2* in particular, while *UGT76E11* and *UGT76E12* have been described to glycosylate flavonoids like quercetin (Li *et al.*, 2018; Lim *et al.*, 2004).

As mentioned, all UGTs in *A. thaliana* share a common structure with two protein domains (see 0) each harboring a conserved catalytic motif for substrate binding (N-terminus) and UDP-binding (C-terminus, Figure 1-5) (Offen *et al.*, 2006). Therefore, *UGT76E1*, *UGT76E2*, *UGT76E11*, and *UGT76E12* were analyzed for these catalytic motifs.

The two UGT-specific motifs of *UGT76E1*, *UGT76E2*, *UGT76E11*, *UGT76E12*, the control *UGT74F1*, and the UGT reference gene of *V. vinifera* *VvGT1* (Figure 1-5) (Offen *et al.*, 2006)

were aligned with the Geneious algorithm. All sequences show the catalytic histidine at the N-terminus at the position 27 of the consensus sequences (Figure 4-3A). In the N-terminal regions, 14 of 57 amino acids of the candidates are similar to the reference VvGT1 (> 60 % similarity, Figure 4-3A). The C-termini of the UGTs show high similarity, too. All six sequences share the UDP-Glc binding motif (Figure 4-3B, see Figure 1-5A). The candidate-UGTs show similarity for 39 of 57 amino acids in comparison to the reference VvGT1 (> 60 % similarity, Figure 4-3B).

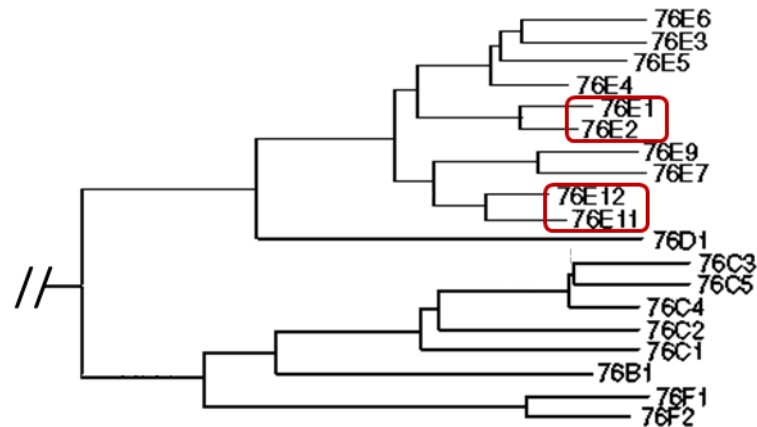


Figure 4-2: Phylogenetic tree of group H UGTs in *A. thaliana*

Phylogenetic tree of 19 out of 107 UGT genes of *A. thaliana*. The selected branch shows the group H (> 60 % motif-similarity). The four UGTs, which are potentially active in the JA-pathway are marked with red boxes. The complete phylogenetic tree is given in Supplemental figure 1. Figure was taken from (Ross *et al.*, 2001).

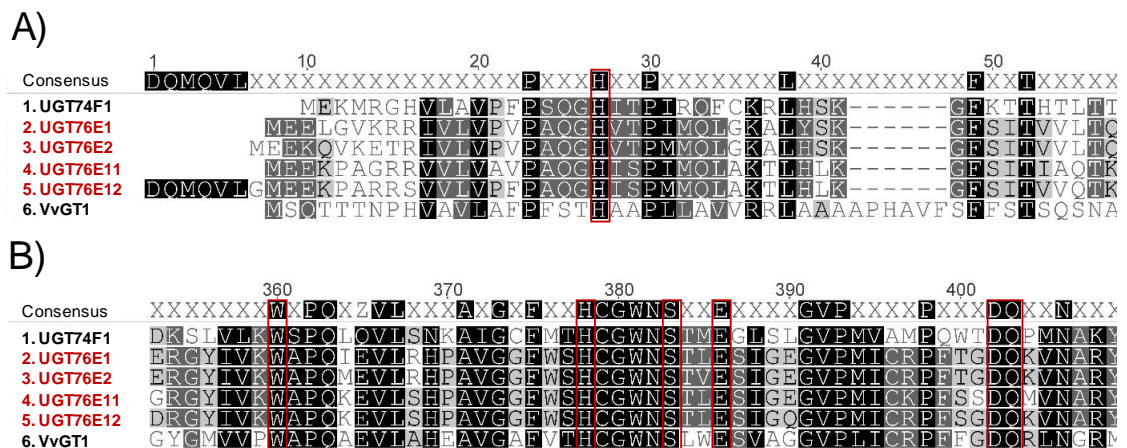


Figure 4-3: UGT76E1, UGT76E2, UGT76E11, and UGT76E12 show the catalytic motifs

Amino acid alignment of the four UGT76Es (2. - 5.), the control UGT74F1 (1.), and the reference VvGT1 (6.). Amino acids, which are conserved in the six indicated UGTs, are highlighted. Amino acids highlighted by black boxes share 100 % identity. Amino acids highlighted by dark grey, light grey or white boxes show 80 to 100 %, 60 to 80 %, or less than 60 % similarity, respectively. **A)** Amino acid alignment and consensus sequence for the N-termini are shown. The catalytic histidine (H) at position 27 is marked by a red box. It was postulated by the x-ray crystal structure of VvGT1 and UGT74F1 (George Thompson *et al.*, 2017; Offen *et al.*, 2006). **B)** Amino acid alignment and consensus sequence of the C-termini. The region is proposed to harbor the UDP-Glc binding motif (shown in red boxes) – postulated by the x-ray crystal structure of VvGT1 with the bound cofactor (Offen *et al.*, 2006). Alignments were created with Geneious algorithm as global alignment with free end gaps and Blosum62 cost matrix in Geneious version 8.1 (Biomatters, New Zealand). Available from <http://www.geneious.com>.

Because the four candidates are highly conserved in the substrate and UDP-Glc binding-motifs, the complete amino acid sequences were compared among each other. UGT76E1 and UGT76E2 show a high amino acid sequence identity of 88 %. Compared to UGT76E11, both, UGT76E1 and UGT76E2, display a sequence identity of 65 %. With UGT76E12, UGT76E1 and UGT76E2 share 65 and 67 % identity respectively. UGT76E11 and UGT76E12 have 84 % of the amino acids in common (Table 4-3). Taken together, all four UGTs are similar on the amino acid level with at least 65 % identity. This confirms the systematic classification to the subfamily E (≥ 60 % amino acid sequence homology) (Mackenzie *et al.*, 1997).

Table 4-3: Amino acid sequence comparison for UGT76E1, UGT76E2, UGT76E11, and UGT76E12

Amino acid identity of the indicated UGTs was calculate and the respective identity is given in %. Alignments were created with the Geneious algorithm as global alignment with free end gaps and Blosom62 cost matrix in Geneious version 8.1 (Biomatters, New Zealand). Available from <http://www.geneious.com>.

Amino acid identity	UGT76E1	UGT76E2	UGT76E11	UGT76E12
UGT76E1		88	65	67
UGT76E2	88		65	65
UGT76E11	65	65		84
UGT76E12	67	65	84	

4.2.3. PROTEIN PARAMETERS OF UGT76E1, UGT76E2, UGT76E11, AND UGT76E12 ARE SIMILAR

To get a better understanding of the four UGTs for the following protein purification and characterization, the protein parameters were estimated using the ProtParam online tool (<https://web.expasy.org/protparam/>). The MWs of the UGTs are about 51 kDa. The specific extinction coefficients at 280 nm are between $55.5 \text{ kM}^{-1}\text{cm}^{-1}$ (UGT76E12) and $66.4 \text{ kM}^{-1}\text{cm}^{-1}$ (UGT76E1). The predicted extinction coefficients were used to determine the exact concentrations of the purified proteins by spectroscopy later on. The predicted pIs of the proteins are acidic and mainly similar for UGT76E2 (pI 5.4), UGT76E11 (pI 5.9), UGT76E12 (pI 6.0), and UGT74F1 (pI 5.5). Interestingly, UGT76E1 has a pI at pH 6.6, which differs most to its homologue UGT76E2 (pI 5.4). Sequence analyses did not identify any signal peptides or transmembrane domains in any of the sequences. In addition, target sequences are not predicted for UGT76E2, UGT76E11, and UGT76E12. Again, UGT76E1 was predicted differently with a putative mitochondrial location. The score was the lowest prediction probability that the TargetP tool gives (Supplemental table 1).

The protein parameters illustrate that the five different UGTs are very similar in respect to their calculated properties. Only, UGT76E1 may show a less acidic pI and an uncertain putative

mitochondrial location (Supplemental table 1). In respect to the characterization of the four candidates, the predictions do not give reasons to remove any motifs from the sequences.

4.3. BIOCHEMICAL CHARACTERIZATION OF UGT76E1, UGT76E2, UGT76E11, AND UGT76E12

After the four candidate genes have been identified by co-expression analyses and first *in silico* investigations have been done, the coding sequences were cloned, the proteins were heterologously expressed in *E. coli*, purified and introduced to biochemical characterizations. Likewise, it was aimed to determine their preferred substrates with various types of activity assays. The four UGTs were tested towards potential substrates, which are typically containing free hydroxy and carboxy groups including the proposed native substrate 12-OH-JA. Additionally, the enzymatic performance of the homogeneous UGTs were analyzed in a native-like environment. Finally, the kinetic parameters for the main substrates were determined in a continuous spectrophotometric assay.

4.3.1. UGT76E1, UGT76E2, UGT76E11, UGT76E12, AND UGT74F1 WERE HETEROLOGOUSLY EXPRESSED IN *E. COLI*

The coding sequences of *UGT76E1*, *UGT76E2*, *UGT76E11*, *UGT76E12*, and *UGT74F1* were amplified from cDNA. These RNA-based templates ensure correct splicing and processing of the gene products, which should result in functional proteins after heterologous expression in *E. coli*. The templates for *UGT76E1*, *UGT76E2*, *UGT76E11*, *UGT76E12* were synthesized from RNA of leaf material 2 hpw. The coding sequence of *UGT74F1* was amplified as splice variant 2 (see 3.2.3.1) from cDNA, which are synthesized from RNA of unwounded root material. The coding sequences of all five genes have been integrated into the open reading frame (ORF) of the pET28a vector (Supplemental figure 10). The vector is optimized for protein expression and harbors an N-terminal HisTag for affinity chromatography purification.

To express the five UGTs in *E. coli* with high efficiency as soluble proteins, different optimizations have been done to the expression system. Best results were obtained for expressing the proteins with the pET28a vector in BL21 Star (DE3) cells in the auto-induction medium ZYP-5052 (Table 3-8) (Studier, 2005).

After protein expression, the heterologously expressed proteins can be visualized by SDS-PAGE in lysates of whole bacteria cells (Figure 4-4). There, signals of the expressed UGTs (~51 kDa) can be seen, which are absent in the empty vector control. However, UGT74F1 is the only expressed protein, which illustrates strong signals at the predicted size of the UGT protein. UGT76E1, UGT76E2, UGT76E11, and UGT76E12 display faint signals at the assumed

molecular weight of the expressed proteins. To detect the expressed proteins specifically in the whole cell lysates, the heterologous proteins were detected by immuno-blotting of their HisTags. The western blot shows a prominent signal for UGT76E2 and UGT74F1 at 51 kDa. In addition, a faint signal is visible for UGT76E11. No staining is visible for UGT76E1 and UGT76E12 (Figure 4-4B), however signals of the SDS-PAGE suggest for protein expression of UGT76E1 and UGT76E12.

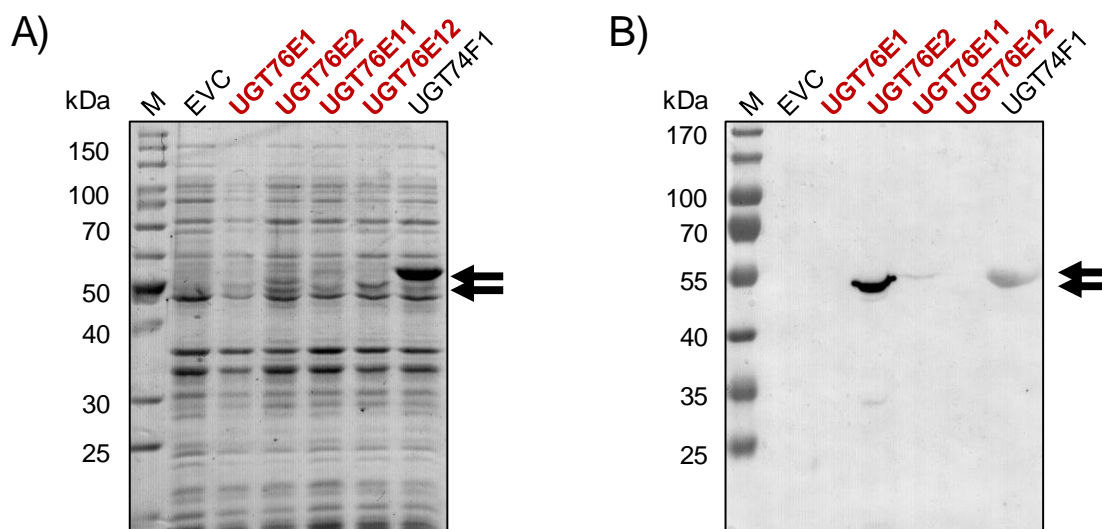


Figure 4-4: UGT76E1, UGT76E2, UGT76E11, UGT7 E12, and UGT74F1 were expressed in *E. coli* Indicated UGTs were fused to an N-terminal His-tags of pET28a vectors and heterologously expressed in *E. coli* BL21 Star (DE3) cells in auto-induction medium for 3 d at 16 °C. The heterologous protein expression was recorded in 100 mL *E. coli* cultures: **A)** Sodium dodecyl sulfate (SDS)-polyacrylamide gel electrophoresis (PAGE) of cultures expressing UGT76E1, UGT76E2, UGT76E11, UGT76E12, UGT74F1, and the empty vector control (EVC). After protein expression, 5 μ L of the samples were loaded onto a 10 % SDS-PAGE for separation. The proteins were stained with 0.01 % Coomassie Brilliant Blue. The arrows indicate the size of UGT proteins at appr. 50 kDa. The expressions and the SDS-PAGE are representative for at least five independent expressions for every enzyme. **B)** Western blot of the UGTs. The his-tagged UGTs were specifically detected via primary and secondary antibody and an activity staining by phosphatase. The arrows indicate the size of UGT proteins of about 51 kDa. The blot was performed like this once.

4.3.2. UGT76E1, UGT76E2, UGT76E11, UGT76E12, AND UGT74F1 WERE PURIFIED TO HOMOGENEITY

The biochemical investigation of so far not characterized enzymes requires homogeneous proteins. Therefore, a two-step protein purification was set up to yield homogeneous UGT76E1, UGT76E2, UGT76E11, UGT76E12 and UGT74F1. Using different separation properties, two purification steps ensure that co-purifications of unspecific proteins are diminished. First, His-tagged proteins are captured from the bacterial lysate by IMAC. Second, the UGTs are further purified by SEC.

Briefly, the cleared lysate was loaded onto the IMAC-column to retard His-tagged proteins from other bacterial proteins. Since those unspecific proteins were not (or rarely) bound to the bivalent cations of the column material, they could be washed away by loading buffer His A. The remaining captured proteins were eluted by imidazole.

Even though UGT76E1, UGT76E2, UGT76E11 and UGT76E12 show very high amino acid sequence homologies (seen Table 4-3), it was not possible to use one common scheme for efficient and reliable purification of all UGTs up to homogeneity. The protein purification of the UGT enzymes required several optimizations for each enzyme.

In this regard, the purification of UGT76E1 was most challenging and different parameters have been improved to produce a sufficient yield of active protein. Firstly, the cell pellet of 0.5 L was resolved in 20 mM Tris/HCl pH 7.5, 50 mM NaCl. Protein elution from the IMAC-material with 150 mM imidazole resulted in a small UGT76E1 protein fraction (Figure 4-5A). However, the enriched UGT76E1 protein precipitated immediately and did not show any glycosyltransferase activity (data not shown). To improve the IMAC-purification step, the culture volume was enlarged stepwise to 2 L and the bivalent cation was exchanged from nickel to cobalt. Cobalt as chelating metal cation forms less strong chelate complexes with the His-tagged proteins and, thus, releases the proteins at lower imidazole concentrations. The reduction to 40 mM imidazole increased the protein stability. Additionally, the concentration of the Tris-buffer, its pH-value and the salt content were optimized to 50 mM Tris/HCl pH 9.0, and 100 mM NaCl. In addition, 0.1 % Tween 20 was added to improve solubility of UGT76E1. Finally, these changes of the IMAC-purification resulted in a sufficient yield of active and stable UGT76E1 (Figure 4-5B-D).

Similar optimizations have been done for UGT76E2, UGT76E11, UGT76E12, and the control protein UGT74F1. The cell pellet of 2 L culture (1 L for UGT74F1) was used for optimized settings. Improving purification procedures resulted in specific buffer requirements for each enzyme (Table 3-16 - Table 3-20) with varying concentrations of Tris/HCl-buffer (20 – 50 mM), NaCl (50 – 100 mM), different pH values (7.5 – 9.0), and in part requirements for 0.1 % Tween 20 or 10 % glycerol. To increase the power of the IMAC purification and to remove impurities, a special wash buffer (50 mM Tris/HCl pH 7.5, 100 mM NaCl, 2 mM DTT, 5 mM ATP, 5 mM MgCl₂, 20 mM imidazole, Table 3-21) was developed for purification of UGT76E2, UGT76E11, and UGT74F1. Here, ATP provides molecular energy to remove chaperons from the column-resin or the proteins of interest. Following, the retained proteins were eluted from the column material by specific imidazole concentrations (appr. 150 mM for nickel- and appr. 40 mM for cobalt-affinity column resin). As second purification step, SEC was used.

After optimization, the IMAC protein purifications of five UGTs show similar behaviors. After cell lysis, the majority of UGT76E1, UGT76E2, and UGT76E11 was soluble in the lysate fraction

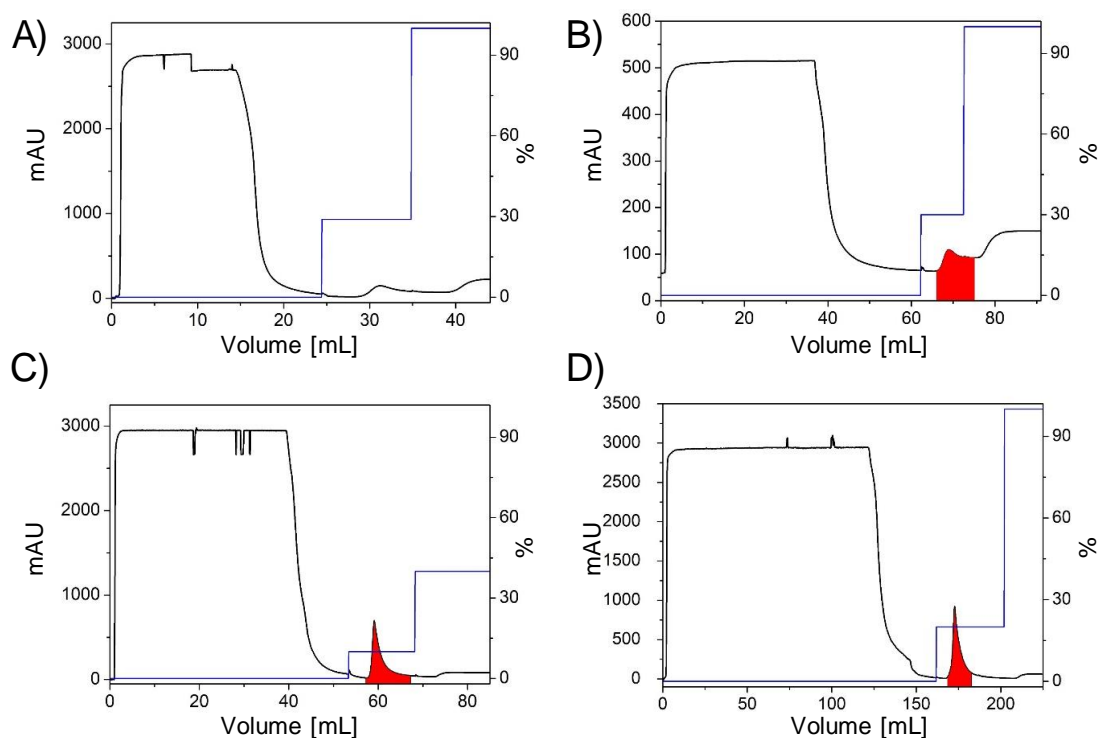


Figure 4-5: Optimization of the protein purification of UGT76E1 by affinity chromatography

UGT76E1 was fused to an N-terminal HisTag, heterologously expressed in *E. coli* BL21 Star (DE3) cells and purified by immobilized metal affinity chromatography (IMAC). The chromatograms illustrate the absorption at 280 nm (milli absorption units (mAU)) and the concentration of elution buffer (%) over the elution volume. Elution of active UGT76E1 is depicted in red area. IMAC for UGT76E1 was optimized in the following way: **A)** 0.5 L *E. coli* lysate with nickel affinity, 20 mM Tris/HCl pH 7.5, 50 mM NaCl. **B)** 1 L *E. coli* lysate with nickel affinity, 50 mM Tris/HCl pH 7.5, 100 mM NaCl. **C)** 1 L *E. coli* lysate, cobalt instead of nickel as binding metal for IMAC, 50 mM Tris/HCl pH 7.5, 100 mM NaCl, 0.1 % Tween 20. **D)** 2 L *E. coli* lysate with cobalt affinity, 50 mM Tris/HCl pH 9.0, 100 mM NaCl, 0.1 % Tween 20. Each profile is representative for at least three independent purifications.

whereas large amounts of UGT76E12 and UGT74F1 remained in the pellet fraction. Following necessary (mainly for UGT76E2, UGT76E11, and UGT74F1) the special wash buffer improved this purification step. As shown in Figure 4-6, all chromatograms display specific protein elution at the applied imidazole concentrations. The fractions show enriched UGTs with some remaining impurities (SDS-PAGE, Figure 4-6). Only, UGT76E2 shows several additional protein signals. The UGT-enriched fractions of the IMAC were introduced to SEC. As shown in Figure 4-6 the chromatograms generally illustrate two protein peaks. For UGT76E1, both fractions were tested for activity (60 μ g protein, 20 μ M ω -OH-16:0, 5 mM UDP-Glc, 16 $^{\circ}$ C, 2 h, LC-MS analysis). The protein, which elutes in the first peak at 48 ml did not show activity and represents hetero-oligomeric UGT76E1 whereas second peak at 63 mL showed UGT-activity and corresponds to the MW of monomeric UGT76E1 (data not shown, cf. Figure 4-7). Hence, the UGT-proteins, which elute later (second peak) were collected and used as purified UGTs for further analysis. The respective samples illustrate homogenous protein signals at the MWs of the five UGTs with some smaller proteins signals at lower MWs. Most likely, those indicate degradation because the signals increase over time (Figure 4-6).

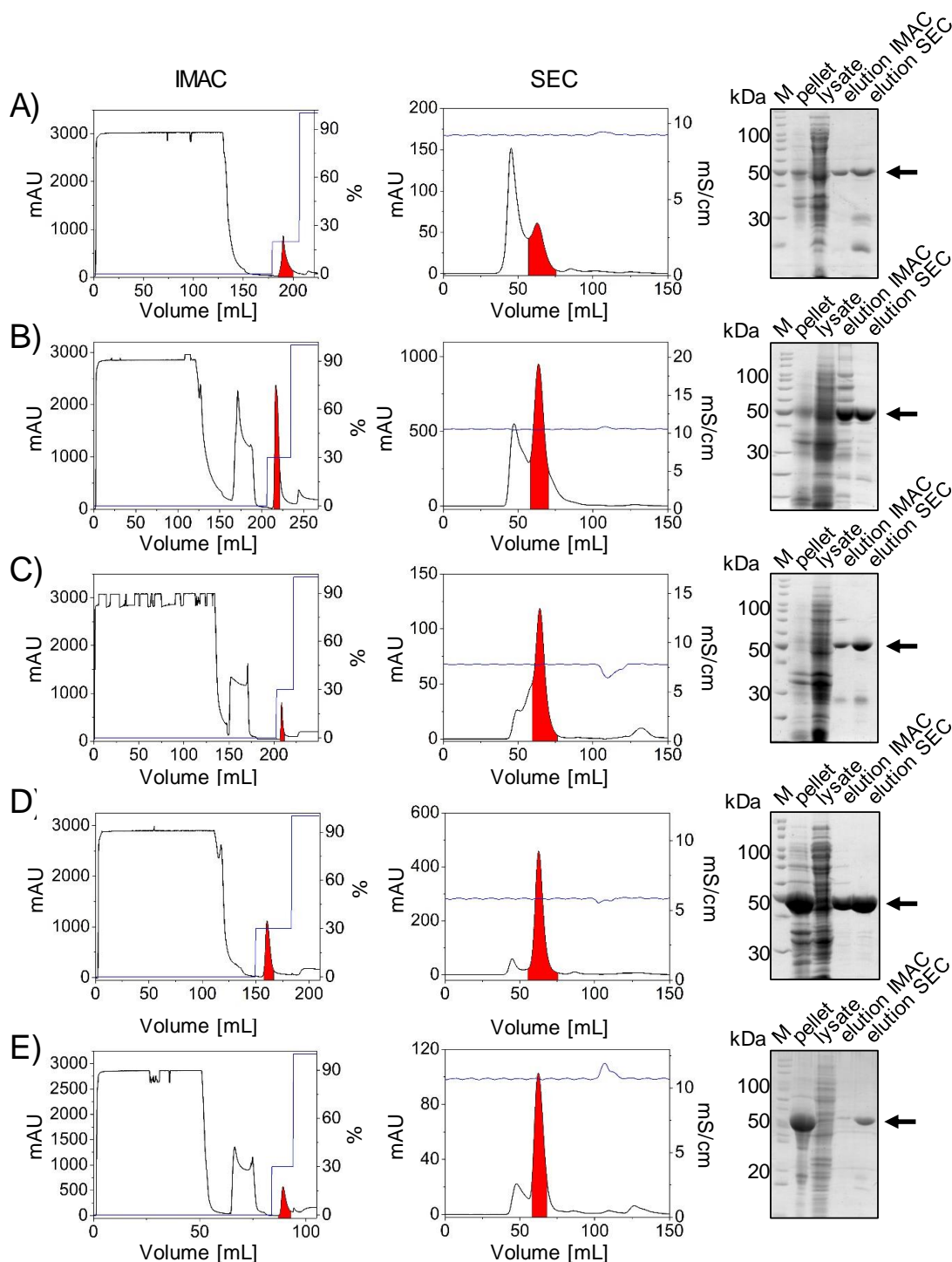


Figure 4-6: Protein purification for UGT76E1, UGT76E2, UGT7E11, UGT76E12, and UGT74F1
 UGTs fused to an N-terminal His-tag and heterologously expressed in *E. coli* BL21 Star (DE3) were purified by a two-step protein purification strategy of immobilized metal affinity chromatography (IMAC) with nickel as bivalent cation and size exclusion chromatography (SEC). Shown are the purification chromatograms and a sodium dodecyl sulfate (SDS)-polyacrylamide gel electrophoresis (PAGE) with samples of pellet, lysate, IMAC eluate, and SEC eluate. Arrows indicate the size of the respective purified protein. Chromatograms illustrate the absorption at 280 nm (milli absorption units (mAU)) during elution. For IMAC, the second y-axis shows the concentration of elution buffer (%). For SEC, the second y-axis shows the conductivity (mS/cm). The volume that contained the protein of interest is marked in red. Purifications of **A)** UGT76E1 **B)** UGT76E2 **C)** UGT76E11 **D)** UGT76E12 **E)** UGT74F1. The depicted purifications are representative for at least four independent purifications for each UGT.

Taken together, the two-step purification strategy resulted in mainly homogeneous proteins of UGT76E1, UGT76E2, UGT76E11, UGT76E12, and UGT74F1. Lowest protein yields were obtained for UGT76E1 (appr. 0.5 mg/L culture) and highest yields were achieved for UGT76E2 (5.0 mg/L culture). In the end, the proteins were concentrated as stocks (> 1 mg/mL) and stored at -80 °C.

4.3.3. UGT76E1, UGT76E2, UGT76E11, UGT76E12, AND UGT74F1 SHOW ACTIVITY TOWARDS ω -OH-HEXADECANOIC ACID AND SOME TOWARDS 12-OH-JA

After heterologous expression and purification of the five UGTs, the uncharacterized UGTs were tested for their catalytic activity. Therefore, two tentative substrates were used: 12-OH-JA and ω -OH-16:0. 12-OH-JA is the expected substrate for the four selected UGTs. The hydroxy-fatty acid ω -OH-16:0 should be used as alternative substrate, which is commercially available in contrast to 12-OH-JA. As mentioned above, P450 enzymes (CYP94B1, CYP94B3, and CYP94C1), which catalyze the oxidation of JA-Ile (see 1.1.3) also tolerate fatty acids for catalysis (Benveniste *et al.*, 2006). Moreover, some UGTs are capable to glycosylate hydroxy-fatty acids (Huang *et al.*, 2015). Hence, UGT76E1, UGT76E2, UGT76E11, and UGT76E12 putatively active on 12-OH-JA might also tolerate FA-derivatives for their catalysis.

In the assay, 10 μ g homogeneous UGT76E1, UGT76E2, UGT76E21, UGT76E12, UGT74F1, and a heat-inactivated control (aliquots of all enzymes) were incubated with 0.1 mM ω -OH-16:0 or 12-OH-JA, respectively, and the reaction products were analyzed by LC-MS. Here, LC-MS analyses provide high sensitivity to detect even small amounts of enzymatic products at a specific retention time (RT). The exact m/z of the expected products was used to extract the specific mass signal. The extracted ion chromatograms (EICs) for ω -glucosyl-*O*-hexadecanoic acid (ω -*O*-Glc-16:0, [M-H]⁻ 433.281) and 12-*O*-Glc-JA ([M-H]⁻ 387.116) are shown in Figure 4-7.

All tested enzymes used ω -OH-16:0 as substrate, at least to a limited extent. The product ω -*O*-Glc-16:0 elutes at 5.8 min. It is formed in different amounts by UGT76E12 (100 %), UGT76E2 (70 %), UGT74F1 (15 %), UGT76E1 (10 %), and only trace amounts by UGT76E11 (Figure 4-7A). Next, the UGTs were tested towards 12-OH-JA. The product 12-*O*-Glc-JA elutes at 3.3 min. Here, the highest activity is depicted by UGT76E2 (100 %), UGT76E1 and UGT76E12 shows 65 %, and UGT76E11 illustrates trace amounts of product. UGT74F1 shows no product signal (Figure 4-7B).

In summary, the activity assay uncovers enzymatic activity of all five UGTs towards the substrate ω -OH-16:0 (for UGT76E11, at least to a minor extent). The reaction serves as positive control for enzymatic activity in the following. 12-OH-JA was used as substrate by UGT76E2,

UGT76E1, and UGT76E12. These enzymes form 12-*O*-Glc-JA *in vitro* and, likewise, can be classified as 12-OH-JA UDP-glycosyltransferases.

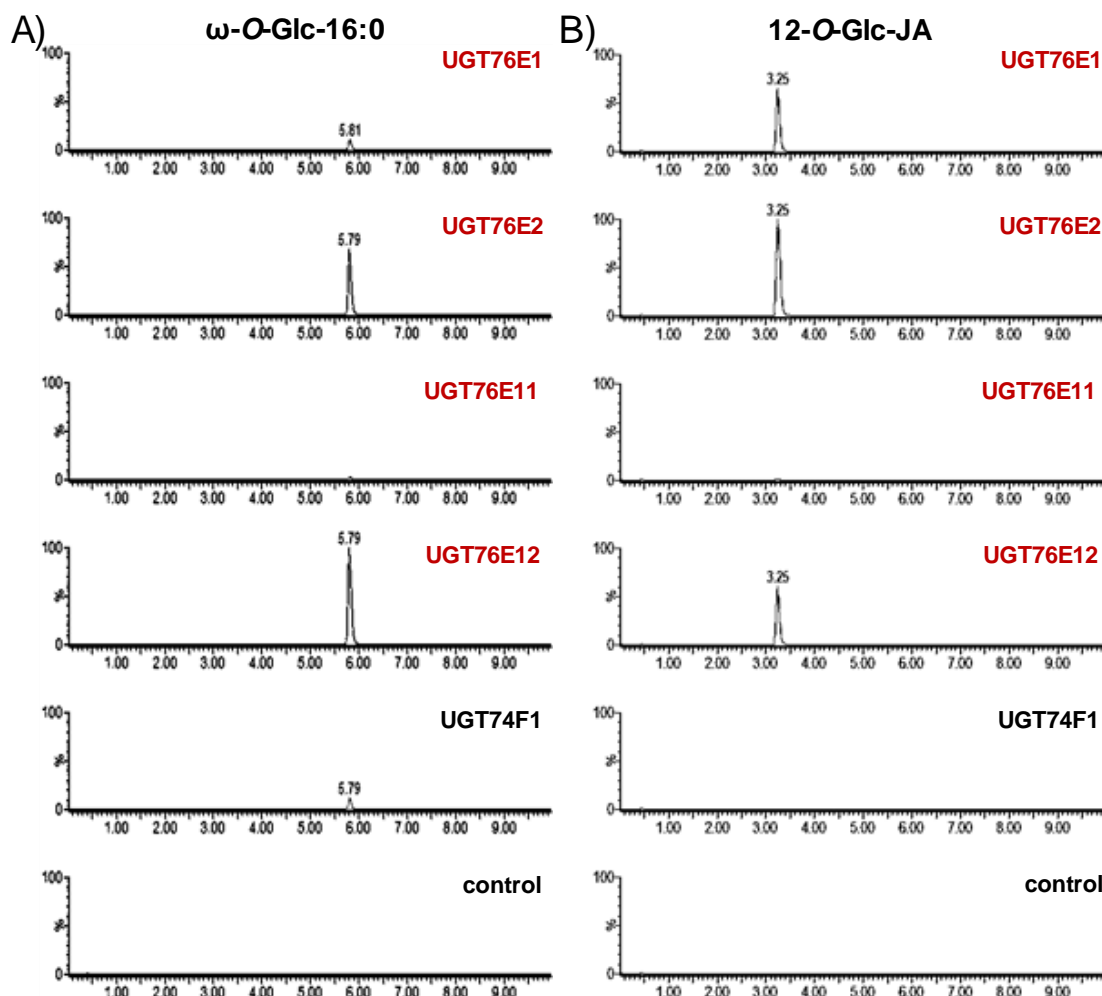


Figure 4-7: LC-MS based activity assays of UGT76E1, UGT76E2, UGT76E11, UGT76E12, and UGT74F1 with ω -OH-hexadecanoic acid and 12-hydroxy-JA as substrates

Activity tests of homogeneous UGT76E1, UGT76E2, UGT76E21, UGT76E12, UGT74F1, and inactivated UGTs as negative control were performed with 0.1 mM ω -hydroxy-hexadecanoic acid or 12-hydroxy-JA and 0.5 mM UDP-Glc for 1 h at 25 °C. The reactions were stopped by adding 25 μ L acetonitrile and analyzed by LC-MS. Extracted ion chromatograms (EICs) are shown for the products **A)** ω -glucosyl-*O*-hexadecanoic acid (ω -*O*-Glc-16:0, [M-H]⁻ 433.281) and **B)** 12-*O*-glucosyl-JA (12-*O*-Glc-JA, [M-H]⁻ 387.116). Y-Axes are scaled to the highest product signal (100 %). Data represent a single experiment. Measurements were performed by Dr. Kirstin Feussner (University of Goettingen, Germany).

To obtain information about the side of glycosylation (at the hydroxyl or the carboxy group of 12-OH-JA), the product of the UGT76E2-reaction with 12-OH-JA (see above) was analyzed and compared to an authentic standard of 12-*O*-Glc-JA (kindly provided by Dr. Otto Miersch, University of Halle/Wittenberg, Germany) by MS/MS analyses. The LC-MS analysis of the enzymatic product shows two signals in the total ion chromatogram (TIC). The second signal could be assigned to the substrate 12-OH-JA. The first signal at 3 min shows the same RT as the

standard (Figure 4-8A, C). Both signals share the m/z of $[M-H]^-$ 387.116 and are identical in respect to their fragmentation patterns. All major fragments could be assigned to 12-*O*-Glc-JA including the analytical fragment of m/z 207.101, which derives from the neutral loss of the Glc-moiety and m/z 59.013, which is specific for the α -carboxy group of jasmonates (Figure 4-8B, D, E). Therefore, 12-*O*-Glc-JA could be unequivocally confirmed as the product of the UGT76E2, UGT76E1 and UGT76E12 catalyzed reaction with 12-OH-JA.

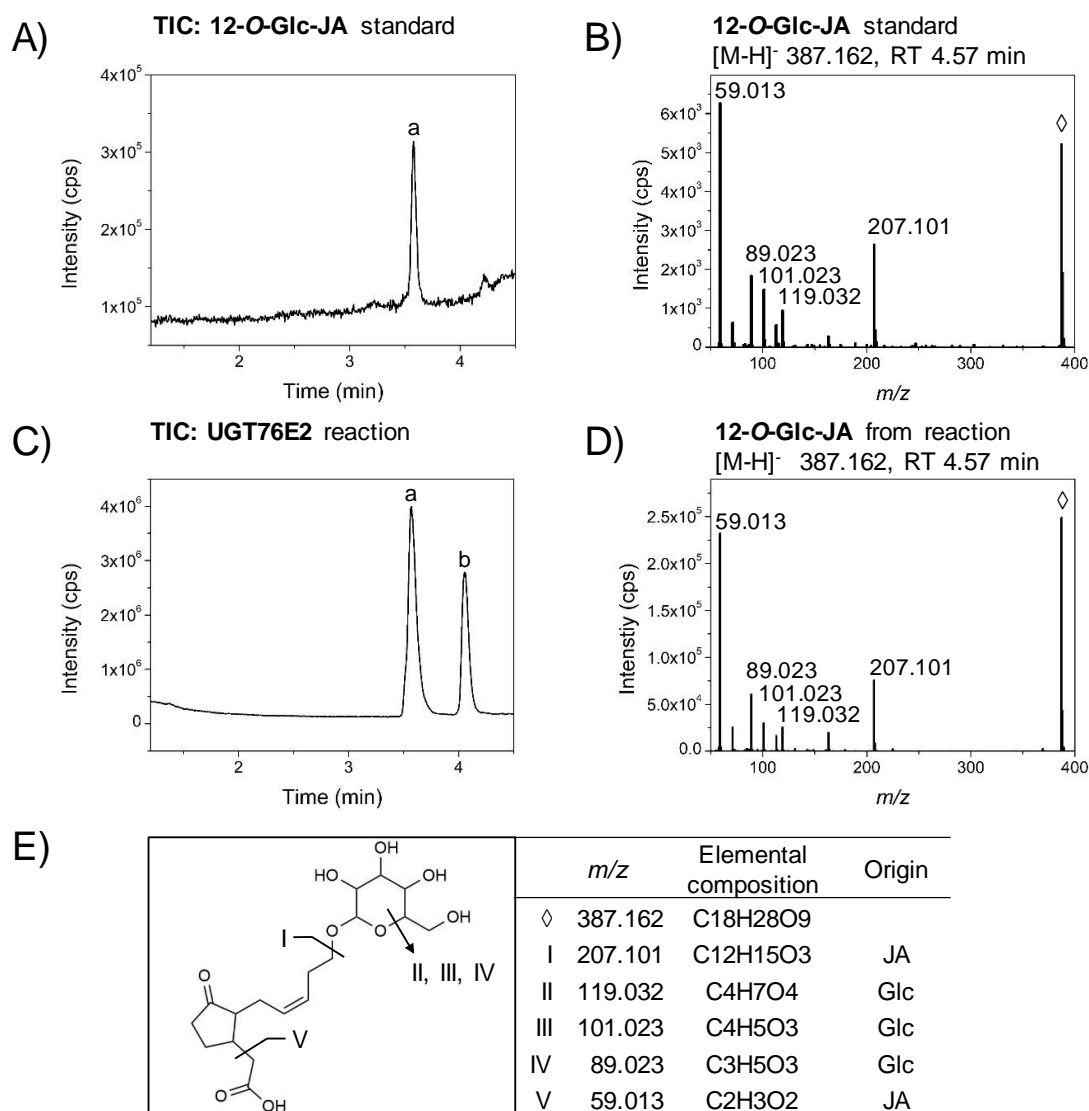


Figure 4-8: Structure confirmation of 12-*O*-glucosyl-JA

An authentic chemical standard of 12-*O*-glucosyl-JA was compared to the reaction product of UGT76E2 with 12-hydroxy-JA (12-OH-JA) by liquid chromatography coupled to tandem mass spectrometry (LC-MS/MS). Shown are total ion chromatograms (TICs) and the MS/MS spectra in the negative ionization mode with collision energies of 20 eV. **A)** The TIC of 12-*O*-Glc-JA standard (**a**) and **B)** the corresponding MS/MS spectrum. **C)** TIC of the *in vitro* reaction of UGT76E2 with 0.1 mM 12-OH-JA and 0.5 mM UDP-Glc (in 50 mM Tris/HCl pH 8.0, 100 mM NaCl, 1 h at 25 °C). The chromatogram shows the signals for the product 12-*O*-Glc-JA (**a**) and the substrate 12-OH-JA (**b**). **D)** MS/MS spectrum of the respective 12-*O*-Glc-JA of the enzymatic reaction. **E)** Assignment of the MS/MS-fragments to the structure of 12-*O*-Glc-JA. LC-MS/MS analysis was performed by Dr. Kirstin Feussner.

4.3.4. THE UGT ENZYMES PREFER MILD ALKALINE pH

With a common substrate in hands, UGT76E1, UGT76E2, UGT76E11, and UGT76E12 can be compared with respect to their optimal parameters. Since, UGTs are generally similar and tend to have rather broad specificities, it is important to characterize them in detail to determine their preferences. The optimal pH and temperature were determined for UGT76E1, UGT76E2, UGT76E11, and UGT76E12 with ω -OH-16:0 as substrate. The formation of ω -O-Glc-16:0 was detected by LC-MS as before. The product intensities were evaluated as relative signal intensities of the signal areas and the highest value was set to 100 %.

The optimal pH values were analyzed in the range of pH 3 to pH 11 in BRB (Britton & Robinson, 1931). UGT76E1 shows two maxima at pH 7 and pH 9 (Figure 4-9A). UGT76E2 displays one optimum at pH 7.5 (Figure 4-9B). UGT76E11 and UGT76E12 show their optimum at pH 8. (Figure 4-9C, D). The pH optima of all four UGTs are rather similar with mild alkaline values of pH 7.0 – 8.0.

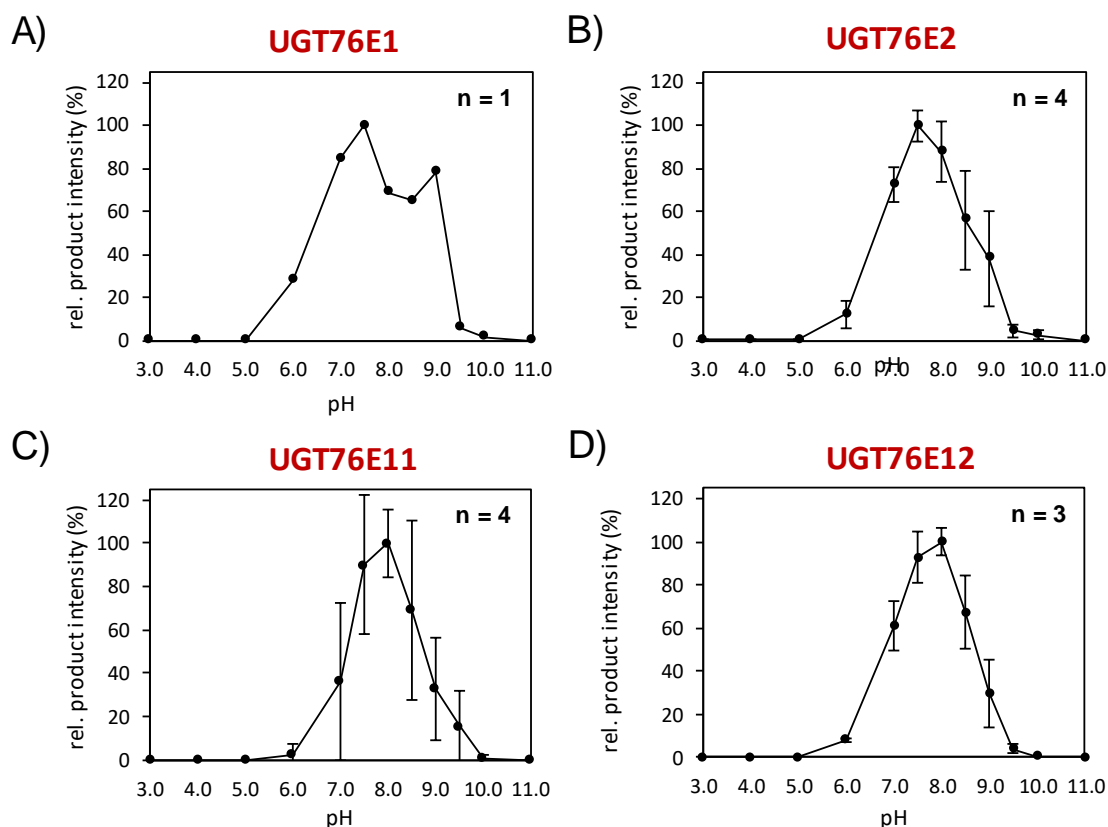


Figure 4-9: Optimum pH of UGT76E1, UGT76E2, UGT76E11, and UGT76E12

pH optima for the indicated UGTs were determined in the range of pH 3 to pH 11 in the Britton-Robinson buffer system. 0.1 mM ω -hydroxy-hexadecanoic acid and 0.5 mM UDP-Glc were incubated with enzyme at 25 °C for 1 h. The product formation was detected by LC-MS and shown as relative signal intensities (%). **A)** UGT76E1. **B)** UGT76E2. **C)** UGT76E11. **D)** UGT76E12. Data represents one experiment for UGT76E1. All other measurements are means with \pm SD of at least three independent experiments.

The optimal temperatures of the UGTs were determined from 4 °C to 50 °C. UGT76E1 shows enzymatic activity (> 20 %) between 4 – 35 °C with an optimum at 20 °C. UGT76E2 shows activity between 15 – 42 °C and an optimum at 30 °C. UGT76E11 and UGT76E12 show enzymatic activity between 10 – 42 °C but with different optima – UGT76E11 at 25 °C and UGT76E12 at 30 °C (Supplemental figure 11).

4.3.5. UGT76E1 AND UGT76E2 SHOW SUBSTRATE PREFERENCE FOR 12-OH-JA

UGT enzymes tend to have rather broad substrate specificities (Bowles *et al.*, 2006). Hence, it is necessary to test the specificities of the four UGTs with different substrates and compare their reaction performance. Therefore, a radioactive approach was established using ¹⁴C-labeled co-substrate. The radioactive carbons are incorporated into the Glc moiety of the UDP-Glc. The UGTs transfer the ¹⁴C(U)-Glc moiety of the UDP-Glc onto the substrate. Like this, every reaction turnover produces the same signal intensity independently of the used substrate and the signal intensities of generated products can be compared to each other.

The substrate specificities of the UGT76E1, UGT76E2, UGT76E11, UGT76E12, and UGT74F1 were analyzed towards a set of different tentative substrates with different functional groups. Some of which harbored a carboxy group, some a hydroxy group, and other both. Hereby, the specificity of the UGTs towards forming GE- or Glc-products can be investigated. One sub-set included fatty acid derived compounds with a chain length of 16 carbons and without or with a hydroxy group at different positions, like hexadecanoic acid (16:0), ω -OH-16:0, 2-hydroxy-16:0 (2-OH-16:0), 3-hydroxy-16:0 (3-OH-16:0). Additionally, a fatty alcohol with a chain length of 16 carbons was used (hexadecanol (OH-C16)). This first set has developed from the activity towards ω -OH-16:0 and evaluates if the carboxy, the hydroxy group, both, or the position of the hydroxy group are essential for catalysis. A second group contained plant hormones and signal compounds as SA, pipelic acid (Pip), ICA, ABA, zeatin, and GA. In addition, BA was included to discriminate against the hydroxy group of SA. This second set arose from the different activities of characterized UGTs towards small aromatic molecules (Lim *et al.*, 2002) and will question a physiological specificity of the UGTs towards some phytohormones. However, the focus was given to a third set of JA-precursors and jasmonates including 12-OPDA, JA, 12-OH-JA, 11-hydroxy-JA (11-OH-JA), 12-hydroxy-JA-methyl ester (12-OH-JA-ME). Here again, structural elements like a free or shielded carboxy group, the presence and position of a hydroxy group and the length of the C-terminus were investigated. Lastly, a fourth set of flavonoids contained quercetin, dihydro-myricetin (dh-myricetin), and dihydro-kaempferol (dh-kaempferol). These substrates can be glycosylated at different positions and have been used for broad activity tests before (Lim *et al.*, 2004). A control was performed with heat-inactivated enzyme. For analysis, the reaction products were extracted with n-butanol (*cf.* Huang *et al.*, 2015; Suzuki *et al.*, 2007) and separated by TLC (*cf.* Augustin *et al.*, 2012). Here, all samples of one UGT were run together

and treated equally. Hence, all product signals of one enzyme towards all substrates can be compared to each other qualitatively.

Noticeable, this assay pointed out side activities of UGT76E12 towards the alcohol-solvent ethanol (Supplemental figure 12). Thus, all substrates were dissolved in ACN. Finally, 20 aglycones with different structural properties were tested with the UGTs (Supplemental table 2).

UGT76E1 illustrates low signal intensities but a clear preference for 12-OH-JA (100 %). Minor activities were detected towards ω -OH-16:0 (38 %), and zeatin (23 %). All three substrates share aliphatic chains with terminal hydroxy groups. In addition, 12-OH-JA and ω -OH-16:0 contain a carboxy group whereas zeatin includes a purine (see Supplemental table 2). UGT76E2 shows similar preferences with higher intensities. The highest product signal is seen for 12-OH-JA (100 %). This enzyme also tolerated 11-OH-JA and 12-OH-JA-ME (both 13 %) as well as ω -OH-16:0, 3-OH-16:0, and zeatin (all appr. 7 %). Here, the exact ω -terminal position of the hydroxy group seems to be less important and UGT76E2 tolerates the methylated carboxyl group of 12-OH-JA-ME as well (see Supplemental table 2). In the case of UGT76E11, the signal intensities are too low to judge them as enzymatic activities. On top of this, no clear specificity or preference can be derived from those signals. For UGT76E12, the highest activities are displayed for ω -OH-16:0 (100 %), dh-kaempferol (63 %), 12-OH-JA (38 %), and quercetin (25 %). Here, UGT76E12 showed dual specificity for the terminal hydroxy group of ω -OH-16:0 and 12-OH-JA as well as for polyphenolic compounds like dh-kaempferol and quercetin (see Supplemental table 2). The control, UGT74F1, shows high product formation with its native substrate SA (100 %). Additional products were formed with BA, ω -OH-16:0, ICA, 12-OPDA, 12-OH-JA, and 11-OH-JA (all 6 %, Figure 4-10). Interestingly, UGT7674F1 displays side-activity towards substrates featuring a carboxy group, but no hydroxyl group (BA, ICA, 12-OPDA, JA, see Supplemental table 2).

Altogether, UGT76E1 and UGT76E2 specifically glycosylate 12-OH-JA with a high specificity and they do not use JA or 12-OH-JA-ME. UGT76E12 displays the highest activity towards ω -OH-16:0 but neither the respective FA nor the fatty alcohol. All three, UGT76E1, UGT76E2 and UGT76E12 prefer substrates featuring both, a terminal hydroxy group and a carboxy function. Thereby, the hydroxy group is necessary but not sufficient for catalysis. Although this experiment cannot distinguish between a glucose ester and a glycoside being formed, the structure analysis has confirmed the glycoside of 12-*O*-Glc-JA (see Figure 4-8). Hence, it is likely that glycosidic products are also formed in this experiment and the additional carboxy group assists catalysis. For UGT76E11 however, the evaluation of the activity and specificity was not possible in this experiment.

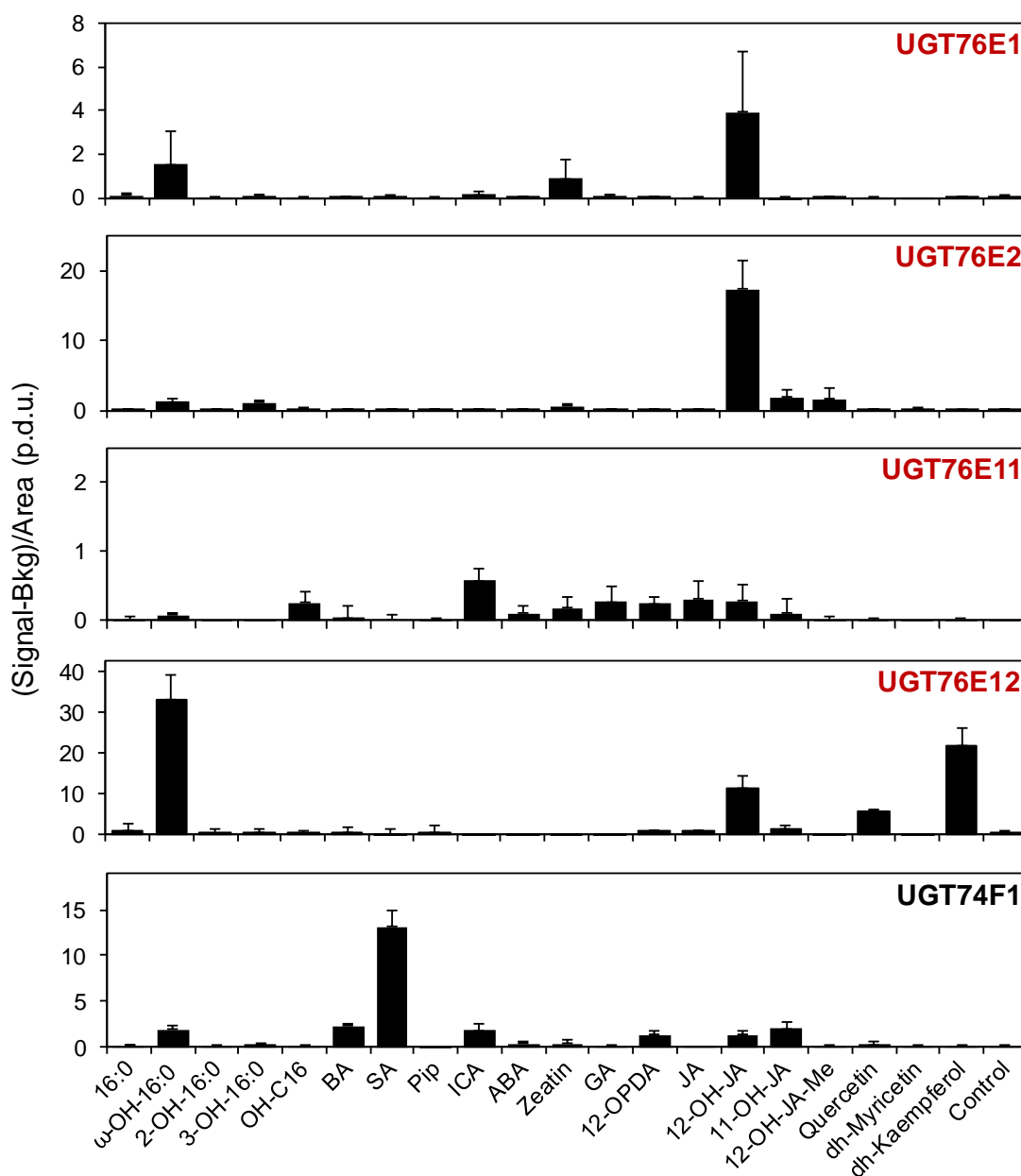


Figure 4-10: Substrate specificity of UGT76E1, UGT76E2, UGT76E11, UGT76E12, and UGT74F1

The substrate specificities of the UGTs were analyzed by an activity assay with ^{14}C -labeled UDP-Glc (UDP- ^{14}C (U)-Glc) and the indicated substrates. The assay was performed in the respective gel filtration buffer with 0.06 mM substrate, 0.03 mM UDP-Glc, 0.02 μCi UDP- ^{14}C (U)-Glc for 1 h at 25 $^{\circ}\text{C}$. After metabolite extraction and thin layer chromatography (TLC), the TLC-plates were incubated on phosphor screens for 3 d and the radioactive signals were detected. Given are product signals minus background over signal area ((Signal-Bkg)/Area). UGT76E1, UGT76E2, UGT76E11, UGT76E12, and UGT74F1 were incubated with a set of different aglycones: hexadecanoic acid (16:0), ω -hydroxy-16:0 (ω -OH-16:0), 2-hydroxy-16:0 (2-OH-16:0), 3-hydroxy-16:0 (3-OH-16:0), hexadecanol (OH-C16), benzoic acid (BA), salicylic acid (SA), pipercolic acid (Pip), indole-3-carboxylic acid (ICA), abscisic acid (ABA), zeatin, gibberellic acid (GA), 12-oxo-phytodienoic acid (12-OPDA), JA, 12-hydroxy-JA (12-OH-JA), 11-hydroxy-JA (11-OH-JA), 12-hydroxy-JA-methyl ester (12-OH-JA-Me), quercetin, dihydro-myricetin (dh-myricetin), dihydro-kaempferol (dh-kaempferol), and a control with inactivated enzyme (control). The data shows means of 3 independent experiments + SE for every UGT.

4.3.6. HOMOGENOUS ENZYMES CAN BE BROUGHT BACK TO THEIR NATIVE SUBSTRATES

Besides single reactions (see 4.3.5), it is important to bring the UGTs in contact with a mixture of different substrates that may be available – like in a living cell. A new approach, which analyzes the enzymes in their native substrate environment, was adapted to the requirements of the four UGTs. To achieve this, enzyme biochemistry was combined with metabolomics; homogenous proteins were incubated with a metabolite rich extract from *A. thaliana* and measured with the non-targeted metabolite fingerprinting platform (Kaefer, 2014). Differential analyses of metabolite rich extracts with and without enzyme can hereby identify specific reaction partners from a natural substrate mixture.

12-OH-JA-Ile may a putative jasmonate substrate of the UGTs since Kitaoka and co-workers, 2014, have found 12-*O*-Glc-JA-Ile in wounded *A. thaliana* (Kitaoka *et al.*, 2014). So far, 12-OH-JA-Ile could not be investigated by the former *in vitro* activity assays (see Figure 4-10) because the compound was not available. At the same time, it is well known that 12-OH-JA-Ile accumulates in response to wounding *in vivo* (Figure 4-18E) (Bruckhoff *et al.*, 2016). Therefore, the biological material of a wounding experiment (see Figure 4-18) was used to provide substrates like 12-OH-JA and 12-OH-JA-Ile and mimic the native environment (see 4.1.3). Due to comprehensibility, attention was given to 2 hpw. At this time point, the substrate availability was best for UGT-activity towards jasmonates: 12-OH-JA and 12-OH-JA-Ile have accumulated and internal abundance of 12-*O*-Glc-JA is still low (Supplemental figure 14, see Figure 4-18).

Nevertheless, the *ex vivo* fingerprinting approach entails several variables due to the complexity of the system. For this reason, different controls were taken to distinguish between enzymatic activities and internal plant metabolites. On the one hand, a negative control (heat-inactivated enzyme) was used to determine substrates and internal features. On the other hand, a positive control was performed to inspect product formation by spiking known substrates into the reaction solutions. Both controls together were thought to provide strong substrate/product patterns to prove the activity of the UGTs and to confirm the existence of the respective substrates. Altogether, the experiment used metabolite rich plant extracts after wounding (2 hpw) including potential jasmonates substrates (12-OH-JA and 12-OH-JA-Ile) that were dissolved in protein buffer (50 mM Tris/HCl, pH 8, 100 mM NaCl). The extracts were incubated (1 h, 25 °C) with 100 µg homogenous UGTs or inactive enzymes (negative control) and 0.1 mM UDP-Glc as general co-substrate. A second set of reaction was performed as positive control with additional substrates spikes into the reactions. Afterwards, both sets were measured with the non-targeted LC-MS analysis and data were processed with the MarVis-tool (Kaefer, 2014). This tool filters features from all reactions by their statistical distribution, clusters them by similar abundances, and identifies them by databank comparisons. The graphical output represents mean intensities of

the features (heat-map representation), which were clustered as one-dimensional self-organizing map (1D-SOMs).

The data of the *ex vivo* metabolite fingerprinting approach for UGT76E1, UGT76E2, UGT76E11, UGT76E12 and UGT74F1 and the controls are given as 1D-SOM with vertical clusters illustrating feature-intensities for every enzyme and the neg. control (horizontal). Globally, both reaction sets of the internal reactions and the positive controls with additional substrates show similar accumulations. The Clusters 1 – 5 are dominated by patterns specific for UGT76E1. Meaning, features in these clusters are accumulating in samples incubated with UGT76E1. Clusters 6 – 10 show specific patterns for different enzymes: cluster 6 sums up features, which could represent products of UGT76E11, cluster 7 summarizes a pattern of tentative UGT76E1-product, cluster 9 is connected to tentative products of UGT76E12, and cluster 10 represents UGT74F1-related features. The majority of features in clusters 11 – 18 seems neither to be related to tentative products nor substrates of the five UGTs. Clusters 19 and 20 show features specific for the additional substrates of the positive controls (Figure 4-11).

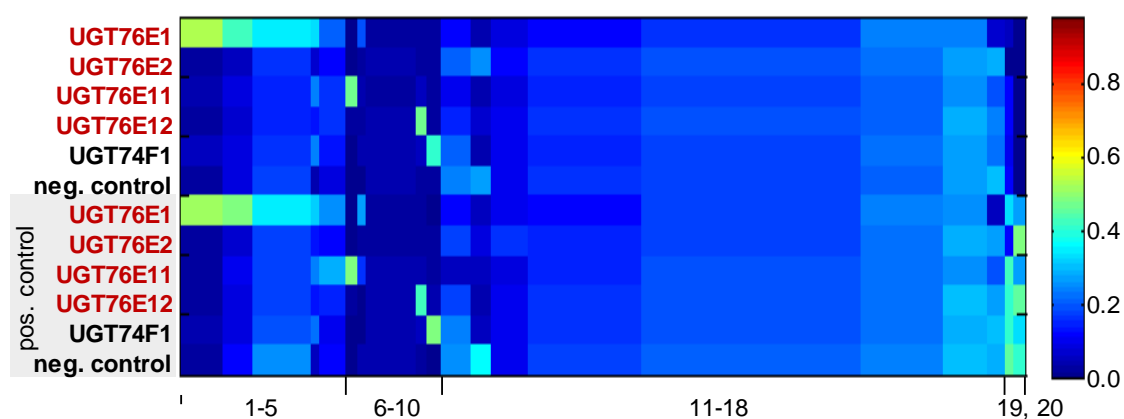


Figure 4-11: Search for native substrates of UGT76E1, UGT76E2, UGT76E11, UGT76E12, UGT74F1 by non-targeted *ex vivo* analysis

For the enzymatic assay with the indicated UGTs total metabolite extracts of wounded *A. thaliana* plants were used. Therefore, plants were grown for six weeks at 22 °C under short day conditions (8 h light/16 h dark). Leaves were wounded three times across the mid vein by squeezing with forceps. Damaged rosette leaves were harvested at 2 hours post wounding (pool of 10 plants per sample), extracted by two-phase-extraction, and used as substrate mix for the *ex vivo* activity assay. The extracts were resolved in 50 mM Tris pH 8, 100 mM NaCl buffer and incubated with 0.1 mM UDP-Glc and 100 µg of the indicated active UGT-enzyme or inactive enzymes (neg. control). As positive control (highlighted in grey), 0.01 mM salicylic acid, ω-hydroxy-hexadecanoic acid, and 12-hydroxy-JA were added to the mixtures. Reactions were incubated at 25 °C for 1 h, stopped by adding acetonitrile and analyzed by LC-MS-based metabolite fingerprinting. 1996 metabolite features ($p\text{Val} < 10^{-6}$) were selected and their intensity profiles were clustered by means of one-dimensional self-organizing maps (1D-SOMs). Shown is the heat map representation of the clustering process by using 20 clusters. The number of features per cluster is proportional to the cluster-width. The data represents three measurements of one experiment that are representative for two independent experiments. Samples were measured by Dr. Kirstin Feussner (University of Goettingen, Germany). Experiment was designed and performed together with Dr. Kirstin Feussner. Data were analyzed with the MarVis tool (Kaefer, 2014).

To streamline the extraction of tentative substrates and products out of the 1996 features of the *ex vivo* data set three criteria for data analysis were established. Tentative pairs of product and substrate are characterized by: (i) an exact mass difference of a Glc moiety (162.016 Da), (ii) a RT-shift of the more hydrophilic product in comparison to the substrate and (iii) inverse intensity pattern to each other.

4.3.7. UGT76E1, UGT76E2, UGT76E12, AND UGT74F1 SHOW ACTIVITY TOWARDS THEIR KNOWN SUBSTRATES

The patterns of the positive controls were used to evaluate the activities of the UGTs and support former findings in a concurrence situation. The substrates ω -OH-16:0, 12-OH-JA and SA were spiked with 10 μ M each into every reaction of the positive controls. Features of both, the spiked substrates and the respective products, were identified in accordance to the three criteria defined above (Figure 4-12). First, SA could be detected in all samples besides those incubated with UGT74F1; UGT74F1 used up SA completely. The levels of the corresponding product, 2-*O*-Glc-SA, are increased 2-fold in UGT76F1-treated samples exclusively. All other samples show 2-*O*-Glc-SA levels, which are similar to the negative control and seem to be natural amounts of 2-*O*-Glc-SA in the *A. thaliana* extracts 2 hpw. The substrate ω -OH-16:0 was used as a control reaction for all UGTs. The amounts of ω -OH-16:0 are reduced in UGT76E1-, UGT76E11-, UGT76E12-, and UGT74F1-treated samples compared to the negative control. On the product level, UGT76E12-treated samples shows the highest intensity of ω -*O*-Glc-16:0. UGT76E1, UGT76E2, and UGT74F1 illustrate similar product intensities about half of that of UGT76E12. The lowest activity is given by UGT76E11 with 1/5 of the maximal value. For 12-OH-JA, UGT76E1- and UGT76E2-treated samples show reduced amounts of the substrate with stronger reduction in the UGT76E2-samples. In accordance to that, UGT76E2-treated samples show the highest amount of the product 12-*O*-Glc-JA, followed by UGT76E1-treated samples and, to a much lower extent, UGT76E12-treated samples (Figure 4-12).

The positive controls of the *ex vivo* experiment confirm the specific activities of the UGTs in a concurrence situation and reflect the activity levels of previous experiments. Moreover, the three criteria for identifying activities for the indicated enzymes could be evaluated with specific substrate and product couples.

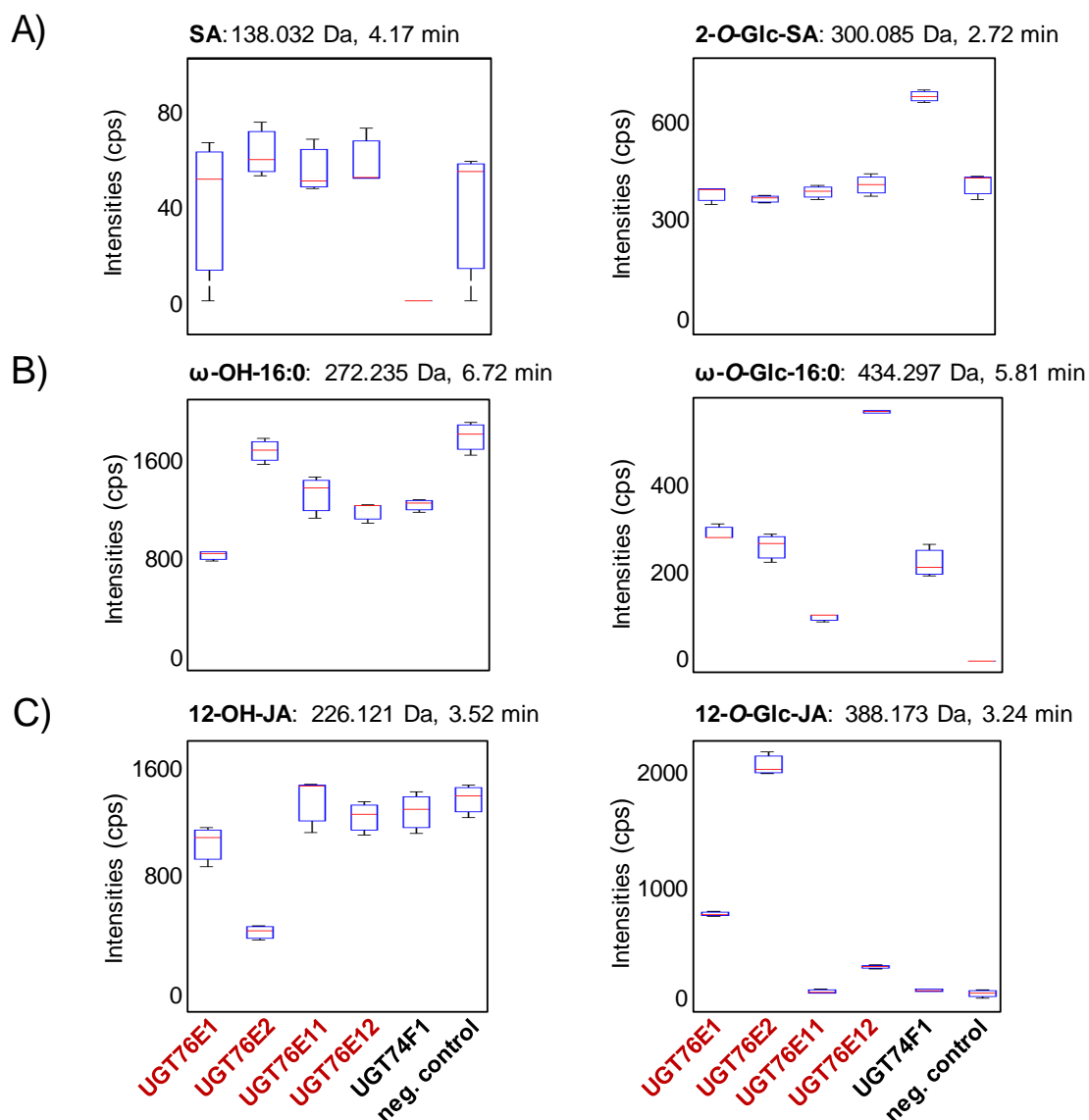


Figure 4-12: Activity of UGT76E1, UGT76E2, UGT76E11, UGT76E12, and UGT74F1 for 12-hydroxy-JA, salicylic acid, and ω -hydroxy-hexadecanoic acid in total metabolite extracts

For the enzymatic assays, total metabolite extracts of wounded *A. thaliana* plants were used. The indicated compounds were added as substrates and used as positive control for the *ex vivo* approach. Plants were grown for six weeks at 22 °C under short day conditions (8 h light/16 h dark). Leaves were wounded three times across the mid vein by squeezing with forceps. Damaged rosette leaves were harvested at 2 hours post wounding (pool of 10 plants per sample), extracted, and used as substrate mix for the *ex vivo* activity assay. The extracts were resolved in 50 mM Tris pH 8, 100 mM NaCl buffer and the assay was performed with 0.1 mM UDP-Glc, 0.01 mM salicylic acid, 0.01 mM ω -hydroxy-hexadecanoic acid, and 0.01 mM 12-hydroxy-JA, 100 μ g of the indicated active UGT-enzyme or inactive enzyme (neg. control) for 1 hour at 25 °C. The reactions were stopped by adding acetonitrile and analyzed by LC-MS with a method, which was developed for non-targeted fingerprinting. Out of 1996 metabolite features with a p Val < 10^{-6} the particular features for A) salicylic acid (SA) and 2-*O*-glucosyl-SA (2-*O*-Glc-SA), B) ω -hydroxy-hexadecanoic acid (ω -OH-16:0) and ω -*O*-glucosyl-16:0 (ω -*O*-Glc-16:0), and C) 12-hydroxy-JA (12-OH-JA) and 12-*O*-glucosyl-JA (12-*O*-Glc-JA) are shown as Box-Whisker-plots with intensities given as counts per second (cps). The data represents three technical replicates of one experiment. Samples were measured by Dr. Kirstin Feussner (University of Goettingen, Germany). Experiment was designed and performed together with Dr. Kirstin Feussner. Data were analyzed with the MarVis tool (Kaefer, 2014).

4.3.8. UGT76E1, UGT76E2, UGT76E11, UGT76E12, AND UGT74F1 SHOW ACTIVITY TOWARDS NATIVE SUBSTRATES

The non-targeted *ex vivo* metabolite fingerprinting approach was initiated to bring back purified enzymes to their native substrate environment aiming to identify new substrates.

Two oxylipins were identified as new substrates of the four UGTs. The reaction pair of 13-HOT (276.210 Da, 6.59 min) and 13-glucosyl-*O*-octadecatrienoic acid (13-*O*-Glc-HOT, 465.274 Da, 5.65 min, Supplemental table 3) is shown in Figure 4-13A. There, UGT76E11 and UGT76E12 used up the substrate from the extracts and depict the highest product levels. UGT76E1 and UGT76E2-treated samples display half substrate levels and corresponding appr. 50 % of the highest product intensity. UGT74F1-treated samples shows negative control patterns with highest substrate intensities and no product intensities (Figure 4-13A). Furthermore, the glycosylation of (7Z9E,13Z)-11-hydroxy-7,9,13-hexadecatrienoic acid (11-HHT, 266.186 Da, 6.08 min) to 11-*O*-glycosyl-hexadecatrienoic acid (11-*O*-Glc-HHT, 428.240 Da, 5.25 min, Supplemental table 3) was identified. Here, UGT76E2, UGT76E11, and UGT76E12 form the high product levels. UGT76E1-treated samples showed about half of that activity and UGT74F1 did not tolerate this substrate with control-like intensities (Figure 4-13B). Both glycosylated oxylipins are not abundant in the extracts as indicated by the negative controls (see Figure 4-13A, B).

Next, the reaction pair of 12-OH-JA to 12-*O*-Glc-JA was also identified as native reaction with substrate from the extracts. Here, UGT76E11, UGT76E12, and UGT74F1-treated samples show highest substrate levels corresponding to the accumulation of 12-OH-JA 2 hpw. UGT76E1-treated samples illustrate slightly reduced amounts whereas UGT76E2 used up completely 12-OH-JA from the extracts. 12-*O*-Glc-JA illustrates a complementary pattern: UGT76E11, UGT74F1, and the negative control display low intensities of the glycoside as present without enzymatic activity. UGT76E12 shows 3-fold, UGT76E1 6-fold, and UGT76E2 12-fold higher product levels (Figure 4-13C).

In addition, an unknown reaction pair for UGT76E11 was identified. The substrate shows no wound-related accumulation in the leaf extracts; it is detectable at 0, 2, and 5 hpw (data not shown). The substrate feature has an exact mass of 198.126 Da, a RT of 5.47 min and a deduced sum formula of C₁₁H₁₈O₃. UGT76E11 used up the substrate exclusively forming high amounts of the corresponding product (Glc-C₁₁H₁₈O₃, 360.179 Da, RT 4.65 min). Glc-C₁₁H₁₈O₃ shows trace intensities in UGT76E1, UGT76E2, UGT76E12, UGT74F1-treated samples, and the negative control (Figure 4-13D). To obtain structural information about the compound MS/MS analyses were performed. The fragmentation of the UGT76E11-specific product (Glc-C₁₁H₁₈O₃) show a loss of a hexose moiety, which leads to the mass signal of the substrate of [M+H]⁺ 199.099 and confirms the finding of the *ex vivo* approach (Fig. 4-13). The MS/MS spectrum of the substrate (C₁₁H₁₈O₃) shows three serial losses of water, which suggests the

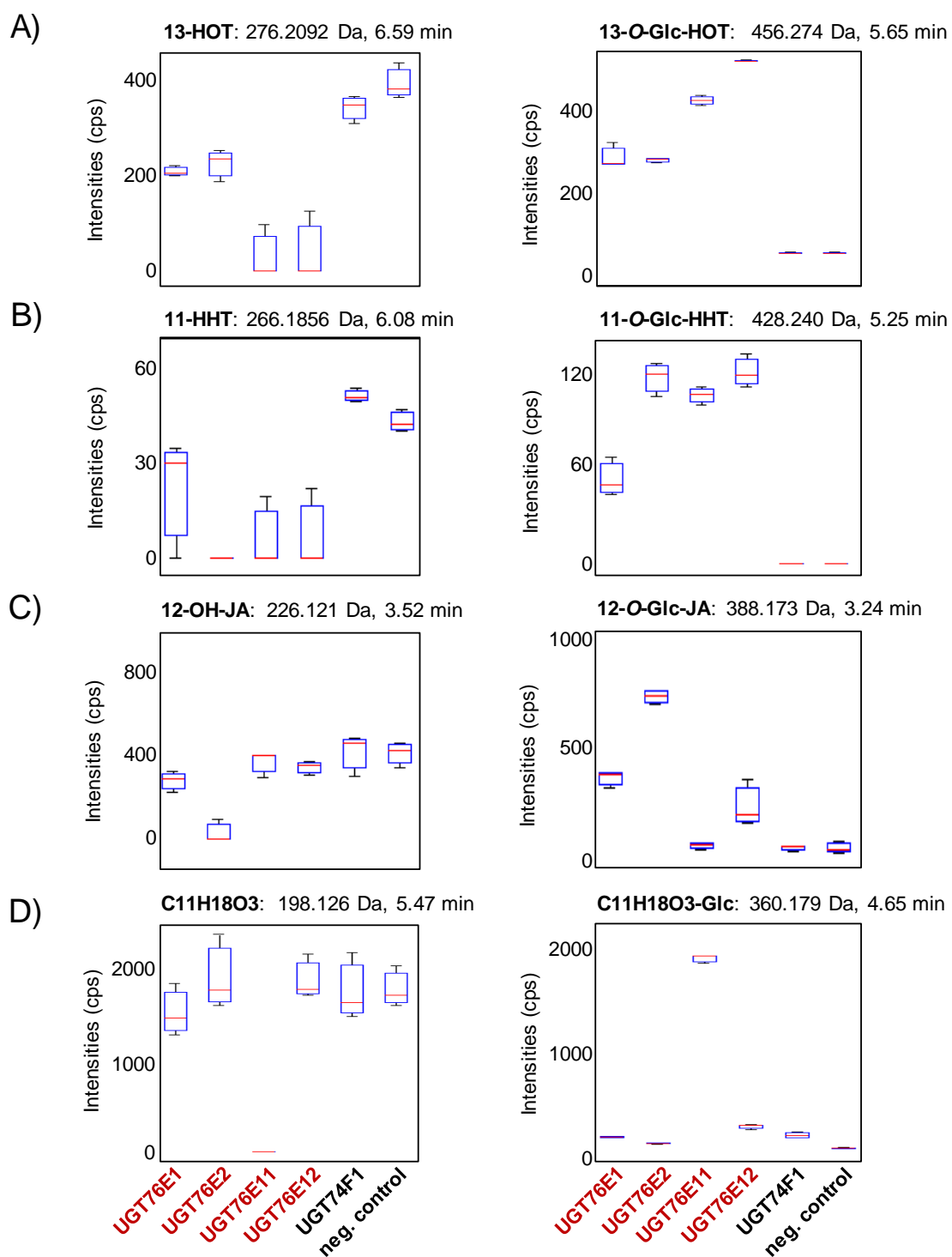


Figure 4-13: Native substrates of UGT76E1, UGT7E2, UGT76E11, UGT76E12, UGT74F1 identified by a non-targeted *ex vivo* analysis

For the enzymatic assays, total metabolite extracts of wounded *A. thaliana* plants were used. Plants were grown for six weeks at 22 °C under short day conditions (8 h light/16 h dark). Leaves were wounded three times across the mid vein by squeezing with forceps. Damaged rosette leaves were harvested at 2 hours post wounding (pool of 10 plants per sample), extracted, and used as substrate mix for the *ex vivo* activity assay. The extracts were resolved in 50 mM Tris pH 8, 100 mM NaCl buffer and the assay was performed with 0.1 mM UDP-Glc and 100 µg of the indicated active UGT-enzyme or inactive enzyme (neg. control) for 1 hour at 25 °C. The reactions were stopped by adding acetonitrile and analyzed by LC-MS with a method, which was developed for non-targeted fingerprinting. Out of 1996 metabolite features

with a $p\text{Val} < 10^{-6}$ the particular features for **A**) 13-hydroxy-octadecatrienoic acid (13-HOT) and 13-*O*-glucosyl-octadecatrienoic acid (13-*O*-Glc-HOT), **B**) 11-hydroxy-hexadecatrienoic acid (11-HHT) and 11-*O*-glucosyl-octadecatrienoic acid (11-*O*-Glc-HHT), **C**) 12-hydroxy-JA (12-OH-JA) and 12-*O*-glucosyl-JA (12-*O*-Glc-JA) and **D**) C11H18O₃ and C11H18O₃-Glc are shown as Box-Whisker-plots with intensities given as counts per second (cps). The data represents three technical replicates of one experiment. Samples were measured by Dr. Kirstin Feussner (University of Goettingen, Germany). Experiment was designed and performed together with Dr. Kirstin Feussner. Data was analyzed with the MarVis tool (Kaefer, 2014).

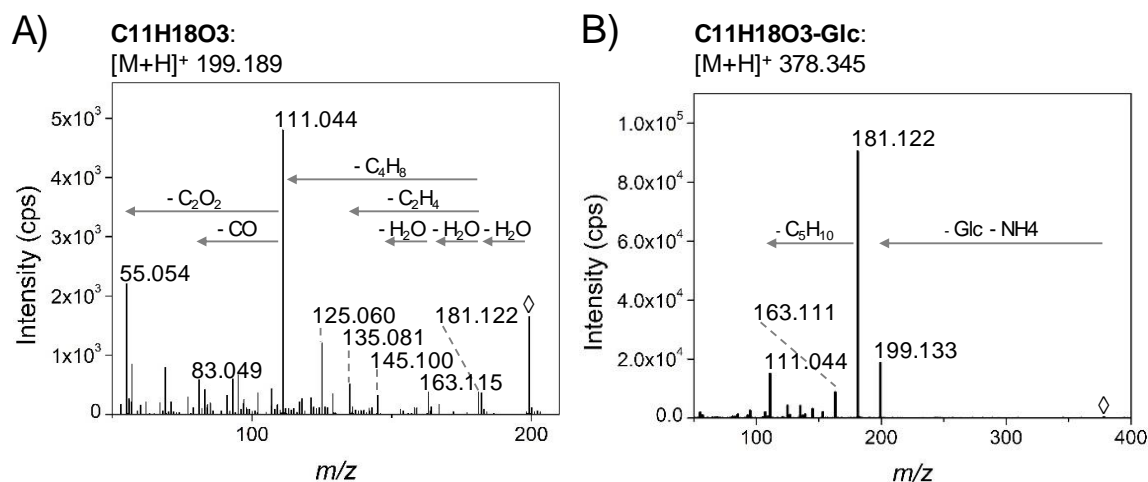


Figure 4-14: MS/MS analysis of the unknown substrate C11H18O₃

The *ex vivo* metabolite fingerprinting experiment identified a reaction pair for UGT76E11: C11H18O₃ to C11H18O₃-Glc. LC-MS/MS analysis were performed with collision energies of 12 eV in the positive ionization mode. MS/MS fragmentation of **A**) the substrate signal (C11H18O₃, [M+H]⁺ 199.099, at 6.01 min) **B**) the product signal (C11H18O₃-Glc, [M+H]⁺ 378.345 at 5.01 min). LC-MS/MS analysis was performed by Dr. Kirstin Feussner. Intensities given as counts per second (cps).

existence of three hydroxy groups. The main fragment of [M+H]⁺ 111.044 equals C₆H₇O₂. The UGT76E11-specific substrate could not be elucidated in more detail. In summary, 13-HOT, 11-HHT are new substrates for UGT76E1, UGT76E2, UGT76E11, and UGT76E12. All four enzymes formed the respective products. Furthermore, the high activity of UGT76E2 towards 12-OH-JA is supported by the *ex vivo* approach, too. In addition, UGT76E1 and UGT76E12 again show activity towards 12-OH-JA. Here, a first hypothesis for a specific, but so far not structurally elucidated substrate for UGT76E11 was generated.

4.3.8.1. 12-OH-JA-ILE IS NO SUBSTRATE FOR THE ANALYZED UGTs

Since 12-OH-JA-Ile was identified in *A. thaliana* after wounding (Kitaoka *et al.*, 2014), the potential glycosylation reaction of 12-OH-JA-Ile to 12-*O*-Glc-JA-Ile was of special interest in this study. Because 12-OH-JA-Ile was abundant in the *ex vivo* extracts after wounding (see Supplemental figure 14, *cf.* Figure 4-18E), it was likewise tested as potential substrate of the different candidate UGTs. By the criteria introduced above, a putative product was searched by the exact mass of 501.257 Da and an earlier RT than 4.9 min (12-OH-JA-Ile). However, a feature of this mass could not be identified in any of the *ex vivo* samples (see Supplemental figure 14).

Meaning, neither UGT76E1, UGT76E2, UGT76E11, UGT76E12, nor UGT74F1 tolerate 12-OH-JA-Ile for catalysis. This finding was supported by a LC-HR-MS analysis of the UGT76E2-treated sample (2 hpw) as second layer of evidence (Supplemental figure 14). Noticeably, these measurements also imply that 12-*O*-Glc-JA-Ile is not present as internal metabolite of *A. thaliana* with or without wounding stimulus here.

Worth mentioning, 12-COOH-JA was detected the first time in wounded leaves of *A. thaliana* here. Before, the metabolite has been described in flowers of *A. thaliana* exclusively (Bruckhoff *et al.*, 2016). From the metabolite rich extracts of the *ex vivo* approach, it was possible to identify the compound by exact mass and RT in the positive as well in the negative ionization mode. The pattern of 12-COOH-JA shows late wound accumulation at 5 hpw and its identity was confirmed by LC-MS/MS fragmentation (Supplemental figure 13).

4.3.9. SUBSTRATE PREFERENCES OF UGT76E1, UGT76E2, UGT76E11, UGT76E12, AND UGT74F1

So far, the characterization of the enzymes UGT76E1, UGT76E2, UGT76E11, and UGT76E12 has given clear substrate preferences but has also indicated additional (side) activities. Therefore, a LC-MS-based activity assay was performed to judge the performances. UGT76E1, UGT76E2, UGT76E11, UGT76E12, and UGT74F1 were tested with the substrates ω -OH-16:0, SA, 12-OH-JA, 9-HOT, 13-HOT. Additionally, (10*E*,15*Z*)-9,12,13-trihydroxy-10,15-octadecadienoic acid (triOH-18:2) and (10*E*)-9,12,13-trihydroxy-10-octadecaenoic acid (triOH-18:1) were included. It should be tested, if the UGTs would tolerate up to three hydroxyl-groups on a fatty acid as a substrate and if several glycosylations could be performed with one substrate molecule.

ω -OH-16:0 is preferably glycosylated by UGT76E12 (100 %). In comparison to that UGT76E2 shows 36 %, UGT76E1 9 %, UGT74F1 4 %, and UGT76E11 illustrates 2 % relative conversion rate. Similarly, both oxylipins, 9-HOT and 13-HOT, are best substrates of UGT76E12. Anyhow, 9-*O*-Glc-HOT and 13-*O*-Glc-HOT are also formed by UGT76E2 (22 %, 94 %) and UGT76E11 (5 %, 98 %). UGT76E1 produces low amounts of 13-*O*-Glc-HOT (6 %) but no 9-*O*-Glc-HOT. SA is the native substrate of UGT74F1 and 2-*O*-Glc-SA is exclusively formed by this enzyme (100 %). 12-*O*-Glc-JA is formed from 12-OH-JA by UGT76E2 (100 %), UGT76E1 (29 %), and UGT76E12 (28 %). The tri-hydroxy fatty acids were detected in the samples but neither mono-, di-, nor tri-glycosylated products could be identified for any of the enzymes (Table 4-4).

Altogether, the evaluation of the substrate preferences supports the specificities and tolerances observed before: UGT76E2 glycosylates preferentially 12-OH-JA. In addition, it uses 13-HOT with a high relative conversion rate as well as ω -OH-16:0 and 9-HOT to lower extent. UGT76E1 forms 12-*O*-Glc-JA very specifically, but with a lower conversion rate as UGT76E2. UGT76E12 shows broader substrate tolerance with highest activities towards the hydroxyl fatty acids and to

a lower extent with 12-OH-JA. UGT76E11 depicts high relative conversion rates with 13-HOT. None of the candidates tolerated tri-hydroxy-oxylipins as substrates.

Table 4-4: Relative substrate preference of UGT76E1, UGT76E2, UGT76E11, UGT76E12, and UGT74F1

Substrates so far identified for UGT76E1, UGT76E2, UGT76E11, UGT76E12, and UGT74F1 are evaluated by an *in vitro* assay. The relative conversion rate (%) was analyzed by LC-MS: ω -hydroxy-hexadecanoic acid (ω -OH-16:0), salicylic acid (SA), 12-hydroxy-JA (12-OH-JA), 9-hydroxy-octadecatrienoic acid (9-HOT), 13-hydroxy-octadecatrienoic acid (13-HOT). In addition, 9,12,15-trihydroxy-octadecadienoic acid (tri-OH-18:2) and 9,12,13-trihydroxy-octadecaenoic acid (tri-OH-18:2) were tested as substrates. In a 100 μ L reaction assay, 10 μ g homogenous enzyme were incubated with 0.05 mM substrate and 0.25 mM UDP-Glc at 25 °C for 30 min. The reactions were stopped with 100 μ L ACN. n. d., not detected. The data are representative for one experiment.

Substrate	UGT76E1	UGT76E2	UGT76E11	UGT76E12	UGT74F1
ω -OH-16:0	9	36	2	100	4
SA	n. d.	n. d.	n. d.	n. d.	100
12-OH-JA	29	100	n. d.	28	n. d.
9-HOT	n. d.	22	5	100	n. d.
13-HOT	6	94	98	100	n. d.
Tri-OH-18:1	n. d.	n. d.	n. d.	n. d.	n. d.
Tri-OH-18:2	n. d.	n. d.	n. d.	n. d.	n. d.

4.3.10. THE KINETIC PARAMETERS OF UGT76E1, UGT76E2, UGT76E11, AND UGT76E12 WERE ESTIMATED BY A COUPLED PHOTOMETRIC

A continuous record of an enzymatic reaction allows determining the initial linear phase, a so-called steady-state kinetic. The initial velocity of a reaction is often measured by a spectrophotometric assay. Since the compounds of the UGT-reaction do not change their photometrical properties upon catalysis, the reaction was coupled to a redox reaction, which includes nicotinamide adenine dinucleotide (NADH/NAD⁺) as reaction partner. In particular, UGTs release UDP as co-product, which (*cf.* Reaction 1) can be linked to pyruvate kinase (PK) and lactate dehydrogenase (LDH) to record the UGT reaction kinetics in 1 : 1 : 1 stoichiometry. The PK natively phosphorylates ADP to ATP by metabolizing phosphoenolpyruvate (PEP) to pyruvate. However, it is also capable to phosphorylate UDP to UTP. Next, LDH catalyzes the reduction of pyruvate to lactate by oxidizing NADH to NAD⁺. NADH shows an absorption maximum at 340 nm, which NAD⁺ does not. (Figure 4-15). Hence, the UGT reaction is indirectly monitored by the decrease of the absorption of NADH at 340 nm and the reaction velocities can be determined from the initial slope (Figure 4-15, Equation 5) (*cf.* Brown *et al.*, 2012). Like this, the steady-state kinetics of UGT76E1, UGT76E2, UGT76E11, and UGT76E12 were determined towards 9-HOT and 13-HOT. Additionally, UGT76E1 and UGT76E2 were measured with their preferred substrate 12-OH-JA. Due to limitations in the availability of 12-OH-JA, the kinetic

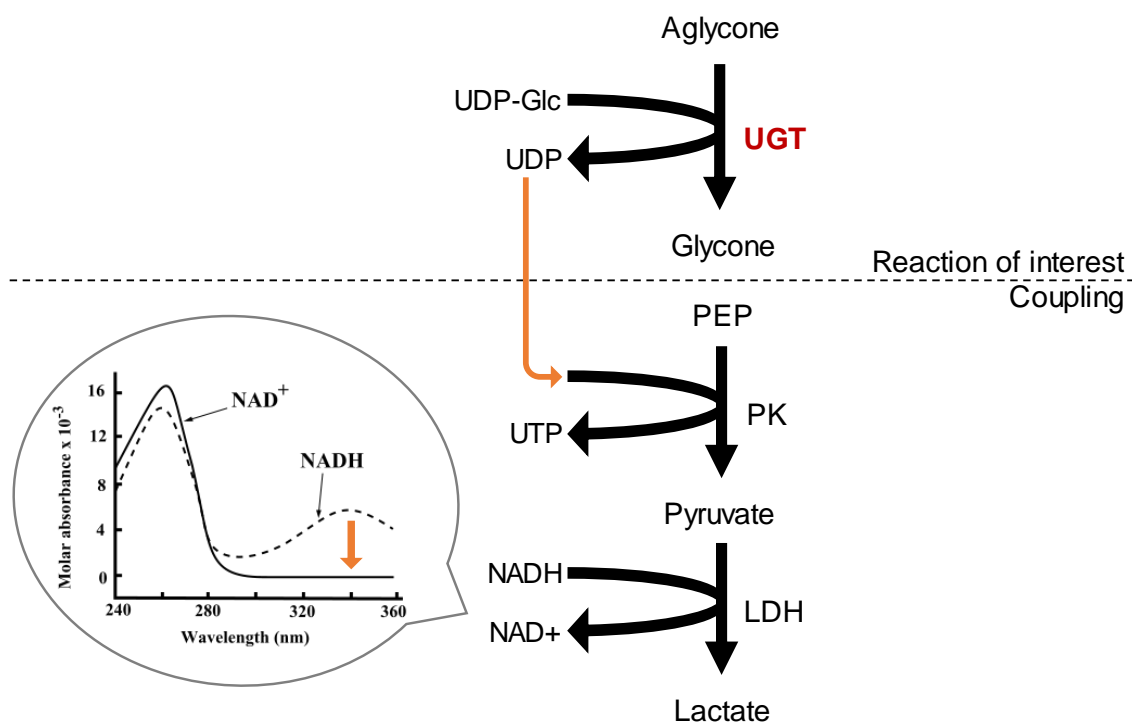


Figure 4-15: Scheme of a coupled spectrophotometric assay to record reactions of uridine diphosphate-dependent glycosyltransferases

Uridine diphosphate (UDP)-dependent glycosyltransferases (UGTs) transfer a glucose (Glc) moiety from UDP-Glc to the hydroxyl-aglycone releasing the respective glycone and UDP. The UGT-reaction has been coupled via the co-product UDP to the pyruvate kinase (PK) and the lactate dehydrogenase (LDH) to record the UGT reaction kinetics in 1 : 1 : 1 stoichiometry: The PK phosphorylates UDP to UTP while metabolizing phosphoenolpyruvate (PEP) to pyruvate. LDH catalyzes the reduction of pyruvate to lactate by oxidizing NADH to NAD⁺, which shows no absorption maximum at 340 nm. The assay was adapted from Brown *et al.*, 2012. The spectrum was taken from https://en.wikipedia.org/wiki/Nicotinamide_adenine_dinucleotide.

parameters of UGT76E12 against 12-OH-JA could not be obtained. In addition, the control enzyme UGT74F1 was measured with SA. First, it must be shown that the coupling reactions (PK- and LDH-reaction) are not rate limiting for determining the reaction parameters of the reaction of interest. Therefore, a positive control (450 μ M UDP) illustrates the capacity of the system. Generally, all UGT-reactions started with a lack phase. Then, the linear reaction phase – steady-state conditions – lasted for at least 100 s (UGT76E2 with 500 μ M 12-OH-JA). The setup recorded specific activities at different substrate concentrations. The respective values of the steady-state slopes were plotted as reaction rate per enzyme concentration ($V/[E]$) against the substrate concentration.

For the kinetic analyses of UGT76E1, 10 μ g of the enzyme were stabilized with BSA and 12-OH-JA was used as substrate in a concentration range from 0 – 1 179 μ M. UGT76E1 showed only little initial reaction velocities, even in the range of substrate saturation at > 393 μ M (Δ 0.02 AU per min). Overall, the conversion of 12-OH-JA to 12-*O*-Glc-JA by UGT76E1 follows the Michaelis-Menten model (Figure 4-16). The reaction rate, which were obtained for 262 μ M 12-OH-JA do not match well with the Michaelis-Menten fit, but the fit still shows a correlation

of 0.982 (Table 4-5). The calculated parameters are the Michaelis-Menten constant (K_M) of 61 μM 12-OH-JA and a turnover number (k_{cat}) of 0.0123 s^{-1} . Before, UGT76E1 has shown low activity rates, which could be resolved here: UGT76E1 shows high catalytic affinity towards the preferred substrate 12-OH-JA (61 μM) but it is characterized as a slow enzyme (k_{cat} of 0.0123 s^{-1}). Since the affinity of UGT76E1 to 12-OH-JA is high, it is most likely that the low turnovers of UGT76E1

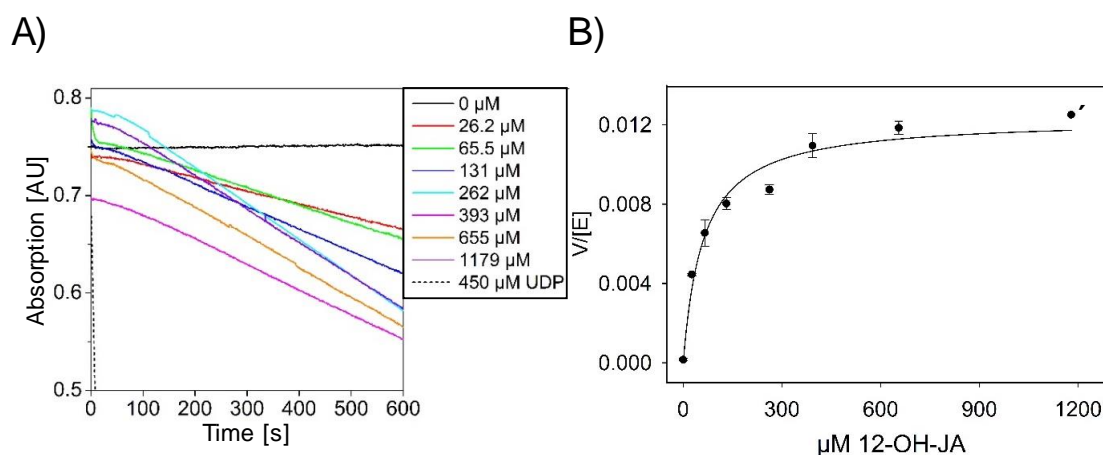


Figure 4-16: Enzyme kinetics of UGT76E1 with 12-hydroxy-JA

The initial velocities of UGT76E1-reaction were determined by a coupled spectrophotometric assay via the co-product UDP to pyruvate kinase and lactate dehydrogenase. The assay was adapted from Brown *et al.*, 2012, and recorded at 340 nm. The reactions were performed at 25 °C with 10 μg UGT76E1 (stabilized with 0.13 % [w/v] bovine serum) in 50 mM Tris/HCl, pH 9.0, 100 mM NaCl, 0.5 mM UDP-Glc, and the indicated concentrations of 12-hydroxy-JA (12-OH-JA). **A)** The initial slopes of the UGT76E1-reactions are shown. The data shows one dataset of three biological replicates. **B)** Michaelis-Menten plot of the UGT76E1-reactions. The data are mean values with standard deviation of three biological replicates. Due to limitations in 12-OH-JA availability, the value for 1179 μM was measured only once.

are caused by restrictive conditions. Likewise, not optimal buffer conditions will influence the kinetic parameters similar to a competitive inhibition resulting in lower turnovers (k_{cat}) but unchanged affinity (K_M).

Next, UGT76E2 was measured with 12-OH-JA. In contrast to UGT76E1, UGT76E2 was not stabilized with BSA and shows much higher activities. The reaction rate of UGT76E2 at 500 μM 12-OH-JA was appr. 100 times faster than that of UGT76E1 (Figure 4-17). The same holds true for the absolute signals: at appr. 500 μM 12-OH-JA, UGT76E2 is around 20-fold faster (Δ 0.300 AU per min) than UGT76E1 (Δ 0.015 AU per min). The values of the UGT76E2-kinetic follow the Michaelis-Menten model and can be fitted (Equation 5) with 0.998 correlation (Table 4-5). Noticeably, the reaction rate does still not show saturation at the highest substrate concentration (500 μM 12-OH-JA). Anyhow, UGT76E2 shows a K_M of 219 μM for 12-OH-JA and a k_{cat} of 1.48 s^{-1} (Table 4-5). Here, the specific affinity of UGT76E2 and 12-OH-JA is 3-fold higher than for UGT76E1 but, at the same time, the turnovers are 100-fold faster. Those

parameters seem to reflect the high activities observed in the former experiments and confirms the specificity and preference of UGT76E2 towards 12-OH-JA.

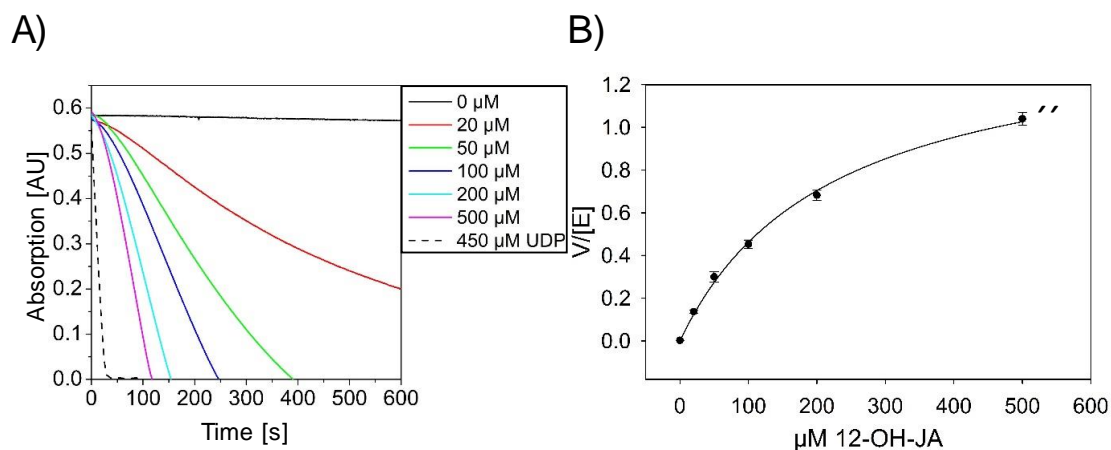


Figure 4-17: Enzyme kinetics of UGT76E2 with 12-hydroxy-JA

The initial velocities of UGT76E2-reaction were determined by a coupled spectrophotometric assay via the co-product UDP to pyruvate kinase and lactate dehydrogenase. The assay was adapted from Brown *et al.*, 2012, and recorded at 340 nm. The reactions were performed at 25 °C with 5 μg UGT76E2 in 50 mM Tris/HCl, pH 8.0, 100 mM NaCl, 0.5 mM UDP-Glc, and the indicated concentrations of 12-hydroxy-JA (12-OH-JA). **A)** The initial slopes of the UGT76E2-reactions are shown. The data shows one dataset of three biological replicates. **B)** Michaelis-Menten plot of the UGT76E2-reactions. The data are mean values with standard deviation of three biological replicates. Due to limitations in 12-OH-JA availability, the value for 500 μM was measured only twice.

Furthermore, the kinetic parameters for UGT76E1, UGT76E2, UGT76E11, and UGT76E12 with the substrates 9-HOT and 13-HOT were determined. 13-HOT was found to be a general substrate of all four UGTs (see Figure 4-11). In case of 9-HOT, no enzymatic activities could be detected for UGT76E1, UGT76E2, and UGT76E11 (Table 4-5). For UGT76E12, a very high affinity with a K_M of 21 μM but at the same time a very low turnover with k_{cat} of 0.0007 s⁻¹ was observed towards 9-HOT (Table 4-5, Supplemental figure 15A). For 13-HOT, it was possible to record the kinetic parameters of UGT76E2, UGT76E11, and UGT76E12. Just UGT76E1 did not show detectable activities towards 13-HOT (Table 4-5). For UGT76E2, the kinetic measurements display linear correlation between reaction velocity and substrate concentrations and no saturation (Supplemental figure 15B). However, the fit to the Michaelis-Menten-model showed a correlation of 0.951, which allows to calculate the parameters for K_M of 4 mM and k_{cat} of 0.5 s⁻¹ (Table 4-5). The fit extrapolates the saturation resulting in 100-fold higher K_M for 13-HOT with UGT76E2. UGT76E11 shows specific but very slow activity towards 13-HOT (K_M of 156 μM, k_{cat} of 0.0007 s⁻¹, Table 4-5, Supplemental figure 15C). UGT76E12 illustrates very high specificity towards 13-HOT but also the slowest turnovers of all kinetics. Nevertheless, the parameters were calculated with K_M of 23 μM and k_{cat} of 0.0005 s⁻¹ (Table 4-5, Supplemental figure 15D). Taken together, the kinetics of UGT76E11 and UGT76E12 with the oxylinpin

substrates show a relative high affinity whereas the turnover rates are extremely low and at the detection limit of the spectrophotometric assay.

The control enzyme UGT74F1 was measured with its native substrate SA. The kinetic parameters were calculated with K_M of 212 μM and k_{cat} of 0.0027 s^{-1} (Table 4-5, Supplemental figure 15E). This kinetic was recorded to relate the kinetics of the candidates to published data of other UGTs of *A. thaliana*. This K_M matches well with the published data and this turnover rate is one order of magnitude lower than the former value (Table 5-1) (Lim *et al.*, 2002). Since the kinetic parameters of the four candidate UGTs show similar values, the control measurements show, that the coupled spectrometric assay is suitable for the estimation of the kinetic parameters.

Table 4-5: Kinetic parameters of the UGT76E1, UGT76E2, UGT76E11, UGT76E12, and UGT74F1 towards their best substrates

Steady-state kinetics were recorded for all four UGTs with the common substrates 9-hydroxyoctadecatrienic acid (9-HOT), 13-hydroxy-octadecatrienoic acid. (13-HOT). UGT76E1 and UGT76E2 were also tested towards 12-hydroxy-JA (12-OH-JA). UGT74F1 was measured with salicylic acid (SA). A coupled spectrophotometric assay with the pyruvate kinase and the lactate dehydrogenase was used to measure the reactions of the UGTs in a 1 : 1 : 1 stoichiometry by the decrease of NADH at 340 nm (Brown *et al.*, 2012). The data were fitted with the hyperbolic function and the correlations are given. The kinetic parameters were calculated as Michaelis-Menten constant (K_M), the turnover rate (k_{cat}), and the catalytic efficiency (k_{cat}/K_M). The data is representative for three biological replicates of one experiment.

	Substrate	Correlation	K_M (μM)	k_{cat} (s^{-1})	k_{cat}/K_M ($\text{s}^{-1}\mu\text{M}^{-1}$)
UGT76E1	12-OH-JA	0.982	61	0.0123	$2.02 \cdot 10^{-4}$
	9-HOT	-	n. d.	n. d.	-
	13-HOT	-	n. d.	n. d.	-
UGT76E2	12-OH-JA	0.998	219	1.4770	$67.44 \cdot 10^{-4}$
	9-HOT	-	n. d.	n. d.	-
	13-HOT	0.951	4 000	0.5000	$1.25 \cdot 10^{-4}$
UGT76E11	9-HOT	-	n. d.	n. d.	-
	13-HOT	0.993	156	0.0007	$0.04 \cdot 10^{-4}$
UGT76E12	9-HOT	0.983	21	0.0007	$0.33 \cdot 10^{-4}$
	13-HOT	0.990	23	0.0005	$0.22 \cdot 10^{-4}$
UGT74F1	SA	0.998	212	0.0027	$0.13 \cdot 10^{-4}$

In summary, the coupled spectrophotometric assay enabled kinetic investigations of UGT76E1, UGT76E2, UGT76E11, UGT76E12, and the control UGT74F1. UGT76E1, UGT76E11, UGT76E12, and UGT74F1 turned out to be slow catalysts with very poor turnover rates (Table 4-5). In this regard, the compromise of three enzymatic reactions coupled might reduce the performance of the UGTs. Exclusively, UGT76E2 show better k_{cat} -values with 12-OH-JA and 13-HOT (Table 4-5). On the other side, the specific affinities of the candidate UGTs were comparable to UGT74F1 (Table 4-5). Thus, the calculated K_M -values of UGT76E1 and UGT76E2 for 12-OH-JA strengthen the hypothesis that these are specific 12-OH-JA UGTs.

4.4. JASMONATES ACCUMULATE AFTER WOUNDING

The metabolite patterns of different jasmonates after wounding are well known (Bruckhoff *et al.*, 2016; Mosblech, 2010). Nevertheless, it was important for this study to ensure a stable and functional wound response in *A. thaliana*. The wounded plant material was the resource for the quantitative expression data and the *ex vivo* metabolite fingerprinting approach (see 4.1.4 and 4.3.6). Therefore, the wounding experiment was set up like in Mosblech, 2010 and harvested at 0, 1, 2, and 5 hpw. The samples were analyzed by the UPLC-ESI-MS/MS-based phytohormone profiling (Iven *et al.*, 2014). Quantitative data are calculated from authentic internal standards given in nmol/g fresh weight (f. w.). Analytes, for which authentic standards were not available, relative intensities (p.d.u.) related to the chemically most similar standard are given.

JA and the active compound JA-Ile rise to maximal values at 1 hpw (JA 3.1 nmol/g f. w., JA-Ile 0.9 nmol/g f. w.) and decrease within the next 4 h (Figure 4-18A, D). The oxidized jasmonates, 11/12-hydroxy-JA (11/12-OH-JA), 12-OH-JA-Ile and 12-COOH-JA-Ile accumulate after wounding with highest values at 5 hpw. The amount of 11/12-OH-JA is enriched to 2.4 nmol/g f. w. at 5 hpw (Figure 4-18B). 12-HSO₄-JA and 12-O-Glc-JA are both formed from 12-OH-JA. 12-HSO₄-JA accumulates after wounding considerably but not significantly (Figure 4-18C), while 12-O-Glc-JA accumulates significantly 2.5-fold at 2 and 6-fold at 5 hpw (Figure 4-18G).

Similar to jasmonates, the precursor 12-OPDA displays significant accumulations at 1 hpw (2 nmol/g f. w.) and at 2 hpw (3 nmol/g f. w.) and reduced levels at 5 hpw (1.3 nmol/g f. w.) (Supplemental figure 16). Additionally, the wounding time course for SA and ABA, their glycosylated forms, 2-O-Glc-SA and ABA-GE as well as IAA and ICA are shown in Supplemental figure 16. This wounding experiment shows a functional wound response of *A. thaliana*. Hence, the biological material tested here was suitable for the quantitative expression analysis and the non-targeted *ex vivo* finger printing activity assay.

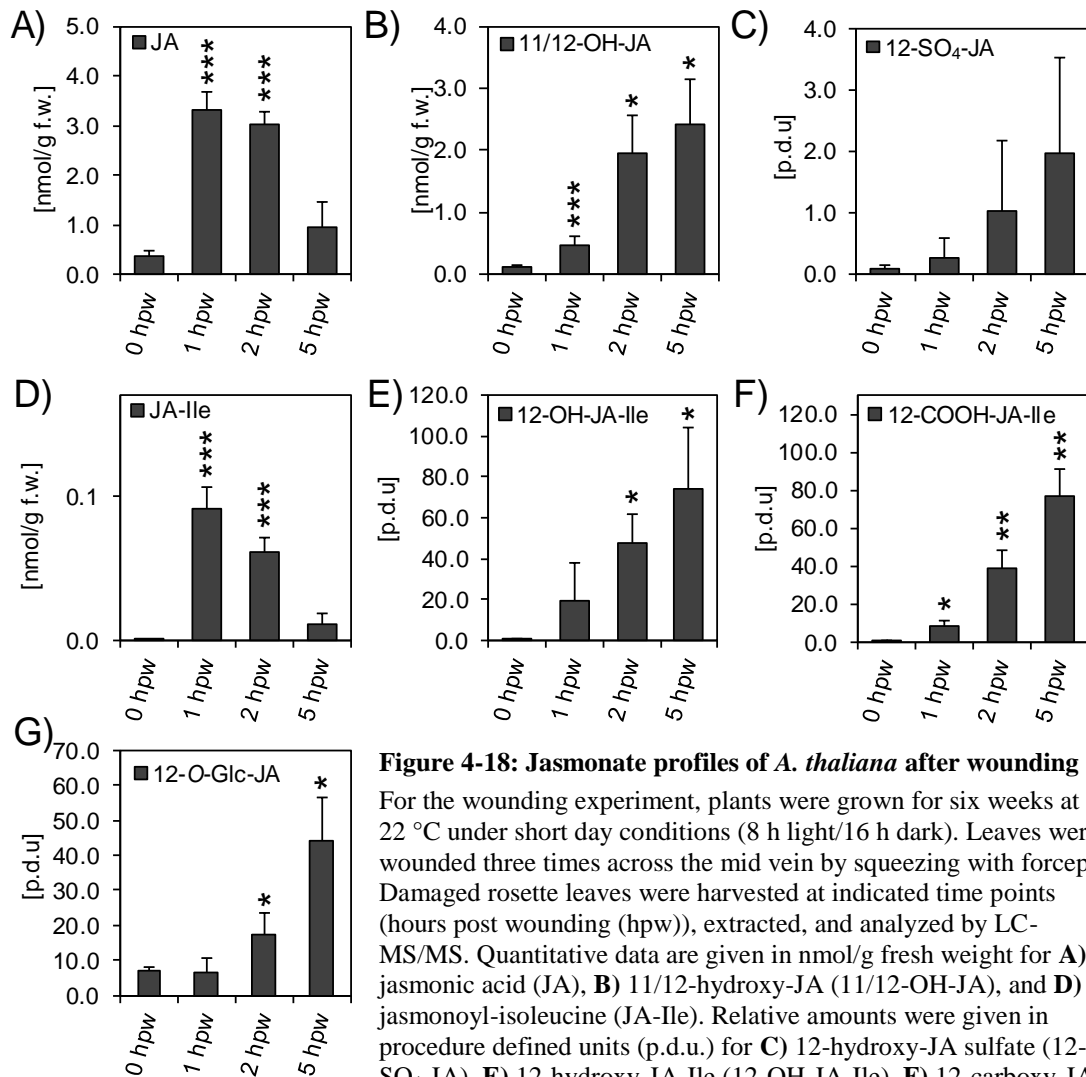


Figure 4-18: Jasmonate profiles of *A. thaliana* after wounding

For the wounding experiment, plants were grown for six weeks at 22 °C under short day conditions (8 h light/16 h dark). Leaves were wounded three times across the mid vein by squeezing with forceps. Damaged rosette leaves were harvested at indicated time points (hours post wounding (hpw)), extracted, and analyzed by LC-MS/MS. Quantitative data are given in nmol/g fresh weight for **A)** jasmonic acid (JA), **B)** 11/12-hydroxy-JA (11/12-OH-JA), and **D)** jasmonoyl-isoleucine (JA-Ile). Relative amounts were given in procedure defined units (p.d.u.) for **C)** 12-hydroxy-JA sulfate (12-SO₄-JA), **E)** 12-hydroxy-JA-Ile (12-OH-JA-Ile), **F)** 12-carboxy-JA-Ile (12-COOH-JA-Ile) and **G)** 12-*O*-glucosyl-JA (12-12-*O*-Glc-JA). Each data point represents the mean value + SD of three biological replicates from three independent experiments. 10 plants were pooled for each time point of one replicate. Asterisks indicate significance by one-sided T-Test with *p<0.05, **p<0.01, ***p<0.005. Samples were measured by Dr. Cornelia Herrfurth (University of Goettingen, Germany).

4.5. GENE EDITING ENABLES INVESTIGATING *UGT76E1*, *UGT76E2*, *UGT76E11*, AND *UGT76E12* IN *A. THALIANA*

Analysis of the *in vivo* roles of the UGTs was initially started through transfer DNA (T-DNA) insertion lines of *UGT76E1* and *UGT76E12*. However, the annotated mutants of *UGT76E1* could not be confirmed in the respective locus and the homozygous mutations in the promotor and the 5' untranslated region of *UGT76E12* did not affect the abundance and distribution of jasmonates after wounding (data not shown) (*cf.* Haroth, 2014). On top of this, the four UGT genes are located in two sets of two neighboring loci each within the *A. thaliana* genome, making it highly unlikely

to obtain respective double mutants by crossing individual mutant lines (oral communication Dr. Amélie Kelly, University of Goettingen, Germany). Therefore, a different approach was initiated in this study, in which all four genes were targeted by a CRISPR/Cas9 gene editing tool to generate stable single as well as higher order mutants (Wang *et al.*, 2015; Xing *et al.*, 2014).

4.5.1. THE OPTIMIZED VECTOR SYSTEM TARGETS FOUR CANDIDATES TO CAS9

Since the here presented work deals with four candidates genes– *UGT76E1*, *UGT76E2*, *UGT76E11*, and *UGT76E12* –, the plant CRISPR/Cas9 vector of Xing *et al.*, 2014 was highly suitable. It was originally designed to carry four targets in separate gRNAs with individual promoters and terminators. Wang and co-workers then improved the vector system of Xing, by introducing egg-cell specific promoters and terminators (pHEE401E vector, available from Addgene, Cambridge, USA), Figure 4-19). This way, the gRNA and Cas9 are both expressed in the single-cell-state of the plant embryo and successful Cas9-activity should thus lead straight to homozygous mutations in all later plant cells. Effective and selective design of the gRNA is crucial for successful gene editing by CRISPR/Cas9. Highly specific target-sequences of *UGT76E1*, *UGT76E2*, *UGT76E11*, and *UGT76E12* were selected based on the following criteria: Presence of a PAM, no likely off-targets, GC-content around 40 %, and an on-target efficiency above 0.5 (Table 4-6). These short sequences were inserted as oligonucleotides into pHEE401E for subsequent *Agrobacterium*-mediated transformation of *A. thaliana*.

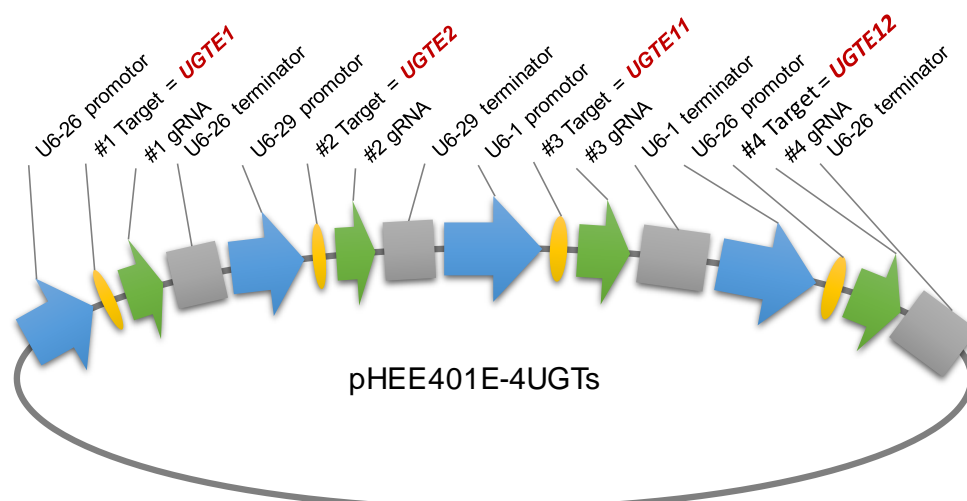


Figure 4-19: Vector maps of the CRISPR-Cas9 constructs for four UGT-target genes

A CRISPR-Cas9 approach was used to generate stable loss-of-function *UGT*-mutant lines of *A. thaliana*. The egg-cell specific promoter activates Cas9 in the one-cell phase making it possible to obtain homozygous mutants in the T1-generation already. A four-target construct was generated to target *UGT76E1*, *UGT76E2*, *UGT76E11*, and *UGT76E12* to Cas9. The vectors are commercially available on www.addgene.org and are described in Wang *et al.*, 2015; Xing *et al.*, 2014.

Table 4-6: CRISPR target sequences for UGT76E1, UGT76E2, UGT76E11, and UGT76E12

Targets were chosen with the help of three online tools: CRISPRdirect (<https://crispr.dbcls.jp/>), CRISPR-P (<http://crispr.hzau.edu.cn/CRISPR2/>), and The Genetic Perturbation Platform for designing sgRNAs for CRISPRko (<http://portals.broadinstitute.org/gpp/public/analysis-tools/sgrna-design>). The best targets are listed which were used integrated into the CRISPR/Cas9 vector.

Target	Sequence	Strand	Off targets	Score	On target efficiency	GC content [%]
<i>UGT76E1</i>	CGGGAAGGCTCTTACTCCAAGG	+	0	99	0.57	55
<i>UGT76E2</i>	CCCAGGCAGCTTAAGTCTG	-	0	95	0.51	50
<i>UGT76E11</i>	CCATTCCAGAAAGCTTACCAGAG	-	1 (<i>UGT76E12</i>)	49	0.51	45
<i>UGT76E12</i>	GGTGAGCTTCAAGGACTGTTGG	+	0	71	0.39	50

4.5.2. CRISPR/CAS9 INITIATES A LOSS-OF-FUNCTION MUTATION IN *UGT76E1*

After plant transformation, T1 seedlings were selected by hygromycin and positive plants propagated. Interestingly, some plants had developed a phenotype that is connected to jasmonates-deficiency (Caldelari *et al.*, 2011; Stintzi & Browse, 2000; von Malek *et al.*, 2002): around 5 % of the transformants of the generation 1 (T1) showed an impaired silique-formation. These plants were sprayed with JA-ME after which they formed seeds in response. These T1 plants were chosen and a total of 76 plants were propagated (T2). It should be noted, that these plants did not display any growth phenotypes and that they set seeds without any application of JA-ME. Anyhow, those 76 plants were screened for alterations in their JA-catabolism as compared to wild type. To ensure seed propagation, the plants were grown under long day conditions (16 h light / 8 h dark) and only three leaves per plant were wounded and harvested at 2 hpw for metabolite analyses (cf. 4.4).

To highlight metabolite differences concerning 12-OH-JA, a coefficient was calculated between the UGT-substrate, the UGT-concurrence reaction, and the UGT-product (amount of 12-OH-JA multiplied with the amount of 12-SO₄-JA over the amount of 12-O-Glc-JA). This coefficient was used to screen the 76 plants. Higher values depict more substrate and concurrence product than 12-O-Glc-JA. Six wild type plants show equal levels. Most of the transformed plants exhibit levels within a maximal 3-fold fluctuation. Exclusively, one plant line shows a 7-fold higher value (Figure 4-20A). For this particular plant, all four candidate loci were sequenced and compared to the wild type. The sequence alignment of *UGT76E1* revealed an insertion of a single thymidine at the expected Cas9-cutting-site (position 98 of the consensus, Figure 4-20B). This insertion causes a frame shift in the ORF of *UGT76E1* and results in a stop codon shortly after (position 136 of the consensus). Therefore, it may be assumed that in this particular plant line, *UGT76E1* is knocked out and not functional anymore. The sequencing was repeated three times independently supporting the mutation and confirming a homozygous *ugt76e1* genotype.

Here, the CRISPR/Cas9 approach has successfully produced a homozygous mutation of *UGT76E1* in the T2-generation. The mutation was identified by altered metabolite levels of the

enzyme's reaction partners. This is so far the only mutation that was obtained by this approach. Obviously, more mutations of the remaining *UGTE76s* are needed for gaining 12-*O*-Glc-JA-deficient plants, which shall be screened for in the progeny of *ugt76e1*.

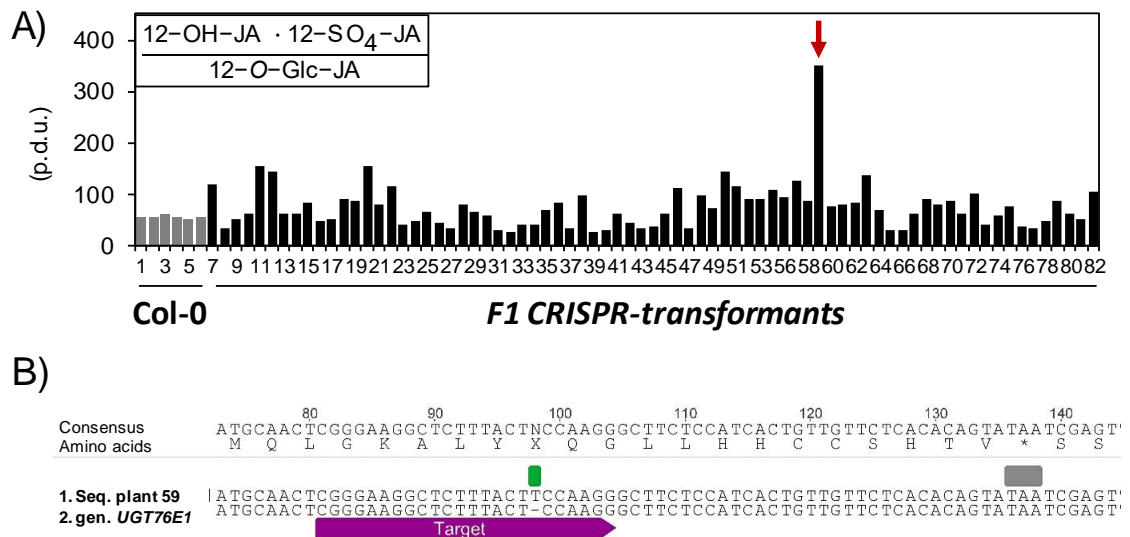


Figure 4-20: Identification of a mutation in the ORF of *UGT76E1* by CRISPR-Cas9 activity

A CRISPR-Cas9 approach was used to introduce mutations in *UGT76E1*, *UGT76E2*, *UGT76E11*, and *UGT76E12* in wild type *A. thaliana* (Col-0). After transformation, plant seedlings were selected by hygromycin. 76 F1-plants (7-82) were screened for alterations in the JA-catabolism in comparison to Col-0 plants (1-6). Leaves were wounded three times across the mid vein by squeezing with forceps. Damaged rosette leaves were harvested at 2 hours post wounding. After extraction, the samples were analyzed by LC-MS/MS. Special focus was given to the following metabolites: 12-hydroxy-JA (12-OH-JA) as substrate of the UGT-reaction, 12-*O*-glucosyl-JA (12-*O*-Glc-JA) as its product and 12-hydroxy-JA sulfate (12-SO₄-JA) as product of a concurrence reaction with 12-OH-JA as substrate. **A)** The product of the relative amounts of 12-OH-JA and 12-SO₄-JA divided by the relative amount of 12-*O*-Glc-JA were calculated and are shown as bar plots for all analyzed lines. Plant 59 exclusively shows the highest value (red arrow). Genomic DNA of plant 59 was sequenced. Jasmonate measurements were performed together with Dr. Krzysztof Zienkiewicz. **B)** Sequence alignment of the target region of plant line 59 and the corresponding *UGT76E1* region in genomic DNA of Col-0. The alignment illustrates an insertion of one thymidine at the Cas9-cutting-site (green annotation). This insertion causes a stop codon in the open reading frame of the edited sequence (grey annotation) and an end of the amino acid sequence (*). The sequencing is representative for three independent experiments. The alignment was done with the Geneious algorithm as global alignment with free end gaps and 65 % cost matrix in Geneious version 8.1 (Biomatters, New Zealand). Available from <http://www.geneious.com>

5. DISCUSSION

The role of jasmonates in plants goes far beyond plant defense towards feeding insects, and necrotrophic pathogens. Therefore, JA, JA-Ile and their derivatives may have functions in other physiological processes (Koo, 2018; Wasternack & Hause, 2013; Wasternack & Song, 2017). Within the catabolic fate of jasmonates, the defense-inactive 12-OH-JA has a special position because it is produced in two ways and gets modified by two reactions (see Figure 1-3) (Miersch *et al.*, 2008). It is synthesized either by oxidation of JA by JOX1-4 (Caarls *et al.*, 2017) or by de-conjugation of the inactive 12-OH-JA-Ile by IAR3 and ILL6 (see Figure 1-3) (Widemann *et al.*, 2015). Although both paths compete with each other (Bruckhoff *et al.*, 2016), it was suggested that the oxidative path is favored after necrotrophic pathogen attack and the de-conjugation is preferred after wounding (Smirnova *et al.*, 2017). The same holds true for the modifications of 12-OH-JA. The levels of 12-HSO₄-JA (Gidda *et al.*, 2003) and 12-O-Glc-JA influence each other but molecular regulations are not known yet (Mugford *et al.*, 2009; Wasternack & Hause, 2013). Interestingly, the enzyme(s) to specifically glycosylate 12-OH-JA were elusive although the reaction product, 12-O-Glc-JA, is known for a long time in plants (Miersch *et al.*, 2008; Seto *et al.*, 2009). The glycoside might have metabolic functions in signaling, inactivation, degradation, storage, or recycling (Bowles *et al.*, 2006; Vogt & Jones, 2000). Thus, this work identified and characterized four UGTs with the aim to describe specific enzymes for the glycosylation of 12-OH-JA to 12-O-Glc-JA. Likewise, it may be possible to complete the set of enzymes acting on jasmonates after wounding (see Figure 1-3) and to improve the knowledge of the metabolic flux around 12-OH-JA. Since 12-OH-JA may be regulated as an inactive jasmonate in regard to defense related JA-Ile responses (Miersch *et al.*, 2008), it is not clear so far, which consequences the glycosylation or the sulfation introduced to 12-OH-JA may have (Koo, 2018; Wasternack & Feussner, 2018). Therefore, the characterizations of the candidate UGTs were achieved by different approaches – as suggested by Vogt & Jones, 2000 – to deal with the expected broad substrate tolerances of the enzymes and to obtain a comprehensive and conclusive picture of the catalytic activities of the JA-related UDP-dependent glycosyltransferases in *A. thaliana*. Furthermore, distinct biochemical data might assist evaluating complex physiological effects *in vivo*.

5.1. COMPREHENSIVE CHARACTERIZATION OF THE JA-RELATED UGTs REVEALED THEIR CATALYTIC PREFERENCES

Briefly, UGT76E1, UGT76E2, UGT76E11, and UGT76E12 were identified as wound-induced and, therefore, JA-related *UGTs*. Sequence-analyses identified the catalytic motifs for substrate binding at the N-terminus and UDP-Glc binding at the C-terminus. Such structural motifs are common for all UGT enzymes with the protein fold B (see Figure 1-5). There, the enzyme consists of two domains connected *via* a large cleft, which harbors the active center (Albesa-Jové & Guerin, 2016; Offen *et al.*, 2006; Wang, 2009). Logically, the substrate-binding at the N-terminal domain is less conserved and cannot be used to predict potential substrates. All four candidates belong to the UGT76 subfamily (Mackenzie *et al.*, 1997), which is classified in the group H by sequence homology of nine conserved regions of all UGTs in *A. thaliana* (see Figure 4-2) (Ross *et al.*, 2001). From the group H, three members – UGT76B1, UGT76C2, and UGT76D1 – have been characterized with catalytic activities to form HMPA-Glc, Glc-DHBA, and cytokinin glycosides, respectively (Hou *et al.*, 2004; Huang *et al.*, 2018; von Saint Paul *et al.*, 2011). Thus, it was also not possible to deduce putative substrates of the candidates from these homologies. Nevertheless, UGT76B1, UGT76C2, and UGT76D1 are involved in defense responses in *A. thaliana* (Hou *et al.*, 2004; Huang *et al.*, 2018; von Saint Paul *et al.*, 2011). In analogy to CYP94B1, CYP94B3, and CYP94C1 (see 1.1.3), which are oxidizing JA-Ile and were identified as FA-oxidases first (Benveniste *et al.*, 2006), specific UGT may have similar catalytic tolerances. In addition to that, UGT76B1 was found to form glycosides with short OH-FA as for its published product HMPA-Glc (von Saint Paul *et al.*, 2011). Since *UGT76E1*, *UGT76E2*, *UGT76E11*, and *UGT76E12* are induced by wounding, they may be related to JA-metabolism and may be active on OH-FAs and 12-OH-JA. This hypothesis was supported by the activity of UGT76E1, UGT76E2, and UGT76E12 showed activity with 12-OH-JA (Table 4-4). On top of this, UGT76E1, UGT76E2, UGT76E12, and to some extent of UGT76E11 towards ω -OH-16:0 and oxylipins like 11-HHT, 9-HOT, and 13-HOT (Figure 4-7, Figure 4-13). Thus, it can be concluded that UGTs active on 12-OH-JA also tolerate oxylipins due to structural similarities.

The four candidate UGTs and the control UGT, UGT74F1, specific for the glycosylation of SA (George Thompson *et al.*, 2017; Lim *et al.*, 2004), were characterized biochemically by different activity assays with the aim to confirm the expected activity towards 12-OH-JA, to describe the substrate preferences and, eventually, to identify new native substrates (see above) (*cf.* Vogt & Jones, 2000). Therefore, an activity assay with radiolabeled co-substrate (UDP-¹⁴C(U)-Glc), a comprehensive assay in a quasi-native substrate environment as well as detailed spectrophotometric analyses for estimating the kinetic constants were used.

As mentioned above, UGT76E1, UGT76E2, UGT76E11, and UGT76E12 showed activity towards ω -OH-16:0 and UGT76E1, UGT76E2, and UGT76E12 were also able to glycosylate 12-OH-JA. For further investigations, the candidates were analyzed towards a set of putative substrates to narrow down their substrate preferences. With different sets of substrates (FA-derived, plant specialized metabolites, jasmonates, and flavonoids) the specificities and necessities of the candidates towards a free or shielded carboxy group, the presence and position of a hydroxy group, and the overall size of the substrate were evaluated by an activity test with radiolabeled UDP-¹⁴C(U)-Glc. Like this, all reactions give the same product signal and can be evaluated for one enzyme but different UGTs cannot be compared to each other. Concerning phytohormones, the UGT76E1, UGT76E2, and UGT76E12 showed product formation with 12-OH-JA exclusively. In addition, a special interest was to compare different general substrates to the preferred substrates. Lim and co-workers have tested the majority of *A. thaliana* UGTs towards BAs (Lim *et al.*, 2002) and flavonoids (Lim *et al.*, 2004). They found that a broad set of UGTs showed activity towards these general substrates. With benzoates, Lim and co-workers identified UGT74F1 to glycosylate SA to 2-*O*-Glc-SA preferably and the SA-GE only to a minor extent (Lim *et al.*, 2002). This behavior could be confirmed in this study. UGT74F1 showed preference to SA and only minor activity to BA. This consistent reproduction of the activity of UGT74F1 served as positive control for the experimental setup and, hence, supports the findings for the candidates UGT76E1 and UGT76E2 as 12-OH-JA UGTs. Later Lim and co-workers found UGT76E12 and UGT74F1 to be active towards quercetin (Lim *et al.*, 2004). The activity with flavonoids could be confirmed here for UGT76E12 but not for UGT74F1. Furthermore, the study of Lim showed minor activities of UGT76E1, UGT76E2, and UGT76E11 towards quercetin. In this study, only trace activities towards quercetin could be identified for UGT76E1, UGT76E2, and UGT76E11. Altogether, distinct specificities could be derived from OH-FAs and jasmonates as substrates: UGT76E1, UGT76E2, and UGT76E12 require – in case of fatty acids or the fatty acid derived oxylipins – a carboxy function and a hydroxy group, which is located in ω -position of the carbon chain (ω -OH-16:0). In addition to this, the *ex-vivo* approach has shown specificity of these UGTs to oxylipins with a hydroxy group in the middle of the aliphatic chain (9-, 13-HOT, 11-HHT, see Figure 4-13). In addition, small aromatic compounds and phytohormones with carboxy and/or hydroxy groups were not tolerated. Side activities towards flavonoids could only be observed with UGT76E12. Nevertheless, strong specificity UGT76E1 and UGT76E2 was found for 12-OH-JA. Jasmonates with differing oxidized groups were not preferred by UGT76E2 and not tolerated by UGT76E1. Again, a side activity of UGT76E12 could be observed with 12-OH-JA but no other jasmonate.

Interestingly, a glycosylation of JA to JA-GE could not be observed in this work. JA-GE was identified as JA-derivative in *N. tabacum* (Swiatek *et al.*, 2004). Although UGT74D1 was published as JGT1 (Song, 2005), this enzyme shows higher activities towards auxins as substrates

(Jin *et al.*, 2013; Tanaka *et al.*, 2014). In this study, no candidate UGT tolerated the free carboxy group of JA for glycosylation. While the free carboxy group of 12-OH-JA was crucial for substrate recognition, neither UGT76E1, UGT76E2, nor UGT76E12 formed GEs with 12-OH-JA as substrate (Figure 4-8). To identify an UGT with the ability to form JA-GE, it might be worth to investigate the UGTs of group L, in which most of the members form GEs (Figure 1-6). Another approach might try to identify a specific JA-GE UGT in *N. tabacum* first, because there the JA-GE has been found in response to JA-application (Swiatek *et al.*, 2004). Also in *N. tabacum*, the respective UGT has still not been identified.

Besides experiments to determine the enzymatic substrate tolerances and specificities, the *ex vivo* metabolite fingerprinting approach was used, which brings back enzymes to their native substrate environment and challenges their selectivity. Like this, it was possible to investigate purified proteins as close as possible to their natural environment. The metabolite rich extracts of *A. thaliana* after wounding mimicked the natural substrate availability, what led to the identification of wound-induced oxylipins like 13-HOT as substrates of the UGTs. However, a drawback of this assay is the missing compartmentation. The plant tissue is homogenized before extraction and all metabolites are extracted equally no matter if the compounds are naturally available for the enzymes or not. Since compartmentation is very important to understand the physiological processes *in vivo* (Ovádi & Saks, 2004), this has to be considered for evaluation of the *ex vivo* data. In this case, plant UGTs are proposed to be cytosolic enzymes (see Supplemental table 1) (Bowles *et al.*, 2006; Lim *et al.*, 2001; Vogt & Jones, 2000). In line with this, oxylipins like 13-HOT, and 11-HHT might not be accessible to the UGTs because they are present in the chloroplast and only 9-HOT is cytosolic like the UGTs (*cf.* Wasternack & Feussner, 2018). Altogether, UGT76E1 and UGT76E2 have been characterized as 12-OH-JA UGTs. UGT76E11 showed activity towards 11-HHT, 13-HOT, and the unknown compound C11H18O3. UGT76E12 showed high activity towards the artificial ω -OH-16:0, several oxylipins and to minor extent 12-OH-JA. In addition, the *in vivo* analyses of the candidates were started. Therefore, the CRISPR/Cas9 approach was used to knock out the candidate genes specifically and a putative loss-of-function *ugt765e1* could be identified by an altered metabolite profile of 12-OH-JA, 12-SO₄-JA, and 12-O-Glc-JA.

5.2. UGT76E1, UGT76E11, AND UGT76E12 ARE SLOW CATALYSTS

The kinetic values of UGT76E1, UGT76E2, UGT76E11, and UGT76E12 were recorded with 9-HOT and 13-HOT in continues spectrophotometric assay. In addition, UGT76E1 and UGT76E2 were measured with 12-OH-JA. As UGT76E12 has the lowest specificity towards 12-OH-JA (Table 4-4), these measurements were skipped due to substrate limitations. The experimental setup showed that the UGTs in this study were generally slow enzymes and kinetic measurements

could just be determined with specific substrates (see Table 4-5). Noticeable, besides this study, only Jackson *et al.*, 2001 has determined the kinetic parameters of plant UGTs with a continuous spectrophotometric assay. However, kinetic measurements are not always reproducible: the reference UGT VvGT1, which was used to determine structural motifs in UGTs (see Figure 1-5, Figure 4-3), was measured with quercetin twice before. The kinetic parameters of Ford *et al.*, 1998 (K_M of 15 μM , k_{cat} of 19 mkatal/kg) differ dramatically from the values of (Offen *et al.*, 2006) (K_M of 680 μM , k_{cat} of 0.085 s^{-1} , appr. 6.0 mkatal/kg). Therefore, the control enzyme UGT74F1 was used to evaluate the spectrophotometric assay and to compare the obtained kinetic values with those from the literature. In this study, the K_M value for the native UGT74F1-substrate SA was 213 μM and the turnover rate was 0.003 s^{-1} (0.4 mkatal/kg). This K_M value is very similar to that determined in a discontinuous assay by Lim and co-workers, 2002, with 230 μM . For the SA-UGTs of *O. sativa* and *N. tabacum*, much higher K_M values were determined with SA, 1 200 μM and 900 μM respectively. The turnover rate of UGT74F1 with SA in this study is 2-fold faster than the SA-UGTs of *N. tabacum* (0.2 mkatal/kg) but, at the same time, 4-fold slower than the turnover of SA-UGTs of *O. sativa* (1.5 mkatal/kg, Table 4-5) (Seto *et al.*, 2011; Seto *et al.*, 2009). The same UGT74F1 from *A. thaliana* was estimated by Lim *et al.*, 2002 as being 10-fold faster (5.8 mkatal/kg) than here. Generally, the turnover of UGT74F1 estimated here is similar to that of UGT76E1 with 12-OH-JA from this study and UGT73B1 with flavonoids (Table 5-1). The affinity of UGT74F1 to SA is similar to many values determined for UGTs with their specific substrates (Table 5-1). In this regard, the kinetic values obtained for UGT74F1 here are comparable to those of several other kinetic studies.

The kinetic parameters of UGT76E2 with 12-OH-JA point to medium affinity and a rather fast turnover rate (K_M of 219 μM , k_{cat} of 1.4 s^{-1}); UGT76E2 was slightly less affine but 100-fold faster than UGT76E1 with the same substrate. It shows similar turnovers than the fastest plant UGTs from the comparison (Table 5-1). However Jackson *et al.*, 2001, used a similar photometric setup and could record maximal reaction velocities, which were up to 3-fold faster than determined for UGT76E2 in this assay (Table 5-1). Compared to the only UGTs, which have been tested with 12-OH-JA before (Seto *et al.*, 2011; Seto *et al.*, 2009), UGT76E2 with 12-OH-HA shows a 6-fold respective 2-fold higher affinity and a 1 500-fold respective 58 000-fold faster turnover rate than the SA-UGT from *N. tabacum* and *O. sativa*. The values of UGT76E2 with 13-HOT (K_M of 4 mM, k_{cat} of 0.5 s^{-1}) show also fast turnovers but unspecific affinity. This affinity is in a similar range than the affinity of the side activities of the SA-UGTs of *O. sativa* and *N. tabacum* with 12-OH-JA what suggested that 13-HOT may not be the best substrate for UGT76E2 (Table 5-1). In summary, UGT76E2 seems to be a general fast UGT, but with clear affinity to its preferred substrate, 12-OH-JA.

UGT76E1 showed high affinity with 12-OH-JA (K_M of 60 μM , k_{cat} of 0.012 s^{-1}). These values are similar to the most affine measurements of comparisons and values of UGT76E12 with oxylipins

(Table 4-5). Since UGT76E1 had to be stabilized with BSA for kinetic measurements, it is likely that the buffer conditions were not optimal for the enzyme impairing its reaction speed. Such limitations will affect the turnover but not the affinity. Certainly, UGT76E1 will show higher reaction rates in optimal conditions. However, the turnover of UGT76E1 with 12-OH-JA is still 2-fold faster than the velocity of the control UGT74F1 with its native substrate SA. Furthermore, the reaction velocity is similar to the turnovers of UGT73B1 with flavonoids and the SA-UGTs from *N. tabacum* and *O. sativa* with SA (Table 4-5). Compared to the activities of SA-UGTs from *N. tabacum* and *O. sativa* with 12-OH-JA (Seto *et al.*, 2011; Seto *et al.*, 2009), UGT76E1 is 22-fold respectively 7-fold more affine and 21-fold respectively 830-fold faster than the SA-UGTs (Table 4-5). Altogether, the high affinity and the moderate turnover still give strong evidence for a natural activity of UGT76E1 towards 12-OH-JA.

Especially, the kinetic constants with oxylipin substrates were very slow. Nevertheless, the very slow turnovers of UGT76E11 and UGT76E12 with 13-HOT are similar to those of UGT73B1

Table 5-1: Comparison of kinetic parameters of UDP-dependent glycosyltransferases

UDP-dependent glycosyltransferases (UGTs) and their gene number (*Arabidopsis thaliana*) are listed with substrate affinity (K_M) and turnover rate (k_{cat}) of indicated substrate. The data for the first five enzymes are results of this work, while the kinetic parameters of the following UGTs are taken from the literature. 12-Hydroxy-jasmonic acid, 12-OH-JA; 13-hydroxy-octadecanoic acid, 13-HOT; salicylic acid, SA; jasmonic acid, JA; indole-3-acetic acid, IAA; indole-3-butyric acid, IBA; indole-3-proponic acid, IPA, SA-UGT from *Nicotina tabacum*, *NtSA-UGT*; SA-UGT from *Oryza sativa*, *OsSA-UGT*; glycosyltransferase 1 from *Vitis vinifera*, *VvGT1*.

Enzyme	Gene	substrate	K_M (μM)	k_{cat} (s^{-1})	k_{cat} (mkatal/kg)	Reference
UGT76E1	<i>At5g59580</i>	12-OH-JA	60	0.012	0.83	this study
UGT76E2	<i>At5g59590</i>	12-OH-JA	219	1.477	58.2	this study
UGT76E2	<i>At5g59590</i>	13-HOT	4 000	0.500	18.95	this study
UGT76E11	<i>At2g46670</i>	13-HOT	156	0.001	0.18	this study
UGT76E12	<i>At2g46660</i>	13-HOT	23	0.001	0.22	this study
UGT76E12	<i>At2g46660</i>	9-HOT	22	0.001	0.33	this study
UGT74F1	<i>At2g43840</i>	SA	213	0.003	0.39	this study
UGT72E2	<i>At5g66690</i>	Sinapic acid	900	-	20.33	Lim <i>et al.</i> , 2001
UGT72E2	<i>At5g66690</i>	Sinapoyl-alcohol	240	-	151.52	Lim <i>et al.</i> , 2001
UGT73B1	<i>At4g34138</i>	Quercetin	18	-	0.33	Kim <i>et al.</i> , 2006
UGT73B1	<i>At4g34138</i>	Kaempferol	26	-	0.25	Kim <i>et al.</i> , 2006
UGT74D1	<i>At2g31750</i>	JA	290	0.035	-	Song 2005
UGT74D1	<i>At2g31750</i>	IAA	540	0.067	-	Song 2005
UGT74F1	<i>At2g43840</i>	SA	230	-	5.79	Lim <i>et al.</i> , 2002
UGT74G1-like	<i>NtSA-UGT</i>	12-OH-JA	1 300	-	0.04	Seto <i>et al.</i> , 2011
UGT74G1-like	<i>NtSA-UGT</i>	SA	900	-	0.23	Seto <i>et al.</i> , 2011
UGT74H5	<i>OsSA-UGT</i>	SA	2 100	-	1.53	Seto <i>et al.</i> , 2009
UGT74H5	<i>OsSA-UGT</i>	12-OH-JA	400	-	0.001	Seto <i>et al.</i> , 2009
UGT78A5	<i>VvGT1</i>	Quercetin	680	0.085	-	Offen <i>et al.</i> , 2006
UGT78A5	<i>VvGT1</i>	Quercetin	15	-	18.88	Ford <i>et al.</i> , 1998
UGT84A1	<i>At4g15480</i>	Coumaric acid	400	-	13.07	Lim <i>et al.</i> , 2001
UGT84A1	<i>At4g15480</i>	Sinapic acid	580	-	6.39	Lim <i>et al.</i> , 2001
UGT84B1	<i>At2g23260</i>	IAA	240	-	180	Jackson <i>et al.</i> , 2001
UGT84B1	<i>At2g23260</i>	IBA	150	-	122	Jackson <i>et al.</i> , 2001
UGT84B1	<i>At2g23260</i>	IPA	140	-	113	Jackson <i>et al.</i> , 2001

with quercetin and kaempferol (Kim *et al.*, 2006). Like for UGT76E1, the slow reaction velocities are thought to be influenced by the buffer conditions. Hence, for UGT76E11 and UGT76E12 with 13-HOT, the focus was given to the affinities (K_M) and not to the reaction velocities (k_{cat}). The affinities of UGT76E12 with 9-HOT and 13-HOT are the highest, which were determined in this work, and similar to the K_M values of UGT76E1 with 12-OH-JA, and VvGT1 and UGT73B1 with quercetin (Table 4-5). Since these affinities were identified to be the native activities of the respective enzymes, it is very likely that UGT76E12 might be involved in the glycosylation of oxylipins and especially 13-HOT as well. UGT76E11 shows similar behavior with 13-HOT. The affinity (156 μ M) is not as high as for UGT76E12 but still comparable to K_M values of natural reaction partners like UGT74F1 with SA, UGT84B1 with auxins, and UGT72E2 with sinapoyl-alcohol (Table 4-5). However, UGT76E11 showed also activity against 11-HHT and C11H18O3, and it has been shown to form flavonoid-glycosides (Li *et al.*, 2018). Those activities have to be considered for a complete characterization of UGT76E11 with detailed kinetic measurements.

In summary, the kinetic data support the high affinity of UGT76E12 towards oxylipins and a potential role in glycosylation of these plant metabolites. Further, the kinetic parameters reveal high affinity but low turnover of UGT76E1 towards 12-OH-JA and fast turnover of UGT76E2 with 12-OH-JA but with lesser affinity. These catalytic differences are likely to influence the physiological function of UGT76E1 and UGT76E2 *in plantae*.

5.3. UGT76E1 GLYCOSYLATES 12-OH-JA WITH HIGH SPECIFICITY

In the beginning, it was postulated that the jasmonate metabolism might be driven by chronological protein biosynthesis of the responsible proteins (see 2). This hypothesis led to the identification of *UGT76E1* by co-regulation with *JOX3* (Table 4-1). The substrate for glycosylation – 12-OH-JA – shows elevated levels from 1 hpw on (see 4.4) and might trigger 12-O-Glc-JA synthesis. This matches with the highest expression of *UGT76E1* in the quantitative expression data as well as the transcriptomic data with accumulations at 2 hpw in a JA-dependent manner (see 4.1.2, 4.1.3). On top of this, *UGT76E1* is co-regulated with genes involved in both synthetic paths of 12-OH-JA (*JOX3* and *ILL6*, Table 4-2). Hence, the expression pattern of *UGT76E1* is temporally connected with reactions producing its substrate and specifically classified into the wound-induced defense pathway in *A. thaliana* (Supplemental figure 4A).

UGT76E1 showed problems in protein purification and protein stability. In contrast to its closest homolog – UGT76E2 (88 % identity) –, the purification of UGT76E1 has needed several optimizations (see Figure 4-5) and yielded the lowest amounts of all purifications. However, this is in analogy with (Vogt & Jones, 2000), who characterize UGTs as generally labile enzymes. Furthermore, Bowles and co-authors suggest that *in vitro* experiments with UGTs are difficult because specific co-factors, protein-protein interactions and metabolic channeling may be missing

in *in vitro* reactions. Thus, the protein stability of UGT76E1 might be caused by the lack of co-factors, assisting or stabilizing proteins. At least *in vitro*, the enzyme might need special conditions regarding the buffer composition as well as additives to stabilize the protein. During kinetic measurements, UGT76E1 had to be stabilized with 0.13 % BSA and still showed slow reaction rates with 12-OH-JA. Due to this low turnover, UGT76E1 showed 30-fold lower catalytic efficiency than UGT76E2 although UGT76E1 had high affinity to 12-OH-JA (K_M of 60 μ M). However, it could be shown by different enzymatic assays (see Figure 4-10, Figure 4-13, Table 4-5) that the glycosylation of 12-OH-JA to 12-*O*-Glc-JA is the preferred reaction of UGT76E1 *in vitro*. Likewise, different functional properties of the substrate could be identified as being crucial for catalysis: UGT76E1 seems to require a hydroxyl group and carboxy function. Though the hydroxy group is glycosylated (Figure 4-8), a free carboxy group is required for catalysis. The fatty alcohol (OH-C16) and 12-OH-JA-derivatives with a shielded carboxy group, like 12-OH-JA-ME (tested in the radiolabeled assay) and the 12-OH-JA-Ile (provided in the *ex vivo* extracts), were not used as substrates by UGT76E1.

Furthermore, UGT76E1 was the only candidate, for which the *in vivo* analysis could be started in this study. A recently described CRISPR/Cas9 toolbox (Wang *et al.*, 2015; Xing *et al.*, 2014) was used to target all four candidates to Cas9 endonuclease activity. As a result, a putative loss-of-function *ugt76e1* single mutant plant could be identified (Figure 4-20B). The specific mutant line was found by an altered distribution of the substrate, concurrence product, and product (12-OH-JA * 12-HSO₄-JA / 12-*O*-Glc-JA, Figure 4-20A). Surprisingly, the abundance of 12-*O*-Glc-JA itself was not reduced in this mutant line (data not shown). Thus, it is likely that UGT76E1, UGT76E2, and UGT76E12 may act redundantly. UGT76E1 and UGT76E2 both were characterized to specifically glycosylate 12-OH-JA *in vitro* and, in addition, UGT76E12 showed minor activity against 12-OH-JA (Table 4-4). In this respect, *UGT76E1* and *UGT76E12* were both significantly induced after wounding (Figure 4-1). Additionally, also *UGT76E2* might compensate for reduced 12-OH-JA-glycosylation *in vivo* although it illustrated a different expression pattern (see Figure 4-1, Supplemental figure 3, Supplemental figure 4). To generate a 12-*O*-Glc-JA-deficient mutant line at least these three UGTs active on 12-OH-JA have to be mutated.

In summary, this study was aware that UGTs tend to be rather unspecific enzymes, which have to be tested with different substrates to identify their native reactions (Bowles *et al.*, 2006; Vogt & Jones, 2000). Thus, the clear preference of UGT76E1 to 12-OH-JA in different activity assays emphasizes a potential role of UGT76E1 as natural 12-OH-JA-UGT in *A. thaliana* (Figure 5-1).

5.4. UGT76E2 FORMS 12-O-GLC-JA WITH HIGH SPECIFICITY AND TURNOVER NUMBERS

The transcript of the next candidate, *UGT76E2*, did not show significant accumulation after wounding in the leaves of *A. thaliana*, which were analyzed by RT-PCR (see Figure 4-1). Nevertheless, *UGT76E2* was identified by co-expression with *ST2a* and shows a similar expression profile as *ST2a* (data not shown, eFP-Browser access 02.05.2018). This shared profile depicted its induction after biotic and abiotic stresses whereas *UGT76E1* showed induction after wounding exclusively. (Supplemental figure 4B) As mentioned before, 12-OH-JA does not inhibit root growth like JA and JA-Ile. However 12-OH-JA and 12-O-Glc-JA were identified as tuber-inducing compounds in *S. tuberosum* (Yoshihara *et al.*, 2014). Therefore, 12-OH-JA and 12-O-Glc-JA may have a physiological role in below-ground parts of plants, at least in growth-regulation of roots. The constitutive expression of *UGT76E2* may be connected to this function but localization and expression studies of *UGT76E2* have to be done to reveal the presence and a putative function of *UGT76E2* roots.

The enzyme showed generally high activities in all experiments and it was the enzyme with the best turnover rate (1.4 s^{-1}) and the highest catalytic efficiency ($67.44 * 10^{-4} \text{ s}^{-1} \mu\text{M}^{-1}$) of the four candidates (Table 4-5). *UGT76E2* is about 100-times faster but also slightly less affine for 12-OH-JA than *UGT76E1*. Its kinetic constants with 12-OH-JA are K_M of 219 μM and a maximal turnover of 1.4 s^{-1} . Surprisingly, the turnover of *UGT76E2* with 13-HOT was also fast with 0.5 s^{-1} though the catalytic affinity was very low and the K_M could just be estimated with 4 mM. Hence, *UGT76E2* is assumed to have a clear preference towards its native substrate, 12-OH-JA (Figure 5-1). Similar to *UGT76E1*, certain structural requirements can be assumed for the substrates of *UGT76E2*: a carboxy function and a hydroxy group of the substrate is required. However, the position of the hydroxy group is less important: *UGT76E2* shows minor activities towards hydroxy groups close to the carboxy group (3-OH-16:0, Figure 4-10), similar activities than *UGT76E1* towards hydroxy groups in the middle of the unsaturated aliphatic chain (11-HHT and 13-HOT, Figure 4-13), and strong activities towards ω -hydroxy groups (ω -OH-16:0, 12-OH-JA, Figure 4-10). In addition to this, *UGT76E2* was the only UGT that tolerates a shielded carboxy group to minor extent (12-OH-JA-ME, Figure 4-10) but bigger groups attached inhibited catalysis (12-OH-JA-Ile, Supplemental figure 14). Hence, the specificity of *UGT76E2* is not as tight as for *UGT76E1* but shows strong preference for 12-OH-JA (Figure 5-1). The reason for this may be its higher activity.

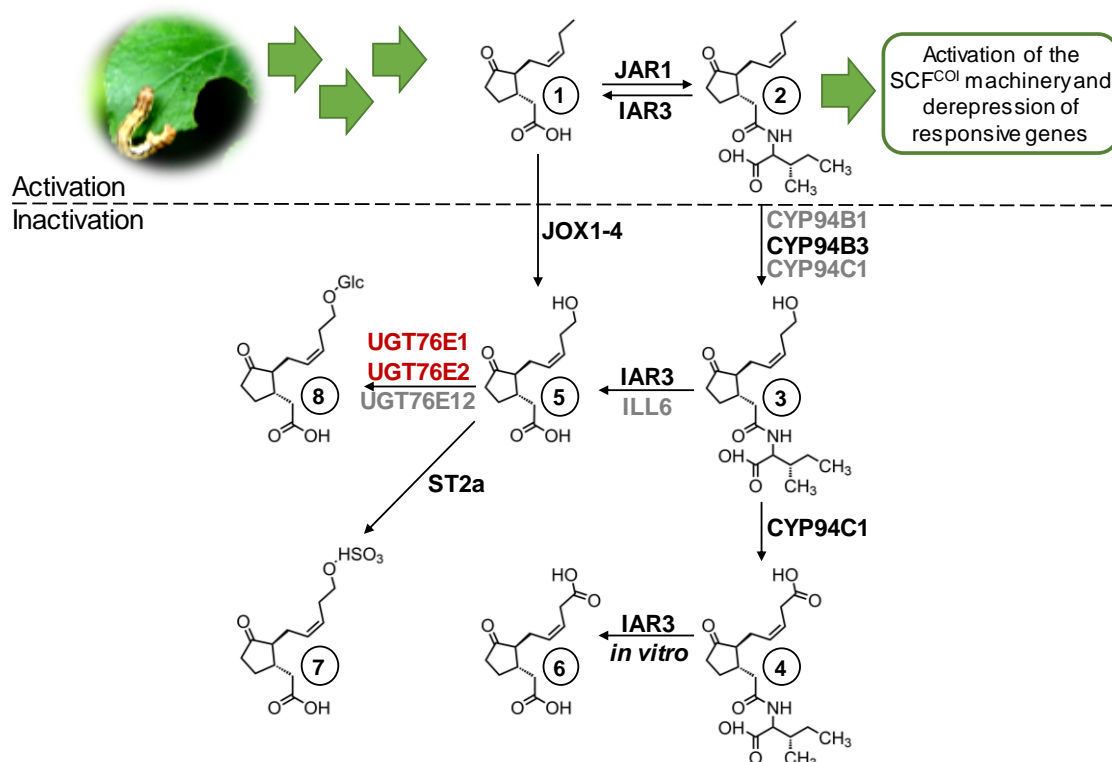


Figure 5-1: UGT76E1, UGT76E2 complete the set of jasmonate-enzymes after wounding

Wound stimuli like feeding insects lead to the activation of jasmonic acid (JA, 1) biosynthesis. JA gets active as hormone by the conjugation to isoleucine. Jasmonoyl-isoleucine (JA-Ile, 2) stimulates de-repression of JA-responsive genes *via* proteasomal degradation. CYP94B1, CYP94B3 and CYP94C1 oxidize JA-Ile to 12-hydroxy-JA-Ile (12-OH-JA-Ile, 3) and CYP94C1 to 12-carboxy-JA-Ile (12-COOH-JA-Ile, 4). JA-Ile, 12-OH-JA-Ile, and 12-COOH-JA-Ile get de-conjugated by IAA-alanine-resistant 3 (IAR3) and IAA-leucine-resistant-like 6 (ILL6) forming JA, 12-hydroxy-JA (12-OH-JA, 5) and 12-carboxy-JA (12-COOH-JA, 6), respectively. JA is oxidized to 12-OH-JA by jasmonate-induced oxidases 1 to 4 (JOX1-4). 12-OH-JA gets modified to 12-OH-JA-sulfate (12-HSO₄-JA, 7) by sulfotransferase 2a (ST2a). This work identified two specific UDP-dependent glycosyltransferases (UGTs, highlighted in red), which glycosylate 12-OH-JA to 12-O-glucosyl-JA (12-O-Glc-JA, 8). A third UGTs showed minor activity forming 12-O-Glc-JA. Scheme modified from Wasternack & Hause, 2013, additions from Caarl's *et al.*, 2017; Kitaoka *et al.*, 2014; Widemann *et al.*, 2016; Zhang *et al.*, 2016. Photo was taken from Iven *et al.*, 2014.

5.5. UGT76E11 SHOWS ACTIVITIES TOWARDS OXYLIPINS AND A SO FAR UNKNOWN METABOLITE

Next, *UGT76E11* showed high expression in *A. thaliana* after wounding in a JA-related manner (Figure 4-1, Supplemental figure 2, Supplemental figure 6). Additionally, the transcription of *UGT76E11* displayed constitutive and high expression after different abiotic stresses Supplemental figure 5. In another study, *UGT76E11* was found to be induced after salinity, drought and hydrogen peroxide treatment in *A. thaliana* (Li *et al.*, 2018). Such an expression profile of *UGT76E11* may be not suitable for specific glycosylation of jasmonates after wounding.

UGT76E11 illustrates overall non-specific and low signals in the radiolabeled substrate assay. In this case, the set of substrates in this experiment was most likely not suitable to identify specific substrates of UGT76E11. The work of Li and co-workers, 2017, has identified flavonoids, like quercetin, kaempferol, and naringenin to be the preferred substrates of UGT76E11 *in vitro* and *in vivo* (Li *et al.*, 2018). However, this behavior could not be confirmed here, the radiolabeled substrate assay as well as the *ex vivo* approach did not identify activities towards quercetin, dh-kaempferol or other flavonoids (Figure 4-10, 4.3.8). On the other side, the *ex vivo* analysis could identify specific activities of UGT76E11 from the metabolite-enriched extracts: 11-HHT, 13-HOT, and a native compound of the elemental composition of C₁₁H₁₈O₃. This unknown metabolite neither gave any databank hit nor could be structurally identified by MS/MS fragmentation analysis. From the overall *ex vivo* data set, it could be concluded that C₁₁H₁₈O₃ is not wound-induced but rather constitutively present in all samples. This is consistent with a more constitutive expression profile of UGT76E11. An identity of the metabolite might enlighten the specific and high activity of UGT76E11 towards this compound. The activity towards 11-HHT and 13-HOT was similar for all four tested UGTs of the 76E-subfamily and might be due to their protein homology. Nevertheless, it may be important to test the different activities of UGT76E11 from this study (11-HHT, 13-HOT, C₁₁H₁₈O₃) with the findings of Li and co-workers (flavonoids). There, they tested specifically and exclusively flavonoids with UGT76E11. Therefore, it may be interesting to compare the activities towards oxylipins with the published activities towards flavonoids determine the best of them.

5.6. UGT76E12 PREFERS OTHER OXYLIPINS OVER 12-OH-JA

UGT76E12 could be identified as well by transcript accumulation after wounding in a JA-dependent manner (see 4.1.2). The TAIR eFP Browser shows for *UGT76E12* strong induction in response to wounding and to osmotic stress. *UGT76E12* has been found as stress-induced *UGT* before (Rehman *et al.*, 2018; von Saint Paul *et al.*, 2011). In a general ranking after biotic and abiotic stress, *UGT76E12* was on the fifth place of all induced *UGTs* in *A. thaliana*. Previous work only investigated the top hit, which was UGT76B1 that forms HMPA-Glc (von Saint Paul *et al.*, 2011). However, this supports the more general stress-related expression of *UGT76E12*. In another study, *UGT76E12* was found to be up-regulated in ABA-sensitive seedlings and after 12-OPDA-application (Rehman *et al.*, 2018). The induction by the JA-precursor 12-OPDA might explain the JA-dependency in this work. However, dissecting responses after 12-OPDA- or JA-application needs additional experiments, because 12-OPDA will be converted *in planta* into JA. In comparison with UGT76E1, UGT76E2 and UGT76E11, UGT76E12 shows the highest rates of product formation with ω -OH-16:0 and oxylipins like 11-HHT, 9-HOT and 13-HOT. In addition, UGT76E12 also accepts 12-OH-JA as substrate but to a lower extent (see Figure 4-13,

Table 4-4). Here again, a free carboxy group together with the hydroxy group are necessary for catalysis because JA, 12-OH-JA-ME, 16:0 and the fatty alcohol OH-C16 were no substrates for UGT76E12. In respect to the position of the functional group, UGT76E12 seems to be more specific than UGT76E2. It tolerates the free hydroxy group at the ω -position (ω -OH-16:0, see Figure 4-10) and in the middle of the molecule (11-HHT, 9-HOT, and 13-HOT, see Figure 4-13 and Table 4-4) but not in the direct neighborhood of the carboxy terminus in α - or β -position (see Figure 4-10). However, the kinetic parameters could be measured with 9-HOT (K_M of 22 μ M) and 13-HOT (K_M of 23 μ M). These are the best substrate affinities, estimated for all analyzed candidates with their preferred substrates. The turnover rates are very low in comparison to the other UGTs tested (see Table 5-1). Surprisingly, the targeted activity assays based on LC-MS measurements showed a high relative product formation for 13-*O*-Glc-HOT and 9-*O*-Glc-HOT (see Table 4-4). The glycosylation of 9-HOT and 13-HOT by UGT76E12 is a very interesting finding (Figure 5-2). It is the first time that UGTs have been described to be specific to these oxylipins. Since oxylipins are FA-derivatives, glycosylation might increase their solubility in the plant cell. Additionally, glycosylated oxylipins have been found in *L. paucicostata* (Kai *et al.*, 2010) but not in *A. thaliana* so far. Because different oxylipins may have different functions in plants (see 1.1.1), UGT76E12 might be involved in different aspects of oxylipin regulation or even signaling. For example, pool of green leaf volatiles may be influenced (Matsui, 2006) or the oxylipin-driven defense against pathogens in *N. tabacum* may be regulated (Mene-Saffrane *et al.*, 2003) with activity against 9-HOT. As 13-HOT is produced by the 13-LOX-pathway, an early interference with the pathway and its by-products is possible by storing glycosylated oxylipins in the plants vacuole after wounding. In this case, 13-HOT accumulates after SA-treatment and 13-HOT alone is sufficient to induce pathogenesis-related genes in *Hordeum vulgare* (Weichert *et al.*, 1999). Altogether, UGT76E12 shows high preference towards the oxylipin substrates and there are different putative functions of oxylipin-glycosides but all these hypotheses have to be evaluated in future work.

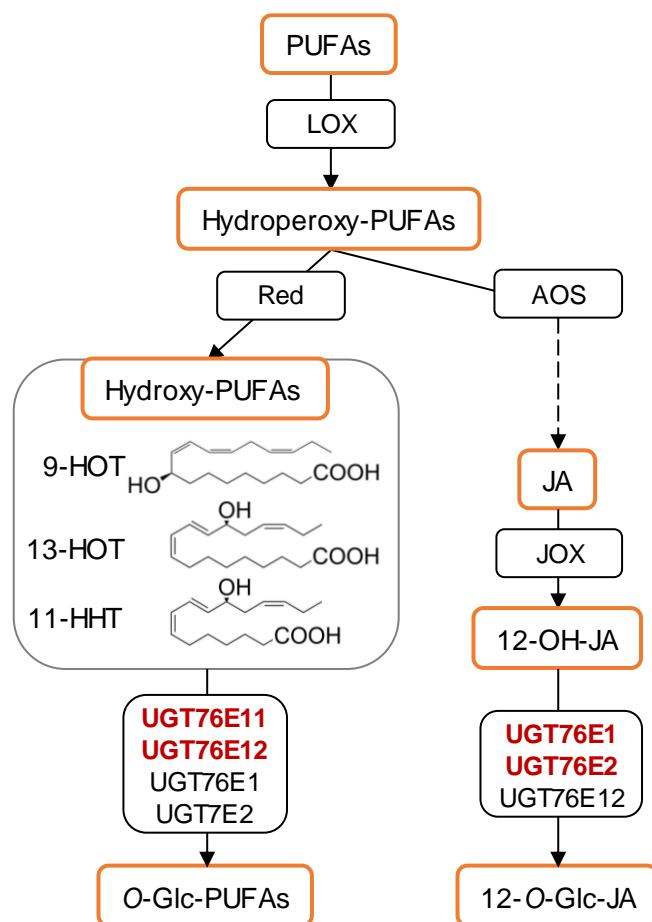


Figure 5-2: The candidate UGTs glycosylate oxylipins

Lipoxygenases (LOXs) oxygenate polyunsaturated fatty acids (PUFAs) to hydroperoxy-PUFAs. Those molecules can be metabolized to diverse oxylipins. In particular, reductases (Red) produce hydroxy-PUFAs like 9-hydroxy-octadecatrienoic acid (9-HOT), 13-hydroxy-octadecatrienoic acid (13-HOT), and 11-hydroxy-hexadecatrienoic acid (11-HHT). In parallel, an allene oxide synthase (AOS) and others initiate synthesis of jasmonic acid (JA). JA may be oxidized to 12-hydroxy-JA (12-OH-JA) by jasmonate-induced PUFAs oxidases (JOX). Both, hydroxy-PUFAs and 12-OH-JA, can be glycosylated by the candidate UDP-dependent glycosyltransferases (UGTs), UGT71E1, UGT76E2, UGT76E11, and UGT76E12. These produce 12-O-glucosyl-JA (12-O-Glc-JA) and O-glucosyl-PUFAs (O-Glc-PUFAs). O-Glc-PUFAs have been described in *Lemna paucicostata* (Kai *et al.*, 2010), but no function has been assigned yet. Figure was modified from Wasternack & Feussner, 2018.

Additionally, UGT76E12 glycosylated flavonoids like quercetin (appr. 33 % of ω -OH-16:0) and dh-kaempferol (appr. 66 % of ω -OH-16:0, see Figure 4-10). This activity has been described before (Lim *et al.*, 2004). In that work, UGT76E12 showed high activity towards quercetin and Lim and co-workers speculated that UGT76E12 may be suitable for industrial application and producing high-value natural glycosides. This behavior could be confirmed in this work although the activity towards flavonoids was not the preferred activity of UGT76E12. Furthermore, UGT76E12 showed minor activity towards 12-O-Glc-JA. Between the candidates, UGT76E12 has produced similar amounts of 12-O-Glc-JA than UGT76E1 (see Figure 4-10, Table 4-4). However, the catalytic efficiency of UGT76E1 with 12-OH-JA ($2.02 \times 10^{-4} \text{ s}^{-1} \mu\text{M}^{-1}$) was 10-fold higher than the efficiency of UGT76E12 with its preferred substrates 9-HOT ($0.33 \times 10^{-4} \text{ s}^{-1} \mu\text{M}^{-1}$) and 13-HOT ($0.22 \times 10^{-4} \text{ s}^{-1} \mu\text{M}^{-1}$, see Table 4-5). Similar to other studies of different UGTs showing side activities with 12-OH-JA (Seto *et al.*, 2011; Seto *et al.*, 2009), the activity of UGT76E12 might be similar due to structural similarities of 12-OH-JA to ω -OH-16:0 and 13-HOT.

5.7. EVIDENCE FOR PHYSIOLOGICAL RELEVANCE OF 12-O-GLC-JA

The metabolite 12-O-Glc-JA has been found in different plants (Miersch *et al.*, 2008; Seto *et al.*, 2009). However, the responsible enzymes have been elusive until now. UGT76E1 and UGT76E2

have shown their preference to catalyze the glycosylation of 12-OH-JA. From here, the logical step is to investigate glycosylation *in vivo*. This was started by a CRISPR-Cas9 approach, which could generate at least a *ugt76e1* single mutant until now. This single mutation was already sufficient to alter the abundance of metabolites, which are connected to 12-OH-JA (Figure 4-20). However, the levels of 12-*O*-Glc-JA alone were not reduced (data not shown). Therefore, generation of double (*ugt76e1/ugt76e2*) or triple (*ugt76e1/ugt76e2/ ugt76e12*) mutants of the *UGTs* might elucidate the role of 12-*O*-Glc-JA further. Thus, the CRISPR/Cas9 approach has to be repeated in homozygous *ugt76e1*-background to obtain double or multiple mutants of the *UGTs*. This might enlighten the physiological role of 12-*O*-Glc-JA and the respective enzymes. Deletion of all *UGTs* responsible for 12-*O*-Glc-JA synthesis is the first possibility to investigate the role of 12-*O*-Glc-JA independently of 12-OH-JA and *vice versa*. So far, it was not possible to assign functions of 12-OH-JA and its glycoside individually. Both seem to induce tuber formation in *S. tuberosum* (Yoshihara *et al.*, 2014), both function as COI/JAZ-independent leaf closing factor in *S. sameni* (Nakamura *et al.*, 2011), and both might be mobile metabolites in *A. thaliana* (Seto *et al.*, 2009). In this regard, it is important to specifically assign the observations to one metabolite and elucidate the function of jasmonates next to wounding.

However, the existing knowledge provides more evidence of a metabolic function of 12-*O*-Glc-JA than for its concurrence product 12-HSO₄-JA. In respect to a re-localization upon glycosylation, it remains to be clarified if 12-*O*-Glc-JA is transported into the vacuole like for 2-*O*-Glc-SA (Dean *et al.*, 2005; Dean *et al.*, 2003) or into the apoplast. An export of glycosylated phytohormones into the apoplast has only been shown for ABA (Dietz *et al.*, 2000). However, JAT1, which seem to transport JA and JA-Ile through the plasma membrane, may have the potential to transport jasmonates like 12-*O*-Glc-JA as well. Preliminary analysis of petiole exudates of wounded *A. thaliana* may hint towards elevated levels of 12-*O*-Glc-JA and other glycosylated plant hormones in the apoplast (data not shown). In addition, a specific hydrolase enzyme in *O. sativa* strengthen a reversible storage function at least in rice (Wakuta *et al.*, 2010).

As described, 12-OH-JA is modified in two reactions, which results in 12-*O*-Glc-JA and 12-HSO₄-JA. Concerning this, it is tempting to speculate why two metabolic modifications are needed. One modification may therefore be necessary to bypass the function of the other (oral communication Prof. Dr. R. Solano, Spanish National Research Council, Madrid, Spain). In this regard, 12-*O*-Glc-JA is more likely to have relevance *in plantae* than its concurrence product 12-HSO₄-JA, for which no function has been assigned until now (see 1.1.3) (Gidda *et al.*, 2003; Koo, 2018). On top of this, UGT76E1 and UGT76E2 are characterized to specifically form 12-*O*-Glc-JA while being differentially expressed in roots and shoots. This might support a distinct physiological relevance of 12-*O*-Glc-JA in different tissues and processes.

5.7.1. 12-O-GLC-JA-Ile CANNOT BE IDENTIFIED IN *A. THALIANA*

So far, 12-*O*-Glc-JA-Ile has been found once in plants by (Kitaoka *et al.*, 2014). In that work, they identified the compound by targeted LC-MS/MS analysis of wounded plant material related to an authentic chemical standard. Therewith, Kitaoka and co-workers were able to detect low amounts of 12-*O*-Glc-JA-Ile at 6 hpw in three plant species: *A. thaliana* (11 ± 5 pmol/g f. w.), *N. tabaccum* (23 ± 6 pmol/g f. w.), and *G. max* (22 ± 5 pmol/g f. w.) (Kitaoka *et al.*, 2014). Nevertheless, these abundances have big deviations and those signals might be at the detection limit of that method since a robust signal of *e. g.* 12-OH-JA-Ile are three orders of magnitude higher (9813 ± 2473 pmol/g f. w.). 12-OH-JA-Ile was also measured in this study. Although, no quantitative levels could be determined, the 12-OH-JA-Ile accumulated to significant levels after wounding. 12-OH-JA-Ile was related to an internal JA-Ile-standard and shows much higher relative levels similar to the abundance in Kitaoka *et al.*, 2014. However, IAR3 accepts 12-*O*-Glc-JA-Ile for hydrolytic cleavage to 12-*O*-Glc-JA *in vitro* (Kitaoka *et al.*, 2014), which may support a physiological existence of 12-*O*-Glc-JA-Ile.

This work showed significant accumulation of 12-OH-JA-Ile after wounding (see Figure 4-18E). Therefore, the potential precursor-molecule was present in *A. thaliana* but the glycoside could not be identified in this study. Since no chemical standard was available here, 12-*O*-Glc-JA-Ile was searched by exact mass in the LC-MS analyses of the *ex vivo* approach with and without of enzymes (Supplemental figure 14). The samples were investigated in both ionization modes with two independent LC-HR-MS-methods. 12-*O*-Glc-JA-Ile could neither be detected as internal metabolite of *A. thaliana* in the enriched metabolite extract 5 hpw nor as product of UGT76E1, UGT76E2, UGT76E11 or UGT76E12 with the native substrate 12-OH-JA-Ile (Supplemental figure 14). Anyhow, it might be possible that so far unknown UGT(s) are responsible for the glycosylation of 12-OH-JA-Ile although the co-expression analysis performed in this work did not give any hit for putative candidates around 12-OH-JA-Ile (see 4.1.1).

Altogether, this study was not able to detect 12-*O*-Glc-JA-Ile in *A. thaliana* after wounding. However, it is concluded that none of the investigated UGTs has the potential to use 12-OH-JA-Ile as substrate. Kitaoka *et al.*, 2014 is still the exclusive recourse of the abundance and future work has to challenge this again with optimized detection methods to prove the physiological presents and relevance of 12-*O*-Glc-JA-Ile.

5.7.2. 12-COOH-JA WAS IDENTIFIED IN WOUNDED LEAVES OF *A. THALIANA*

Up to now, the new metabolite 12-COOH-JA has been identified in flowers of *A. thaliana* (Bruckhoff *et al.*, 2016). In addition, 12-COOH-JA and 12-OH-JA-Ile accumulated in a *jox2* mutant without wounding resulting in an elevated defense responses (Smirnova *et al.*, 2017).

Here, the compound was identified as wound-induced metabolite in *A. thaliana* leaves in the extracts of the *ex vivo* metabolite fingerprinting experiment (see 4.3.6). This finding supports the mutant analysis of Smirnova and co-workers, 2016, and puts 12-COOH-JA not only in the context of flower development but also in the wound response of *A. thaliana*. Nevertheless, it is not clear how the molecule is formed. Most likely, 12-COOH-JA is produced by hydrolytic cleavage of 12-COOH-JA-Ile by IAR3. This is supported by different approaches: the accumulation of 12-COOH-JA is dependent of CYP94C1 (Bruckhoff *et al.*, 2016), it is produced by de-conjugation of 12-COOH-JA-Ile by IAR3 *in vitro* (Zhang *et al.*, 2016), and its abundance is strongly related to 12-COOH-JA-Ile levels (Smirnova *et al.*, 2017; Widemann *et al.*, 2016). This hypothesis has to be challenged in future experiments with detailed phytohormone analysis of wounded *A. thaliana* in wild type, the *cyp94c1* and the *iar3* mutants of *A. thaliana*. The wound-induction of 12-COOH-JA gives new insights in the complex metabolic fate of jasmonates and offers a new approach to study a putative metabolic function of 12-COOH-JA.

6. OUTLOOK

This study provided detailed biochemical characterizations of UGT76E1, UGT76E2, UGT76E11, and UGT76E12. Thereby, UGT76E1 and UGT76E2 could be identified as specific 12-OH-JA-UGTs *in vitro*. UGT76E12 showed minor activity to 12-OH-JA. Its preferred substrates are oxylipins.

The next step in the project has to be the physiological investigation of the UGTs. It started by now with the generation of a *ugt76e1* single mutant by a CRISPR-Cas9 approach. The metabolite analysis showed that the 12-O-Glc-JA-content *in planta* was not reduced. However, the ratio of metabolites, which are connected to 12-OH-JA, was altered (Figure 4-20). Therefore, it is important to generate also double (*ugt76e1/ugt76e2*) or triple (*ugt76e1/ugt76e2/ ugt76e12*) mutants of the UGTs to deplete 12-O-Glc-JA *in vivo*. Thereby, it might be possible to investigate the role of 12-O-Glc-JA independently of 12-OH-JA and *vice versa* in *A. thaliana*. Still, the CRISPR/Cas9 approach is favored to obtain such double or multiple mutants, because UGT76E1 and UGT76E2 as well as UGT76E11 and UGT76E12 are located as direct neighbors on the *A. thaliana* genome. Likewise, the putative function of 12-O-Glc-JA in storage and transport of jasmonates can be investigated (see 5.7). UGT76E1 and UGT76E2 showed a differential expression pattern in expression analyses (Supplemental figure 4). Therefore, localization studies might help to obtain hints to the relevance of the two enzymes in roots and shoots. This will also help to understand the role of 12-OH-JA and 12-O-Glc-JA in different plant tissues and may help to discover differential functions and regulations of the UGTs and the metabolic products.

In addition to jasmonates, oxylipins like 11-HHT, 9-HOT, and 13-HOT were glycosylated by all four candidate UGTs in this study. Oxylipins are involved in regulatory processes and stress responses in plants (see 1.1.1). Glycosylation of these FA-derived compounds might increase their solubility in the plant cell. As 11-HHT, 9-HOT, and 13-HOT are produced by the LOX-pathway, an early interference with the pathway and its by-products is possible and may be part of the regulation of the oxylipin pool. However, oxylipin-glycosides have been found in *L. paucicostata* (Kai *et al.*, 2010) but not in *A. thaliana*. In this respect, also the analytical methods have to be optimized to detect and identify glycosylated oxylipins in *A. thaliana*. With improved analytical methods, it may be possible to investigate the relevance of glycosylated oxylipins in the stress responses *e. g.* after wounding in *A. thaliana*. Such findings may enlarge the picture of the wound-response beside from jasmonates. Concerning jasmonates, this study has produced large amounts of 12-O-Glc-JA in the different activity assays. For 12-O-Glc-JA, the authentic chemical standard is missing for quantitative and qualitative phytohormones measurements.

Purifying 12-*O*-Glc-JA from the *in vitro* reactions of UGT76E1 and UGT76E2 will yield an authentic chemical standard for analytical methods in the future.

From the phylogenetic investigation, it was obvious that the group H of plant UGTs has not been investigated in detail and structural information are only available for UGT74F2. In contrast to UGT74F2, the enzymes in this work, UGT76E1, UGT76E2, UGT76E11, and UGT76E12, and UGT76B1 (von Saint Paul *et al.*, 2011) seem to have substrate specificity towards hydrophobic or FA-derived substrates. Hence, crystal structures of candidate UGTs will bring detailed information about the reaction mechanism and the coordination of 12-OH-JA and oxylipins. A crystal structure would help to understand the function of the different functional groups that were identified as necessary for catalysis. Especially, UGT76E2 is a good candidate for this since it can be purified in high amounts from the expression cultures.

7. REFERENCES

- Albesa-Jové, D. and Guerin, M. E. (2016). The conformational plasticity of glycosyltransferases. *Current Opinion in Structural Biology*, **40**, 23-32. doi: <http://dx.doi.org/10.1016/j.sbi.2016.07.007>.
- Andreou, A., Brodhun, F. and Feussner, I. (2009). Biosynthesis of oxylipins in non-mammals. *Progress in Lipid Research*, **48**, 148-170. doi: [10.1016/j.plipres.2009.02.002](https://doi.org/10.1016/j.plipres.2009.02.002).
- Arnold, M. D., Gruber, C., Floková, K., Miersch, O., Strnad, M., Novák, O., Wasternack, C. and Hause, B. (2016). The Recently Identified Isoleucine Conjugate of *cis*-12-Oxo-Phytodienoic Acid Is Partially Active in *cis*-12-Oxo-Phytodienoic Acid-Specific Gene Expression of *Arabidopsis thaliana*. *PLoS ONE*, **11**, e0162829. doi: [10.1371/journal.pone.0162829](https://doi.org/10.1371/journal.pone.0162829).
- Augustin, J. M., Drok, S., Shinoda, T., Sanmiya, K., Nielsen, J. K., Khakimov, B., Olsen, C. E., Hansen, E. H., Kuzina, V., Ekstrom, C. T., Hauser, T. and Bak, S. (2012). UDP-glycosyltransferases from the UGT73C subfamily in *Barbarea vulgaris* catalyze saponin 3-*O*-glucosylation in saponin-mediated insect resistance. *Plant Physiol*, **160**, 1881-1895. doi: [10.1104/pp.112.202747](https://doi.org/10.1104/pp.112.202747).
- Ausubel, F. M., Brent, R. E., Kingston, D. D., Seidmann, J. R., Smith, J. A. and Struhl, K. (1993). *Current Protocols in Molecular Biology*, Green Publishing Associates and John Wiley and Sons Inc., New York.
- Bensinger, S. J. and Tontonoz, P. (2008). Integration of metabolism and inflammation by lipid-activated nuclear receptors. *Nature*, **454**, 470-477. doi: [10.1038/nature07202](https://doi.org/10.1038/nature07202).
- Benveniste, I., Saito, T., Wang, Y., Kandel, S., Huang, H., Pinot, F., Kahn, R. A., Salaun, J.-P. and Shimoji, M. (2006). Evolutionary relationship and substrate specificity of *Arabidopsis thaliana* fatty acid omega-hydroxylase. *Plant Science*, **170**, 326-338.
- Blée, E. (2002). Impact of phyto-oxylipins in plant defense. *Trends in Plant Science*, **7**, 315-322.
- Bligh, E. G. and Dyer, W. J. (1959). A rapid method of total lipid extraction and purification. *Canadian journal of biochemistry and physiology*, **37**, 911-917.
- Bowles, D., Lim, E.-K., Poppenberger, B. and Vaistij, F. n. E. (2006). GLYCOSYLTRANSFERASES OF LIPOPHILIC SMALL MOLECULES. *Annual Review of Plant Biology*, **57**, 567-597. doi: [doi:10.1146/annurev.arplant.57.032905.105429](https://doi.org/10.1146/annurev.arplant.57.032905.105429).
- Britton, H. T. S. and Robinson, R. A. (1931). Universal buffer solutions and the dissociation constant of veronal. *Journal of the Chemical Society (Resumed)*, 1456-1462.
- Brown, C., Leijon, F. and Bulone, V. (2012). Radiometric and spectrophotometric *in vitro* assays of glycosyltransferases involved in plant cell wall carbohydrate biosynthesis. *Nat Protoc*, **7**, 1634-1650. doi: [10.1038/nprot.2012.089](https://doi.org/10.1038/nprot.2012.089).
- Bruckhoff, V., Haroth, S., Feussner, K., König, S., Brodhun, F. and Feussner, I. (2016). Functional characterization of CYP94-genes and identification of a novel jasmonate catabolite in flowers. *PLoS ONE*, **11**, e0159875. doi: [10.1371/journal.pone.0159875](https://doi.org/10.1371/journal.pone.0159875).
- Caarls, L., Elberse, J., Awwanah, M., Ludwig, N. R., de Vries, M., Zeilmaier, T., Van Wees, S. C. M., Schuurink, R. C. and Van den Ackerveken, G. (2017). Arabidopsis JASMONATE-INDUCED OXYGENASES down-regulate plant immunity by hydroxylation and inactivation of the hormone jasmonic acid. *Proceedings of the National Academy of Sciences*, **114**, 6388-6393. doi: [10.1073/pnas.1701101114](https://doi.org/10.1073/pnas.1701101114).
- Caldelari, D., Wang, G., Farmer, E. and Dong, X. (2011). Arabidopsis *lox3 lox4* double mutants are male sterile and defective in global proliferative arrest. *Plant Molecular Biology*, **75**, 25-33. doi: [10.1007/s11103-010-9701-9](https://doi.org/10.1007/s11103-010-9701-9).
- Campbell, J. A., Davies, G. J., Bulone, V. and Henrissat, B. (1997). A classification of nucleotide-diphospho-sugar glycosyltransferases based on amino acid sequence similarities. *Biochemical Journal*, **326**, 929.
- Chauvin, A., Caldeleri, D., Wolfender, J.-L. and Farmer, E. E. (2012). Four 13-lipoxygenases contribute to rapid jasmonate synthesis in wounded *Arabidopsis thaliana* leaves: a role

- for lipoxygenase 6 in responses to long-distance wound signals. *New Phytologist*, **197**, 566–575. doi: 10.1111/nph.12029.
- Chehab, E. W., Kaspi, R., Savchenko, T., Rowe, H., Negre-Zakharov, F., Kliebenstein, D. and Dehesh, K.** (2008). Distinct roles of jasmonates and aldehydes in plant-defense responses. *PLoS ONE*, **3**, e1904.
- Chini, A., Monte, I., Zamarréño, A. M., Hamberg, M., Lassueur, S., Reymond, P., Weiss, S., Stintzi, A., Schaller, A., Porzel, A., García-Mina, J. M. and Solano, R.** (2018). An OPR3-independent pathway uses 4,5-didehydrojasmonate for jasmonate synthesis. *Nature Chemical Biology*, **14**, 171-178. doi: 10.1038/nchembio.2540.
- Clough, S. J. and Bent, A. F.** (1998). Floral dip: a simplified method for *Agrobacterium*-mediated transformation of *Arabidopsis thaliana*. *Plant Journal*, **16**, 735-743.
- Coleman, J., Mechteld, M. and Blake-Kalff, E. D.** (1997). Detoxification of xenobiotics by plants: chemical modification and vacuolar compartmentation. *Trends in plant science*, **2**, 141-151.
- Davis, B. J.** (1964). Disc electrophoresis—II method and application to human serum proteins. *Annals of the New York Academy of Sciences*, **121**, 404-427.
- Dean, J. V., Mohammed, L. A. and Fitzpatrick, T.** (2005). The formation, vacuolar localization, and tonoplast transport of salicylic acid glucose conjugates in tobacco cell suspension cultures. *Planta*, **221**, 287-296. doi: 10.1007/s00425-004-1430-3.
- Dean, J. V., Shah, R. P. and Mohammed, L. A.** (2003). Formation and vacuolar localization of salicylic acid glucose conjugates in soybean cell suspension cultures. *Physiologia Plantarum*, **118**, 328-336.
- Demole, E., Lederer, E. and Mercier, D.** (1962). Isolement et détermination de la structure du jasmonate de méthyle, constituant odorant caractéristique de l'essence de jasmin. *Helvetica Chimica Acta*, **45**, 675-685. doi: 10.1002/hlca.19620450233.
- Dietz, K. J., Sauter, A., Wichert, K., Messdaghi, D. and Hartung, W.** (2000). Extracellular β -glucosidase activity in barley involved in the hydrolysis of ABA glucose conjugate in leaves. *Journal of Experimental Botany*, **51**, 937-944.
- Dong, T., Xu, Z. Y., Park, Y., Kim, D. H., Lee, Y. and Hwang, I.** (2014). Abscisic acid uridine diphosphate glucosyltransferases play a crucial role in abscisic acid homeostasis in *Arabidopsis*. *Plant Physiol*, **165**, 277-289. doi: 10.1104/pp.114.239210.
- Doyle, J. and Doyle, J.** (1987). Genomic plant DNA preparation from fresh tissue-CTAB method. *Phytochem Bull*, **19**, 11-15.
- Duan, H., Huang, M.-Y., Palacio, K. and Schuler, M. A.** (2005). Variations in *CYP74B2* (hydroperoxide lyase) gene expression differentially affect hexenal signaling in the Columbia and Landsberg *erecta* ecotypes of *Arabidopsis*. *Plant Physiology*, **139**, 1529-1544.
- Farmer, E. E.** (2007). Plant biology: Jasmonate perception machines. *Nature*, **448**, 659-660.
- Feussner, I. and Wasternack, C.** (2002). The lipoxygenase pathway. *Annual Review of Plant Biology*, **53**, 275-297. doi: DOI: 10.1146/annurev.arplant.53.100301.135248.
- Ford, C. M., Boss, P. K. and Høj, P. B.** (1998). Cloning and characterization of *Vitis vinifera* UDP-Glucose: flavonoid 3-*O*-glucosyltransferase, a homologue of the enzyme encoded by the *maize bronze-1* Locus that may primarily serve to glucosylate anthocyanidins *in vivo*. *Journal of Biological Chemistry*, **273**, 9224-9233.
- Gasperini, D., Chetelat, A., Acosta, I. F., Goossens, J., Pauwels, L., Goossens, A., Dreos, R., Alfonso, E. and Farmer, E. E.** (2015). Multilayered Organization of Jasmonate Signalling in the Regulation of Root Growth. *PLoS Genet*, **11**, e1005300. doi: 10.1371/journal.pgen.1005300.
- George Thompson, A. M., Iancu, C. V., Neet, K. E., Dean, J. V. and Choe, J. Y.** (2017). Differences in salicylic acid glucose conjugations by UGT74F1 and UGT74F2 from *Arabidopsis thaliana*. *Sci Rep*, **7**, 46629. doi: 10.1038/srep46629.
- Ghareeb, H., Becker, A., Iven, T., Feussner, I. and Schirawski, J.** (2011). Sporisorium reilianum Infection Changes Inflorescence and Branching Architectures of Maize. *Plant Physiology*, **156**, 2037-2052. doi: 10.1104/pp.111.179499.

- Gidda, S. K., Miersch, O., Levitin, A., Schmidt, J., Wasternack, C. and Varin, L. (2003). Biochemical and molecular characterization of a hydroxyjasmonate sulfotransferase from *Arabidopsis thaliana*. *J. Biol. Chem.*, **278**, 17895-17900.
- Glauser, G., Dubugnon, L., Mousavi, S. A. R., Rudaz, S., Wolfender, J.-L. and Farmer, E. E. (2009). Velocity estimates for signal propagation leading to systemic jasmonic acid accumulation in wounded *Arabidopsis*. *Journal of Biological Chemistry*, **284**, 34506-34513. doi: 10.1074/jbc.M109.061432.
- Guo, Q., Major, I. T. and Howe, G. A. (2018). Resolution of growth–defense conflict: mechanistic insights from jasmonate signaling. *Current Opinion in Plant Biology*, **44**, 72-81. doi: <https://doi.org/10.1016/j.pbi.2018.02.009>.
- Haroth, S. (2014). Catabolism of jasmonates. Vol. Master Göttingen.
- Heitz, T., Widemann, E., Lugan, R., Miesch, L., Ullmann, P., Desaubry, L., Holder, E., Grausem, B., Kandel, S., Miesch, M., Werck-Reichhart, D. and Pinot, F. (2012). Cytochromes P450 CYP94C1 and CYP94B3 catalyze two successive oxidation steps of plant hormone jasmonoyl-isoleucine for catabolic turnover. *Journal of Biological Chemistry*, **287**, 6296-6306. doi: 10.1074/jbc.M111.316364.
- Hofer, R., Boachon, B., Renault, H., Gavira, C., Miesch, L., Iglesias, J., Ginglinger, J. F., Allouche, L., Miesch, M., Grec, S., Larbat, R. and Werck-Reichhart, D. (2014). Dual function of the cytochrome P450 CYP76 family from *Arabidopsis thaliana* in the metabolism of monoterpenols and phenylurea herbicides. *Plant Physiol*, **166**, 1149-1161. doi: 10.1104/pp.114.244814.
- Hou, B., Lim, E. K., Higgins, G. S. and Bowles, D. J. (2004). *N*-glucosylation of cytokinins by glycosyltransferases of *Arabidopsis thaliana*. *J Biol Chem*, **279**, 47822-47832. doi: 10.1074/jbc.M409569200.
- Howe, G. A. and Jander, G. (2008). Plant immunity to insect herbivores. *Annual Review of Plant Biology*, **59**, 41-66. doi: 10.1146/annurev.arplant.59.032607.092825.
- Huang, F. C., Hinkelmann, J. and Schwab, W. (2015). Glucosylation of aroma chemicals and hydroxy fatty acids. *J Biotechnol*, **216**, 100-109. doi: 10.1016/j.jbiotec.2015.10.011.
- Huang, X., Zhu, G.-q., Liu, Q., Chen, L., Li, Y.-J. and Hou, B.-K. (2018). Modulation of plant salicylic acid-associated immune responses via glycosylation of dihydroxybenzoic acids. *Plant Physiology*. doi: 10.1104/pp.17.01530.
- Ishimaru, Y., Hayashi, K.-i., Suzuki, T., Fukaki, H., Prusinska, J., Meesters, C., Quareshy, M., Egoshi, Y., Matsuura, H., Takahashi, K., Kato, N., Kombrink, E., Napier, R. M., Hayashi, K. and Ueda, M. (2018). Jasmonic acid inhibits auxin-induced lateral rooting independently of the CORONATINE INSENSITIVE 1 receptor. *Plant Physiology*, **177**, 704–1716. doi: 10.1104/pp.18.00357.
- Iven, T., Feussner, K., Herrfurth, C. and Herbig, E. (2014). Signalstoffe der pflanzlichen Abwehr. *LABO Life sciences*, **12**, 43-47.
- Jackson, R. G., Lim, E. K., Li, Y., Kowalczyk, M., Sandberg, G., Hoggett, J., Ashford, D. A. and Bowles, D. J. (2001). Identification and biochemical characterization of an *Arabidopsis* indole-3-acetic acid glucosyltransferase. *J Biol Chem*, **276**, 4350-4356. doi: 10.1074/jbc.M006185200.
- Jin, S. H., Ma, X. M., Han, P., Wang, B., Sun, Y. G., Zhang, G. Z., Li, Y. J. and Hou, B. K. (2013). UGT74D1 is a novel auxin glycosyltransferase from *Arabidopsis thaliana*. *PLoS One*, **8**, e61705. doi: 10.1371/journal.pone.0061705.
- Kaever, A. (2014). Development of a statistical framework for mass spectrometry data analysis in untargeted Metabolomics studies. Vol. Dissertation Göttingen.
- Kaever, A., Landesfeind, M., Feussner, K., Morgenstern, B., Feussner, I. and Meinicke, P. (2014). Meta-analysis of pathway enrichment: combining independent and dependent omics data sets. *PLoS ONE*, **9**, e89297. doi: 10.1371/journal.pone.0089297.
- Kai, K., Akaike, R., Iida, K., Yokoyama, M. and Watanabe, N. (2010). C14-Oxylipin glucosides isolated from *Lemna paucicostata*. *Phytochemistry*, **In Press, Corrected Proof**.
- Kellenberger, E. (1968). Studies on the morphopoiesis of the head of phage T-even: V. The components of the T4 capsid and of other, capsid-related structures. *Virology*, **34**, 549-561.

- Kessler, A. and Baldwin, I. T.** (2001). Defensive Function of Herbivore-Induced Plant Volatile Emissions in Nature. *Science*, **291**, 2141-2144. doi: 10.1126/science.291.5511.2141.
- Khan, B. R., Wherritt, D. J., Huhman, D., Sumner, L. W., Chapman, K. D. and Blancaflor, E. B.** (2016). Malonylation of glucosylated *N*-lauroylethanolamine: a new pathway that determines *N*-acylethanolamine metabolic fate in plants. *J Biol Chem*, **291**, 27112-27121. doi: 10.1074/jbc.M116.751065.
- Kilian, J., Whitehead, D., Horak, J., Wanke, D., Weinl, S., Batistic, O., D'Angelo, C., Bornberg-Bauer, E., Kudla, J. and Harter, K.** (2007). The AtGenExpress global stress expression data set: protocols, evaluation and model data analysis of UV-B light, drought and cold stress responses. *Plant J*, **50**, 347-363. doi: 10.1111/j.1365-313X.2007.03052.x.
- Kim, J. H., Kim, B. G., Park, Y., Ko, J. H., Lim, C. E., Lim, J., Lim, Y. and Ahn, J. H.** (2006). Characterization of flavonoid 7-*O*-glucosyltransferase from *Arabidopsis thaliana*. *Biosci Biotechnol Biochem*, **70**, 1471-1477. doi: 10.1271/bbb.60006.
- Kitaoka, N., Kawaide, H., Amano, N., Matsubara, T., Nabeta, K., Takahashi, K. and Matsuura, H.** (2014). CYP94B3 activity against jasmonic acid amino acid conjugates and the elucidation of 12-*O*- β -glucopyranosyl-jasmonoyl-*L*-isoleucine as an additional metabolite. *Phytochemistry*, **99**, 6-13. doi: <http://dx.doi.org/10.1016/j.phytochem.2013.12.019>.
- Kitaoka, N., Matsubara, T., Sato, M., Takahashi, K., Wakuta, S., Kawaide, H., Matsui, H., Nabeta, K. and Matsuura, H.** (2011). Arabidopsis CYP94B3 encodes jasmonyl-*L*-isoleucine 12-hydroxylase, a key enzyme in the oxidative catabolism of jasmonate. *Plant and Cell Physiology*, **52**, 1757-1765. doi: 10.1093/pcp/pcr110.
- Koo, A. J.** (2018). Metabolism of the plant hormone jasmonate: a sentinel for tissue damage and master regulator of stress response. *Phytochemistry Reviews*, **17**, 51-80. doi: 10.1007/s11101-017-9510-8.
- Koo, A. J., Thireault, C., Zemelis, S., Poudel, A. N., Zhang, T., Kitaoka, N., Brandizzi, F., Matsuura, H. and Howe, G. A.** (2014). Endoplasmic reticulum-associated inactivation of the hormone jasmonoyl-*L*-isoleucine by multiple members of the cytochrome P450 94 family in Arabidopsis. *Journal of Biological Chemistry*, **289**, 29728-29738. doi: 10.1074/jbc.M114.603084.
- Koo, A. J. K., Chung, H. S., Kobayashi, Y. and Howe, G. A.** (2006). Identification of a peroxisomal acyl-activating enzyme involved in the biosynthesis of jasmonic acid in *Arabidopsis*. *J. Biol. Chem.*, **281**, 33511-33520.
- Koo, A. J. K., Cooke, T. F. and Howe, G. A.** (2011). Cytochrome P450 CYP94B3 mediates catabolism and inactivation of the plant hormone jasmonoyl-*L*-isoleucine. *Proceedings of the National Academy of Sciences*, **108**, 9298-9303. doi: 10.1073/pnas.1103542108.
- Koo, A. J. K. and Howe, G. A.** (2009). The wound hormone jasmonate. *Phytochemistry*, **70**, 1571-1580.
- Lackman, P., González-Guzmán, M., Tilleman, S., Carqueijeiro, I. s., Pérez, A. C. l., Moses, T., Seo, M., Kanno, Y., Häkkinen, S. T., Van Montagu, M. C. E., Thevelein, J. M., Maaheimo, H., Oksman-Caldentey, K.-M., Rodriguez, P. L., Rischer, H. and Goossens, A.** (2011). Jasmonate signaling involves the abscisic acid receptor PYL4 to regulate metabolic reprogramming in Arabidopsis and tobacco. *Proceedings of the National Academy of Sciences*, **108**, 5891-5896. doi: 10.1073/pnas.1103010108.
- Laemmli, U. K.** (1970). Cleavage of Structural Proteins during the Assembly of the Head of Bacteriophage T4. *Nature*, **227**, 680. doi: 10.1038/227680a0.
- Lairson, L. L., Henrissat, B., Davies, G. J. and Withers, S. G.** (2008). Glycosyltransferases: structures, functions, and mechanisms. *Annu Rev Biochem*, **77**, 521-555. doi: 10.1146/annurev.biochem.76.061005.092322.
- Lee, S., Yang, D. S., Uppalapati, S. R., Sumner, L. and Mysore, K.** (2013). Suppression of plant defense responses by extracellular metabolites from *Pseudomonas syringae* pv. *tabaci* in *Nicotiana benthamiana*. *BMC Plant Biology*, **13**, 65.
- Lesk, A. M.** (1995). Systematic representation of protein folding patterns. *Journal of molecular graphics*, **13**, 159-164.

- Li, Q., Yu, H.-M., Meng, X.-F., Lin, J.-S., Li, Y.-J. and Hou, B.-K. (2018). Ectopic expression of glycosyltransferase UGT76E11 increases flavonoid accumulation and enhances abiotic stress tolerance in *Arabidopsis*. *Plant Biology*, **20**, 10-19. doi: 10.1111/plb.12627.
- Li, Q., Zheng, J., Li, S., Huang, G., Skilling, S. J., Wang, L., Li, L., Li, M., Yuan, L. and Liu, P. (2017). Transporter-Mediated Nuclear Entry of Jasmonoyl-Isoleucine Is Essential for Jasmonate Signaling. *Molecular Plant*. doi: <http://dx.doi.org/10.1016/j.molp.2017.01.010>.
- Lim, E. K., Ashford, D. A., Hou, B., Jackson, R. G. and Bowles, D. J. (2004). *Arabidopsis* glycosyltransferases as biocatalysts in fermentation for regioselective synthesis of diverse quercetin glucosides. *Biotechnol Bioeng*, **87**, 623-631. doi: 10.1002/bit.20154.
- Lim, E. K., Doucet, C. J., Li, Y., Elias, L., Worrall, D., Spencer, S. P., Ross, J. and Bowles, D. J. (2002). The activity of *Arabidopsis* glycosyltransferases toward salicylic acid, 4-hydroxybenzoic acid, and other benzoates. *J Biol Chem*, **277**, 586-592. doi: 10.1074/jbc.M109287200.
- Lim, E. K., Li, Y., Parr, A., Jackson, R., Ashford, D. A. and Bowles, D. J. (2001). Identification of glucosyltransferase genes involved in sinapate metabolism and lignin synthesis in *Arabidopsis*. *J Biol Chem*, **276**, 4344-4349. doi: 10.1074/jbc.M007263200.
- Louis, J., Lorenc-Kukula, K., Singh, V., Reese, J., Jander, G. and Shah, J. (2010). Antibiosis against the green peach aphid requires the *Arabidopsis thaliana* *MYZUS PERSICAE-INDUCED LIPASE1* gene. *Plant J*, **64**, 800-811. doi: 10.1111/j.1365-313X.2010.04378.x.
- Mackenzie, P. I., Owens, I. S., Burchell, B., Bock, K. W., Bairoch, A., Belanger, A., Fournel-Gigleux, S., Green, M., Hum, D. W. and Iyanagi, T. (1997). The UDP glycosyltransferase gene superfamily: recommended nomenclature update based on evolutionary divergence. *Pharmacogenetics*, **7**, 255-269.
- Matsui, K. (2006). Green leaf volatiles: hydroperoxide lyase pathway of oxylipin metabolism. *Current Opinion in Plant Biology*, **9**, 274-280.
- Matyash, V., Liebisch, G., Kurzchalia, T. V., Shevchenko, A. and Schwudke, D. (2008). Lipid extraction by methyl-tert-butyl ether for high-throughput lipidomics. *Journal of Lipid Research*, **49**, 1137-1146. doi: 10.1194/jlr.D700041-JLR200.
- Mene-Saffrane, L., Esquerre-Tugaye, M. T. and Fournier, J. (2003). Constitutive expression of an inducible lipoxygenase in transgenic tobacco decreases susceptibility to *Phytophthora parasitica* var. *nicotianae*. *Molecular Breeding*, **12**, 271-282.
- Meng, M., Geisler, M., Johansson, H., Harholt, J., Scheller, H. V., Mellerowicz, E. J. and Kleczkowski, L. A. (2009). UDP-glucose pyrophosphorylase is not rate limiting, but is essential in *Arabidopsis*. *Plant Cell Physiol*, **50**, 998-1011. doi: 10.1093/pcp/pcp052.
- Miersch, O., Neumerkel, J., Dippe, M., Stenzel, I. and Wasternack, C. (2008). Hydroxylated jasmonates are commonly occurring metabolites of jasmonic acid and contribute to a partial switch-off in jasmonate signaling. *New Phytologist*, **177**, 114-127.
- Miersch, O., Preiss, A., Sembdner, G. and Schreiber, K. (1987). (+)-7-iso-jasmonic acid and related compounds from *Botryodiplodia theobromae*. *Phytochemistry*, **26**, 1037-1039. doi: 10.1016/S0031-9422(00)82345-6.
- Mizutani, M. and Sato, F. (2010). Unusual P450 reactions in plant secondary metabolism. *Archives of Biochemistry and Biophysics*, **In Press, Accepted Manuscript**.
- Monte, I., Ishida, S., Zamarreño, A. M., Hamberg, M., Franco-Zorrilla, J. M., García-Casado, G., Gouhier-Darimont, C., Reymond, P., Takahashi, K., García-Mina, J. M., Nishihama, R., Kohchi, T. and Solano, R. (2018). Ligand-receptor co-evolution shaped the jasmonate pathway in land plants. *Nature Chemical Biology*. doi: 10.1038/s41589-018-0033-4.
- Mosblech, A. (2010). Requirement of phosphoinositol-derived signals in the wounding response of *Arabidopsis thaliana*. Vol. Dissertation Göttingen.
- Mugford, S. G., Yoshimoto, N., Reichelt, M., Wirtz, M., Hill, L., Mugford, S. T., Nakazato, Y., Noji, M., Takahashi, H., Kramell, R., Gigolashvili, T., Flugge, U. I., Wasternack, C., Gershenzon, J., Hell, R., Saito, K. and Kopriva, S. (2009). Disruption of adenosine-5'-phosphosulfate kinase in *Arabidopsis* reduces levels of sulfated secondary metabolites. *Plant Cell*, **21**, 910-927. doi: 10.1105/tpc.109.065581.

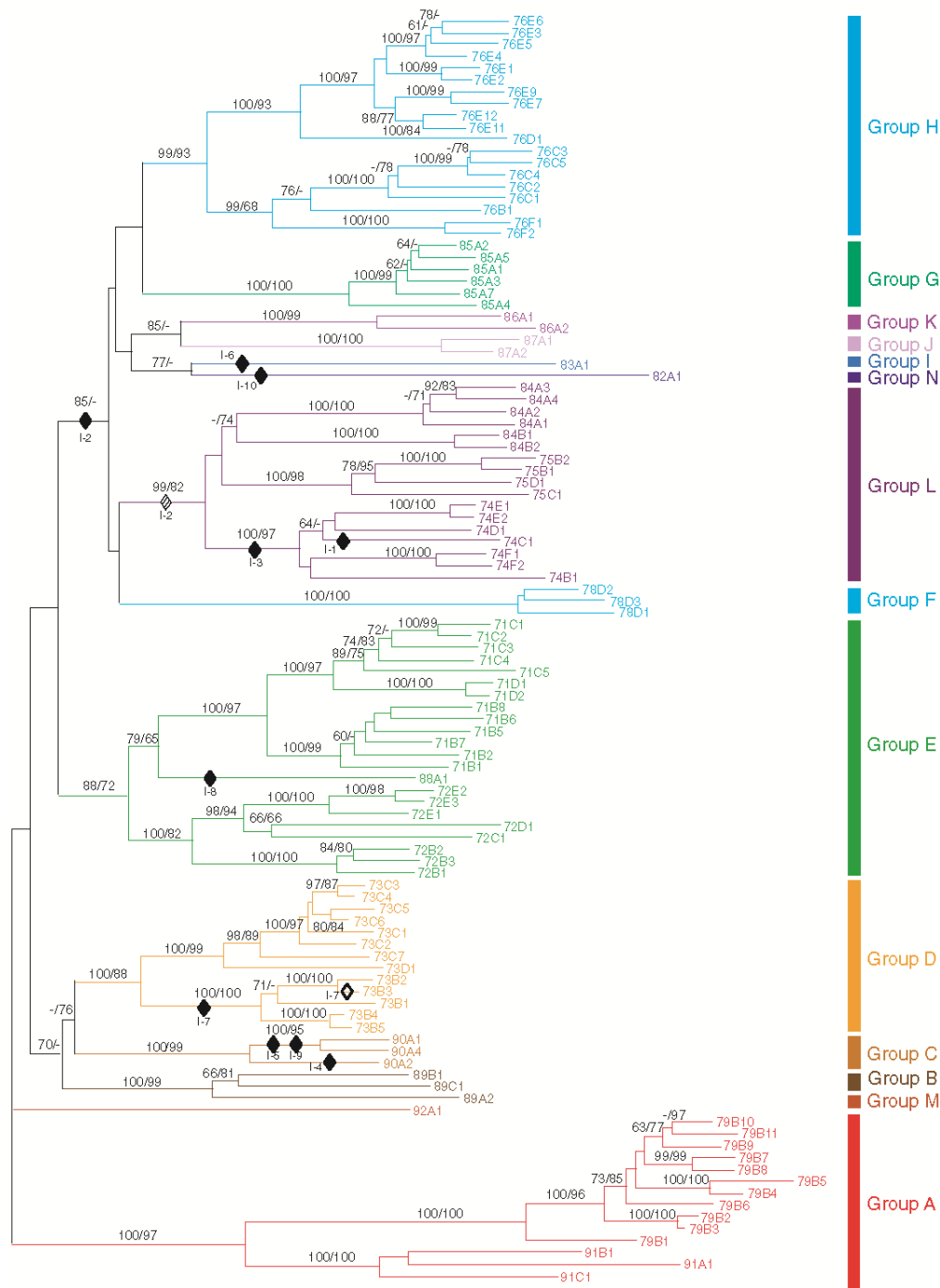
- Nahlik, K., Dumkow, M., Bayram, Ö., Helmstaedt, K., Busch, S., Valerius, O., Gerke, J., Hoppert, M., Schwier, E., Opitz, L., Westermann, M., Grond, S., Feussner, K., Göbel, C., Kaefer, A., Meinicke, P., Feussner, I. and Braus, G. H. (2010). The COP9 signalosome mediates transcriptional and metabolic response to hormones, oxidative stress protection and cell wall rearrangement during fungal development. *Molecular Microbiology*, **78**, 964–979. doi: 10.1111/j.1365-2958.2010.07384.x.
- Nakamura, Y., Mithofer, A., Kombrink, E., Boland, W., Hamamoto, S., Uozumi, N., Tohma, K. and Ueda, M. (2011). 12-Hydroxyjasmonic Acid Glucoside Is a COI1-JAZ-Independent Activator of Leaf-Closing Movement in *Samanea saman*. *Plant Physiology*, **155**, 1226-1236. doi: 10.1104/pp.110.168617.
- Nguyen, C. T., Martinoia, E. and Farmer, E. E. (2017). Emerging Jasmonate Transporters. *Molecular Plant*. doi: <http://dx.doi.org/10.1016/j.molp.2017.03.007>.
- Offen, W., Martinez-Fleites, C., Yang, M., Kiat-Lim, E., Davis, B. G., Tarling, C. A., Ford, C. M., Bowles, D. J. and Davies, G. J. (2006). Structure of a flavonoid glucosyltransferase reveals the basis for plant natural product modification. *The EMBO journal*, **25**, 1396-1405.
- Onate-Sanchez, L. and Vicente-Carbajosa, J. (2008). DNA-free RNA isolation protocols for *Arabidopsis thaliana*, including seeds and siliques. *BMC Res Notes*, **1**, 93. doi: 10.1186/1756-0500-1-93.
- Ornstein, L. (1964). Disc electrophoresis-i background and theory. *Annals of the New York Academy of Sciences*, **121**, 321-349.
- Ovádi, J. and Saks, V. (2004). On the origin of intracellular compartmentation and organized metabolic systems. *Molecular and cellular biochemistry*, **256**, 5-12.
- Park, J.-H., Halitschke, R., Kim, H. B., Baldwin, I. T., Feldmann, K. A. and Feyereisen, R. (2002). A knock-out mutation in allene oxide synthase results in male sterility and defective wound signal transduction in *Arabidopsis* due to a block in jasmonic acid biosynthesis. *The Plant Journal*, **31**, 1-12.
- Pauwels, L., Barbero, G. F., Geerinck, J., Tilleman, S., Grunewald, W., Perez, A. C., Chico, J. M., Bossche, R. V., Sewell, J., Gil, E., Garcia-Casado, G., Witters, E., Inze, D., Long, J. A., De Jaeger, G., Solano, R. and Goossens, A. (2010). NINJA connects the co-repressor TOPLESS to jasmonate signalling. *Nature*, **464**, 788-791.
- Pieterse, C. M. J., Leon-Reyes, A., Van der Ent, S. and Van Wees, S. C. M. (2009). Networking by small-molecule hormones in plant immunity. *Nature Chemical Biology*, **5**, 308-316. doi: 10.1038/nchembio.164.
- Pieterse, C. M. J., Poelman, E., Van Wees, S. C. M. and Dicke, M. (2013). Induced plant responses to microbes and insects. *Frontiers in Plant Science*, **4**. doi: 10.3389/fpls.2013.00475.
- Rehman, H. M., Nawaz, M. A., Shah, Z. H., Ludwig-Muller, J., Chung, G., Ahmad, M. Q., Yang, S. H. and Lee, S. I. (2018). Comparative genomic and transcriptomic analyses of Family-1 UDP glycosyltransferase in three *Brassica* species and *Arabidopsis* indicates stress-responsive regulation. *Sci Rep*, **8**, 1875. doi: 10.1038/s41598-018-19535-3.
- Ross, J., Li, Y., Lim, E.-K. and Bowles, D. J. (2001). Higher plant glycosyltransferases. *Genome Biology*, **2**, reviews3004.3001. doi: 10.1186/gb-2001-2-2-reviews3004.
- Saito, H., Oikawa, T., Hamamoto, S., Ishimaru, Y., Kanamori-Sato, M., Sasaki-Sekimoto, Y., Utsumi, T., Chen, J., Kanno, Y., Masuda, S., Kamiya, Y., Seo, M., Uozumi, N., Ueda, M. and Ohta, H. (2015). The jasmonate-responsive GTR1 transporter is required for gibberellin-mediated stamen development in *Arabidopsis*. *Nature Communications*, **6**, 6095. doi: 10.1038/ncomms7095.
- Sambrook, J., Fritsch, E. F. and Maniatis, T. (1989). *Molecular cloning: a laboratory manual*, 2nd edn. edn. Cold Spring Harbor Laboratory, Cold Spring Harbor NY.
- Seto, Y., Hamada, S., Ito, H., Masuta, C., Matsui, H., Nabeta, K. and Matsuura, H. (2011). Tobacco salicylic acid glucosyltransferase is active toward tuberonic acid (12-hydroxyjasmonic acid) and is induced by mechanical wounding stress. *Biosci Biotechnol Biochem*, **75**, 2316-2320. doi: 10.1271/bbb.110454.
- Seto, Y., Hamada, S., Matsuura, H., Matsushige, M., Satou, C., Takahashi, K., Masuta, C., Ito, H., Matsui, H. and Nabeta, K. (2009). Purification and cDNA cloning of a wound

- inducible glucosyltransferase active toward 12-hydroxy jasmonic acid. *Phytochemistry*, **70**, 370-379. doi: <http://dx.doi.org/10.1016/j.phytochem.2009.01.004>.
- Smirnova, E., Marquis, V., Poirier, L., Aubert, Y., Zumsteg, J., Ménard, R., Miesch, L. and Heitz, T.** (2017). Jasmonic Acid Oxidase 2 (JAO2) hydroxylates jasmonic acid and represses basal defense and resistance responses against *Botrytis cinerea* infection. *Molecular Plant*, **10**, 1159-1173. doi: <https://doi.org/10.1016/j.molp.2017.07.010>.
- Somssich, I. E., Wernert, P., Kiedrowski, S. and Hahlbrock, K.** (1996). *Arabidopsis thaliana* defense-related protein ELI3 is an aromatic alcohol: NADP⁺ oxidoreductase. *Proceedings of the National Academy of Sciences*, **93**, 14199-14203.
- Song, J. T.** (2005). Biochemical characterization of an *Arabidopsis* glucosyltransferase with high activity toward jasmonic acid. *Journal of Plant Biology*, **48**, 422-428.
- Staswick, P. E. and Tiryaki, I.** (2004). The oxylipin signal jasmonic acid is activated by an enzyme that conjugates it to isoleucine in *Arabidopsis*. *The Plant Cell*, **16**, 2117-2127. doi: DOI 10.1105/tpc.104.023549.
- Stintzi, A. and Browse, J.** (2000). The *Arabidopsis* male-sterile mutant, *opr3*, lacks the 12-oxophytodienoic acid reductase required for jasmonate synthesis. *Proceedings of the National Academy of Sciences of the United States of America*, **97**, 10625-10630.
- Studier, F. W.** (2005). Protein production by auto-induction in high-density shaking cultures. *Protein Expression and Purification*, **41**, 207-234. doi: <http://dx.doi.org/10.1016/j.pep.2005.01.016>.
- Suzuki, H., Hayase, H., Nakayama, A., Yamaguchi, I., Asami, T. and Nakajima, M.** (2007). Identification and characterization of an *Ipomoea nil* glucosyltransferase which metabolizes some phytohormones. *Biochemical and Biophysical Research Communications*, **361**, 980-986. doi: <http://dx.doi.org/10.1016/j.bbrc.2007.07.147>.
- Swiatek, A., Dongen, W. V., Esmans, E. L. and Onckelen, H. V.** (2004). Metabolic fate of jasmonates in Tobacco bright yellow-2 cells. *Plant Physiology*, **135**, 161-172.
- Tanaka, K., Hayashi, K., Natsume, M., Kamiya, Y., Sakakibara, H., Kawaide, H. and Kasahara, H.** (2014). UGT74D1 catalyzes the glucosylation of 2-oxindole-3-acetic acid in the auxin metabolic pathway in *Arabidopsis*. *Plant Cell Physiol*, **55**, 218-228. doi: 10.1093/pcp/pct173.
- Theodoulou, F. L., Job, K., Slocombe, S. P., Footitt, S., Holdsworth, M., Baker, A., Larson, T. R. and Graham, I. A.** (2005). Jasmonic acid levels are reduced in COMATOSE ATP-binding cassette transporter mutants. Implications for transport of jasmonate precursors into peroxisomes. *Plant Physiology*, **137**, 835-840.
- Ueda, J. and Kato, J.** (1980). Isolation and Identification of a Senescence-promoting Substance from Wormwood (*Artemisia absinthium* L.). *Plant Physiology*, **66**, 246-249. doi: 10.1104/pp.66.2.246.
- Vogt, T. and Jones, P.** (2000). Glycosyltransferases in plant natural product synthesis: characterization of a supergene family. *Trends in Plant Science*, **5**, 380-386. doi: [http://dx.doi.org/10.1016/S1360-1385\(00\)01720-9](http://dx.doi.org/10.1016/S1360-1385(00)01720-9).
- von Malek, B., van der Graaff, E., Schneitz, K. and Keller, B.** (2002). The *Arabidopsis* male-sterile mutant *dde2-2* is defective in the *ALLENE OXIDE SYNTHASE* gene encoding one of the key enzymes of the jasmonic acid biosynthesis pathway. *Planta*, **216**, 187-192.
- von Saint Paul, V., Zhang, W., Kanawati, B., Geist, B., Faus-Kessler, T., Schmitt-Kopplin, P. and Schäffner, A. R.** (2011). The *Arabidopsis* Glucosyltransferase UGT76B1 Conjugates Isoleucic Acid and Modulates Plant Defense and Senescence. *The Plant Cell*, **23**, 4124-4145. doi: [tpc.111.088443](https://doi.org/10.1105/tpc.111.088443) [pii]
- 10.1105/tpc.111.088443.
- Wakuta, S., Hamada, S., Ito, H., Matsuura, H., Nabeta, K. and Matsui, H.** (2010). Identification of a beta-glucosidase hydrolyzing tuberonic acid glucoside in rice (*Oryza sativa* L.). *Phytochemistry*, **71**, 1280-1288. doi: 10.1016/j.phytochem.2010.04.025.
- Wang, X.** (2009). Structure, mechanism and engineering of plant natural product glycosyltransferases. *FEBS Lett*, **583**, 3303-3309. doi: 10.1016/j.febslet.2009.09.042.
- Wang, Z.-P., Xing, H.-L., Dong, L., Zhang, H.-Y., Han, C.-Y., Wang, X.-C. and Chen, Q.-J.** (2015). Egg cell-specific promoter-controlled CRISPR/Cas9 efficiently generates

- homozygous mutants for multiple target genes in *Arabidopsis* in a single generation. *Genome Biology*, **16**. doi: 10.1186/s13059-015-0715-0.
- Wasternack, C.** (2015). How jasmonates earned their laurels: Past and present. *Journal of Plant Growth Regulation*, 1-34. doi: 10.1007/s00344-015-9526-5.
- Wasternack, C. and Feussner, I.** (2018). The oxylipin pathways: Biochemistry and function. *Annual Review of Plant Biology*, **69**, 363-386. doi: 10.1146/annurev-arplant-042817-040440.
- Wasternack, C. and Hause, B.** (2013). Jasmonates: biosynthesis, perception, signal transduction and action in plant stress response, growth and development. An update to the 2007 review in *Annals of Botany*. *Annals of Botany*, **111**, 1021-1058. doi: 10.1093/aob/mct067.
- Wasternack, C., Miersch, O., Kramell, R., Hause, B., Ward, J., Beale, M., Boland, W., Parthier, B. and Feussner, I.** (1998). Jasmonic acid: biosynthesis, signal transduction, gene expression. *Fett/Lipid*, **100**, 139-146.
- Wasternack, C. and Song, S.** (2017). Jasmonates: biosynthesis, metabolism, and signaling by proteins activating and repressing transcription. *Journal of Experimental Botany*, **68**, 1303-1321. doi: 10.1093/jxb/erw443.
- Weber, H., Vick, B. A. and Farmer, E. E.** (1997). Dinor-oxo-phytodienoic acid: A new hexadecanoid signal in the jasmonate family. *Proceedings of the National Academy of Sciences of the United States of America*, **94**, 10473-10478.
- Weichert, H., Stenzel, I., Berndt, E., Wasternack, C. and Feussner, I.** (1999). Metabolic profiling of oxylipins upon salicylate treatment in barley leaves - preferential induction of the reductase pathway by salicylate. *FEBS Letters*, **464**, 133-137.
- Weigel, D. and Glazebrook, J.** (2002). *Arabidopsis: a laboratory manual*, CSHL Press.
- Westfall, C. S., Sherp, A. M., Zubieta, C., Alvarez, S., Schraft, E., Marcellin, R., Ramirez, L. and Jez, J. M.** (2016). *Arabidopsis thaliana* GH3.5 acyl acid amido synthetase mediates metabolic crosstalk in auxin and salicylic acid homeostasis. *Proceedings of the National Academy of Sciences*, **113**, 13917-13922. doi: 10.1073/pnas.1612635113.
- Westfall, C. S., Zubieta, C., Herrmann, J., Kapp, U., Nanao, M. H. and Jez, J. M.** (2012). Structural Basis for Prereceptor Modulation of Plant Hormones by GH3 Proteins. *Science*, **336**, 1708-1711. doi: 10.1126/science.1221863.
- Widemann, E., Grausem, B., Renault, H., Pineau, E., Heinrich, C., Lugan, R., Ullmann, P., Miesch, L., Aubert, Y., Miesch, M., Heitz, T. and Pinot, F.** (2015). Sequential oxidation of jasmonoyl-phenylalanine and jasmonoyl-isoleucine by multiple cytochrome P450 of the CYP94 family through newly identified aldehyde intermediates. *Phytochemistry*, **117**, 388-399. doi: <http://dx.doi.org/10.1016/j.phytochem.2015.06.027>.
- Widemann, E., Miesch, L., Lugan, R., Holder, E., Heinrich, C., Aubert, Y., Miesch, M., Pinot, F. and Heitz, T.** (2013). The Amidohydrolases IAR3 and ILL6 contribute to jasmonoyl-isoleucine hormone turnover and generate 12-hydroxyjasmonic acid upon wounding in *Arabidopsis* leaves. *Journal of Biological Chemistry*, **288**, 31701-31714. doi: 10.1074/jbc.M113.499228.
- Widemann, E., Smirnova, E., Aubert, Y., Miesch, L. and Heitz, T.** (2016). Dynamics of jasmonate metabolism upon flowering and across leaf stress responses in *Arabidopsis thaliana*. *Plants*, **5**, 4.
- Winter, D., Vinegar, B., Nahal, H., Ammar, R., Wilson, G. V. and Provart, N. J.** (2007). An "Electronic Fluorescent Pictograph" browser for exploring and analyzing large-scale biological data sets. *PLoS ONE*, **2**, e718. doi: 10.1371/journal.pone.0000718.
- Woodward, A. W. and Bartel, B.** (2005). Auxin: regulation, action, and interaction. *Ann Bot*, **95**, 707-735. doi: 10.1093/aob/mci083.
- Wu, J. and Baldwin, I. T.** (2010). New Insights into Plant Responses to the Attack from Insect Herbivores. *Annual Review of Genetics*, **44**, 1-24. doi: 10.1146/annurev-genet-102209-163500.
- Xing, H.-L., Dong, L., Wang, Z.-P., Zhang, H.-Y., Han, C.-Y., Liu, B., Wang, X. and Chen, Q.-J.** (2014). A CRISPR/Cas9 toolkit for multiplex genome editing in plants. *BMC Plant Biology*, **14**, 327.

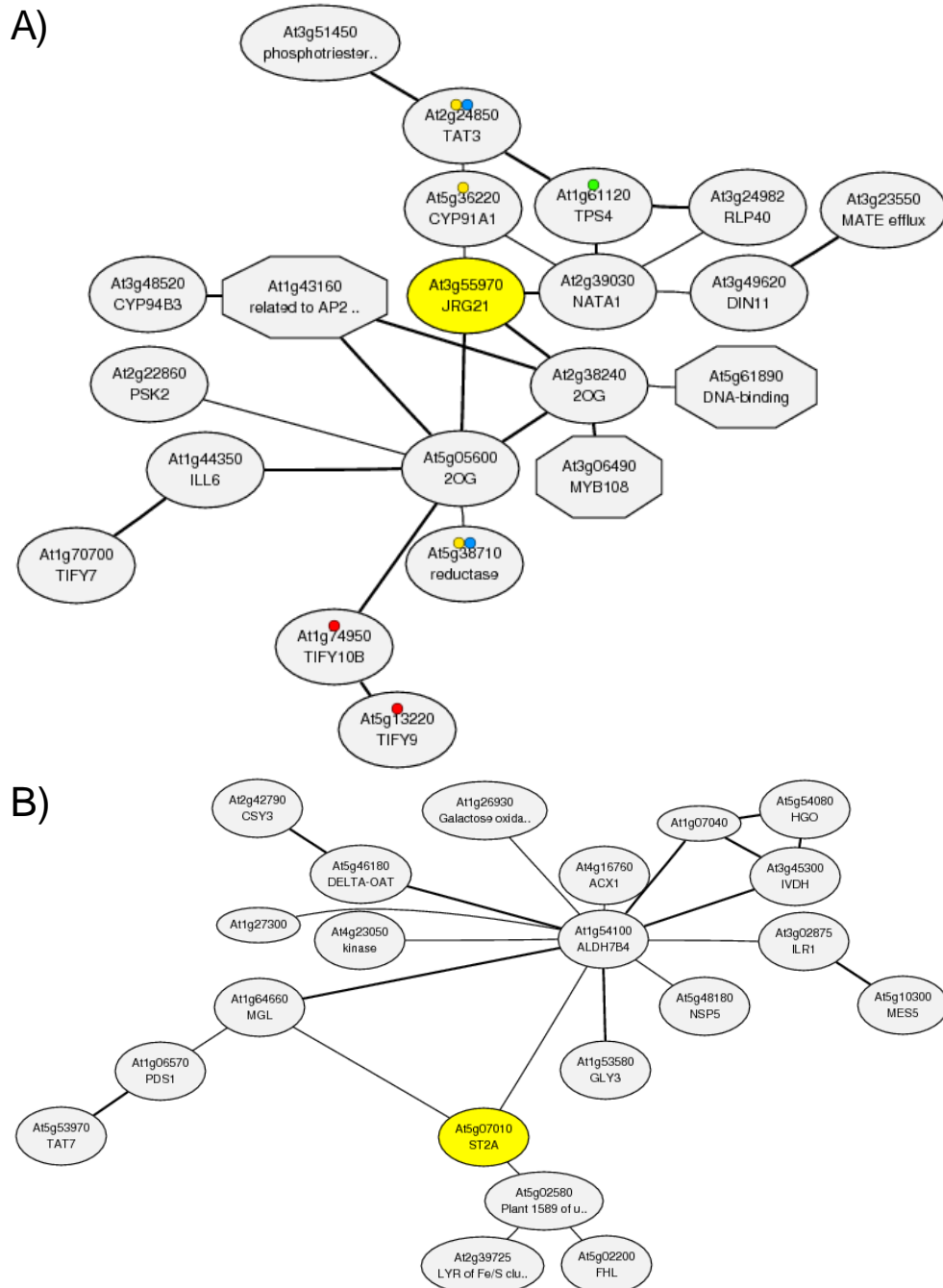
-
- Xu, Y., Chang, P. F. L., Liu, D., Narasimhan, M. L., Raghothama, K. G., Hasegawa, P. M. and Bressan, R. A.** (1994). Plant defense genes are synergistically induced by ethylene and methyl jasmonate. *The Plant Cell*, **6**, 1077-1085.
- Yoshida, Y., Sano, R., Wada, T., Takabayashi, J. and Okada, K.** (2009). Jasmonic acid control of GLABRA3 links inducible defense and trichome patterning in Arabidopsis. *Development*, **136**, 1039-1048. doi: 10.1242/dev.030585.
- Yoshihara, T., Omir, E.-S. A., Koshino, H., Sakamura, S., Kkuta, Y. and Koda, Y.** (2014). Structure of a Tuber-inducing Stimulus from Potato Leaves (*Solanum tuberosum* L.). *Agricultural and Biological Chemistry*, **53**, 2835-2837. doi: 10.1080/00021369.1989.10869712.
- Zhang, T., Poudel, A. N., Jewell, J. B., Kitaoka, N., Staswick, P., Matsuura, H. and Koo, A. J.** (2016). Hormone crosstalk in wound stress response: wound-inducible amidohydrolases can simultaneously regulate jasmonate and auxin homeostasis in *Arabidopsis thaliana*. *Journal of Experimental Botany*, **67**, 2107-2120. doi: 10.1093/jxb/erv521.
- Zhu, Z., An, F., Feng, Y., Li, P., Xue, L., A, M., Jiang, Z., Kim, J. M., To, T. K., Li, W., Zhang, X., Yu, Q., Dong, Z., Chen, W. Q., Seki, M., Zhou, J. M. and Guo, H.** (2011). Derepression of ethylene-stabilized transcription factors (EIN3/EIL1) mediates jasmonate and ethylene signaling synergy in *Arabidopsis*. *Proc Natl Acad Sci U S A*, **108**, 12539-12544. doi: 10.1073/pnas.1103959108.

8. SUPPLEMENTAL DATA



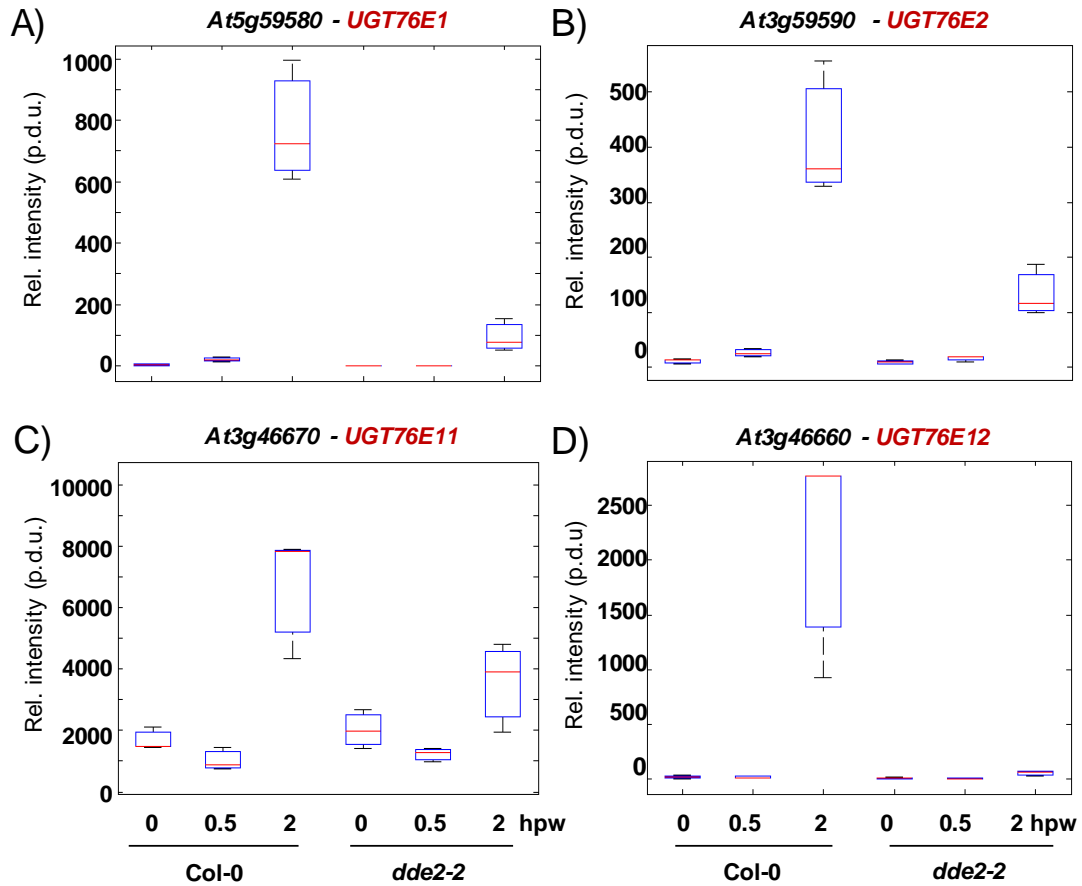
Supplemental figure 1: Phylogenetic tree of glycosyltransferases of *A. thaliana*

Phylogenetic analysis of 107 UGTs in *A. thaliana*. “Neighbor-joining and parsimony-based analysis of nine conserved amino acid sequences. Bootstrap values over 60 % are indicated above the nodes, with the number on the left indicating neighbor-joining and that on the right indicating parsimony. Dashes indicate bootstrap values under 60%. Hypothetical intron gains and losses are indicated by diamonds with the intron number (I). Postulated intron gains are indicated by filled diamonds, intron losses by unfilled diamonds and the questionable intron loss by a striped diamond.” Colors indicate phylogenetic groups (A-N) with a bootstrap support greater than 90 % in the distance analysis. Figure and text taken from Ross *et al.*, 2001.



Supplemental figure 2: Search for glucosyltransferase genes products by co-expression analysis

Micro-array co-expression analysis of gene products involved in 12-hydroxy-JA metabolism. **A)** Co-expression gene network around Jasmonic acid oxidase 3 (*JOX3*, *At3g55970*, yellow circle). *JOX3* is co-expressed with genes involved in plant hormone signal transduction (red marks), biosynthesis of secondary metabolites (yellow marks), diterpenoid biosynthesis (green marks), and biosynthesis of antibiotics (blue marks). **B)** Co-expression gene network of sulfotransferase 2a (*ST2a*, *At5g07010*, yellow circle). Octagonal shape indicates transcription factors and circular shape others. Networks are drawn based on Mutual Ranks (MR) giving an average correlation of two genes indicating stronger correlation by smaller values (MR = 1-5: bold lines, MR = 5-30: normal lines, MR > 30: weak lines). Marks indicate a common KEGG pathway. Access 02.05.2018; the page was prepared on Dec. 14. 2017 for ATTED-II version 9.1



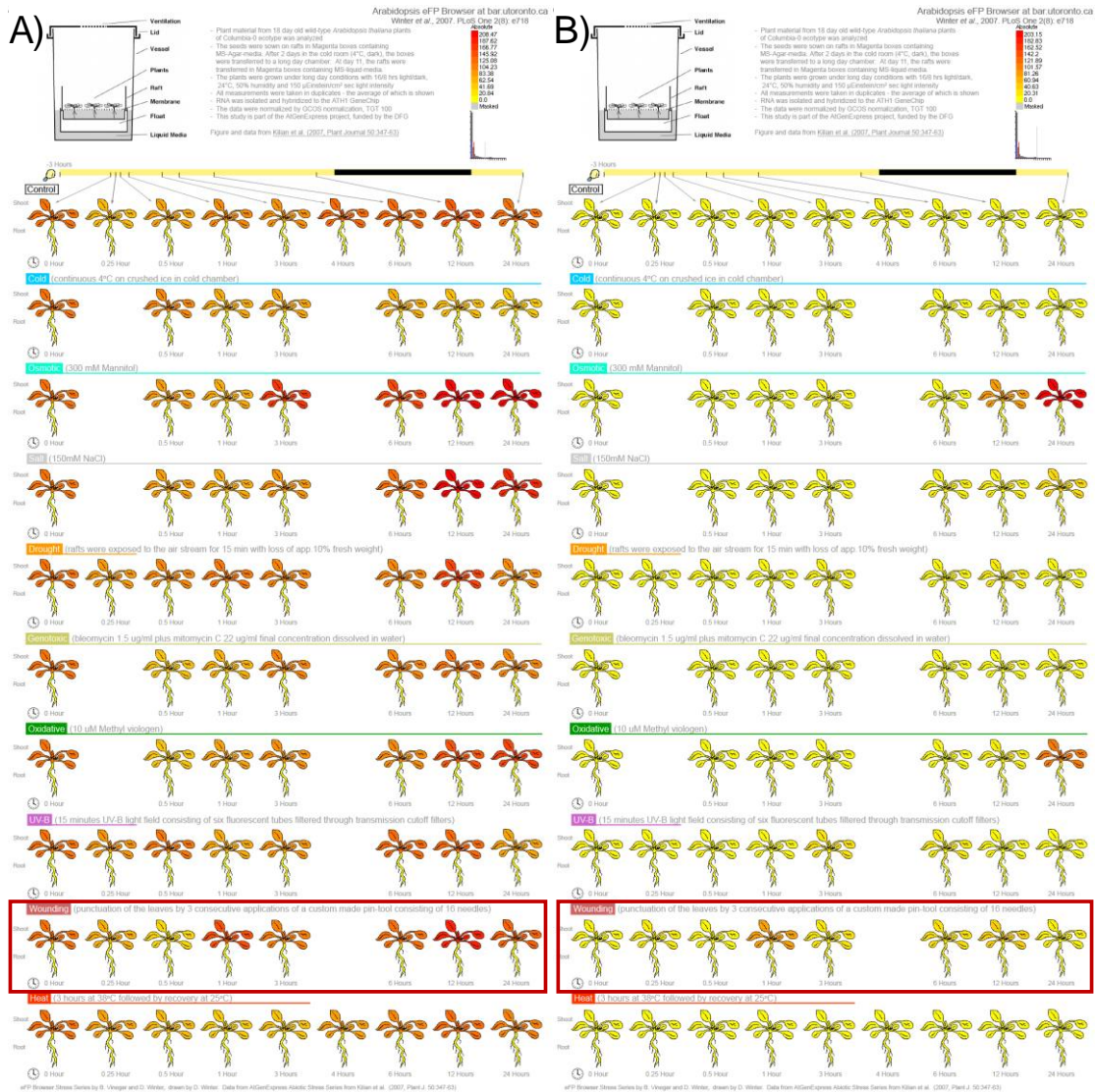
Supplemental figure 3: Expression of *UGT76E1*, *UGT76E2*, *UGT76E11*, and *UGT76E12* in *A. thaliana* leaves after wounding

Transcriptomic analysis of Col-0 and a JA-deficient mutant (*dde2-2*). Plants were grown for six weeks at 22°C under short day conditions (8 h light/16 h dark). Leaves were wounded three times across the mid vein by squeezing with forceps. Damaged rosette leaves were harvested at indicated time points (hours post wounding (hpw)). RNA was isolated and used for micro-array analysis. The transcriptomics data was recorded by a 44 k Affimetrix micro-array analysis and the readout is given in relative intensities (procedure defined units (p.d.u.)). Given are Box-Whisker-plots of the relative intensities of **A)** *At5g59580*, *UGT76E1*, **B)** *At3g59590*, *UGT76E2*, **C)** *At3g46670*, *UGT76E11*, and **D)** *At3g46660*, *UGT76E12*. The data represents medians of three experiments. Data from Dr. A. Mosblech, Dr. K. Feussner and Prof. Dr. I. Heilmann, 2010 unpublished.



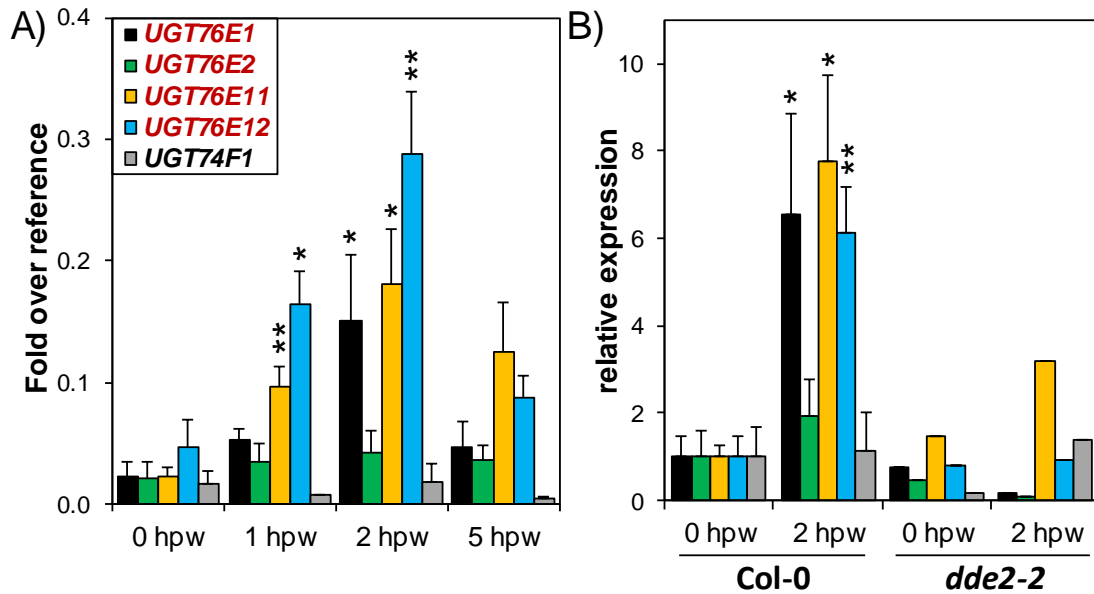
Supplemental figure 4: Expression of UGT76E1 and UGT7E2 after abiotic stresses

Expression analysis of indicated genes after abiotic stresses: cold, osmotic, alt, drought, genotoxic, oxidative, UV-B, wounding, and heat. Stress responses are illustrated from 0 -24 hours after stimulus **A)** Expression pattern of *UGT76E1*. Response after wounding is highlighted (red box). **B)** Expression pattern of *UGT76E2*. Response after wounding is highlighted (red box). The graphics are taken from Arabidopsis eFP-Browser; original data from Winter *et al.*, 2007. Access 02.05.2018



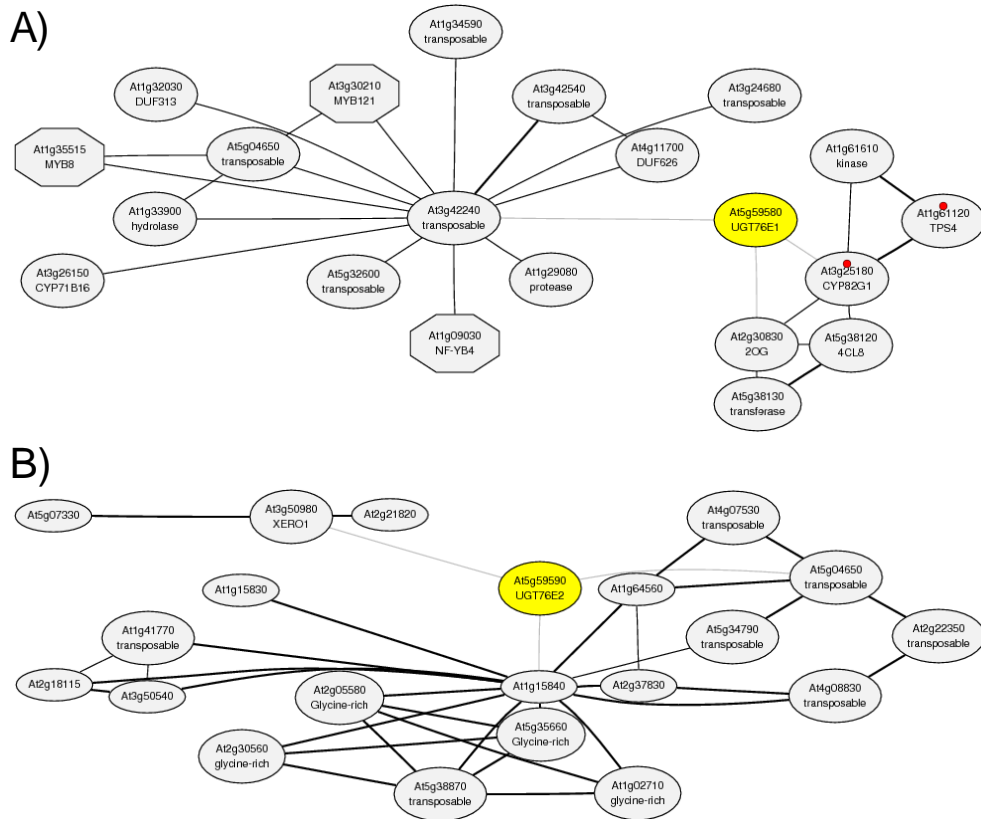
Supplemental figure 5: Expression of *UGT76E11* and *UGT7E12* after abiotic stresses

Expression analysis of indicated genes after abiotic stresses: cold, osmotic, alt, drought, genotoxic, oxidative, UV-B, wounding, and heat. Stress responses are illustrated from 0 -24 hours after stimulus **A**) Expression pattern of *UGT76E11*. Response after wounding is highlighted (red box). **B**) Expression pattern of *UGT7E12*. Response after wounding is highlighted (red box). The graphics are taken from Arabidopsis eFP-Browser; original data from Winter *et al.*, 2007. Access 02.05.2018.



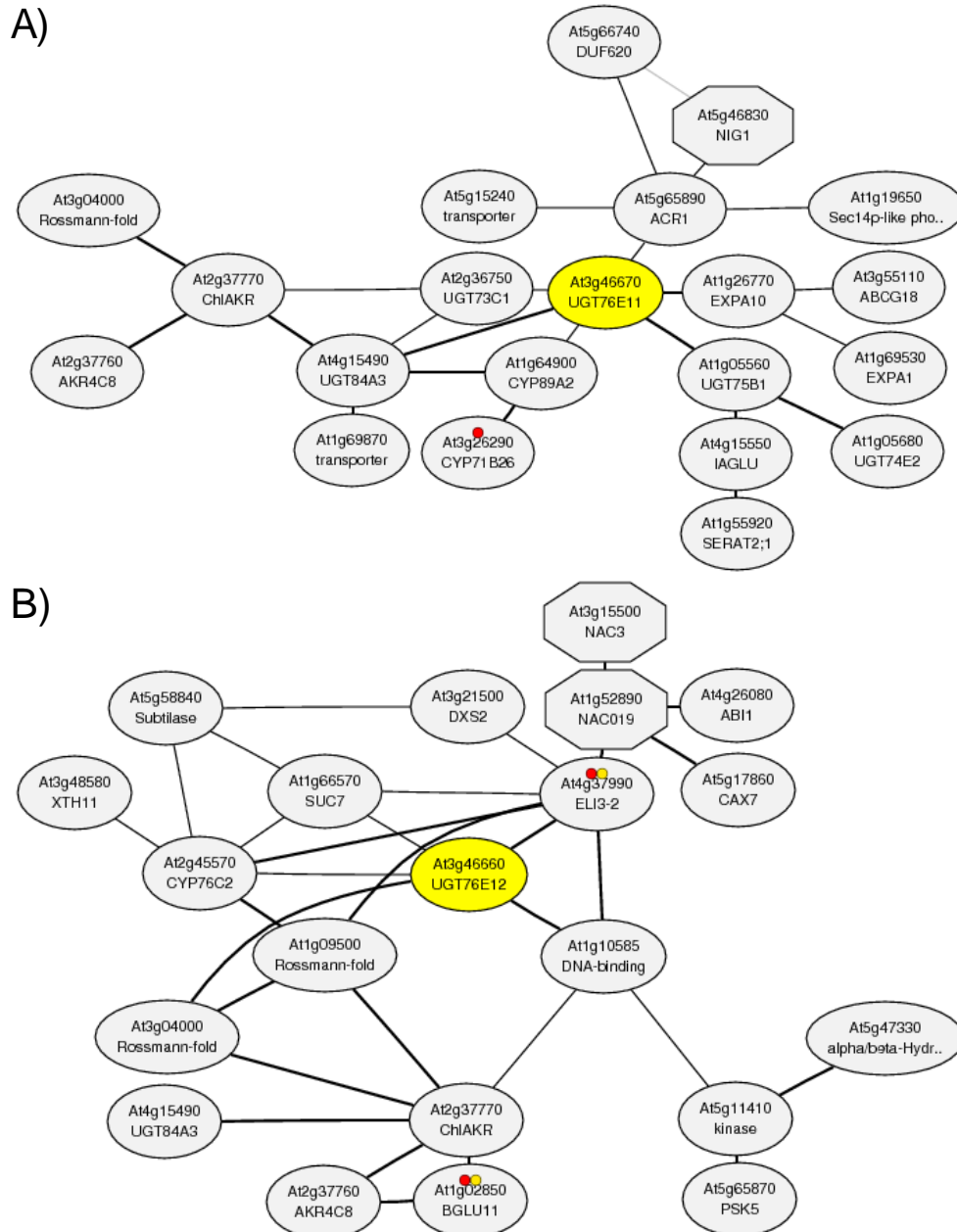
Supplemental figure 6: Expression of *UGT76E1*, *UGT76E2*, *UGT76E11*, *UGT76E12*, and *UGT74F1* in Col-0 and JA-deficient mutant after wounding

Quantitative real-time PCR of *UGT76E1* (red), *UGT76E2* (green), *UGT76E11* (orange), *UGT76E12* (blue), and *UGT74F1* (grey). Col-0 and JA-deficient (*dde2-2*) plants were grown for six weeks at 22 °C under short day conditions (8 h light/16 h dark). Leaves were wounded three times across the mid vein by squeezing with forceps. Damaged rosette leaves were harvested at indicated time points (hours post wounding (hpw)), RNA was isolated, and appr. 1 µg transcribed complementary DNA were used for PCR. All expression values are normalized to actin 8 as reference. Relative expression of the transcripts normalized to their respective expression levels at 0 hpw in Col-0 and *dde2-2*. Col-0-data represents the mean value + SD of three biological replicates, *dde2-2*-data presents one experiment. 10 plants per time point were pooled for one replicate. Asterisks indicate significance by one-sided T-Test with *p<0.05, **p<0.01.



Supplemental figure 7: Co-expression analysis of *UGT76E1* and *UGT76E2*

Micro-array co-expression analysis of gene products of indicated genes. **A)** Co-expression gene network around *UGT76E1* (*At5g59580*, yellow circle). *UGT76E1* is co-expressed with genes involved in diterpenoid biosynthesis (red marks). **B)** Co-expression gene network of *UGT76E2* (*At5g59590*, yellow circle). Octagonal shape indicates transcription factors and circular shape others. Networks are drawn based on Mutual Ranks (MR) giving an average correlation of two genes indicating stronger correlation by smaller values (MR = 1-5: bold lines, MR = 5-30: normal lines, MR > 30: weak lines). Marks indicate a common KEGG pathway. Access 02.05.2018; the page was prepared on Dec. 14. 2017 for ATTED-II version 9.1



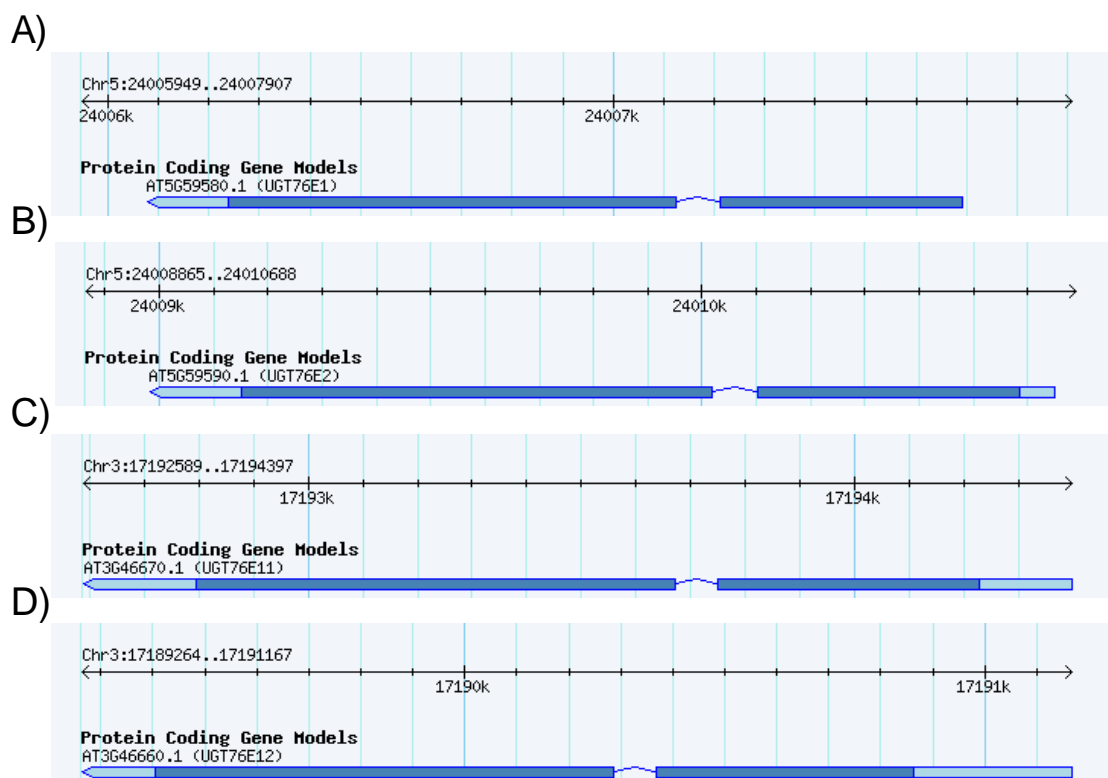
Supplemental figure 8: Co-expression analysis of *UGT76E11* and *UGT76E12*

Micro-array co-expression analysis of gene products of indicated genes. **A)** Co-expression gene network around *UGT76E11* (*At3g46670*, yellow circle). *UGT76E11* is co-expressed with genes involved in biosynthesis of secondary metabolites (red marks). **B)** Co-expression gene network of *UGT76E12* (*At3g46660*, yellow circle). *UGT76E12* is co-expressed with genes involved in biosynthesis of secondary metabolites (red marks) and genes of the phenylpropanoid biosynthesis (yellow marks). Octagonal shape indicates transcription factors and circular shape others. Networks are drawn based on Mutual Ranks (MR) giving an average correlation of two genes indicating stronger correlation by smaller values (MR = 1-5: bold lines, MR = 5-30: normal lines, MR > 30: weak lines). Marks indicate a common KEGG pathway. Access 02.05.2018; the page was prepared on Dec. 14. 2017 for ATTED-II version 9.1

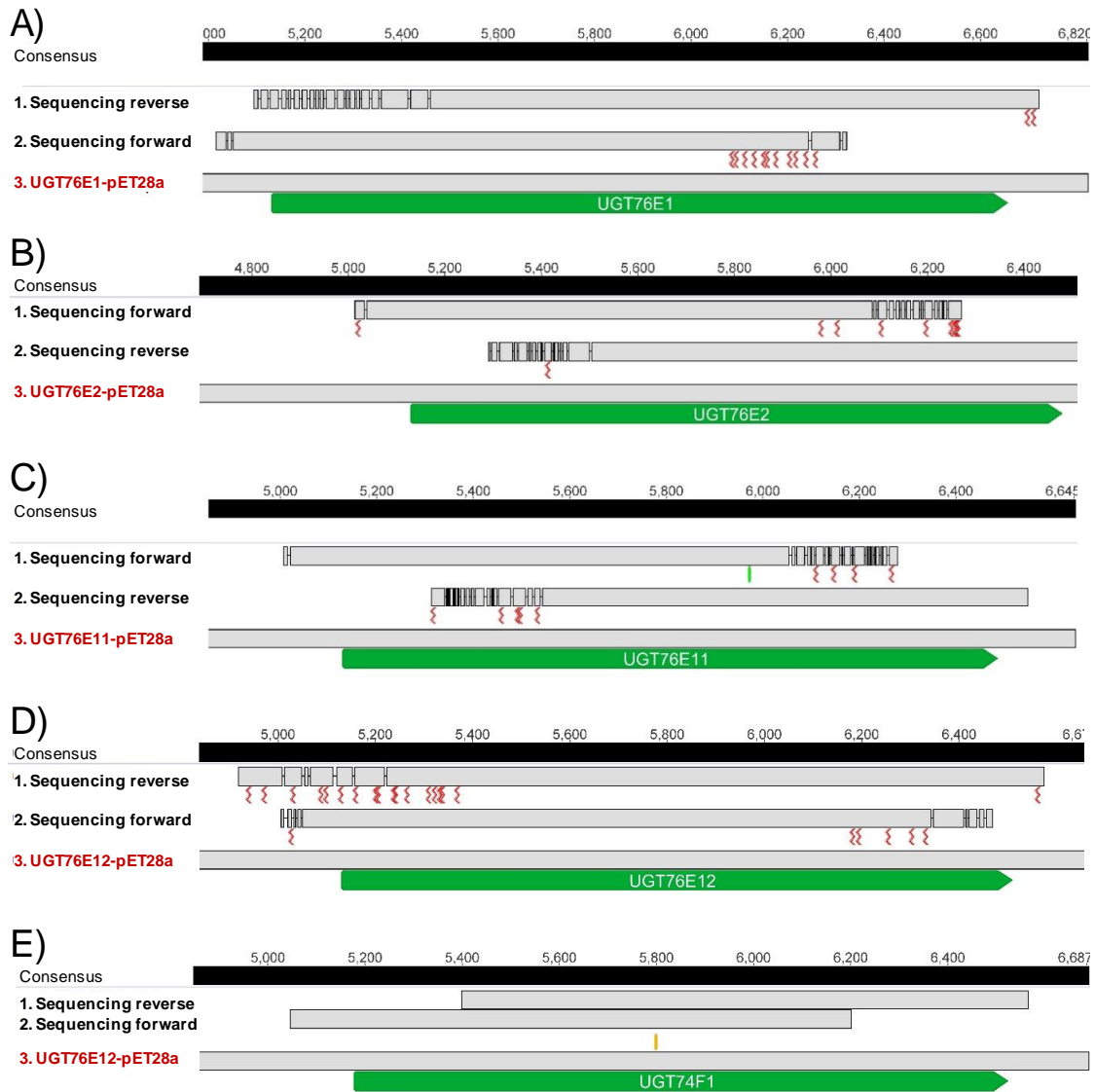
Supplemental table 1: Calculated protein parameters and predicted localizations for UGT76E1, UGT76E2, UGT76E11, UGT76E12 and UGT74F1

Information about the proteins were calculated from their primary amino acid sequences with different online-tools. The table depicts the molecular weight (MW), the specific extinction coefficient at 280 nm (ϵ), the theoretical isoelectric point (pI), the presents of a signal peptide (SignalP), target peptides (TargetP), and the number of transmembrane domains (TMHMM) for UGT76E1, UGT76E2, UGT76E11, UGT76E12, and UGT74F1. The protein parameters were calculated with ProtParam and localization predictions were done with SignalP, TargetP (plant settings), and TMHMM online tools. Access was 04.05.2018.

Parameter	UGT76E1	UGT76E2	UGT76E11	UGT76E12	UGT74F1
MW (kDa)	50.8	50.1	50.6	51.7	50.3
ϵ (kM ⁻¹ cm ⁻¹)	66.4	63.5	58.0	55.5	62.4
pI	6.6	5.4	5.9	6.0	5.5
SignalP	/	/	/	/	/
TargetP	mitochondrial	/	/	/	/
TMHMM (no.)	0	0	0	0	0

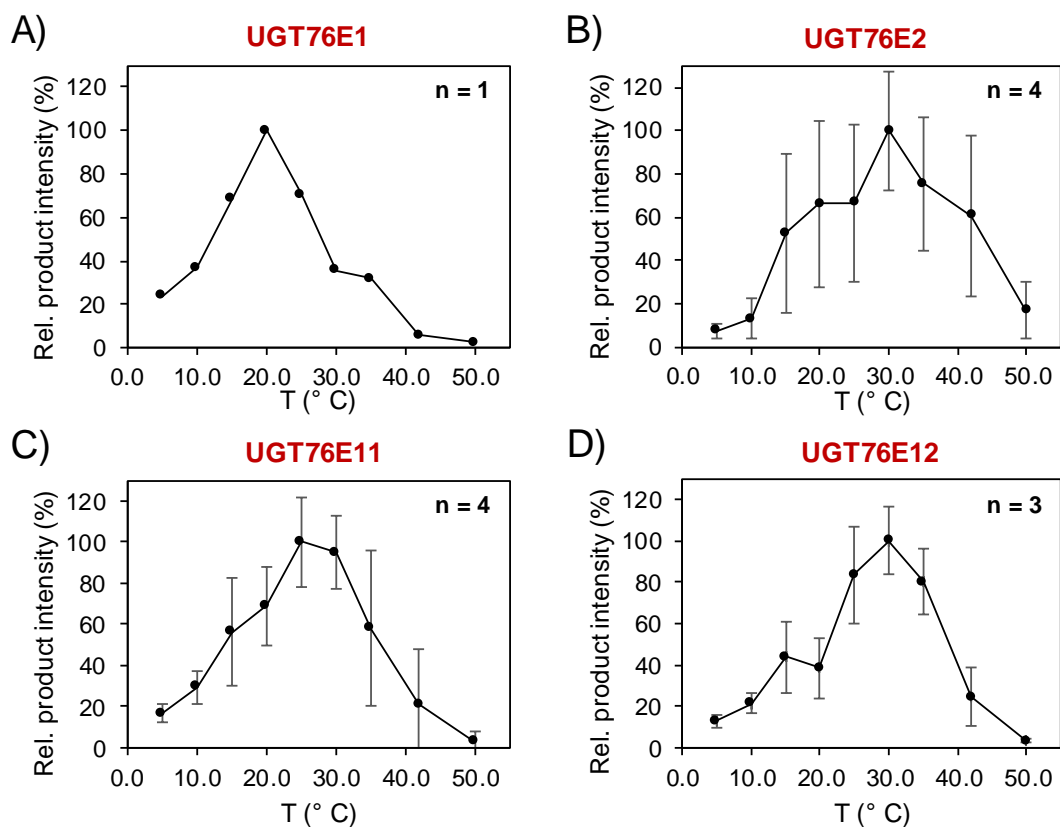
**Supplemental figure 9: Gene structures of UGT76E1, UGT76E2, UGT76E11, and UGT76E12 in *A. thaliana* genome**

Gene maps of the indicated *UGTs* in the *A. thaliana* genome. Nucleotide bar depicts the location in the chromosome (black bar). Gene structure is shown in coding region (dark blue), untranslated region (light blue), and introns (arrow up lines). Shown are gene maps of **A)** *UGT76E1*, **B)** *UGT76E2*, **C)** *UGT76E11*, and **D)** *UGT76E12*. Graphics taken from The Arabidopsis Information Resource (TAIR), access 02.05.2018.



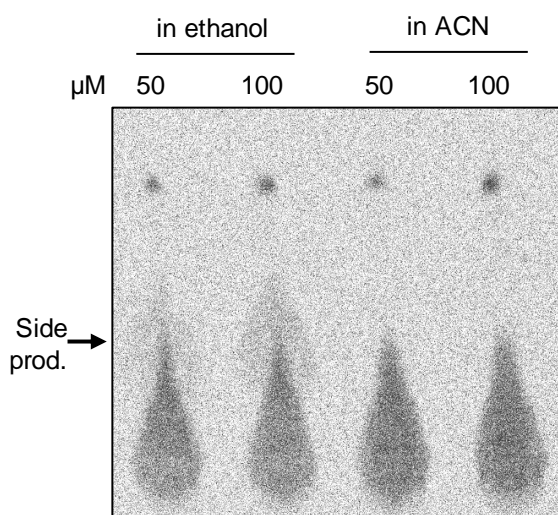
Supplemental figure 10: Sequencing results of *UGT76E1*, *UGT76E2*, *UGT76E11*, *UGT76E12*, and *UGT74F1* integrated into the expression vector

The coding sequences of indicated genes were amplified from complementary DNA (cDNA) 2 hours post wounding. The sequence of *UGT74F1* was amplified from root cDNA. Indicated UGT-sequences (green annotations) were fused to an N-terminal His-tags of pET28a vectors for heterologous protein expression in *E. coli*. Correct cloning was checked by sequencing from two directions (forwards and reverse). Poor sequencing results are marked with red tildes, manual insertion is given as green line, and differing sequence is marked with yellow line. Complete and correct sequencing results are shown for **A)** *UGT76E1*, **B)** *UGT76E2*, **C)** *UGT76E11*, and **D)** *UGT76E12*. **E)** The sequence of *UGT74F1* illustrates a splice variant of the template. All alignments were done with the Geneious algorithm as global alignment with free end gaps and 65 % cost matrix in Geneious version 8.1 (Biomatters). Available from <http://www.geneious.com>



Supplemental figure 11: Optimum temperature of UGT7E1, UGT76E2, UGT76E11, and UGT7E12

Temperature optima for the indicated UGTs were determined in the range of 4 to 50 °C. 0.1 mM ω -hydroxy-hexadecanoic acid and 0.5 mM UDP-Glc in the gel filtration buffer of the receptive enzyme were equilibrated at the indicated temperatures for 1 h. The product formation was detected by LC-MS and shown as relative signal intensities (%) over temperature for **A)** UGT76E1, **B)** UGT76E2, **C)** UGT76E11, and **D)** UGT76E12. Data represents one experiment for UGT76E1. All other measurements are means with \pm SD of and at least three independent experiments



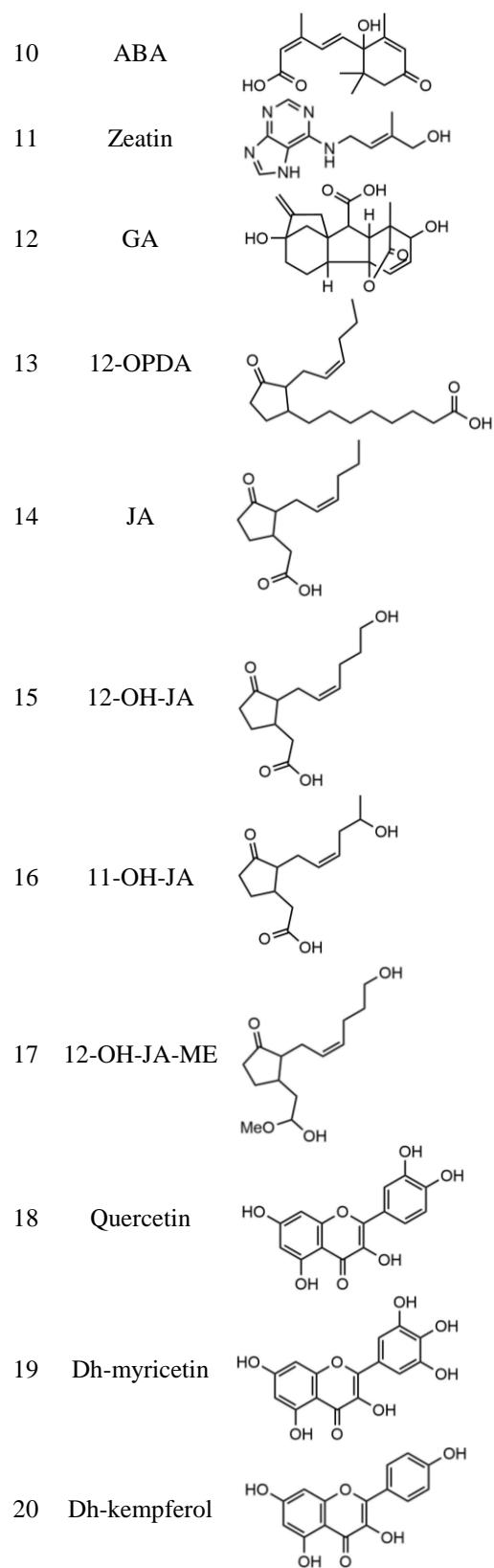
Supplemental figure 12: UGT76E12 shows side activity towards ethanol

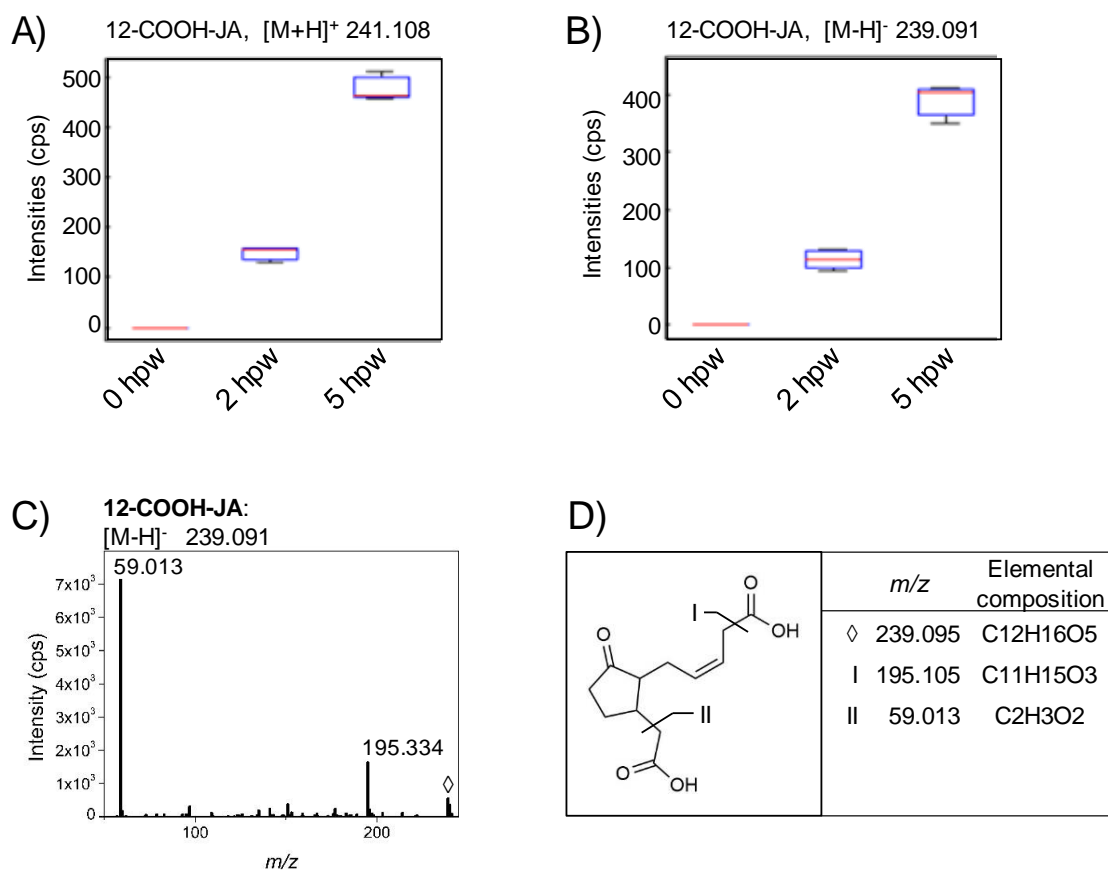
The substrate specificities of UGT76E12 was analyzed by an activity assay with uniformly labeled UDP-¹⁴C(U)-Glc towards ω -hydroxy-hexadecanoic acid. The assay was performed with 5 μ g homogeneous UGT76E12, 50 μ M or 100 μ M ω -hydroxy-hexadecanoic acid dissolved in ethanol or acetonitrile (ACN) and 30 μ M UDP-Glc, 0.02 μ Ci UDP-¹⁴C(U)-Glc in the buffer (20 mM tris/HCl, pH 7.5, 50 mM NaCl). The reaction took place for 1 h at 25 °C. After metabolite extraction and thin layer chromatography (TLC), the TLC-plates were incubated on phosphoscreens for 5 days and the radioactive signals detected. The arrow indicates a side product (side-prod.) with ethanol. The data represents one experiment.

Supplemental table 2: Chemical structures of the UGT-substances

Chemical structures of hexadecanoic acid (16:0), ω -hydroxy-16:0 (ω -OH-16:0), 2-hydroxy-16:0 (2-OH-16:0), 3-hydroxy-16:0 (3-OH-16:0), hexadecanol (OH-C16), benzoic acid (BA), salicylic acid (SA), pipercolic acid (Pip), indole-3-carboxylic acid (ICA), abscisic acid (ABA), zeatin, gibberellic acid (GA), 12-oxo-phytodienoic acid (12-OPDA), JA, 12-hydroxy-JA (12-OH-JA), 11-hydroxy-JA (11-OH-JA), 12-hydroxy-JA-methyl ester (12-OH-JA-ME), quercetin, dihydro-myricetin (dh-myricetin), and dihydro-kaempferol (dh-kaempferol).

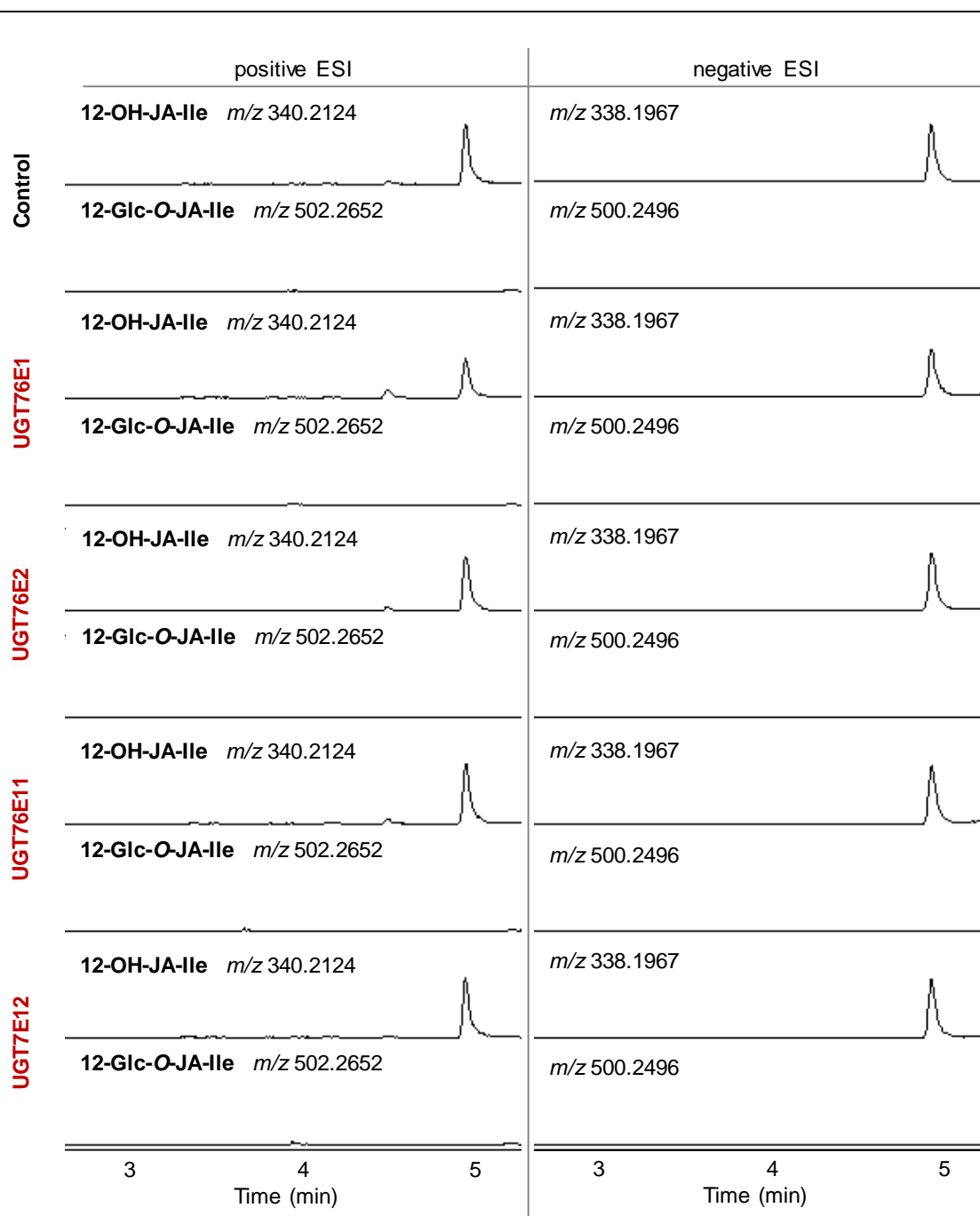
Substrates	Structure
1 16:0	
2 ω -OH-16:0	
3 2-OH-16:0	
4 3-OH-16:0	
5 OH-C16	
6 BA	
7 SA	
8 Pip	
9 ICA	





Supplemental figure 13: 12-carboxy-JA was identified in leaves after wounding

The metabolite 12-carboxy-JA (12-COOH-JA) was identified in the *ex vivo* metabolite fingerprinting analysis. Therefore, plants were grown for six weeks at 22 °C under short day conditions (8 h light/16 h dark). Leaves were wounded three times across the mid vein by squeezing with forceps. Damaged rosette leaves were harvested at 0, 2, and 5 hours post wounding (hpw), extracted, and used as substrate mix for the *ex vivo* activity assay. The extracts were resolved in 50 mM Tris pH 8, 100 mM NaCl buffer and 20 μ l acetonitrile. This samples were analyzed by mass spectrometry with a method, which was developed for non-targeted fingerprinting. Out of 1996 metabolite features with a $pVal < 10^{-6}$ the particular features of 12-COOH-JA were found in the **A)** positive ionization mode and **B)** in the negative ionization mode shown as Box-Whisker-plots. The data represents three measurements of one experiments. 10 plants were pooled for each time point of one replicate. Data was analyzed with the MarVis tool (Kaefer, 2014). **C)** The compound with the mass-to-charge ratio (m/z) 239.091(◇) was fragmented with a collision energy of 12 eV. **D)** Structure analyses of the main fragments can be assigned to 12-COOH-JA. Analysis was performed by Dr. Kirstin Feussner. Intensities given as counts per second (cps)



Supplemental figure 14: 12-O-glucosyl-jasmonoyl-isoleucine is not detected in plants

Plants were grown for six weeks at 22 °C under short day conditions (8 h light/16 h dark). Leaves were wounded three times across the mid vein by squeezing with forceps. Damaged rosette leaves were harvested at 5 hours post wounding (pool of 10 plants per sample), extracted, and used as substrate mix for the *ex vivo* activity assay. The extracts were resolved in 50 mM Tris pH 8, 100 mM NaCl buffer and the assay was performed with 0.1 mM UDP-Glc and 100 µg of the indicated active UGT-enzymes or inactive enzyme (control) for 1 h at 25 °C. The reactions were stopped by adding acetonitrile and analyzed by mass spectrometry with a method, which was developed for non-targeted fingerprinting (1996 features with $p\text{Val} < 10^{-6}$). Given are the extracted ion chromatograms of 12-hydroxy-jasmonoyl-isoleucine (12-OH-JA-Ile) in the negative ionization mode (mass-to-charge ratio (m/z) 338.1967) and in the positive ionization mode (m/z 340.2124) as well as for 12-O-glucosyl-jasmonoyl-isoleucine (12-O-Glc-JA-Ile) in the positive ionization mode (m/z 502.2652), and the negative ionization (m/z 500.2496). All chromatograms show relative signal intensities fixed to 10^4 counts per second over the time. The data is representative for three measurements of one experiments. Samples were measured by Dr. Kirstin Feussner. Data was analyzed with the MarVis tool (Kaefer, 2014).

Supplemental table 3: Identification of specific metabolite markers by fragmentationSpecific metabolites of the *ex vivo* metabolite fingerprinting analysis were identified by mass spectrometry and fragmentation (MS/MS).

ID	Metabolite marker	RT (min)	Exact mass (Da)	Detected ion	Sum formula	Reference	Identity confirmed by	Specific fragments	CE (eV)
1	12-OH-JA	3.52	226.1205	M-H	C12H18O4		B, D	[M-H] ⁻ 225.1132, 59.0128	12
2	12-O-Glc-JA	3.24	388.1733	M-H	C18H28O9		B, D	[M-H] ⁻ 387.1608, 207.0981, 59.0122	25
3	SA	4.17	138.0316	M-H	C7H6O3	MID 616	A	[M-H] ⁻ 137.0221, 93.0330	12
4	2-O-Glc-SA	2.72	300.0845	M-H	C13H16O8	MID 616	C	[M-H] ⁻ 299.0756, 137.0225, 93.0328	12
5	ω -OH-16:0	6.72	272.2351	M-H	C16H32O3	MID 85386	A, D	[M-H] ⁻ 271.2267, 253.218, 225.2191, 59.0139	32
6	ω -O-Glc-16:0	5.81	434.2879	M-H	C18H42O8	MID 85386	C	[M-H] ⁻ 433.2742, 415.2679, 271.2281, 59.0139	25
7	UDP-Glc	0.72	566.0550	M-H	C15H24N2O17P2	MID 97	A	[M-H] ⁻ 565.0449, 384.9825, 323.0267, 241.0108, 78.9583	18
8	UDP	0.86	404.0021	M-H	C9H14N2O12P2	MID 5886	A	[M-H] ⁻ 402.9882, 305.0114, 272.9530, 158.9226, 111.017,	20
9	11-HHT	6.1	266.1881	M-H	C16H26O3	Montillet <i>et al.</i> , 2004	A	[M-H] ⁻ 265.1790, 247.1695, 195.1026, 167.1083	18
10	11-O-Glc-HHT	5.63	428.2410	M-H	C22H36O8	Montillet <i>et al.</i> , 2004	C	[M-H] ⁻ 427.23129, 265.1785, 247.1681	25
11	13-HOT	7.11	294.2194	M-H	C18H30O3	Montillet <i>et al.</i> , 2004	A, D	[M-H] ⁻ 293.2117, 275.162	15
12	13-O-Glc-HOT	6.05	456.2723	M-H	C24H40O8	Montillet <i>et al.</i> , 2004	C	[M-H] ⁻ 455.2660, 293.2117, 275.1950, 223.1275	25
13	C11H18O3	6.01	198.1255	M+H	C11H18O3			[M+H] ⁺ 199.1888, 181.1221, 125.0595, 111.0438, 55.0541	12
14	C11H18O3-Glc	5.01	360.1784	M+NH4	C17H28O8			[M+H] ⁺ 378.2452, 199.1327, 181.1221, 163.1112, 111.0440	18
15	12-COOH-JA	4.31	240.0998	M-H	C12H16O5	Bruckhoff <i>et al.</i> , 2016	A	[M-H] ⁻ 239.095, 195.105, 59.013	12
16	12-OH-JA-Ile	4.94	339.2045	M-H M+H	C18H29N1O5		E		

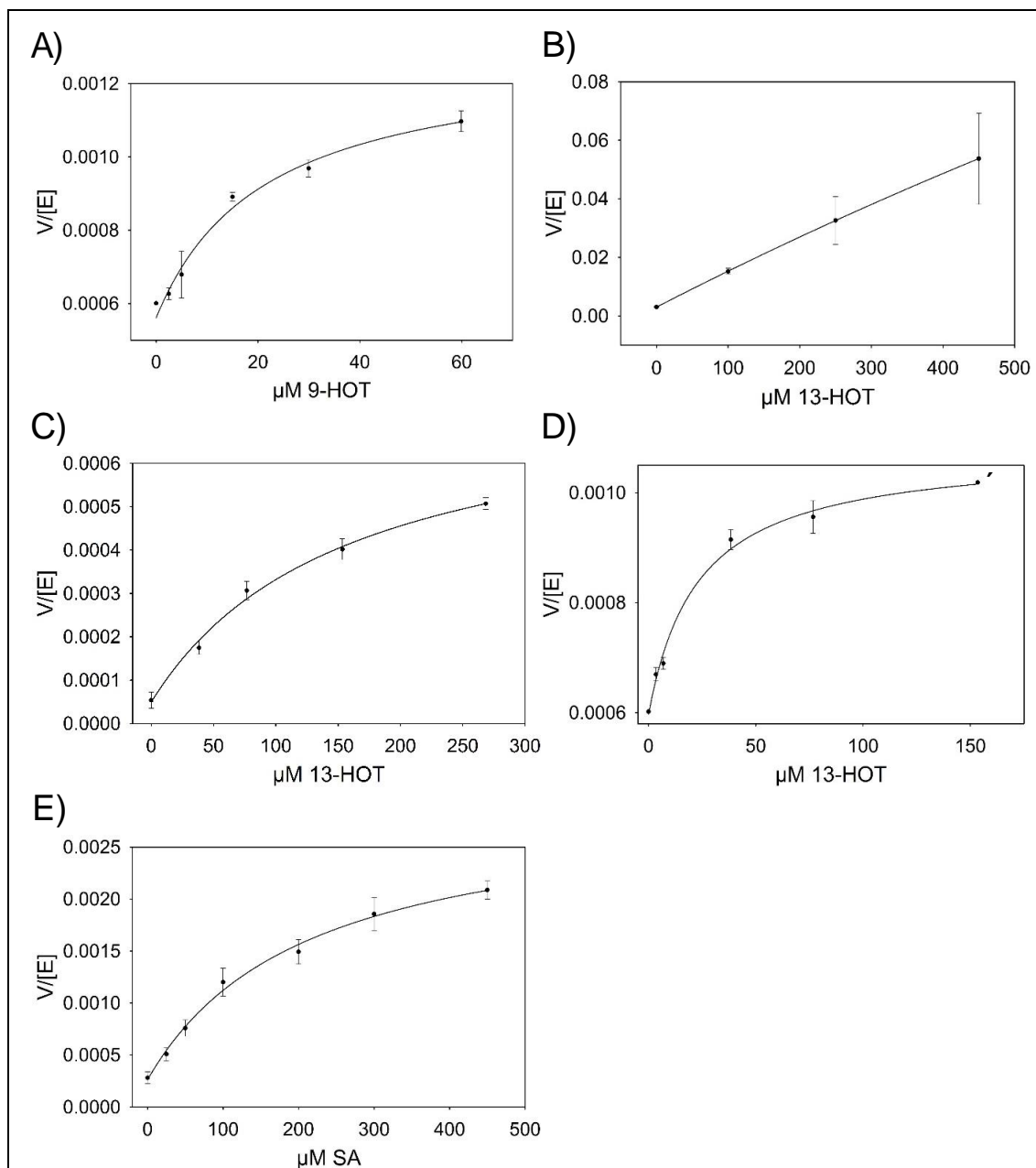
A) MS/MS fragment information from literature/data base

B) MS/MS fragment information from identical standard

C) MS/MS fragment information of non-glycosylated standard

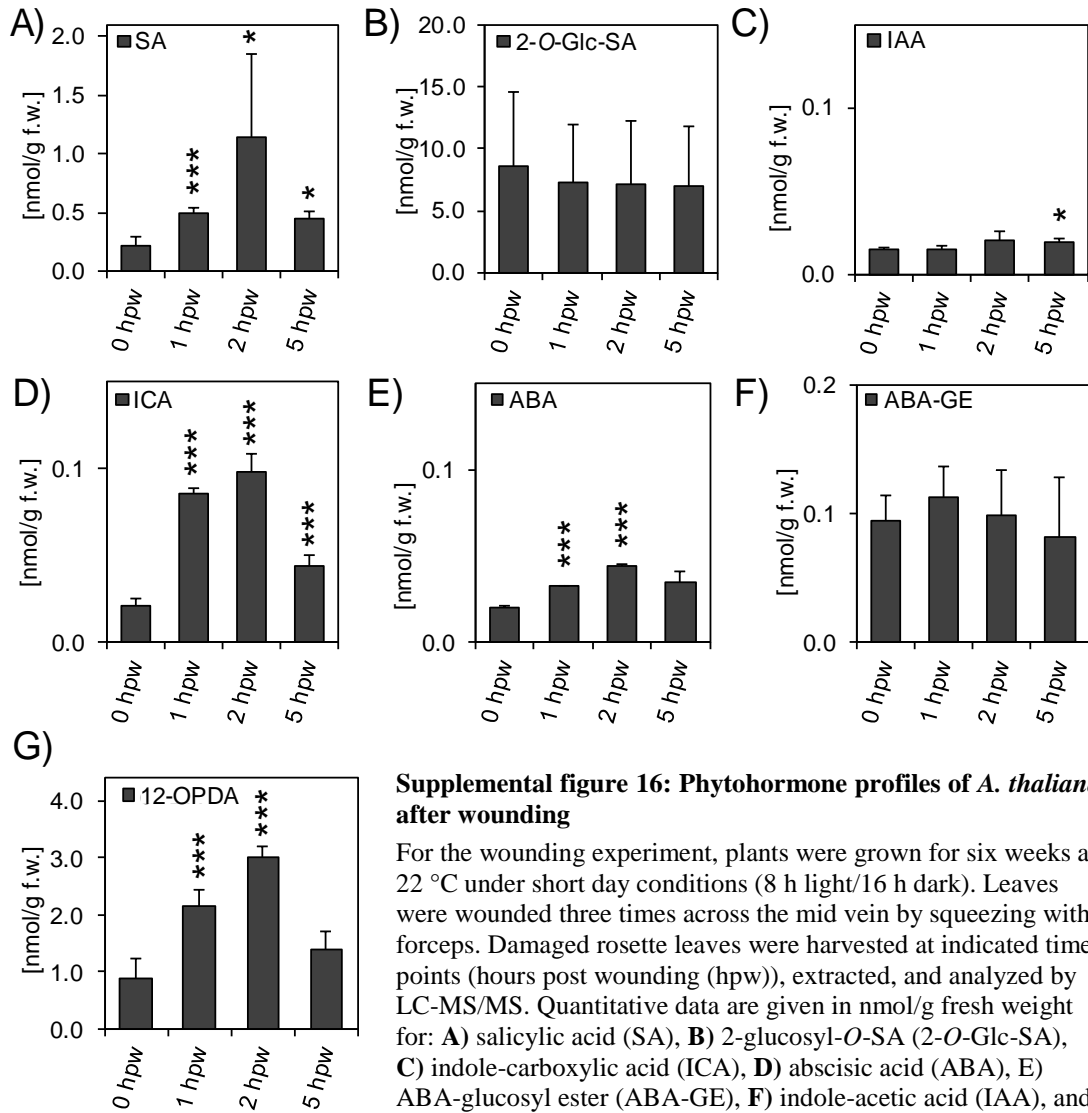
D) Coelution with authentic standard

E) Exact mass measurement only



Supplemental figure 15: Enzyme kinetics with 9- and 13-hydroxy-octadecatrienoic acid

The enzymatic kinetics of UGT76E2, UGT76E11, UGT76E12, and UGT74F1 were determined by spectrophotometric measurements. The UGT-reactions were coupled via the co-product UDP to the pyruvate kinase (PK) and the lactate dehydrogenase (LDH) in 1 : 1 : 1 stoichiometry. The PK phosphorylates UDP to UTP while metabolizing phosphoenolpyruvate to pyruvate. LDH catalyzes the reduction of pyruvate to lactate by oxidizing NADH to NAD⁺, which shows no absorption maximum at 340 nm. The assay was adapted from Brown *et al.*, 2012. The reactions were performed with 5 μg UGT76E2 in gel filtration buffer of the respective enzyme, 500 μM UDP-Glc, and indicated substrates concentration at 25 °C. The reactions were coupled to 50 μg pyruvate kinase, 50 μg lactate dehydrogenase, 0.8 mM phosphoenolpyruvate, and 0.15 mM NADH and monitored at 340 nm for 600 s. **A)** Kinetics of UGT76E12 with 9-hydroxy-octadecatrienoic acid (9-HOT) and Michaelis-Menten fit of the measurements. **B)** Kinetics of UGT76E2 with 13-hydroxy-octadecatrienoic acid (13-HOT) and Michaelis-Menten fit of the measurements. **C)** Kinetics of UGT76E11 with 13-HOT and Michaelis-Menten fit of the measurements. **D)** Kinetics of UGT76E12 with 13-HOT and Michaelis-Menten fit of the measurements. Due to limitations in 13-HOT availability, the value for 150 μM was measured only once. **E)** Kinetics of UGT74F1 with salicylic acid (SA) and Michaelis-Menten fit of the measurements. The data are mean values with standard deviation of three biological replicates.



Supplemental figure 16: Phytohormone profiles of *A. thaliana* after wounding

For the wounding experiment, plants were grown for six weeks at 22 °C under short day conditions (8 h light/16 h dark). Leaves were wounded three times across the mid vein by squeezing with forceps. Damaged rosette leaves were harvested at indicated time points (hours post wounding (hpw)), extracted, and analyzed by LC-MS/MS. Quantitative data are given in nmol/g fresh weight for: **A)** salicylic acid (SA), **B)** 2-glucosyl-*O*-SA (2-*O*-Glc-SA), **C)** indole-carboxylic acid (ICA), **D)** abscisic acid (ABA), **E)** ABA-glucosyl ester (ABA-GE), **F)** indole-acetic acid (IAA), and **G)** 12-oxophytodienoic acid (12-OPDA). Each data point represents the mean value + SD of three biological replicates from three independent experiments. 10 plants were pooled for each time point of one replicate. Asterisks indicate significance by one-sided T-Test with * $p < 0.05$, ** $p < 0.01$, *** $p < 0.005$. Samples were measured by Dr. Cornelia Herrfurth.

CURRICULUM VITAE

Sven Haroth

PERSONAL INFORMATION

Date of birth: 01.06.1986
 Place of birth: Alfeld, Germany
 Nationality: German

EDUCATION

Since 01/2015	<i>Doctor rerum naturalium</i> Department of Plant Biochemistry, Albrecht-von-Haller-Institute for Plant Science, University of Goettingen within the doctoral program “Plant Responses To Eliminate Critical Threats” of the Georg-August University School of Science (GAUSS, Member of the excellence cluster „Göttingen Graduate School for Neurosciences, Biophysics, and Molecular Biosciences”) Thesis title: Metabolic fate of jamonates
10/2012 – 01/2015	Master of Science Department of Plant Biochemistry, Albrecht-von-Haller-Institute for Plant Science, University of Goettingen within the master program „Microbiology and biochemistry“ Thesis title: Catabolic fate of jasmonates
10/2009 – 09/2012	Bachelor of Science Department of Plant Biochemistry, Albrecht-von-Haller-Institute for Plant Science, University of Goettingen Thesis title: Generation, purification, and characterization of Lipoxygenase 2 and Lipoxygenase 4 mutants from <i>Arabidopsis thaliana</i>
10/2007 – 09/2012	Studies of Chemistry, University of Goettingen without degree
07/2007 – 03/2007	Civilian service at the German Red Cross, Alfeld, Germany
08/1993 – 06/2006	General qualification for university entrance Gymnasium Alfeld, Germany Orientation level Alfeld, Germany Primary school „Dohnser Schule Alfeld“, Germany

PUBLICATIONS:

- Bruckhoff, V., Haroth, S., Feussner, K., König, S., Brodhun, F. and Feussner, I.** (2016). Functional characterization of CYP94-genes and identification of a novel jasmonate catabolite in flowers. *PLoS ONE*, **11**, e0159875. doi: 10.1371/journal.pone.0159875.
- Ding, P., Rekhter, D., Ding, Y., Feussner, K., Busta, L., Haroth, S., Xu, S., Li, X., Jetter, R., Feussner, I. and Zhang, Y.** (2016). Characterization of a pipecolic acid biosynthesis pathway required for systemic acquired resistance. *The Plant Cell*, **28**, 2603-2615. doi: 10.1105/tpc.16.00486.
- Eng, F., Haroth, S., Feussner, K., Meldau, D., Rekhter, D., Ischebeck, T., Brodhun, F. and Feussner, I.** (2016). Optimized jasmonic acid production by *Lasiodiplodia theobromae* reveals formation of valuable plant secondary metabolites. *PLoS ONE*, **11**, e0167627. doi: 10.1371/journal.pone.0167627.

